

**COMPUTATIONAL ASSESSMENT OF THE
STRUCTURE AND FUNCTION OF CYSTIC
FIBROSIS LUNG DISEASE PATHOGENESIS**

MAGED AWADALLA

**Computational assessment of the
structure and function of cystic fibrosis
lung disease pathogenesis**

By

Maged Awadalla

Thesis submitted for the degree of

Doctor of Philosophy

In

Biomedical and Biomechanical Engineering

Flinders University, Adelaide, Australia

2015

Research Supervisor: Professor Geoffrey McLennan (Deceased) M.D., Ph.D.

University of Iowa, Iowa City, USA

Research Supervisor: Associate Professor David Stoltz M.D., Ph.D.

University of Iowa, Iowa City, USA

Engineering research Supervisor: Professor Ching-Long Lin, Ph.D.

University of Iowa, Iowa City, USA

Principal academic Supervisor: Professor Karen Reynolds, Ph.D.

Flinders University, Adelaide, Australia

The research described in this thesis was conducted at the University of Iowa under the Iowa/ South Australia Transnational Alliance (ISATNA).

Table of Contents

Abstract	ix
Declaration	xi
Acknowledgements	xii
Publications	xvii
Honours and awards	xix
List of figures	xx
List of tables	xli
List of symbols and abbreviations	xliv
Chapter 1. Motivation, significance and innovation	1
1.1.Introduction.....	1
1.2.Cystic fibrosis effects on physical and mental health.....	3
1.3.Thesis aim and research direction.....	6
1.4.Conclusion	9
1.5.Statement of original contribution	10
Chapter 2. Cystic fibrosis	14
2.1. Cystic fibrosis (CF) history	14
2.2. CFTR structure	18
2.3. CFTR synthesis and trafficking	24
2.4. CFTR mutations	28
Chapter 3. Cystic fibrosis disease clinical manifestations and complications ...	35
3.1. Primary complications	35
3.1.1. Respiratory symptoms	35
3.1.2. Pancreatic insufficiency	41
3.1.3. Gastro-intestinal abnormalities	44
3.1.4. Hepatobiliary involvement	44
3.1.5. Reproductive system	47
3.1.6. Nutrition	47
3.2. Secondary complications	49
3.2.1. Cystic fibrosis related diabetes	49
3.2.2. Low bone mineral density	49
3.2.3. Gastro-intestinal	50
3.2.4. Psychological	51

3.3. Current treatments	52
3.3.1. Inhaled treatments	52
3.3.2. Chest physiotherapy	53
3.3.3. Antibiotics	56
3.4. Latest breakthrough therapies	58
Chapter 4. The respiratory system	63
4.1. The respiratory system structure and function	63
4.2. Ventilation	66
4.2.1. Conducting region	66
4.2.2. Transitional and respiratory region	69
4.3. Perfusion	69
4.4. Respiratory cycle	70
4.5. Methods of quantifying lung structure and function	71
4.6. Using QCT for studying pulmonary function.....	76
Chapter 5. Cell culture and animal models of cystic fibrosis	79
5.1. Introduction	79
5.2. CF in vitro cell culture models	79
5.3. CF mouse model	81
5.4. CF ferret model	83
5.5. CF pig model	85
5.6. Conclusions	88
Chapter 6. Early airway structural changes in cystic fibrosis pigs as a determinant of particle distribution and deposition	91
6.1. Introduction	91
6.2. Methods	93
6.2.1. CT imaging	93
6.2.2. Image analysis	94
6.2.3. Computational fluid dynamics solver	97
6.2.4. Lagrangian particle tracking algorithm	98
6.2.5. Statistical analysis	100
6.3. Results.....	101
6.3.1. Airway structure in newborn non-CF and CF pigs	101
6.3.2. Airflow characteristics in non-CF and CF airways	101
6.3.3. Effect of CF airway structural abnormalities on particle distribution and deposition patterns	104

6.3.4. Factors that cause higher particle deposition in the CF airway	111
6.3.5. Enhanced particle ventilation to the right CF lung	112
6.4. Discussion.....	116
6.5. Conclusion	121
Chapter 7. CFD modelling of airflow and particle deposition in older cystic fibrosis pigs	123
7.1. Introduction	123
7.2. Methods	126
7.2.1. CT imaging	126
7.2.2. Image analysis	129
7.2.3. Computational fluid dynamics solver	131
7.2.4. Lagrangian particle tracking algorithm	131
7.2.5. Statistical analysis	131
7.3. Results.....	132
7.3.1. Demographics, lung, airways characteristics in newborn and three week old non-CF and CF pigs	132
7.3.2. Airflow characteristics in three week old non-CF and CF pig airways .	138
7.3.3. Particle distribution and deposition patterns in non-CF and CF three week old pigs	140
7.3.4. Factors that lead to enhanced particle ventilation to the CF upper lobes	149
7.4. Discussion.....	156
7.5. Conclusion	165
Chapter 8. Analysing the global and local lung structure and function in adult human CF lungs	167
8.1. Introduction	167
8.2. Methods	171
8.2.1. Human subject data sets	171
8.2.2. Image analysis	173
8.2.3. Air trapping	176
8.2.4. Structural variables	177
8.2.5. Flow parameters	177
8.2.6. Construction of the 3-D Hybrid CL-CT-based model	179
8.2.7. Geometric laryngeal model	180
8.2.8. CFD mesh generation and boundary conditions	181

8.2.9. Computational fluid dynamics solver	183
8.2.10. Lagrangian particle tracking algorithm	183
8.2.11. Statistical analysis	183
8.3. Results.....	184
8.3.1. CF lung structure and function	184
8.3.1.1. Demographics	184
8.3.1.2. PFTs	186
8.3.1.3. Fixed lung volume analysis	187
8.3.1.4. Image registration	189
8.3.1.5. The effect of abnormal local lung function on particle ventilation and deposition	191
8.3.1.6. Airway and lung properties in the CF lung that lead to increased particle ventilation and deposition in the right upper lobe	195
8.3.2. The effect of disease severity in CF patients on lung structure and function	199
8.3.2.1. Demographics	199
8.3.2.2. PFTs	200
8.3.2.3. Fixed volume lung analysis	203
8.3.2.4. Image registration	209
8.3.2.5. The effect of disease severity on local and segmental airflow ventilation and tissue deformation	214
8.4. Discussion.....	226
8.5. Conclusion	233
Chapter 9. Summary and concluding remarks	235
9.1. Summary	235
9.2. Pathogenesis of CF lung disease	236
9.2.1. CF lung abnormalities at birth	236
9.2.2. CF lung abnormalities three weeks after birth	237
9.2.3. CF lung abnormalities at adulthood	237
9.3. Implications	239
9.4. Future directions	241
9.5. Final remarks and conclusion	243
References	249

Abstract

The pathogenesis of cystic fibrosis (CF) airway disease is not well understood. CF is an autosomal recessive genetic disease. Approximately, 1 in 25 people carry one of over 1,500 disease causing mutations in the gene that encodes the cystic fibrosis transmembrane conductance regulator (Strom, *Genet Med* 6:136-140). The World Health Organization estimates that 1 in 3,000 European newborns, in Australia 1 in 2,800, and in the United States 1 in 3,500 are born with CF disease (Stoltz, D., Welsh, *Sci Trans Med*, 2: p. 29ra31, 2010; Welsh, M.J., McGraw-Hill.5121-5189, 2001; Cystic Fibrosis Foundation, 2010). The CF phenotype that causes most of the morbidity and mortality is respiratory disease (Zielenski Julian, *Respiration*, 2000, 67:117-33).

The aim of this thesis is to investigate CF lung disease pathogenesis from birth to adulthood by analysing the local and global lung structure and function at three time points (birth, 3 weeks of age, and adulthood) in two species (pigs and humans).

There is increasing evidence that human CF lung disease, including airflow obstruction, is present earlier than originally thought, even within months after birth (Hoo, A.F., *Thorax*, 2012, 67: 874- 81) (Mott, L.S., *J Pediatr*, 2013, 163: 243- 48) (Sly, P.D., *Am J Respir Crit Care Med*, 2009, 180: 146- 52). However, technical and ethical constraints limit our ability to investigate the human lung at even earlier time points.

A porcine CF model was recently generated, in which animals develop lung disease similar to humans with CF. Unexpectedly, before infection and inflammation, newborn CF pigs have airways that are irregularly shaped and have a reduced calibre compared to non-CF pigs. I investigated the effect of the airway abnormalities seen in newborn CF pigs and I examined its effect on the lung function at two time points,

ix

birth and three weeks after birth. I used computational fluid dynamics (CFD) and airway geometries obtained by computed x-ray tomography to investigate the effect of early airway structure abnormalities on airflow. I found that newborn CF airways exhibited higher air velocity and resistance compared to non-CF. I also examined particle distribution and deposition. I found that at birth there was increased particle ventilation fraction to the right lung and higher deposition in the right lower lobe (Awadalla, M., *Annals of Biomedical Engineering*, 24 (4): 915-27, 2014). Three weeks after birth, I found that particle ventilation fraction to the lower lobes decreased while particle ventilation fraction to the right upper lobes increases. This suggests that upper lung lobes disease predominance might be secondary to the effect of congenital airway narrowing in CF. This thesis subsequently investigates progression of CF lung disease pathogenesis in adulthood. I examined the global and local lung structure and function in adult humans with CF. I found that people with CF had lower global pulmonary function compared to healthy subjects. I also found that people with CF had elevated air trapping compared to healthy subjects. I also examined particle distribution and deposition. I found that particle ventilation and deposition to the right upper lobe was also elevated in adults with CF. This was, in part, due to airway structural abnormalities in CF. These findings might have important implications for better understanding the pathogenesis of CF airway disease and the development of inhaled therapeutics in CF.

Declaration

I certify that this thesis does not incorporate without acknowledgement any material previously submitted for a degree or diploma in any university; and that to the best of my knowledge and belief it does not contain any material previously published or written by another person except where due reference is made in the text.

Maged Awadalla

Acknowledgements

Though only my name appears on the cover of this thesis, this large collection of work could not have been accomplished without the guidance of my advisors, help from friends, and support from my family. I owe my sincere gratitude to all those people who have made this thesis possible and because of whom my graduate experience has been one that I will cherish forever.

First and foremost I offer my sincerest and deepest gratitude to my supervisor at University of Iowa, Associate Professor David Stoltz, for his steadfast support, numerous insightful conversations, and his belief in my abilities during the early phases of my career. I attribute the level of my doctorate to his encouragement and effort. Without him, this thesis, too, would not have been completed or written. One simply could not wish for a better friend and supervisor. He allowed me to grow both scientifically and personally. It's been an honour and a great privilege to work with such a renowned scientist. I will forever be grateful.

My sincere appreciation also goes to my co-advisor at the University of Iowa, Professor Ching-Long Lin. The academic guidance he has facilitated provided me with an extensive understanding of the materials and methods involved in the computational study of fluid dynamics in human lungs. I was truly fortunate to have worked with him. His constant motivation, encouragement, and patience since I first met him seven years ago will always be appreciated.

In addition, I would like to thank my principle advisor at Flinders University, Professor Karen Reynolds, for all of her academic guidance, continual support, and encouragement. I could not have had a better cross-institutional supervision. Over the last 10 years, she has assisted me in numerous ways to develop many of the technical

skills that I am using today in my personal and professional life. I'm earnestly thankful Karen.

I will forever be indebted to my first PhD advisor at the University of Iowa, Professor Geoffrey McLennan. I had the privilege to work with Professor McLennan for six months during my work placement. Professor McLennan passed away three months after I started my PhD under his supervision. I was amazingly fortunate to have had the opportunity to work with someone who was truly inspirational. While working with him, he always gave me the freedom to explore the fields of science on my own, and at the same time he provided me with the guidance when my steps faltered. I lost an inspirational advisor and a dear friend. Rest in peace Geoff. Remember don't forget.

In addition, I would like to exceptionally thank my parents, for their support over the years. Also, I would like to thank them for their never ending love and constantly encouraging me to dream big and challenge myself. My dad taught me that nothing in life comes easily. His advice has always been a beacon guiding me throughout my life. I would like to thank my brother and sister for believing in me and encouraging me to always achieve my dreams. I would like to extend a special thanks to my sister Mona Awadalla for always being there for me not matter how busy she might be. In addition, I would like to thank her for always being excited to hear from me, and always being encouraged and inspired by everything I do. Mona I love you.

I'm also grateful for all the help and constant support Christine McLennan provided me throughout my PhD. Chris has been there for me in every good and bad moment. She truly helped be become a better person.

I would like to specially thank the Stoltz Lab members: Ryan Adam, Andrew Michalski, Michael Rector, Alex Tucker, and Drew Hannah. Also would like to

thank the Ching-Long Lin lab members: Dan Wu, Shinjori Miyawaki, Sanghun Choi, Jiwoong Choi, and Youbing Yin. In addition I would like to specially thank the Welsh lab and the Zabner lab members: Mike Welsh, Paula Ludwig, Lynda Ostedgaard, Mark Hoegger, Theresa Mayhew, Phil Karp, Joe Zabner, Alejandro Pezzulo, Peter Taft, Nick Gansemer, Emma Hornick, David Dickey, Ben Steines, and James Min.

I would like to thank all my friends: Alejandro Pezzulo, Peter Taft, Nick Gansemer, Emma Hornick, David Dickey, Ben Steines, Josh Weber, Brad van Sant, Brayden van Sant, Micheal Weaver, Katherine Fretland, Kelsey Andersen, Chris Gansemer, Sarah Tomlinson, Sascia Suminski, Justin Bates, Juan Baez, Morgan Gossman, Alan Schaefer, Sam de Groen, Sarah Arbaje, Per Hyldahl, Liz Swanton, John Goncalves, Tyler Mosher, Cody Wyborny, Nyassa Kollie, Claire Diver, David Dickey, Katir Pletcher, Melissa Jayne Wilson, Tanner Wallen, Grethe Nothling, Marie Edwards, Lizette Ortega, TaShanna Jarvis, Ashley Weaver, Chelsea Jacobsen, Leah Williams, Ciera Turner, Nicole Kelly, Rachelle Browne, Erica Bartley, Eman Namati, Anna Reissetter, Jeffrey Samuels, Jordon McLaughlin, Kevin Bell, Rachel Lipson, Rebecca Erin, Kelli Mohn, April Turley, Matt McCoy, Mark Hollender, Blake Daly, Christopher Tam, Rowshni Ahmed, Stephany Anie, Michael Rector, Nathan Rossen, Grant Lindburg, Asami Hagiwara, Breianne Rozendaal, Hisham Kabbara, Aileen Pappler, Kara Prior, Arielle Lipman, Julia Jessen, Ashley Groh, Shane Kellow, Salma Shabayek, Ouided Rouabhi, Bartosz Kowalski, Amy Hoehne, Sahba Shayani, Nasian Yazdani, Kami Lecamwasam, Agnieszka Saff, Ryan Herzberger, Andy Stessman, Liza Shrestha, Taylor Waldrop, Kiera Morrill, Alex Tucker, Shareef El Attar, Angela Mazza, Taysha Woods, Brittney Hesse, and James Min.

I would like to specially thank David Dickey. David, you have been an amazing friend. You were truly there for me. You generously invited me to stay at your place when I had no place to stay in Iowa. You always treated me like family and I believe you are the only one who cried when I mentioned that I'm leaving Iowa for good.

David we are not friends, we are brothers. I love you man.

I would like to specially thank Josh Weber and Brad van Sant. Since the first time we met you have treated me like an old friend. I always felt like I was at home when I visited you. Thank you for inviting me to all the gatherings you had. Thank you for introducing me to Iowa. Thank you for helping me stay sane through these difficult years. I truly miss you. I greatly value your friendship and deeply appreciate your support.

I would like to thank Morgan Krapfl. You were there for me throughout my PhD. Thank you for all your support. Also I would like to personally thank you for always putting a smile on my face. You are truly the best friend any person can wish for. Thank you for always being in touch even when I was not. A real friend is one who walks in when the rest of the world walks out. You are a real friend. I'm forever grateful.

I would like to specially thank Alexandra Bagley. Lexi you were there for me at the most difficult part of my PhD. I'm truly thankful for your support. You assisted me getting through the hard times and celebrated all the great times with me too. You truly helped me become a better person, and I am forever grateful. I'm extremely lucky to have such a great friend. Thank you.

Last but not least, I would also like to thank both Australia and The United States of America. Both countries have always provided me with numerous opportunities and allowed me to be who I am today. I owe special thanks to The United States of

America and everyone I met there. In America, I learned who I wanted to be and what I should strive for in life. It was truly home away from home. May God always bless the land of the free.

Publications

International journal articles

1. Adam R.J., et al., Air trapping and airflow obstruction in newborn cystic fibrosis piglets, *Am J Respir Crit Care Med*, 188 (12):1434-41, 2013.
2. Fletcher A., et al., The effect of geniglossal advancement on airway flow using a computational flow dynamics model, *Laryngoscope*, 123(12): 3227-32, 2013.
3. Hoegger M.J., et al., Assessing mucociliary transport of single particles in vivo shows variable speed and preference for the ventral trachea in newborn pigs, *Proc Natl Acad Sci U S A*, 111(6):2355-60, 2014.
4. Awadalla M., et al., Early airway structure changes in cystic fibrosis pigs as a determinant of particle distribution and deposition, *Ann Biomed Eng*, 42(4): 915-27, 2014.
5. Hoegger M.J., et al., Cystic fibrosis. Impaired mucus detachment disrupts mucociliary transport in a piglet model of cystic fibrosis, *Science*, 345(6198): 818-22, 2014.
6. Awadalla M., et al., Longitudinal numerical analysis of airflow and particle deposition in newborn and three weeks old cystic fibrosis pigs, under review by advisors.
7. Awadalla M., et al., Computational investigation of airflow and particle behavior in G551D adult cystic fibrosis humans, under review by advisors.
8. Awadalla M., et al., The effect of disease severity on local and global lung function in G551D adult cystic fibrosis patients before and after Ivacaftor treatment, under review by advisors.

Conference and symposium proceedings

1. Poster: “Computational study of particle deposition in CF and non-CF pig airways”, Department of Internal Medicine Research Day, University of Iowa, Iowa City, IA, USA. 2011.
2. Poster: “Effect of airway structure on particle behavior in CF and non-CF pig airways”, 9th Annual Research Open House, College of Engineering, University of Iowa, Iowa City, IA, USA. 2011.
3. Poster: “Computational study of particle deposition in CF and non-CF pig airways”, Translational Genomics Health Science Research Week, University of Iowa, Iowa City, IA, USA. 2011.
4. Poster: “Computational study of particle deposition in CF and non-CF pig airways”, College of Medicine Research Day, University of Iowa, Iowa City, IA, USA. 2011.
5. Oral Presentation/ Poster: “Computational study of particle deposition in CF and non-CF pig airways”, 25th Annual North American Cystic Fibrosis Conference (NACFC), Anaheim, CA, USA. 2011.
6. Poster: “Computational Assessment of the Effect of Airway Morphological Abnormalities in Cystic Fibrosis Pigs on Airflow and Particle Distribution Pattern”, Engineering Open House, University of Iowa, IA, USA. 2012.
7. Poster: “Early airway structural changes in cystic fibrosis pigs as a determinant of particle distribution and deposition”, Research Day, Department of Internal Medicine, University of Iowa, IA, USA. 2013.
8. Poster: “CFD Modeling Of Airflow And Particle Deposition In Newborn And Older Cystic Fibrosis Pigs”, American Thoracic Society International Conference, San Diego, CA, USA. 2014.

Honours and awards

1. Best Hydroscience and Engineering Poster, Engineering Open House, The University of Iowa, 2012.
2. Best Clinical/ Translational Poster, Research Day, The University of Iowa, Department of Internal Medicine, 2013.

List of figures

Figure 1.1. Picture of Holly van Geffen 22 year old cystic fibrosis patient.

Adapted from (Collin, 2013). 2

Figure 1.2. Picture of CF patient Holly van Geffen holding all the tablets she takes every day. Holly is at the end stage of the disease and she is on the double lung transplant list. Adapted from (UK, 2010).

..... 5

Figure 2.1. Dorothy Andersen early description of the CF disease. (A) a

photograph of Dorothy Andersen M.D. Adapted from (Vertex, 2013). (B)

Histological image of the pancreas of the patient Dr. Dorothy treated. The pancreas responded to treatment however this patient later passed away due to bronchiectasis.

This is the earliest description of cystic fibrosis as a lung and pancreas disease. (C)

Metaplasia found in the trachea of the same patient Dr. Dorothy examined. Once

again this is evidence that CF is not part of celiac disease. Adapted from (Andersen

D.H., 1938). 16

Figure 2.2. First described that CF sweat gland ducts are relatively

impermeable to Cl⁻ by Paul Quinton. The figure shows a simplified model of

normal (non-CF) and CF sweat duct. It emphasizes the basic abnormalities lead to

reduced Cl⁻ permeability. The schematic above shows the biochemical events

(starting by the activation of the acinar cells by agonists, which leads to biochemical

process causing the activation of protein kinase A and opening of the Cl⁻ channel) in

both non-CF and CF cells. Paul Quinton reports that all components appear to be

intact including the receptor and Cl⁻ channels in both non-CF and CF. However, at

some point distal to the activation of protein kinase A the biochemical processes stop

causing the abnormalities in Cl⁻ channel function. Adapted from (Quinton, 1989). . 17

Figure 2.3. The basic structure of the CFTR channel. (A) Schematic diagram of the CFTR channel structure. CFTR similar to all ATP-binding-cassette (ABC) transporter proteins have two cytoplasmic nucleotide-binding domains (NBDs) and two transmembrane domains (TMDs) which connect to the NBDs. However, unlike other ABC transporter proteins, CFTR also contains a regulatory domain (RD). The RD splits the protein into semi-symmetrical halves with one NBD and TMD on each half. The gray box indicates the probable location of the membrane lipid bilayer (cell wall). The numbers (1 to 12) represents the components and subunits of the channel TMDs. The lines between TMDs subunits represent strands in both above (ER lumen) and below (cytosol) the membrane of the cell. N is the cytoplasmic amino and C is the carboxyl termini (Hwang & Kirk, 2013). (B) The protein backbone of an ABC channel. Ribbons represent a homodimeric protein meaning protein with similar subunits. TMDs 1 and 2 are represented in purple and blue colours and NBDs 1 and 2 represented in green and gold colours. The TMD numbers 1 to 12 in figure 1.3. (A) are each represented by a helical structure in this image. R-domain is not included in this figure. Adapted from (S. J. Kim, 2012)..... 19

Figure 2.4. Schematic showing the gating regulated process of CFTR channel by forming NBD dimer. (A) Schematic of the CFTR channel. The schematic shows the structure of CFTR with TMD 1 and 2 represented by gray vertical boxes. NBD1 is represented by a green oval and NBD2 represented by a blue oval. R domain represented by a white box with R on it. There are two ATP-binding sites on the CFTR NBDs. N is the cytoplasmic amino and C is the carboxyl termini. (B) Schematic showing only NBD 1 and 2. Panel on the left is the back bone of NBD 1 and 2 protein. Ribbons represent a homodimeric protein meaning protein with similar subunits. Green is NBD1 and Blue is NBD2. Yellow is the ATP molecules at the interface between NBD 1 and 2. Panel on the left is a drawn schematic of the

right panel. (C) Schematic showing the process in which NBD forms a dimer to open the CFTR channel. CFTR can only hydrolyze ATP at one site which is NDB2. When ATP bound to NDB2 is hydrolyzed, the channel closes into a partial dimer. This prevents ATP from dissociating from NDB1 and allows the flow of ATP to NDB2. C1 shows CFTR channel closed with ATP unhydrolyzed and site 2 between NBD 1 and 2 open. O1 shows CFTR channel with site 2 connected and channel open. O2 shows the NBD2 hydrolyzing ATP at NBD2 site 2. C2 show shows the final process of site 2 between NBD 1 and 2 open allowing ADP (the output product of hydrolyzing ATP) to be removed a replaced by ATP to allow the channel to open again. Adapted from (Csanady, 2013)..... 20

Figure 2.5. Schematic showing the gating regulation process of CFTR channel by phosphorylation of the R domain. Left panel, shows the structure of the CFTR channel. The TMDs represented by vertical aligned brown boxes. NBDs represented by horizontally aligned blue boxes. R-domain by a square green box. Right panel, shows two CFTR channels one before phosphorylation of the R domain and the other after the phosphorylation of the R domain. The two large brown box like structure is the TMDs. The blue circular like structure attached the TMDs are the NBDs 1 and 2. The green box attached to one of the NBDs is the R domain. The figure shows the TMDs remain closed until R domain (cyclic AMP) is phosphorylated and ATP is binded to NBDs site one and two. Adapted from (Verkman & Galietta, 2009). 22

Figure 2.6. The protein backbone of the CFTR channel. Dark green helices are TMD1. Lime helices are TMD2. Pink helices and lines are NBD1. Purple helices and lines are NBD2. Gray tubes and lines are R-domain. This figure shows how the R domain is directly connected to NBD1 and TMD2 in the cytoplasmic region. It is proposed that the phosphorylated R domain can interact directly with the CFTR

channel TMD2 cytoplasmic region. The R domain then affects the conformational change within the TMD2 cytoplasmic region and opening the CFTR channel without NBD dimerization. Adapted from (Serohijos et al., 2008). 23

Figure 2.7. The location of the *CFTR* gene in the human chromosome. (A) The 23 pairs of chromosome normally found in human cells. Adapted from Shamsi M.B., Indian Journal of Urology, 27(1): 110-20, 2011, website: <http://www.indianjurol.com/article.asp?issn=0970-1591;year=2011;volume=27;issue=1;spage=110;epage=120;aualast=Shamsi>. (B) A pair of chromosome 7 where *CFTR* is located. Adapted from Patel C., European Journal of Human Genetics 19, 634-9, 2011, doi: 10. 1038/ejhg.2010.238. (C) Schematic showing the location of CFTR at one of the long arm of chromosome 7 position 7q31.2. Adapted from (Lewis, 2002). 25

Figure 2.8. The process of producing CFTR channel from the nucleus to the cell membrane. (1) Chromosome 7 containing the *CFTR* gene in the nucleus. (2) The *CFTR* gene is made up of 250,000 DNA nucleotides containing all the information required to produce a functional CFTR channel. (3) Inside the cell's nucleus the gene is transcribed into a messenger RNA (mRNA). (4) mRNA then leaves the nucleus and is transported to the endoplasmic reticulum (ER). (5) In the ribosomes the mRNA is translated into protein. (6) The protein is then folded in the ER by other proteins called chaperone. (7) The CFTR proteins then move to Golgi apparatus where it undergoes final processing and packaging. (8) The completed CFTR channel leaves the Golgi apparatus and heads towards the cell surface. (9) CFTR channel reaches the cell membrane and starts its function as a chloride transporter. Adapted from (JohnHopkins, 2014). 26

Figure 2.9. Mechanism in which the mutation of the *CFTR* gene can lead to defective or inactive CFTR channel. Class I mechanism, *CFTR* gene in chromosome 7 produces a nonsense mRNA during transcription of the gene. Therefore Class I patients do not have a functioning *CFTR* protein or channels, e.g. G542X. Class II mechanism, *CFTR* gene is missing some essential amino-acids. Therefore when the channel is produced it gets labelled by the cell defence mechanism as defective and then destroyed, Some of these channel do reach the cell surface, however they fail to function, e.g. F508del. Class III mechanism, *CFTR* channel is not folded and packaged correctly in the endoplasmic reticulum and the Golgi apparatus. Therefore, although the channel reaches the cell surface it is unable to properly function, e.g. G551D. Class IV mechanism, *CFTR* channel reaches the cell surface but its function is poor, e.g. R117H. Class V mechanism, although *CFTR* is produced correctly and function normally, there is a decreased production of the *CFTR* channel, e.g. A455E. adapted from (JohnHopkins, 2014). 29

Figure 2.10. The location of F508del in the backbone structure of the *CFTR* channel. (A) Blue helices are TMD1. Sand yellow helices are TMD2. Cyan helices and lines are NBD1. Orange helices are NBD2. Dark green ribbons and helices are R-domain. Red is the location of amino acid F508. The most common disease inducing mutation in *CFTR* is caused by the deletion of three base pairs, which results in loss of a phenylalanine residue at amino acid position 508. The $\Delta F508$ mutation causes folding defects in NBD1 which in turn affects the coupled domain folding. (B) The impairment in the coupled domain folding affects the assembly of NBD1 and the TMDs. This leads to incorrectly folded NBD2 which trigger the channel to be destroyed by the cell defence mechanism. Even if the channel passes the cell defence mechanism it will not be able to function since the ATP binding site

on NBD2 is not functioning due to incorrect folding. Adapted from (Molinski et al., 2012)..... 30

Figure 3.1. Thick viscous mucus observed in CF patient's airways. The airway observed in this figure was obtained from a lung transplant performed on a 15 year old patient. Two types of mucus plugging can be observed in this image. Semi-liquid ivory mucus and translucent elastic mucus (shown in the figure to stretch from the bronchus). Adapted from (J. J. Wine, 2010) 38

Figure 3.2. Histological view of the effect of CFTR on pancreas structure and function. (A) The thick mucus blocking pancreatic duct. H&E (Hematoxylin and Eosin) stain is the gold standard histological staining mechanism used for medical diagnosis mostly used to indicate the location of cells by staining the nucleus dark purple. PAS (Periodic acid-Schiff) stain is used in detecting mucus by staining it dark purple. In (A), our research group observed that the location of the cells forming the pancreatic duct represented by dark purple dots in the H&E stain. Our research group also observed in the PAS stain that that the pancreatic duct is blocked with mucus. In addition, our research group observed that the mucus generating cells on the duct wall, indicated by the white arrow with green border, is also filled with mucus. Bar represents 50 μ m. (B), (C), and (D) shows the microscopic structure of the pancreas, which consists of acini sacks (secretes enzymes) and ductules and ducts which connects all the acini sacks (secretes bicarbonate rich solutions). This is also known as parenchyma (the functional tissue), and the adipose (connective) tissue. In (B), (C), and (D) Our research group compared the healthy pancreas (CFTR +/+) with CF pancreas (CFTR -/-). (B) Abnormal ductules and acini in CF pancreas. Black arrow shows pancreatic duct plugged by concentrically lamellar secretion. Bar represents 33 μ m. H&E stain. (C) shows plugging of the CF pancreatic duct and

shrinking in the CF islets of langerhans which is responsible for generating insulin (indicated by the black arrow heads). (D) Loss in the CF pancreas parenchyma tissue. Bar represents 100 μ m. All these figures were obtained from the CF pig model. Adapted from (Rogers, Stoltz, et al., 2008)..... 42

Figure 3.3. The effect of CF disease on the gallbladder. (A) The gallbladder of a healthy (CFTR +/+) and a CF pig(CFTR -/-). Gallbladder is a small organ attached to the liver and it act as a storage for bile. Bile is fluid produced by the liver and acts as a surfactant allowing the mixing of lipids with water in food. After eating, the gallbladder discharge all the stored bile into the duodenum (first section of the small intestine) to assist in mixing and digesting food. In (A) after sectioning the CFTR +/+ gallbladder bile drained rapidly. However, after sectioning CFTR -/-, bile did not drain, it was coagulated against the lumen of the gallbladder (indicated by the white arrow). Bar, 0.5 cm. B) H&E (Hematoxylin and Eosin) and PAS (Periodic acid-Schiff) stain of the gallbladder. H&E indicates the location of cells by staining the nucleus dark purple. PAS detects mucus by staining it dark purple. CFTR +/+ H&E show a healthy gallbladder duct. CFTR -/- H&E show the inflammation in the gallbladder duct tissue. The asterisks indicated coagulated bile. Black arrows in CFTR -/-, H&E and white arrows in CFTR -/-, PAS indicate coagulated bile and abnormal mucus production. Bars, 500 μ m. All these figures were obtained from the CF pig model. Adapted from (Rogers, Stoltz, et al., 2008)..... 44

Figure 3.4. The effect of CF disease on the liver. The liver of a healthy (CFTR +/+) and CF pig (CFTR -/-). The figure show H&E (Hematoxylin and Eosin) staining which (Hematoxylin and Eosin). The figure shows inflammation and abnormalities in the CFTR-/- liver compared to CFTR +/+. Bars, 100 μ m. All these figures were obtained from the CF pig model. Adapted from (Rogers, Stoltz, et al., 2008). 45

Figure 3.5. Effect of CF disease on the male reproductive system. The figure above illustrates bilateral absence of the vas deferens in CF patients compared to healthy non-CF subjects. Vas deferens is a duct that conveys sperm from the testicles to the urethra. Almost all CF males (98 percent) are azoospermic, meaning that they do not have a measurable amount of sperm within their semen. Adapted from (JohnHopkins, 2014). 47

Figure 3.6. Effect of CF disease on bone material density. The figure shows low bone mineral density in CF patients compared to non-CF healthy subjects. Low bone mineral density occurs in over three quarters of CF adults. It occurs due to poor absorption of fat, low vitamin D levels, insufficient sunlight exposure, insufficient exercise, and delayed onset of puberty. Adapted from (JohnHopkins, 2014)..... 51

Figure 3.7. Positive Expiratory Pressure (PEP) mask. It works by creating higher pressure in the airways forcing more air to distal regions. The resistance is created by exhaling through a mask mouthpiece. The increasing resistance is thought to break up thick mucus secretions. Adapted from (Elettromedicali)..... 54

Figure 3.8. High-frequency chest compression vest. This vest uses air pressure and pulses to create vibrations on the CF patient's chest. It has been shown to loosen, thin, and increase mucociliary clearance by increasing expiration and creating forces leading to coughing. Adapted from (Respiritech). 55

Figure 4.1. Human lung. A. diagram showing all lung lobes positions. Adapted from (LVNG, 2006). B. human lung cast. Left lung: displays the bronchial tree. Right lung: displays arteries shown in red and veins shown in blue. The zoomed in box highlights that the airway and arterial trees mirror each other all of the way out to the terminal branches. Adapted from (Glenny, 2011)..... 65

Figure. 4.2. Gas exchange between tissues in the body and the environment. The figure shows the air going through the conducting airways and then to the respiratory airways, the site of gas exchange. Adapted from (Levitzky, 1995). 67

Figure. 4.3. Scanning electron micrograph of the surface and cross section of the alveoli. The image contains three alveoli. A= alveolus; D=alveolar duct; PK= Pores of Kohn; AR= alveolar entrance to duct; *= connective tissue fibers. Adapted from (Weibel, 1973)..... 68

Figure. 4.4. The airway tree structure. The figure depicts the conducting, transitional, and respiratory regions in the lung. Dimensions are approximate. Adapted from (Weibel, 1963) 68

Figure. 4.5. Lung volumes. The figure depicts different lung volumes during the respiratory cycle and there definitions. Dimensions are approximate. Adapted from (Levitzky, 1995) 71

Figure 6.1. Lung structure and lobar airflow ventilation fraction acquired using computed tomography at 0 and 20 cm H₂O. (A) Front view of non-CF lung at 0 and 20 cmH₂O. The colour codes indicate each individual lobe in the pig lung. Gold-right cranial (RCr), blue-right middle (RM), purple-right accessory (RAc), yellow-right caudal (RCa), red-left cranial (LCr), and green-left caudal (RCa). (B) Airflow ventilation fraction to each lobe in newborn non-CF and CF pigs (n = 5 for each genotype)..... 96

Figure 6.2. Computational fluid dynamic modeling of air pressure and velocity in newborn non-CF and CF porcine airways. (A) Air pressure (Pa) and velocity (m/s) in non-CF and CF airways. (B) The cross-sectional area in the subglottis (SG), the average along the tracheal (T), the right mainstem bronchus (RMB), and left

mainstem bronchus (LMB) in non-CF and CF. (C) The pressure drop at the SG, T, RMB, and LMB in non-CF and CF. (D) The average air velocity at the SG, T, RMB, and LMB in non-CF and CF. (E) The average airway resistance in the area of the SG, T, RMB, and LMB in non-CF and CF. Data for B-E were obtained from horizontal slices extracted from the 3D airway geometry, perpendicular to the centreline using Tecplot. R denotes right side, L denotes left side, A denotes anterior, and P denotes posterior. * denotes statistical significance between non-CF and CF data ($p < 0.05$) ($n = 5$ for each genotype)..... 103

Figure 6.3. Particle distribution and deposition in non-CF and CF airways. 10- μ m particle flow path and deposition pattern at 50 and 400 ms in non-CF and CF airways. Particle colour denotes particle states (black = in-transit, red = deposited, blue = escaped)..... 107

Figure 6.4. CFD prediction of airflow characteristics in non-CF and CF trachea. Shown are tracheal cross-sections at 5 different levels: glottis, above the tracheal angle (above TA), below the tracheal angle (below TA), above the tracheal lobe (above TL), and below the tracheal lobe (below TL). Top panel shows data from a representative non-CF trachea where greater anterior particle deposition was observed. Middle and lower panels show data from a representative non-CF trachea (middle panel) and CF trachea (lower panel) where more circumferential particle deposition was observed. The velocity profile ($m.s^{-1}$) at each level is shown. A denotes anterior, and P denotes posterior. TA denotes tracheal angle..... 108

Figure 6.5. The effects of increasing particle size on deposition efficiency to the left and right lung. Particle deposition efficiency was defined as the number of particles depositing in the right (excluding the right cranial lobe since the right cranial lobe bronchus branches from the trachea) or left lung divided by the number

of particles that entered the right or left lung, respectively. * denotes statistical significance between non-CF and CF data ($p < 0.05$) ($n = 5$ for each genotype). ... 109

Figure 6.6. Particle deposition efficiency for lobar airways in non-CF and CF airway geometries. Shown are the effects of increasing particle size on particle deposition efficiency for lobar airways included in non-CF and CF airway geometries. Particle deposition efficiency was defined as the number of particles depositing in a specific lobar airway divided by the number of particles that entered that lobar airway. * denotes statistical significance between non-CF and CF data ($p < 0.05$) ($n = 5$ for each genotype). 110

Figure 6.7. 10- μ m particle trajectory in newborn non-CF and CF porcine airways. (A) Particle trajectory in non-CF and CF airways at 0.04 s. Note the formation of a fork shape at the front tip of the particle bolus in CF indicating that the particles follow a secondary flow. (B) Particle trajectory in non-CF and CF airway at 0.055 s. Note the particles tend to travel near the right side of the trachea. (C) Particle trajectory in non-CF and CF airways at 0.065 s. The particles are colour based upon their status - black = in-transit and red = deposited. 114

Figure 6.8. The effect of the carina bifurcation angle relative to the trachea on particle ventilation to the right and left lung. (A) Visual comparison between non-CF and CF carina position, and bifurcation angle to right and left main stem bronchus relative to the trachea. (B) The bifurcation angle ratio of the carina relative to the trachea. Note the carina angle ratio was computed by dividing the angle of the left mainstem bronchus by right mainstem bronchus. * denotes statistical significance between non-CF and CF data ($p < 0.05$) ($n = 5$ for each genotype). (C) The formation of the particle bolus while entering the right and left mainstem bronchi.

The particles are colour based upon their status - black = in-transit and red = deposited. R denotes right side and L denotes left side..... 115

Figure 7.1. Lobar airflow ventilation fraction as the lung expands from 0 to 20 cm H₂O in non-CF and CF pigs at two time point birth and 3 weeks after. (A) Airflow ventilation fraction to each lobe in newborn non-CF and CF pigs (n = 5 for each genotype). RCr denotes right cranial, RM denotes right middle, RAc denotes right accessory, RCa denotes right caudal, LCr denotes left cranial, LCa denotes left caudal. (B) Airflow ventilation fraction to each lobe in 3 week old non-CF and CF pigs (n = 5 for each genotype). * denotes statistical significance. 130

Figure 7.2. Airway cross-sectional area, air pressure, and velocity obtained from computational fluid dynamics modeling of three week old non-CF and CF porcine airways. (A) The cross-sectional area in the subglottis (SG), the average along the tracheal (T), the right mainstem bronchus (RMB), and left mainstem bronchus (LMB) in non-CF and CF. (B) The pressure drop at the SG, T, RMB, and LMB in non-CF and CF with inhalation flow rate of 55 ml/s. (C) The average air velocity at the SG, T, RMB, and LMB in non-CF and CF with inhalation flow rate of 55 ml/s. (D) The pressure drop at the SG, T, RMB, and LMB in non-CF and CF with inhalation flow rate of 70 ml/s. (E) The average air velocity at the SG, T, RMB, and LMB in non-CF and CF with inhalation flow rate of 70 ml/s. (F) The pressure drop at the SG, T, RMB, and LMB in non-CF and CF with inhalation flow rate of 85 ml/s. (G) The average air velocity at the SG, T, RMB, and LMB in non-CF and CF with inhalation flow rate of 85 ml/s. * denotes statistical significance..... 137

Figure 7.3. Particle ventilation fraction in 3 week old non-CF and CF lung lobes at three different inhalation flow rate. (A) Particle ventilation fraction in all lung lobes at inhalation flow rate of 55mL/s. RCr denotes right cranial, RM denotes right

middle, RAc denotes right accessory, RCa denotes right caudal, LCr denotes left cranial, LCa denotes left caudal. (B) Particle ventilation fraction in all lung lobes at inhalation flow rate of 70 mL/s. (C) Particle ventilation fraction in all lung lobes at inhalation flow rate of 85 mL/s. * denotes statistical significance 143

Figure 7.4. The relationship between particle ventilation fraction to the upper lobes vs. the middle and lower lobes for three week old non-CF and CF pigs.

For all three graphs, in the y-axis, U denotes upper lobes which consists of right cranial (RCr), right middle (RM), and left cranial (LCr). M denotes middle lobe which consists of right accessory (RAc). L denotes lower lobes which consist of right caudal (RCa) and left caudal (LCa). (A) The relationship between particle ventilation fraction in upper lung lobes vs. the middle and lower lung lobes at inhalation flow rate of 55mL/s. (B) The relationship between particle ventilation fraction in upper lung lobes vs. the middle and lower lung lobes at inhalation flow rate of 70mL/s. (C) The relationship between particle ventilation fraction in upper lung lobes vs. the middle and lower lung lobes at inhalation flow rate of 85mL/s. * denotes statistical significance..... 144

Figure 7.5. The relationship between particle ventilation fraction to the upper lobes vs. the middle and lower lobes for three week old non-CF and CF pigs at each genotype physiological flow rate.

(A) The relationship between particle ventilation fraction in upper lung lobes vs. the middle and lower lung lobes. Non-CF inhalation flow rate of 85mL/s. CF inhalation flow rate of 55mL/s. In the y-axis, U denotes upper lobes which consists of right cranial (RCr), right middle (RM), and left cranial (LCr). M denotes middle lobe which consists of right accessory (RAc). L denotes lower lobes which consist of right caudal (RCa) and left caudal (LCa). (B) Particle ventilation fraction in the right cranial lobe. RCr denotes right cranial. Non-

CF inhalation flow rate of 85mL/s. CF inhalation flow rate of 55mL/s. * denotes statistical significance..... 145

Figure 7.6. Particle deposition efficiency in 3 week old non-CF and CF lung lobes at three different inhalation flow rate. (A) Particle deposition efficiency in all lung lobes at inhalation flow rate of 55mL/s. RCr denotes right cranial, RM denotes right middle, RAc denotes right accessory, RCa denotes right caudal, LCr denotes left cranial, LCa denotes left caudal. (B) Particle deposition efficiency in all lung lobes at inhalation flow rate of 70 mL/s. (C) Particle deposition efficiency in all lung lobes at inhalation flow rate of 85 mL/s. * denotes statistical significance. 147

Figure 7.7. Air velocity in the right cranial airway at three different inhalation flow rates. (A) Air velocity at the right cranial (RCr) airway at a inhalation flow rate of 55, 70, 85 ml/s. (B) Air velocity at the right cranial (RCr) airway at each genotype physiological flow rate. Non-CF inhalation flow rate of 85mL/s. CF inhalation flow rate of 55mL/s. * denotes statistical significance..... 153

Figure 7.8. Tracheal angle and right cranial lobe airway bifurcation angle. (A) Left panel: comparing non-CF and CF tracheal angle. Right panel: diagram demonstration the location the tracheal angle was measured. (B) Left panel: Comparing non-CF and CF right cranial (RCr) lobe airway bifurcation angle. This angle was measured in relation to the straight line connecting the centres of the right and left main bronchus at the carina bifurcation point. Right panel: diagram demonstration the location and method the right cranial bifurcation angle was measured. Arrow denotes the posterior region of the airway. * denotes statistical significance ($p < 0.05$)..... 154

Figure 7.9. A slice of a computed x-ray tomography representing upper lung lobe disease in humans and porcine with CF. In a computed x-ray tomography

image air appear black, tissue appear gray, and bone appear white. If a huge portion of the lung appears light gray, it is an indication of lobe disease or collapse. (A) Upper lobe disease in a human CF patient. (B) Upper lobe disease in the right cranial lobe (RCr) in a year old CF pig. Arrow denotes the location of the upper lobe and the disease. 164

Figure 8.1. Comparing global lung function between healthy non-CF subjects and CF patients using PFTs. (A) FEV1% is forced expiratory volume in one second. (B) FVC% is forced vital capacity. (C) FEF 25-75% is forced (mid) expiratory flow rate. (D) FEV1/FVC % is the ratio between FEV1 and FVC. * denotes statistical significance ($P < 0.05$). Black filled circle (normal, on the x-axis) denotes each individual healthy non-CF patients. Black filled triangle denotes each individual CF patient. 186

Figure 8.2. Supine computed tomography fixed volume global and local values. (A) Total lung volume (global) at residual volume (RV) and total lung capacity (TLC). Normal denotes non-CF patients. CF denotes CF patients. (B) Lobar lung volume at RV normalized by total lung volume at TLC for each individual patient's lobe. UL denotes upper left lung lobe. LL denotes lower left lung lobe. UR denotes upper right lung lobe. MR denotes middle right lung lobe. LR denotes lower right lung lobe. * denotes statistical significance ($P < 0.05$). (C) Lobar lung volume at TLC normalized by total lung volume at TLC for each individual patient's lobe. (D) Lobar lung compliance measures the dynamic change in lobe volume from TLC to RV normalized by the lobe volume for each individual patient total lung volume at TLC. (E) Tissue density at the RV scan. Tissue density is defined as any voxel with a Hounsfield unit greater than -55. (F) Lobar air trapping. TL denotes total lung. 188

Figure 8.3. The effect of lung expansion from RV to TLC on total lung dimensions, shape, volume expansion and tissue deformation in non-CF and CF.

(A) Total lung dimensions: the depth (the distance from the ventral to the dorsal side), the height (the distance from the apical to the basal side), and the width (distance from the left to the right lateral side). Normal denotes non-CF patients. CF denotes CF patients. * denotes statistical significance ($P < 0.05$). (B) Lung shape defined as height (Z) over depth (Y) and height (Z) over width (X). (C) The ratio of lobar air and tissue volume change as the lung expands from RV to TLC. (D) The non-symmetrical deformation in the tissue ratio also know as anisotropic deformation index (ADI)..... 191

Figure 8.4. Selecting three representative CF patients for computational fluid dynamics (CFD) study based on maximum air trapping in all lobes.

(A) Air trapping in all CF patients (CF-all) compared to the selected representative CF patients for CFD study (CF-CFD). UL denotes upper left lung lobe. LL denotes lower left lung lobe. UR denote upper right lung lobe. MR denotes middle right lung lobe. LR denotes lower right lung lobe. (B) Total lung volume in all CF patients compared to the selected representative CF-CFD patient. RV denotes residual lung volume. TLC denotes total lung capacity. (C) Lobar RV volume normalized in all CF patients compared to the selected representative CF-CFD patients. Each lobe at RV was normalized by total lung volume at TLC from each individual patient. (D) Lobar TLC volume normalized in all CF patients compared to the selected representative CF-CFD patients. Each lobe at TLC was normalized by the total lung volume at TLC from each individual patient..... 193

Figure 8.5. Factors that lead to increase particle ventilation into the right upper lobe.

(A) Mass flow rate at the airway supplying right upper lobe (RUL Airway) in

healthy non-CF subjects and CF patient. Normal denotes healthy non-CF subjects. CF denotes CF patients. UL denotes upper left lung lobe. LL denotes lower left lung lobe. UR denotes upper right lung lobe. MR denotes middle right lung lobe. LR denotes lower right lung lobe. * denotes statistical significance ($P < 0.05$). (B) Cross-sectional area of the RUL airway. (C) Airway resistance at the RUL airway. (D) Pressure drop at the RUL airway. (E) Airflow velocity at the RUL airway. 197

Figure 8.6. Factors that lead to increase particle deposition into the airways considered in right upper lobe. (A) Turbulent kinetic energy at the airway supplying right upper lobe (RUL airway) in healthy non-CF subject and CF patient. Normal denotes healthy non-CF subject. CF denotes CF patient. (B) Particle Stokes number in a log scale. Stokes number indicates the ability of the particle to deviate from the stream line due to its speed or mass. Particle sizes considered varied from 0.5 to 10 μm 198

Figure 8.7. Comparing global lung function between non-CF, mild CF patients, and severe CF patients using predicted PFTs. FEV1% is force expiratory volume in one second. FVC is forced vital capacity. FEF 25-75% is forced (mid) expiratory flow rate. FEV1/FVC % is the ratio between FEV1 and FVC. * denotes statistical significance ($P < 0.05$). Normal denotes non-CF patients. CF-L denotes patients with low FEV1 ($\text{FEV1\%} < 55\%$). CF-H denotes patients with high FEV1 ($\text{FEV1\%} > 55\%$). 202

Figure 8.8. Supine computed tomography fixed volume global and local value. (A) Total lung volume (global) at residual volume (RV) and total lung capacity (TLC). Normal denotes non-CF patients. CF-L denotes patients with low FEV1 ($\text{FEV1\%} < 55\%$). CF-H denotes patients with high FEV1 ($\text{FEV1\%} > 55\%$). * denotes statistical significance ($P < 0.05$). (B) Lobar lung volume at RV normalized

by total lung volume at TLC for each individual patient's lobe. UL denotes upper left lung lobe. LL denotes lower left lung lobe. UR denotes upper right lung lobe. MR denotes middle right lung lobe. LR denotes lower right lung lobe. (C) Lobar lung volume at TLC normalized by total lung volume at TLC for each individual patient's lobe. (D) Lobar lung compliance, measures the dynamic change in lobe volume from TLC to RV normalized by the lobe volume for each individual patient total lung volume at TLC. (E) Lobar air trapping. 206

Figure 8.9. Static and dynamic airway values. All the airways measured were has grouped based on their diameter at TLC (less than 4.5 mm, between 4.5 to 6, between 6 to 7.5, between 7.5 to 9, between 9 to 13.5, and finally larger than 13.5 mm). Airway diameter at total lung capacity (TLC) was picked since it is more stable and less based on patient effort. (A) Airway cross-sectional area at TLC (static). Normal denoted non-CF patients. CF-L denotes patients with low FEV1 (FEV1% < 55%). CF-H denotes patients with high FEV1 (FEV1% > 55%). * denotes statistical significance (P < 0.05). (B) Airway cross-sectional area at residual volume (RV) (static). (C) Airway dispensability (dynamic). The change in airway area from TLC to RV normalized by airway area at TLC. 208

Figure 8.10. Comparing total lung dimensions and shape between non-CF, mild CF patients, and severe CF patients. (A) Total lung dimensions: the depth (the distance from the ventral to the dorsal side), the height (the distance from the apical to the basal side), and the width (distance from the left to the right lateral side). Normal denotes non-CF patients. CF-L denotes patients with low FEV1 (FEV1% < 55%). CF-H denotes patients with high FEV1 (FEV1% > 55%). * denotes statistical significance (P < 0.05). (B) Lung shape defined as height (Z) over depth (Y) and height (Z) over width (X). 211

Figure 8.11. Comparing dynamic volume and tissue properties between non-CF, mild CF patients and severe CF patients. (A) The change in lobar air volume as each lobe expands from residual volume (RV) to total lung capacity (TLC). Normal denotes non-CF patients. CF-L denotes patients with low FEV1 (FEV1% < 55%). CF-H denotes patients with high FEV1 (FEV1% > 55%). * denotes statistical significance ($P < 0.05$). UL denotes upper left lung lobe. LL denotes lower left lung lobe. UR denotes upper right lung lobe. MR denotes middle right lung lobe. LR denotes lower right lung lobe. Total denotes all lung lobes. (B) The ratio of lobar air and tissue volume change as the lung expands from RV to TLC. (C) The non-symmetrical deformation in the tissue ratio also known as anisotropic deformation index (ADI). 212

Figure 8.12. Selecting one representative severe CF patient and mild CF patient based on maximum air trapping in the upper lobe. (A) Air trapping in all severe (CF-L-all) patients compared to the selected representative severe patient (CF-L-IR). UL denotes upper left lung lobe. LL denotes lower left lung lobe. UR denotes upper right lung lobe. MR denotes middle right lung lobe. LR denotes lower right lung lobe. TL denotes all lung lobes (B) Air trapping in all mild patients (CF-H-all) compared to the selected representative mild patient (CF-H-IR). (C) Total lung volume in all severe patients compared to the selected representative severe patient. RV denotes lung residual volume. TLC denotes total lung capacity. (D) Total lung volume in all mild patients compared to the selected representative mild patient. (E) Lobar RV volume normalized in all severe patients compared to the selected representative severe patient. Each lobe at RV was normalized by total lung volume at TLC from each individual patient. (F) Lobar RV volume normalized in all mild patients compared to the selected representative mild patient. (J) Lobar TLC volume normalized in all severe patients compared to the selected representative severe

patient. Each lobe at TLC was normalized by the total lung volume at TLC from each individual patient. (K) Lobar TLC volume normalized in all mild patients compared to the selected representative mild patient..... 217

Figure 8.13. Comparing dynamic volume and tissue properties between a representative non-CF subject, mild CF patient and severe CF patient using extracted vertical and horizontal slices. (A) Vertical lung slices representing air volume change, extracted at a lateral depth of 15, 30, 70, and 85% of the non-CF subject's (control, black box), mild CF patient's (mild CF, red box) and severe CF patient's (severe CF, orange box) lung. Air volume change from residual volume (RV) to total lung capacity (TLC) is represented by a heat map. Red denotes high volume change. Blue denotes low volume change. (B) Horizontal lung slices representing air volume change, extracted at 20, 40, 60, and 80% of the height of the non-CF subject's, mild CF patient's, and severe CF patient's lung. (C) Vertical lung slices representing the ratio of air volume change, extracted at lateral depth of 15, 30, 70, and 85% of the non-CF subject's, mild CF patient's and severe CF patient's lung. The ratio of air volume change from residual volume (RV) to total lung capacity (TLC) is represented by a heat map. Red denotes high ratio of volume change. Blue denotes low ratio of volume change. (D) Horizontal lung slices representing ratio of air volume change, extracted at 20, 40, 60, and 80% of the height of the non-CF subject's, mild CF patient's, and severe CF patient's lung. (E) Vertical lung slices representing the ratio of non-uniform tissue deformation of anisotropic deformation index (ADI), extracted at a lateral depth of 15, 30, 70, and 85% of the non-CF subject's, mild CF patient's and severe CF patient's lung. The ADI from residual volume (RV) to total lung capacity (TLC) is represented by a heat map. Red denotes high ADI. Blue denotes low ADI. (F) Horizontal lung slices representing ADI,

extracted at 20, 40, 60, and 80% of the height of the non-CF subject's, mild CF patient's, and severe CF patient's lung219-225

Figure 9.1. A picture of Holly van Geffen suffering from surgical emphysema.

Adapted from (Collins, 2015) 246

Figure 9.2. A picture of Holly van Geffen on the left next to her parents Nick and Jayne. The picture was taken during the transplant games this year. Adapted

from (Collins, 2015) 247

List of tables

Table 6.1. Particle ventilation fraction in non-CF and CF airways. The particle ventilation fraction and particle Stokes number in the trachea for each corresponding animal are shown. Particle ventilation fraction was determined for the right lung (particles entering the right mainstem bronchus), left lung (particles entering the left mainstem bronchus), and right cranial lobe (particles entering the right cranial lobe bronchus) divided by the total number of particles entering the right mainstem, left mainstem, and right cranial lobe bronchi. I separated the right cranial lobe from the “right lung” since the right cranial lobe bronchus branches from the trachea and not the right mainstem bronchus. Each line represents data from a pair of non-CF and CF pigs. Mean \pm SEM for the group are in bold. #denotes statistical significance between non-CF and CF data ($p < 0.05$)..... 106

Table 6.2. Particle Stokes number and Reynolds number at the airway inlet of each individual lobe in non-CF and CF newborn pigs. #denotes statistical significance between non-CF and CF data ($p < 0.05$) ($n = 5$ for each genotype). ... 111

Table 7.1. The demographical and physiological data from all the newborn non-CF and CF pigs selected for the study of lung structure and function. Age units is in days. Weight in kilograms (kg). Lung volume in millilitres (mL). Trachea major and minor diameter in millimetre (mm). The physiological data represents the lung at two inflation position 0 cmH₂O and 25 cmH₂O. # denotes statistical significance between non-CF and CF ($p < 0.05$)..... 135

Table 7.2. The demographical and physiological data from all the 3 week old non-CF and CF pigs selected for the study of lung structure and function. Age units is in days. Weight in kilograms (kg). Lung volume in millilitres (mL). Trachea

major and minor diameter in millimetre (mm). The physiological data represents the lung at two inflation position 0 cmH₂O and 25 cmH₂O. # denotes statistical significance between non-CF and CF (p < 0.05)..... 136

Table 7.3. Particle Stokes number in the trachea for 3 week old non-CF and CF pigs at three different inspirational flow rates. mL/s denotes the flow rate unites millilitres per second. 55 mL/s denotes the value of the inhalation flow rate in non-CF and CF. 70 mL/s denotes the value of the inhalation flow rate in non-CF and CF. 85 mL/s denotes the value of the inhalation flow rate in non-CF and CF. * denotes statistical significance between non-CF inhalation flow rate of 85mL/s and CF inhalation flow rate of 55mL/s (p < 0.05). # denotes statistical significance between non-CF and CF at the same inhalation flow rate (p < 0.05)..... 146

Table 8.1. The demographical data from all the subjects selected for lung structure and function of CF patients compared to healthy non-CF subjects study. Age units is in years. Weight in kilograms (kg). Height in centimetre (cm). BMI is body mass index which is a ratio between weight and height. BMI = Weight/(height*height) 172

Table 8.2. The scanner and scanning protocol used for both non-CF and G551D CF patients. Two different scanners were used to scan each group of patients. The same coached breath-holds at TLC and RV in the supine position were used on both groups. The slice thickness is smaller in the CF data. However, the slice thickness in both data sets are below 0.8 mm which is the quantitative computed tomography threshold. Slice thickness and voxel dimensions are in millimetre (mm). Tube voltage is measured in kilovolts (Kvolt) 172

Table 8.3. Particle ventilation fraction for CF patients compared to healthy non-CF subjects. Ventilation fraction is the number of particles that entered a specific

lobe divide by the total number of particles that entered all the lobes. Two particle sizes were considered in the study 0.5 µm and 1 µm. UL denotes upper left lung lobe. LL denotes lower left lung lobe. UR denotes upper right lung lobe. MR denotes middle right lung lobe. LR denotes lower right lung lobe. * denotes statistical significance ($P < 0.05$). ± denotes standard error..... 194

Table 8.4. Particle deposition efficiency for CF patients compared to healthy non-CF subjects. Deposition efficiency is the number of particles that deposited in a specific lobe divided by the total number that entered that same lobe. Two particle sizes were considered in the study 0.5 µm and 1 µm. UL denotes upper left lung lobe. LL denotes lower left lung lobe. UR denotes upper right lung lobe. MR denotes middle right lung lobe. LR denotes lower right lung lobe. * denotes statistical significance ($P < 0.05$). ± denotes standard error..... 194

Table 8.5. The demographical data from all the subjects selected for the effect of disease severity study. Disease severity was determined by FEV1 value. 8 non-CF subjects, 6 mild G551D cystic fibrosis (CF) patients with FEV1 > 55%, and 3 severe G551D CF patients with FEV1 < 55%. Age units is in years. Weight in kilograms (kg). Height in centimetre (cm). BMI is body mass index which is a ratio between weight and height. $BMI = \text{Weight}/(\text{height}*\text{height})$ 199

List of symbols and abbreviations

$\beta_{\text{air}}^f(\mathbf{T}(\mathbf{x}))$	Air fraction
β_{air}	Fixed air fraction
$\beta_{\text{air}}(\mathbf{x})$	Air fraction
$\beta_{\text{tissue}}(\mathbf{x})$	The tissue fraction
λ	The eigenvalue
ρ	The fluid density
ρ_f	The density of the air
ρ_p	The particle density
1D	One dimensional
3D	Three dimensional
ABC	ATP-binding-cassette
ADI	Anisotropic deformation index
ADP	Adenosine diphosphate
ASL	Airway surface liquid
ATP	Adenosine triphosphate
ATPases	Hydrolyzing ATP
BCC	Burkholderia cepacia complex
BMD	Bone mineral density

BMI Body mass index

cAMP..... Cyclic adenosine monophosphate

C_c The Cunningham slip correction factor

CF.....Cystic fibrosis

CFD Computational fluid dynamics

CFRD..... Cystic fibrosis-related diabetes

CFTR.....Cystic fibrosis transmembrane conductance regulator

CL..... Centerline model

CLCT hybrid Centerline computed tomography

cmH₂O..... Pressure in centimetres of water units

CSA Cross-sectional area

CT..... Computed tomography

d The diameter of a particle

DBSCAN.....Density Based Spatial Clustering of Applications with Noise

delF508..... *CFTR* mutation

D_l Length scales

DNADeoxyribonucleic acid

EBUEndobronchial ultrasound

ENaC Epithelial sodium channel

ER.....Endoplasmic reticulum

ERAD.....Endoplasmic reticulum-associated degradation

fThe frictional coefficient

FCE.....Fiberoptic confocal endomicroscopy

f_{Di}The particle drag force per unit mass

FEF25-75%.....Forced (mid) expiratory flow rate

FEV1.....Forced expiratory volume in 1 second

FVC.....Forced vital capacity

G542X.....*CFTR* mutation

G551D.....*CFTR* mutation

g_iThe i -component of the gravitational acceleration

H&E.....Hematoxylin and Eosin

HU_{air}The Hounsfield unit for air

HU_{tissue}The Hounsfield unit for tissue

idirection

$I(\mathbf{T}(\mathbf{x}))$CT intensity value

$I(\mathbf{x})$The Hounsfield unit of the voxel

JJacobian

KCoefficient of minor loss

L..... Lower lobes

LCa..... The left caudal lobe

LCr..... The left cranial lobe

LL..... Lower left lobe

LMB..... The left mainstem bronchus

LR..... Lower right lobe

M..... Middle lobes

MCC..... Mucociliary clearance

MCT..... Mucociliary transport

MDCT..... Multi-detector row computed tomography

MR..... Middle right lobe

MRI..... Hyperpolarized magnetic resonance imaging

mRNA..... Messenger RNA

MRSA..... Methicillin resistant *S. aureus*

MUC5AC & MUC5B..... mucin glycoproteins

NBDs..... Nucleotide-binding domains

OCT..... Optical coherence tomography

P..... The pressure

PAS..... Periodic acid-Schiff

PEP Positive expiratory pressure

PE T pancreatic enzyme replacement therapy

PET Positron emission tomography

PFT Pulmonary function tests

PhD Doctorate of philosophy

PKA Protein kinase A

QCT Quantitative computed tomography

RAc The right accessory lobe

rAVV Adeno-associated virus

RCa The right caudal lobe

RCr The right cranial lobe

RD Regulatory domain

RDA Recommended dietary allowance

Re Reynolds number

RM Right middle lobe

RMB The right mainstem bronchus

RNA Ribonucleic acid

$r_{Q,b}$ The flow rate ratio between the branch to trachea

RTC Ribosome-translocon complex

RUL.....Airway right upper lobe airway

RUL..... Right upper lobe

RV Residual volume

SCNT..... Somatic cell nuclear transfer

SEM..... Standard error of the mean

SG.....Subglottis

SGS..... The subgrid-scale

SPECT..... Single photon emission CT

SSTVD The sum of square tissue volume difference

Stk..... The Stokes number

T..... Tracheal

TA..... Tracheal angle

TL Total lung

TLC Total lung capacity

TM..... Transmembrane

TMDs..... Transmembrane domains

TSI..... Tobramycin solution for inhalation

U Upper lobes

u_i Velocity

UK United Kingdom

U_l Local velocity

UL..... Upper left lobe

UPS..... Ubiquitin proteasome system

UR Upper right lobe

$V_{\text{air}}(\mathbf{x})$ Air volume

v_{fi} The fluid velocity

v_{pi} The i-component particle velocity

$V_{\text{tissue}}(\mathbf{x})$ Tissue volume

ν The kinematic viscosity

ν_T The subgrid-scale

“The greatest obstacle to discovery is not ignorance -- it is the illusion of knowledge. Never tell people how to do things. Tell them what to do and they will surprise you with their ingenuity. ”

General George S. Patton

Chapter 1. Motivation, significance and innovation

1.1. Introduction

Take a deep breath in and hold it for as long as possible. Right before you had to exhale did you feel the claustrophobic sensation of the tightening in the lungs? Did you feel the strong pain on your chest wall and diaphragm? Did you feel the strong spasms and involuntary contraction of your chest wall? This is how patients with a severe case of a disease called Cystic fibrosis (CF) feel every time they take a breath. “When I was young I imagined an object stuck in my chest.” “I would hold my chest and feel what was stuck inside..... I would imagine it as a brick” “Before I really understood the disease, I always thought one day the ... brick ... would just be removed and I’d be fine.” “I wake up in the morning and I feel my lungs... I don’t feel the rest of my body or give it much acknowledgment. I do feel my chest. I feel the air flow, or lack thereof” This is an actual description of the disease from a patient with cystic fibrosis (Thompson, 2014). Holly van Geffen, also a CF patient,

describes breathing as hard work and tiring and she never felt like she got much air (Collin, 2013).

Over the length of my PhD, I personally followed Holly's battle with cystic fibrosis (Figure 1.1.). Although there are numerous data and publications (I reviewed in next few chapters) that discuss the effect of CF genetic disorder on every organ in the body, I personally believe no amount of purely physical data can truly describe the severity of CF on its patients (Jackson, 1982). However, through purely physical data we can understand disease pathogenesis, prognosis and develop the correct treatment to improve Holly's and so many other CF patient's life. Therefore, I decided to first introduce the reader to CF as perceived by a CF patient then in the next few chapters I will discuss the purely physical data that examine the prognosis of CF and how I can use engineering and biomechanical techniques to understand the pathogenesis that may, in part, provide an improvement to the current treatment methods.



Figure 1.1. Picture of Holly van Geffen 22 year old cystic fibrosis patient. Adapted from (Collin, 2013).

1.2. Cystic fibrosis effects on physical and mental health

I would like to introduce the reader to Holly van Geffen's story. Holly was born in the UK with a healthy weight. Right after birth, Jayne and Nick van Geffen knew that their baby daughter Holly wasn't well. In the first few days of Holly's life, Holly was feeding constantly so much so her parents had to start supplemental feeds with formula milk. Also her parents noticed oil in Holly's Pampers, which is a sign of steatorrhea (occurs when the body cannot break down dietary fat by lipase or absorb it). Six weeks after birth, the standard heel prick test performed on every newborn revealed that Holly had cystic fibrosis (Collin, 2013). Cystic fibrosis (CF) is one of the most common life-threatening inherited diseases (Matsui et al., 1998; Stutts, 1999; Welsh M.J., 1996). Over two million people in the UK carry the faulty gene that causes cystic fibrosis and about one million in Australia- around 1 in 25 of the population. Roughly each week, in the UK, five babies are born with CF. In Australia, two babies are born with CF each week (JohnHopkins, 2014; Molinski et al., 2012)

As Holly grew, she got sicker. She spent as much time in the hospital as she did at her family home. Some days she was so weak, she couldn't even get out of bed and she had to be on oxygen. Breathing, which we take for granted, is a struggle for her. As soon as she wakes up, Holly starts her lung treatment, she starts with the nebulizer to open up her airways and then physiotherapy for twenty minutes. After the physiotherapy, Holly will cough a lot of mucus and she will feel a lot better. "The stuff I cough up, it's so thick and green you could hang it from the ceiling", "Sometime, I can't move it, it's just too sticky. It's like coughing up a toad. It tastes horrible. It's laden with bacteria and I'm something of a connoisseur when it comes to bacteria!" says Holly. Over her childhood, Holly had to develop a breathing

technique which helps move bacteria from the bottom of her lung for her to cough it out (Collin, 2013).

Holly needs 3000 calories a day to stay healthy. It's really hard for her to consume that much due to her loss of appetite and her body's inability to breakdown and absorb fat. Holly relies on liquid supper delivered through a feeding tube (a tubes that goes through her nose, down her throat and into her stomach). All this treatment and feeding routine affects Holly's sleep dramatically, increasing her exhaustion every day (Collin, 2013).

At 21 years of age, Holly is very sick. She suffers from a collapsed lung; her lung capacity is functioning at 30 per cent of what is normal. She needs to take 50 tablets every day to stay alive. This is considered to be the end-stage of the disease (Figure 1.2.).

CF did not only affect Holly physically it also affected her a great deal mentally. As a child Holly spent a lot of time in the hospital or at home. There was no holiday from CF. "As a teenager, I fought against it. It wanted to be spontaneous and go out with my mates all the time. I was so angry at the world. I was a battle with my mum to get me to see how important doing my treatment properly was" says Holly (Collin, 2013).



Figure 1.2. Picture of CF patient Holly van Geffen holding all the tablets she takes every day. Holly is at the end stage of the disease and she is on the double lung transplant list. Adapted from (UK, 2010).

In her adulthood, Holly wanted to leave home and go to University. She suffered from a collapsed lung a few months after she left. Holly said “It’s so frustrating when my mind’s full of things, but my body can’t keep up”. Holly had to postpone her university education. She added “I’m on antidepressants, I was so fed up never getting a break from it, taking one step forward and 10 steps back. I didn’t want to get out of bed. I wouldn’t talk to anyone about anything. One day, when my Mum and Dad were on holiday and I was home alone, I stepped on to the balcony and attempted to climb on to the roof. I was that low”. Holly had to accept so many issues because of CF including not being able to have children of her own.

Depression in CF is the part that does not receive enough awareness. Holly mentions “Everyone sees the physical, but the mental health gets neglected. There are all these things going around your head, this disease is a ticking time bomb and they don’t go away.” Holly is not afraid of dying, what really worries her is suffering from end-stage lung disease. “Sometimes, I wake up in the night coughing, and in those moments, waiting to catch my breath-it’s just terrifying. I do worry about dying, but the suffering at the end worries me more, being degraded and hopeless.” says Holly (Collin, 2013). Each week two young lives are lost to cystic fibrosis in the UK and in Australia one life is lost every ten days to cystic fibrosis (JohnHopkins, 2014; Molinski et al., 2012). Currently Holly is in the end stage of the disease; her only option of survival is a double lung transplant.

1.3. Thesis aim and research direction

The aim of this thesis is to understand the pathogenesis of cystic fibrosis lung disease from the early stages before infection and inflammation until adulthood. Through our understanding of the pure physical data of CF lung disease, we will be able to advance the knowledge that can help Holly and so many other CF patients live a healthier life. To achieve this aim I have to investigate the biomechanical structure

and function of the lung in healthy normal subjects and cystic fibrosis patients. This investigation would be done globally by studying the whole lung and locally by studying a specific lung segment. To accomplish these thesis aims I had to understand the different mutations of the cystic fibrosis gene. I also needed to understand the method in which synthesis and trafficking of the mutated CF gene can lead to the disease. In addition, I needed to understand the clinical manifestations, symptom severity, and complications of the CF disease.

In chapter two, I discussed the cystic fibrosis transmembrane conductance regulator (CFTR) channel structure and function. I also reviewed the different mutations of the *CFTR* gene and highlighted the most common one. In addition, I analysed how different mutations of the *CFTR* gene can cause disease. I also examined *CFTR* synthesis, trafficking, stability, function, and regulation of the ion channel.

In chapter three, I examined the complications caused by CF. I also discussed the organs that don't normally have CFTR channels that can be affected by the CF disease. In addition, I analysed the disease clinical manifestations, symptom severity, and complications.

In chapter four, I examined the different animal models that will enable us to study the early stages of lung disease in CF prior to infection and inflammation. I also discussed in depth why the mouse and ferret model was not ideal for our study. I examined several parameters that influence the choice of alternative species to model CF. First, are the types of cells found in the animal model airways in comparison to humans similar? Second, is the conservation of CFTR structure and function in comparison to human similar? Third, are the reproductive parameters of the species rapid enough to make it feasible to conduct these studies? In addition, I discussed in depth the reasons for choosing the porcine model for our study.

In chapter five, I introduced the reader to the respiratory system. I also discussed the structure and function of the lung in more details.

In chapter six, I investigated the effect of pig airway irregular shaped and reduced calibre found in newborn CF pigs prior to infection and inflammation on the biomechanical local and global lung function. I introduced the reader to computational fluid dynamics (CFD) and how I can use it to study the dynamic function of the lungs and airways. Then I discussed in depth our findings and its implications.

In chapter seven, I discussed the effect of postnatal lung and airway development in CF pigs on the biomechanical function of the lungs compared to healthy pigs. I examined three week old CF pig's lung structure and dynamic function. I used computation fluid dynamics to examine the dynamic function of the lung and the effect of airway structure abnormality on particle distribution and deposition pattern. I compared our findings to healthy three week old pigs and newborn healthy and CF pigs.

In chapter eight, unlike the previous two chapters where I have investigated the early stages of the cystic fibrosis disease in pig models, I investigated the disease pathogenesis in adult human patients. I introduced the reader to image registration and I used it to examine the global and local lung structure and function. In addition I discussed the similarity between lung abnormality investigated in animal model and disease pathogenesis in adult human. I also investigated the effect of disease severity on global and local lung functions.

In chapter nine, I discuss the outcome of this thesis. I examine in depth on the significance of our finding in each chapter and the relationship between all chapters. I also highlight the implication of each chapter and the thesis. In addition, I

investigate future direction for the research in this field. Finally, I provide the most current update about Holly's health condition.

1.4. Conclusion

Every CF patient has a very similar story to Holly's. Holly's story highlights the effect of recurring lung infection and inflammation on the life of every CF patient. In fact, 90% of patients with CF lose their life from loss of lung function (Boucher, Lands, Hay, & Hornby, 1997; Lands, Heigenhauser, & Jones, 1992; Marcotte, Grisdale, Levison, Coates, & Canny, 1986). The treatment cost over the life time of a CF patient is quite expensive. The mean life time cost of treatment is US\$638,000 (van Gool, Norman, Delatycki, Hall, & Massie, 2013). This does not include the cost of new CFTR mutation specific treatments such as Kalydeco costing US\$373,000 per patient per year or Orkambi costing US\$259,000 per patient per year (O'Sullivan, Orenstein, & Milla, 2013; Weisman, 2015). These channel based treatments are actually not suitable for patients at the end stage of the disease. For patients such as Holly at the end stage of the disease a double lung transplant can cost US\$797,000 per patient ((UNOS), 2014). This is also only considering the effect of CF on its patient and not considering the mental and physical effect and cost of CF on the patient's parents, partners, and families.

1.5. Statement of original contribution.

The following is a list of the original contribution made by the candidate towards the work presented in the thesis in the field of CF research.

Chapter 6: Early Airway Structural Changes in Cystic Fibrosis Pigs as a Determinant of Particle Distribution and Deposition.

- Used computed tomography x-ray images obtained from newborn pigs to construct a three dimensional airway tree.
- Used CFD to simulate airflow in the pig's airways.
- Analysed the airflow pattern and secondary flow properties in newborn non-CF and CF pigs.
- Used physiologically correct boundary conditions based on lobar volume change and airway cross-sectional area in the newborn non-CF and CF pig animal model.
- Used particle simulation based on the CFD analysis to examine the location where it's more likely for bacteria to accumulate in the newborn non-CF and CF pig model.
- Explored if current therapeutic aerosols will accumulate at the same density in the same location as the bacteria in the newborn non-CF and CF pig model.
- Used computational analysis to study the change in the dynamic function of in the newborn non-CF and CF pig model.

Chapter 7: CFD modelling of airflow and particle deposition in older cystic fibrosis pigs.

- Examined the effect of postnatal lung and airway development on the biomechanical function of the lung in the three week old non-CF and CF pig model.

- Used computed tomography x-ray images obtained from 3 week old CF pigs to construct a three dimensional airway tree.
- Examined the effect of CF on the development of pig's lung structure.
- Compared the lung structure and function between non-CF and CF pig at birth and 3 weeks after birth.
- Determined the change in lung function by examining the x-ray data and CFD analysis data in the three week old non-CF and CF pig model.
- Used physiologically correct boundary conditions based on lobar volume change and airway cross-sectional area. Also based on the estimated tidal volume of the non-CF and CF three week old pigs.
- Used particle simulation based on the CFD analysis to examine the location where it's more likely for a bacteria to accumulate in the three week old CF pigs airways
- Explored if current therapeutic aerosols will accumulate at the same density in the same location where bacteria deposited in the three week old non-CF and CF pig model.
- Used computational analysis to study the longitudinal change in the structure and dynamic function in non-CF and CF pigs.

Chapter 8: Analysing the global and local lung structure and function in adult human CF lungs.

- Investigated the lung's global and local structure and function in CF patients compared to normal.
- Examined the relationship between the commonly used pulmonary function test (PFT) and new techniques such as image registration and CFD.

- Using PFT, fixed CT volume analysis, image registration, and CFD to provide a new understanding of lung function and CF disease pathogenesis in humans.
- Investigated the effect of CF disease severity on the local and global lung function by using PFT, fixed CT volume analysis, image registration, and CFD.
- Used the same subjects to study the effect of CF in general on lung function and the effect of disease severity on lung function compared to normal healthy subjects. This gives us the ability to understand which group influences the analysis. Also it provides an example of the effect of using patients with different disease severity in a study.
- Provided an actual value for disease severity in each lobe in individual CF patients using CT density compared to healthy subjects.
- Accounting for multi-centre scanner calibration differences between CF subjects when measuring air trapping by normalizing the air in lung by the air value in the centre of the trachea for each individual subject. This is not novel in the lung research field but novel in CF research.
- Used particle simulation based on the CFD analysis and image registration to examine the location where it's more likely for bacteria to accumulate in healthy and CF human airways.
- Explored if current therapeutic aerosols will accumulate at the same density in the same location where bacteria deposited in healthy and CF human airways.

“Nothing tends so much to the advancement of knowledge as the application of a new instrument. The native intellectual powers of men in different times are not so much the causes of the different success of their labours, as the peculiar nature of the means and artificial resources in their possession.”

Sir Humphrey Davy

Chapter 2. Cystic fibrosis

2.1. Cystic fibrosis (CF) history.

The study of cystic fibrosis has attracted a great deal of research effort in the last 80 years (Andersen D.H., 1938; Dickinson et al., 2002; Grubb & Boucher, 1999; Knowles, Clarke, & Boucher, 1991; Quinton, 1989, 2008; Scholte, Davidson, Wilke, & De Jonge, 2004; Smith, Kohart, Newmyer, & Cline, 2009; Steagall, Elmer, Brady, & Kelley, 2000; Welsh M.J., 1996; J.J. Wine, 1999). The earliest comprehensive description of CF was by Dr. Dorothy Andersen in 1938 (Figure 2.1) (Andersen D.H., 1938).

Dr. Paul Quinton first described that CF sweat gland ducts are relatively impermeable to Cl^- (Figure 2.2) (Quinton, 1989). This discovery was followed by evidence showing defective Cl^- transport in CF airway epithelia (Knowles et al.,

1991). It was later shown that the defect in CF epithelia was present at the apical membrane of the epithelia cells (Widdicombe, 1986). These findings helped to explain the reason for increased Cl^- concentration in CF sweat ducts and in unifying the hypothesis about CF disease: CF causes abnormal epithelial Cl^- transport. The unified hypothesis was important as it provided a description of the physiological and biochemical defect in airway epithelia (Welsh & Ramsey, 1998).

In 1989, Drs. Lap-Chee Tsui, John Riordan, Francis Collins, and their collaborators reported the discovery of the gene that is mutated in CF (Riordan et al., 1989). The gene was named *Cystic Fibrosis Transmembrane Conductance Regulator (CFTR)*. This discovery provided the opportunity to correct the defective CFTR Cl^- channel on cultured cells that provided a formal proof that CFTR is responsible for CF disease (Dickinson et al., 2002; Grubb & Boucher, 1999; Quinton, 2008; Scholte et al., 2004; Steagall et al., 2000; Welsh & Ramsey, 1998; J.J. Wine, 1999).

Finding that CFTR caused a defect in an epithelial Cl^- channel regulated by phosphorylation provided a description of the function of the gene and helped propel the understanding of CFTR structure, synthesis, trafficking, and mutation.

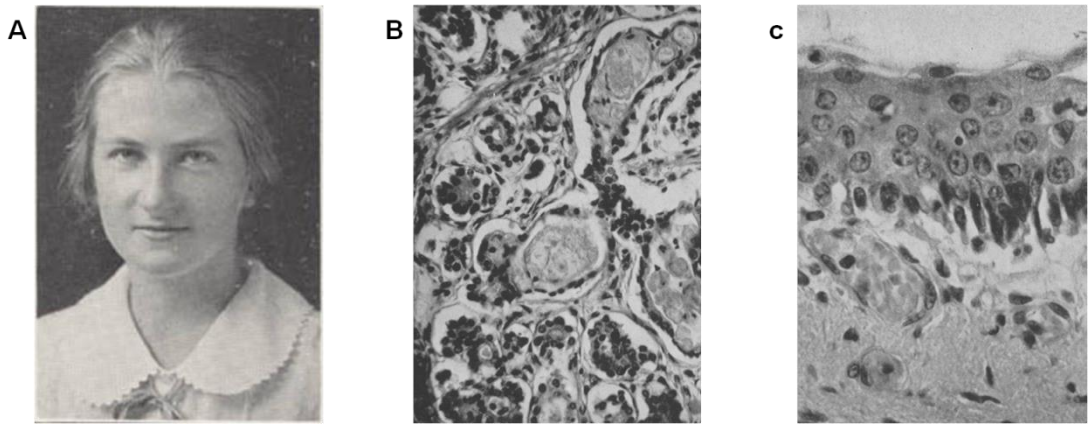


Figure 2.1. Dorothy Andersen early description of the CF disease. (A) a photograph of Dorothy Andersen M.D. Adapted from (Vertex, 2013). (B) Histological image of the pancreas of the patient Dr. Dorothy treated. The pancreas responded to treatment however this patient later pasted away due to bronchiectasis. This is the earliest description of cystic fibrosis as a lung and pancreas disease. (C) Metaplasia found in the trachea of the same patient Dr. Dorothy examined. Once again this is evidence that CF is not part of celiac disease. Adapted from (Andersen D.H., 1938).

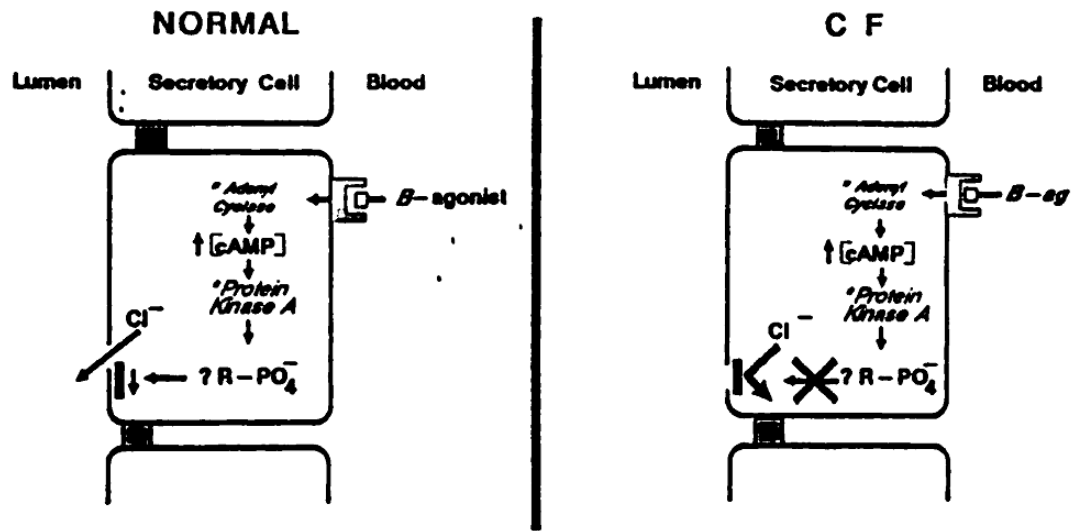


Figure 2.2. First described that CF sweat gland ducts are relatively impermeable to Cl^- by Paul Quinton. The figure shows a simplified model of normal (non-CF) and CF sweat duct. It emphasizes the basic abnormalities lead to reduced Cl^- permeability. The schematic above shows the biochemical events (starting by the activation of the acinar cells by agonists, which leads to biochemical process causing the activation of protein kinase A and opening of the Cl^- channel) in both non-CF and CF cells. Paul Quinton reports that all components appear to be intact including the receptor and Cl^- channels in both non-CF and CF. However, at some point distal to the activation of protein kinase A the biochemical processes stop causing the abnormalities in Cl^- channel function. Adapted from (Quinton, 1989).

2.2. CFTR structure.

CFTR is a glycoprotein and is a member of the superfamily of ATP-binding-cassette (ABC) transporter proteins. It is located at the apical membrane of epithelia cells and the only known member of ABC to function as an ion channel (Gadsby, Vergani, & Csanady, 2006; Ramjeesingh, Kidd, Huan, Wang, & Bear, 2003). All of the members of the ABC protein superfamily contain two cytoplasmic nucleotide-binding domains (NBDs). ABC transporters also contain two transmembrane domains (TMDs) which connect to the NBDs. CFTR, unlike other ABC transporter proteins, also contains a regulatory domain (RD). The RD splits the protein into semi-symmetrical halves with one NBD and TMD on each half (Figure 2.3) (Hwang & Kirk, 2013; Riordan, 2008).

ABC transporters have the ability to move substances against their concentration gradient by hydrolyzing ATP (ATPases). CFTR, unlike most of the other ABC transporters, only hydrolyzes ATP at one site and allows passive diffusion of chloride and bicarbonate ions (Figure 2.4) (Riordan, 2008). CFTR essentially allows the flow of chloride and bicarbonate ions due to their concentration gradient. However it is considered to be an active channel since it requires ATP to open and close the channel (Riordan, 2008).

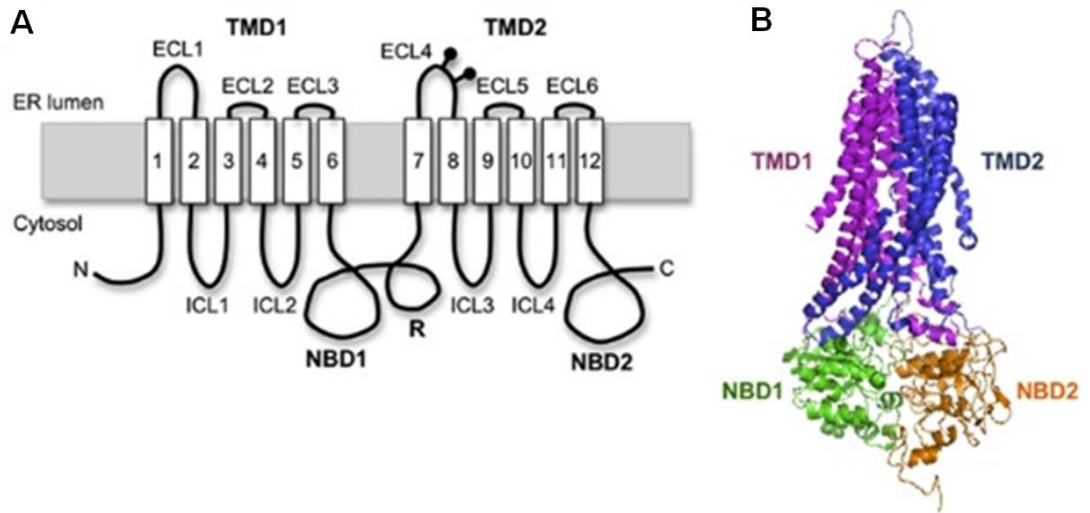


Figure 2.3. The basic structure of the CFTR channel. (A) Schematic diagram of the CFTR channel structure. CFTR similar to all ATP-binding-cassette (ABC) transporter proteins have two cytoplasmic nucleotide-binding domains (NBDs) and two transmembrane domains (TMDs) which connect to the NBDs. However, unlike other ABC transporter proteins, CFTR also contains a regulatory domain (RD). The RD splits the protein into semi-symmetrical halves with one NBD and TMD on each half. The gray box indicates the probable location of the membrane lipid bilayer (cell wall). The numbers (1 to 12) represents the components and subunits of the channel TMDs. The lines between TMDs subunits represent strands in both above (ER lumen) and below (cytosol) the membrane of the cell. N is the cytoplasmic amino and C is the carboxyl termini (Hwang & Kirk, 2013). (B) The protein backbone of an ABC channel. Ribbons represent a homodimeric protein meaning protein with similar subunits. TMDs 1 and 2 are represented in purple and blue colours and NBDs 1 and 2 represented in green and gold colours. The TMD numbers 1 to 12 in figure 1.3. (A) are each represented by a helical structure in this image. R-domain is not included in this figure. Adapted from (S. J. Kim, 2012).

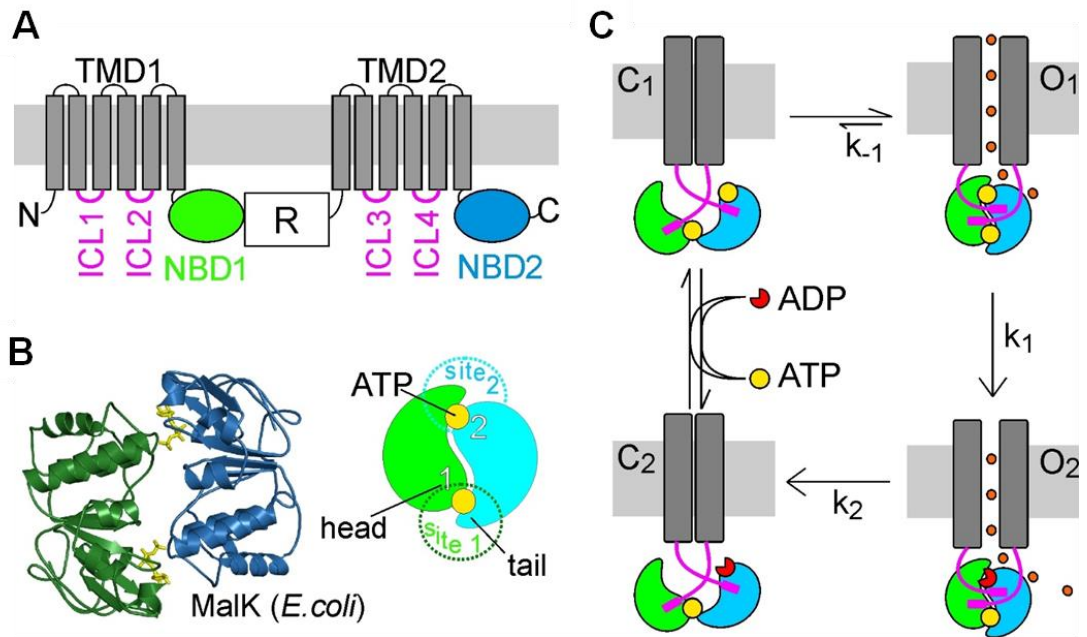


Figure 2.4. Schematic showing the gating regulated process of CFTR channel by forming NBD dimer. (A) Schematic of the CFTR channel. The schematic shows the structure of CFTR with TMD 1 and 2 represented by gray vertical boxes. NBD1 is represented by a green oval and NBD2 represented by a blue oval. R domain represented by a white box with R on it. There are two ATP-binding sites on the CFTR NBDs. N is the cytoplasmic amino and C is the carboxyl termini. (B) Schematic showing only NBD 1 and 2. Panel on the left is the back bone of NBD 1 and 2 proteins. Ribbons represent a homodimeric protein meaning protein with similar subunits. Green is NBD1 and Blue is NBD2. Yellow is the ATP molecules at the interface between NBD 1 and 2. Panel on the left is a drawn schematic of the right panel. (C) Schematic showing the process in which NBD forms a dimer to open the CFTR channel. CFTR can only hydrolyze ATP at one site which is NBD2. When ATP bound to NBD2 is hydrolyzed, the channel closes into a partial dimer. This prevents ATP from dissociating from NBD1 and allows the flow of ATP to NBD2. C1 shows CFTR channel closed with ATP unhydrolyzed and site 2 between NBD 1 and 2 open. O1 shows CFTR channel with site 2 connected and channel open. O2 shows the NBD2 hydrolyzing ATP at NBD2 site 2. C2 show shows the final process of site 2 between NBD 1 and 2 open allowing ADP (the output product of hydrolyzing ATP) to be removed a replaced by ATP to allow the channel to open again. Adapted from (Csanady, 2013).

Second, CFTR gating is regulated by phosphorylation of the R domain by protein kinase A (PKA). CFTR has six phosphorylation sites; CFTR channel gating control with phosphorylation is considered to be the best understood channel regulation mechanism (Hwang & Kirk, 2013). The theory is that the phosphorylation of CFTR by PKA at the R domain, which stimulates binding of ATP to NBD2 resulting in reduced affinity for NBD1. This in turn allows the formation of the NBD dimer and the opening of the CFTR channel. The phosphorylation of CFTR is induced by increased cyclic AMP in the cell, which leads to activation of the CFTR channel and therefore phosphorylation (Figure 2.5) (Baker et al., 2007). On the other hand, in the absence of cyclic AMP at the CFTR channel, the R domain will remain unphosphorylated which inhibits the opening of the channel and the channel will remain closed (Gadsby et al., 2006).

There are other proposed theories to explain the mechanisms of CFTR channel gating. For example, it is proposed that the phosphorylated R domain can interact directly with the CFTR channel cytosolic loop. The R domain then affects the conformational change within the cytosolic loop and opening the CFTR channel without NBD dimerization (Figure 2.6). To summarize the CFTR channel gating is very complex and its regulation can be controlled in multiple ways (Hwang & Kirk, 2013; Kanelis, Hudson, Thibodeau, Thomas, & Forman-Kay, 2010). However to produce a functioning CFTR channel, CFTR must be synthesized, folded, and transported to the apical membrane correctly.

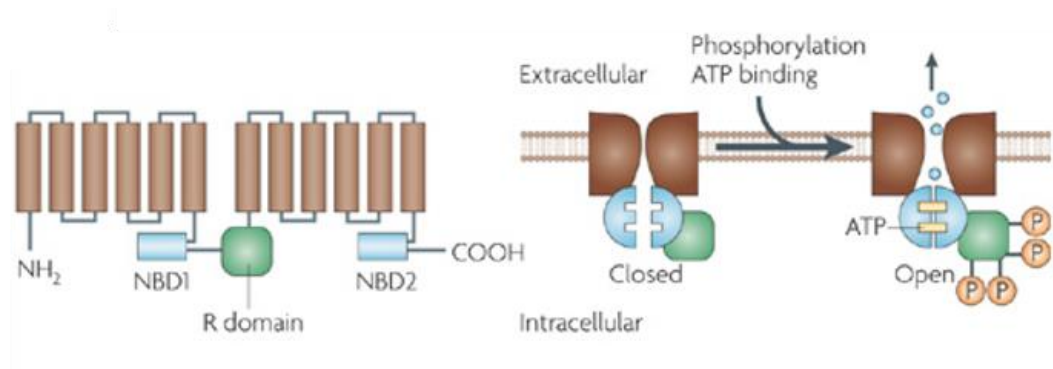


Figure 2.5. Schematic showing the gating regulation process of CFTR channel by phosphorylation of the R domain. Left panel shows the structure of the CFTR channel. The TMDs represented by vertical aligned brown boxes. NBDs represented by horizontally aligned blue boxes. R-domain by a square green box. Right panel, shows two CFTR channels one before phosphorylation of the R domain and the other after the phosphorylation of the R domain. The two large brown box like structure is the TMDs. The blue circular like structure attached the TMDs are the NBDs 1 and 2. The green box attached to one of the NBDs is the R domain. The figure shows the TMDs remain closed until R domain (cyclic AMP) is phosphorylated and ATP is binded to NBDs site one and two.

Adapted from (Verkman & Galietta, 2009).

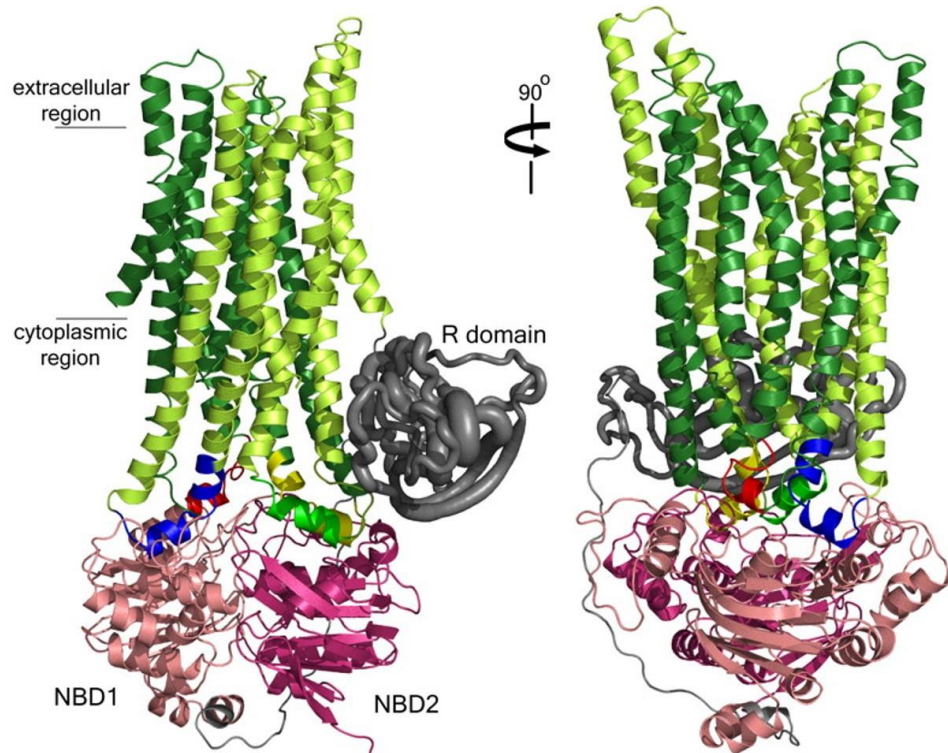


Figure 2.6. The protein backbone of the CFTR channel. Dark green helices are TMD1. Lime helices are TMD2. Pink helices and lines are NBD1. Purple helices and lines are NBD2. Gray tubes and lines are R-domain. This figure shows how the R domain is directly connected to NBD1 and TMD2 in the cytoplasmic region. It is proposed that the phosphorylated R domain can interact directly with the CFTR channel TMD2 cytoplasmic region. The R domain then affects the conformational change within the TMD2 cytoplasmic region and opening the CFTR channel without NBD dimerization. Adapted from (Serohijos et al., 2008).

2.3. CFTR synthesis and trafficking.

CFTR is a complex protein made up of 1480 amino acids (compared to 510 to 920 amino acids in the ENaC channel) (Gadsby et al., 2006; Rogan, Stoltz, & Hornick, 2011; Snyder, McDonald, Stokes, & Welsh, 1994). To ensure the CFTR protein functions properly the cell has set up a stringent quality control that monitors protein synthesis, folding and later CFTR channel function in general throughout its life.

This scrutinized quality control system makes it harder for CFTR protein to pass the quality test (Gelman & Kopito, 2003; T. J. Jensen et al., 1995; Riordan, 2008; Sato, Ward, & Kopito, 1998; Ward, Omura, & Kopito, 1995). For example, 100% of other ABC transporters such as P-glycoprotein and MRP1 leave the ER. However, only 33% of CFTR folds correctly in wild-type and is allowed to leave the ER (Loo et al., 1998).

Creating a fully functioning CFTR channel requires the involvement of many proteins found in the pathway from the nucleus to the plasma membrane. The first step starts in the nucleus where the *CFTR* gene found on the long arm of chromosome 7 is transcribed into mRNA (Figure 2.7). mRNA is then translated in the ribosome attached to the ER (Rogan et al., 2011). During translation the polypeptide is pushed into the ribosome-translocon complex (RTC). The nascent polypeptide chain being translated provides information to the RTC on how to fold, orient and integrate the transmembrane (TM) section of the CFTR to the ER. Therefore the translation and folding of the CFTR happens simultaneously.

Several quality control systems are involved during folding of the CFTR cytosolic part and ER membrane part (Cheung & Deber, 2008; Pind, Riordan, & Williams, 1994; Riordan, 2008).

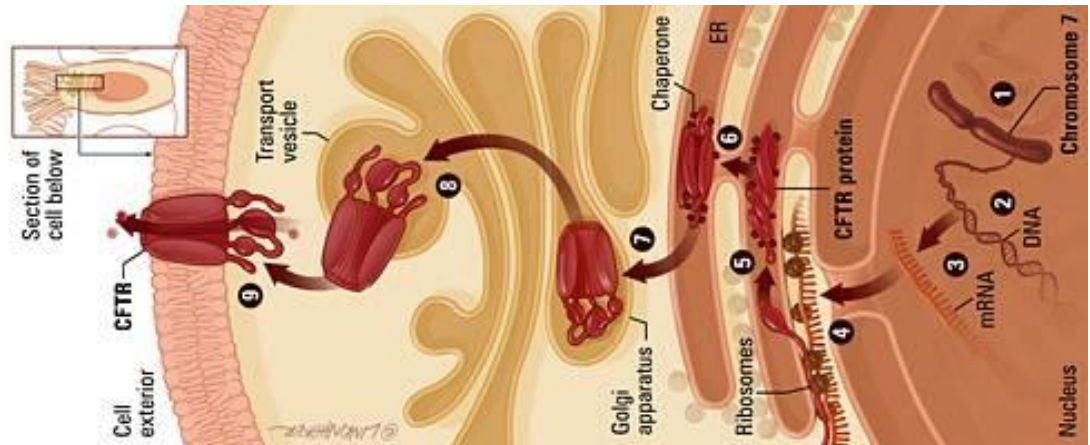


Figure 2.8. The process of producing CFTR channel from the nucleus to the cell membrane. (1) Chromosome 7 containing the *CFTR* gene in the nucleus. (2) The *CFTR* gene is made up of 250,000 DNA nucleotides containing all the information required to produce a functional CFTR channel. (3) Inside the cell's nucleus the gene is transcribed into a messenger RNA (mRNA). (4) mRNA then leaves the nucleus and is transported to the endoplasmic reticulum (ER). (5) In the ribosomes the mRNA is translated into protein. (6) The protein is then folded in the ER by other proteins called chaperone. (7) The CFTR proteins then move to Golgi apparatus where it undergoes final processing and packaging. (8) The completed CFTR channel leaves the Golgi apparatus and heads towards the cell surface. (9) CFTR channel reaches the cell membrane and starts its function as a chloride transporter. Adapted from (JohnHopkins, 2014).

2.4. CFTR mutations.

Cystic fibrosis (CF) disease phenotype can be caused by over 1500 different mutations in the *CFTR* gene (Spicuzza et al., 2012). Most of the CF disease causing mutations can be sorted into one of six categories based on the mechanism in which the mutation alters CFTR function leading to the manifestation of the CF disease.

Mechanism 1, premature termination, frame shifts or non-sense mutation. This can be caused by premature truncation during the translation period of CFTR resulting in a protein production defect. This mutation is found in approximately 10% of CF patients.

Mechanism 2, the mutation causes defective protein processing. Although the protein might still be able to function if it reaches the cell membrane surface, defects in the protein structure hinder its ability to pass through the intracellular trafficking process. This is in-part due to the deletion or absence of phenylalanine (located at nucleotide binding domain 1). This mutation is found in approximately 85% of CF patients.

Mechanism 3, a mutation disrupts the regulation of channel opening. This means that the protein exhibits normal synthesis, trafficking, and processing. However, CFTR will still exhibit abnormal gating of the ion-channel or altered conductance of ion transport. This is in-part due to replacement of specific amino acids by aspartate residues. This mutation is found in approximately 3% of CF patients.

Mechanism 4, mutations produce channels with defective ion conductance. This results in a production of a protein with a reduced channel function.

Mechanism 5, fully functioning CFTR channels are produced. However they are produced at a low percentage due to reduced synthesis.

Mechanism 6, fully functioning CFTR channels are produced. However it is less stable in the cell membrane, leading to reduction in CFTR channel percentage. This is in-part due to increased endocytosis and degradation of CFTR in the lysosomes. The mutations of mechanism 5 and 6 are

found in less than 0.1% of CF patients (Figure 2.9) (Gibson, Burns, & Ramsey, 2003; Rowntree & Harris, 2003; Turnbull et al., 2007).

Having a clear understanding of the effect of each CF mutation and how it causes disease is significantly important for treatment. The most common mutation in *CFTR* is caused by the deletion of three base pairs, which results in loss of a phenylalanine residue at amino acid position 508 (Figure 2.10). This mutation is called delta phe508 ($\Delta F508$), and accounts for 70% of the *CFTR* mutations in North America (S. H. Cheng et al., 1990; Denning et al., 1992; Du, Sharma, & Lukacs, 2005; Lukacs & Verkman, 2012).

The second most common CF mutation is G542X. G542X mutation is considered a nonsense mutation, since no protein is produced in this mutation due to the presence of a premature stop codon instead of glycine residue at a position of 542 in the *CFTR* amino acid. The stop codon triggers the ribosome to stop the translation prematurely before any protein is produced. Therefore G542X is considered to be a class I mutation and it is found in roughly 10% of CF patients (Bedwell et al., 1997; Castaldo et al., 1997).

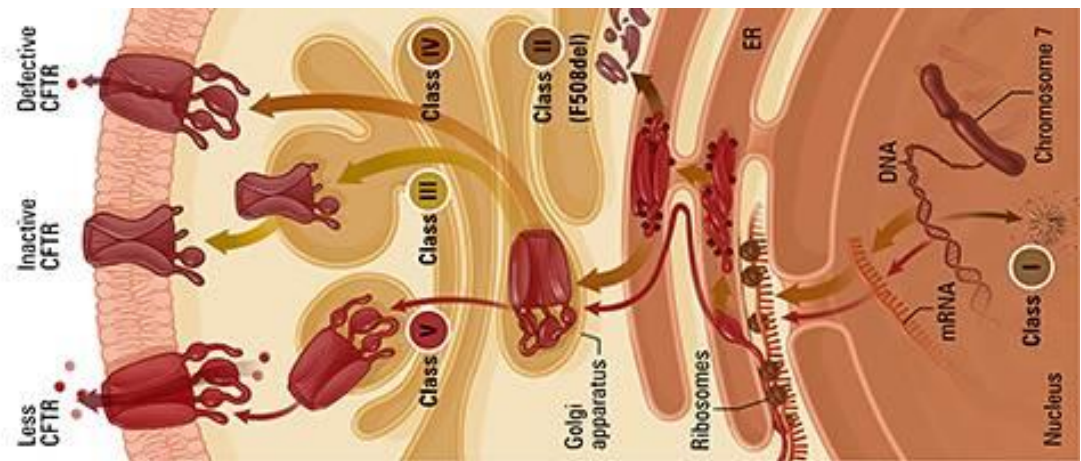


Figure 2.9. Mechanism in which the mutation of the *CFTR* gene can lead to defective or inactive CFTR channel. Class I mechanism, *CFTR* gene in chromosome 7 produces a nonsense mRNA during transcription of the gene. Therefore Class I patients do not have a functioning *CFTR* protein or channels, e.g. G542X. Class II mechanism, *CFTR* gene is missing some essential amino-acids. Therefore when the channel is produced it gets labelled by the cell defence mechanism as defective and then destroyed, Some of these channel do reach the cell surface, however they fail to function, e.g. F508del. Class III mechanism, *CFTR* channel is not folded and packaged correctly in the endoplasmic reticulum and the Golgi apparatus. Therefore, although the channel reaches the cell surface it is unable to properly function, e.g. G551D. Class IV mechanism, *CFTR* channel reaches the cell surface but its function is poor, e.g. R117H. Class V mechanism, although *CFTR* is produced correctly and function normally, there is a decreased production of the *CFTR* channel, e.g. A455E. adapted from (JohnHopkins, 2014).

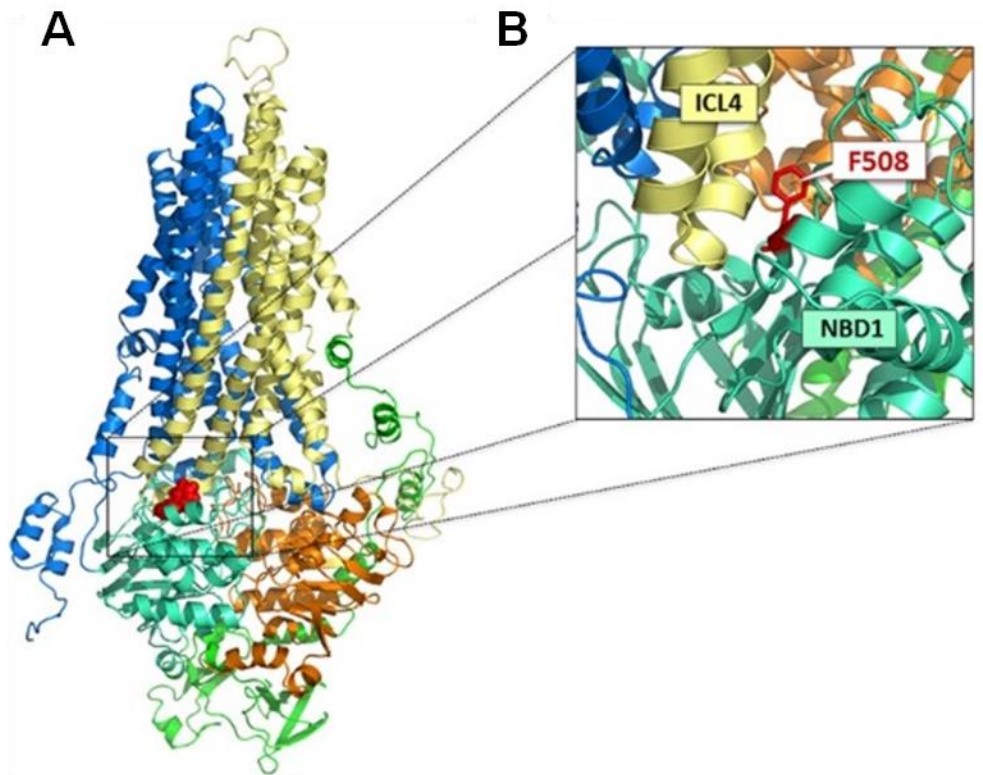


Figure 2.10. The location of F508del in the backbone structure of the CFTR channel.

(A) Blue helices are TMD1. Sand yellow helices are TMD2. Cyan helices and lines are NBD1. Orange helices are NBD2. Dark green ribbons and helices are R-domain. Red is the location of amino acid F508. The most common disease inducing mutation in *CFTR* is caused by the deletion of three base pairs, which results in loss of a phenylalanine residue at amino acid position 508. The $\Delta F508$ mutation causes folding defects in NBD1 which in turn affects the coupled domain folding. (B) The impairment in the coupled domain folding affects the assembly of NBD1 and the TMDs. This leads to incorrectly folded NBD2 which trigger the channel to be destroyed by the cell defence mechanism. Even if the channel passes the cell defence mechanism it will not be able to function since the ATP binding site on NBD2 is not functioning due to incorrect folding. Adapted from (Molinski et al., 2012).

The third most common CF mutation is G551D. In this mutation the glycine residue at position 551 is replaced by an aspartate residue which is a negative charged amino-acid. This change in the amino acid has a significant effect on CFTR channel efficiency specifically at ATP-binding site 2. Unlike the previous mutations discussed, G551D exhibits normal synthesis, trafficking, processing, and membrane stability. Although G551D R domain can be phosphorylated normally, the channel activation time by cAMP is greatly reduced with increased closing time (Bompadre, Sohma, Li, & Hwang, 2007; Xu et al., 2014). Therefore, G551D is classified as class III mutation.

Although it is hypothesized that lung disease severity is most related to the specific CFTR mutation (Turnbull et al., 2007), recent research suggests that CFTR mutations are not solely responsible for disease severity. Other factors such as modifier genes and environmental factors are suggested to have a significant impact on disease severity in the pulmonary and gastrointestinal system (such as liver hepato-biliary) (Bartlett et al., 2009; Collaco & Cutting, 2008; Cutting, 2010; Merlo & Boyle, 2003). However, data in the literature on whether CFTR mutations have an effect on disease severity are divergent. A study examining G551D mutation has shown no differences in age of diagnosis, sweat chloride concentration, nutritional status, lung function and exocrine pancreatic function compared to F508 del mutation (Hamosh et al., 1992). Another study used US CF registry data concluded that there were statistically significant differences in sweat chloride concentration, height, and weight (McKone, Emerson, Edwards, & Aitken, 2003). Furthermore, other studies have concluded that individuals with the G551D mutation have a statistically higher forced expiratory volume in 1 second (FEV1), lower yearly rate of decline of FEV1, higher body mass index (BMI), lower pancreatic insufficiency (not easily affected or modified by environmental factors) (Cutting, 2005) and less

inhaled antibiotic use when compared to F508del (Comer et al., 2009). Accurate genotype-phenotype studies of these mutations are challenging due to small sample size of the disease itself; there are only 70,000 people known to have CF and their age can vary from 1 day to 70 years old or older. Small sample size is observed in most of these CF publications (Hamosh et al., 1992; Parad, 1996).

To conclude, trying to find correlation between the mutation and the severity of lung disease phenotype is important but other factors in addition to *CFTR* mutation alone can affect the patient outcome. Different phenotype in the same genotype can be observed in siblings and identical twins with CF (Mickle & Cutting, 2000).

*“Our greatest weakness lies
in giving up. The most
certain way to succeed is
always to try just one more
time”*

Thomas A. Edison

Chapter 3. Cystic fibrosis disease clinical manifestations and complications

3.1. Primary complications.

The clinical manifestations, symptom severity, and complications of CF disease may vary depending on the *CFTR* mutations, modifier genes and environmental factors. Here I discuss the clinical manifestations in patients with classical CF disease. The primary and secondary CF disease manifestations in the whole body can have a major effect on the current and the longitudinal local and global lung structure and function. In this chapter, I discuss in depth the disease manifestation and treatment in the respiratory system and other major organs that can have a secondary effect on the respiratory system function and structural development.

3.1.1. Respiratory symptoms.

Cystic Fibrosis causes multiple health complications. The primary effect of CF is within the airways and submucosal glands (Gibson et al., 2003). *CFTR* is expressed throughout the lungs where it helps to maintain the proper chloride and bicarbonate

levels. A common observation in CF patient's airways, small intestine, pancreas, gallbladder and female reproductive system is thick viscous mucus (Figure 3.1) Unravelling the physiological process which leads to thicker mucus has been the pursuit of many scientists in the last two decades.

The aim of this thesis is to understand the global and local lung function in CF patients. Thicker viscous mucus can have a significant effect on the lung function and infection rate. Therefore a full understanding of physiological process that leads to thicker viscous mucus is crucial.

There are multiple pathophysiology concepts that explain the rationale behind the viscous mucus in CF. A classic concept is the low volume hypothesis which postulates that CFTR causes loss in the inhibition of the sodium channel ENaC. This leads to sodium hyper-absorption which dehydrates the airway surface liquid (ASL) which in turn increases mucus viscosity. This hypothesis has been challenged by recent findings in the CF pig model where no signs of sodium hyper-absorption or decrease in ASL height were present. Moreover the ENaC hypothesis was based on a culture model where mucus cannot escape, and submucosal glands which are estimated to produce 95% of the mucus are absent (J. J. Wine & Joo, 2004). The outcome of the CF pig model has shown that in the absence of increased ENaC channel activity, the gastro-intestinal tract can still be obstructed with viscous mucus (J. H. Chen et al., 2010).

Another hypothesis is that bicarbonate is essential for the expansion of mucins. It was demonstrated ex-vivo that absence of bicarbonate leads to the formation of viscous mucus. Therefore, it was reasonable to speculate that the absence of bicarbonate leads, in part, to impaired mucociliary transport (MCT) and therefore CF related disease (Garcia, Yang, & Quinton, 2009; Quinton, 2008, 2010). However, in

an ex-vivo study, when a trachea was bathed in bicarbonate free saline or a saline containing bumetanide which inhibits chloride from entering the cell from the basolateral side (Trout, King, Feng, Inglis, & Ballard, 1998), it was demonstrated that neither the absence of bicarbonate or chloride alone can cause mucus build up. However, when the chloride and bicarbonate channels were both inhibited on a non-CF trachea, mucus strands were observed to develop similar to those found in CF (Hoegger, Fischer, et al., 2014).

Another hypothesis states that abnormalities in CFTR channel regulation lead to increased intracellular chloride concentration and a decrease in the extracellular level. The chloride imbalance causes water hyper-absorption by the epithelia cell leading to dehydration of the mucus layer and thicker viscous mucus (Reeves, Molloy, Pohl, & McElvaney, 2012). However, in a recent ex-vivo study, a newborn CF pig trachea was flooded with saline in a volume bigger than a thousand times the ASL, and it was observed that CF mucus defect was still present (Hoegger, Fischer, et al., 2014).

A recent findings demonstrated that, in mutant CFTR, the chloride and bicarbonate levels are not able to be regulated properly. This can alter airway surface pH and mucus properties (Hoegger, Fischer, et al., 2014; Pezzulo et al., 2012). The altered surface pH impairs the destruction of bacteria and the altered mucus fail to detach from the submucosal gland. Either of these factors in isolation or combination can impair lung function capabilities. Mucus that remains tethered to the gland duct impairs MCT. Other mucus strands can become attached to the tethered strand forming a thicker mucus layer around the strand where inhaled particles and bacteria can deposit (Hoegger, Fischer, et al., 2014). Since bacterial destruction is impaired in CF (Pezzulo et al., 2012), bacteria can grow rapidly on the static mucus tethered

strand causing an unstoppable cycle of inflammation and infection. Regardless of what causes this viscous mucus, it eventually builds up in the CF patients' airways and causes significant morbidity and ultimately mortality in CF patients.

As mentioned before, the thick mucus lining the CF airways provides a perfect home for various bacterial infections. Shortly after birth, signs of lung disease such as wheezing, coughing, and difficulty breathing can be seen in infants. Infants and young children with CF are most likely to be infected with *Staphylococcus aureus* (Jain & Smyth, 2012). There are different strains of *S. aureus*. The strain that causes most morbidity and mortality in CF patients is methicillin resistant *S. aureus* (MRSA). Up until the 1960s, lung infections were treated by penicillin. However, during the 1960 almost 80 percent of *S. aureus* became resistant to it. Moreover, in 1959, 2 years after the introduction of methicillin, *S. aureus* strains resistant to methicillin started to be observed in the hospitals. MRSA has gained a lot of attention due to its ability to establish itself in CF airways and its resistance to many antimicrobial therapies.



Figure 3.1. Thick viscous mucus observed in CF patient's airways. The airway observed in this figure was obtained from a lung transplant performed on a 15 year old patient. Two types of mucus plugging can be observed in this image. Semi-liquid ivory mucus and translucent elastic mucus (shown in the figure to stretch from the bronchus). Adapted from (J. J. Wine, 2010).

Almost 25 percent of CF patients are infected with MRSA (Goss & Muhlebach, 2011). Patients infected with MRSA as a primary pathogen have lower lung function, higher hospitalization rates, and higher use of antibiotics to control but not stop MRSA infection (Ren et al., 2007). Some studies have investigated methods of eradication of MRSA and in rare cases it works with systematic antibiotic therapy (Goss & Muhlebach, 2011). Within many children an infection with *Haemophilus influenzae* is common. *Haemophilus influenzae* is non-typeable meaning that the regular childhood immunization cannot prevent this infection (Goss & Muhlebach, 2011).

In teens and adults, coughing becomes a daily occurrence, usually accompanied by sputum. During later stages of the disease, it is not uncommon to find blood-streaked sputum (Gibson et al., 2003). As CF patients age into their late twenties or early thirties, other microorganisms start infecting the lung, the most common being *Pseudomonas aeruginosa*. *P. aeruginosa* which infects approximately 80 percent of adult CF patients. It is hypothesized that the infection comes from the environment since there are usually different strains of these bacteria infecting the lungs. A chronic *P. aeruginosa* infection takes a while to develop. When a chronic infection is developed the *P. aeruginosa* bacteria would have already caused major damage to lung tissue by all the previous recurrent, intermittent colonization.

Another resilient pathogen has also made its way into the CF community within recent years. This devastating bacterium is the Burkholderia cepacia complex (BCC). It can be found in multiple environments, including agricultural crops and aqueous solutions such as detergent solutions and intravenous fluids commonly found in hospitals. BCC was not a prominent pathogen within CF until recently, because patients had a shorter life expectancy. Now that patients with CF are living longer,

BCC has been able to take hold and can be found in about ten percent of adult CF patients. A pulmonary infection of BCC can persist for months or even years. BCC can lead to severe disease or death within as little as six months. However, every individual reacts to BCC differently, with some patients not even experiencing a decline in clinical status after infection (Gautam, Singhal, & Ray, 2011).

Managing CF patients infected with BCC is problematic as BCC is resistant to most antimicrobials and no new antibiotics have been produced that can kill this pathogen. BCC might be susceptible to some antimicrobials, but once it encounters a new antibiotic, it quickly develops a resistance. This leaves doctors with the problem of trying to treat a patient with a pathogen that is resistant to all known antimicrobials. There have been some reports of successful treatment of BCC in CF patients, but these reports are rare. The fact that CF individuals can become infected with BCC from the environment or from other fellow patients has led to great anxiety amongst the CF community. Infection control procedures were soon put in place to help prevent the spread of BCC. CF summer camps were shut down and patients with BCC were segregated from all other CF individuals. BCC infected individuals are no longer allowed to go to any CF gatherings such as fundraisers, and CF patients in general are told to keep their distance from each other in order to help prevent any unintentional spreading of BCC (Gautam et al., 2011).

3.1.2. Pancreatic insufficiency.

The thick mucus in the digestive tract can block pancreatic secretion of digestive enzymes that aid in the digestion and absorption of food (Figure 3.2). At birth, approximately 70% of CF patients suffer from exocrine pancreatic insufficiency. An additional 20% of CF patients will develop pancreatic insufficiency later in childhood (Couper et al., 1992). Exocrine pancreatic insufficiency is characterized by

insufficient production of digestive enzymes, leading to malabsorption of nutrients. The reduced lipase secretion combined with a decreased intestinal pH, leads to malabsorption of fat and fat soluble vitamins (Rowe et al., 2014). Therefore, in the absence of newborn CF screening, signs of CF can be detected by a patient's failure to thrive and the presence of steatorrhoea. The main treatment of pancreatic insufficiency involves supplementation with pancreatic enzymes and fat soluble vitamins and a high caloric diet. Pancreatic insufficient CF patients are more likely to develop episodes of acute and chronic pancreatitis (Augarten et al., 2008).

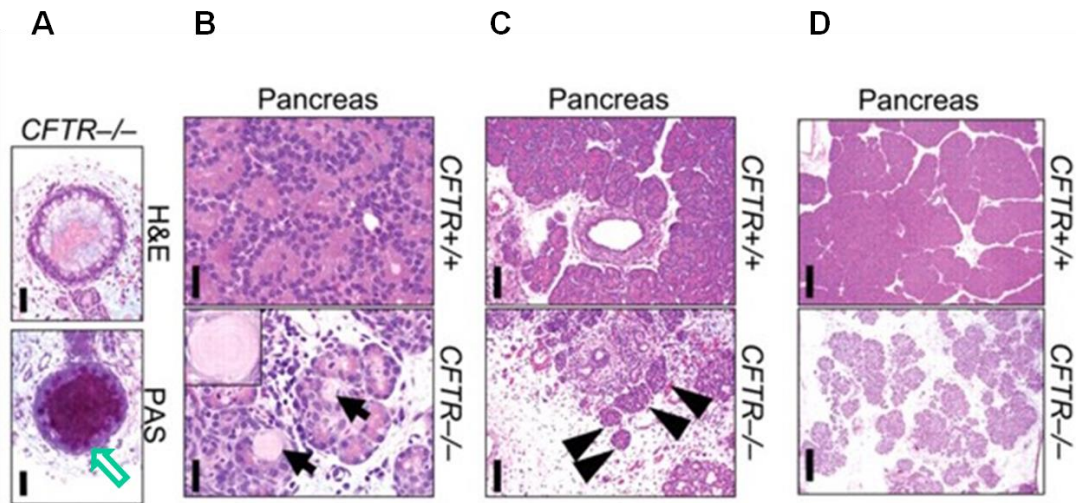


Figure 3.2. Histological view of the effect of CFTR on pancreas structure and function.

(A) The thick mucus blocking pancreatic duct. H&E (Hematoxylin and Eosin) stain is the gold standard histological staining mechanism used for medical diagnosis mostly used to indicate the location of cells by staining the nucleus dark purple. PAS (Periodic acid-Schiff) stain is used in detecting mucus by staining it dark purple. In (A), Our research group observed the location of the cells forming the pancreatic duct represented by dark purple dots in the H&E stain. Our research group also observed in the PAS stain that that the pancreatic duct is blocked with mucus. Our research group can also observed that the mucus generating cells on the duct wall, indicated by the white arrow with green border, is also filled with mucus. Bar represents 50 μ m. (B), (C), and (D) shows the microscopic structure of the pancreas, which consists of acini sacks (secretes enzymes) and ductules and ducts which connect all the acini sacks (secretes bicarbonate rich solutions). This is also known as parenchyma (the functional tissue), and the adipose (connective) tissue. In (B), (C), and (D) Our research group compared the healthy pancreas (CFTR +/+) with CF pancreas (CFTR -/-). (B) Abnormal ductules and acini in CF pancreas. Black arrow shows pancreatic duct plugged by concentrically lamellar secretion. Bar represents 33 μ m. H&E stain. (C) shows plugging of the CF pancreatic duct and shrinking in the CF islets of Langerhans which is responsible for generating insulin (indicated by the black arrow heads). (D) Loss of CF pancreas parenchyma tissue. Bar represents 100 μ m. All these figures were obtained from the CF pig model. Adapted from (Rogers, Stoltz, et al., 2008).

3.1.3. Gastro-intestinal abnormalities.

Another major complication found with CF is within the digestive system. Similar to the lungs, patients with CF have a coating of thick mucus within their intestines. This in turn leads to constipation and mucus filled stool. Constipation caused by *CFTR* mutations helps to prevent death by cholera, which is a leading theory that *CFTR* mutations is so prevalent because it has evolutionary advantage for some of the population to be immune to cholera (Murek, Kopic, & Geibel, 2010). Intestinal obstruction syndromes are a common problem in CF patients. Around 10-20% of CF newborns present with meconium ileus at birth, a condition in which the meconium (the first stool of the infant) is thickened and can severely obstruct the distal small intestine. Meconium ileus is often the first sign for CF being found in 10- 20% of CF infants (Gorter, Karimi, Sleeboom, Kneepkens, & Heij, 2010; Raia, Fuiano, & Staiano, 2010). Older children with CF can suffer from distal intestinal obstruction syndrome and constipation. Intestinal obstruction can be treated with oral laxatives and/or intestinal lavage, or if very severe, with surgical intervention (Gorter et al., 2010).

3.1.4. Hepatobiliary involvement.

CFTR is expressed in the gallbladder and intra- and extra-hepatic bile ducts (Cohn et al., 1993). *CFTR* can cause multiple dysfunctions in the gallbladder such as gallbladder cysts, micro-gallbladder, cholelithiasis and cholestasis (Figure 3.3) (Borowitz et al., 2005). Approximately, 30 percent of CF patients develop CF liver disease (CFLD) (Figure 3.4) (Colombo & Battezzati, 2004; Colombo et al., 2002; Herrmann, Dockter, & Lammert, 2010; Nash et al., 2008). CFLD is considered to be the third leading cause of death in CF patients after pulmonary disease and

complications of lung transplantation (Colombo et al., 2002). There is no clear relation between the development of CFLD and CFTR mutations, therefore it is hypothesized that CFLD is caused in part by modifier genes (i.e. α 1-antitrypsin Z-allele) and environmental factors (Colombo et al., 2002; Wilschanski et al., 1999). A common treatment of CFLD is with the use of ursodeoxycholic acid (UDCA) which is thought to improve the liver biochemical abnormalities (K. Cheng, Ashby, & Smyth, 2000).

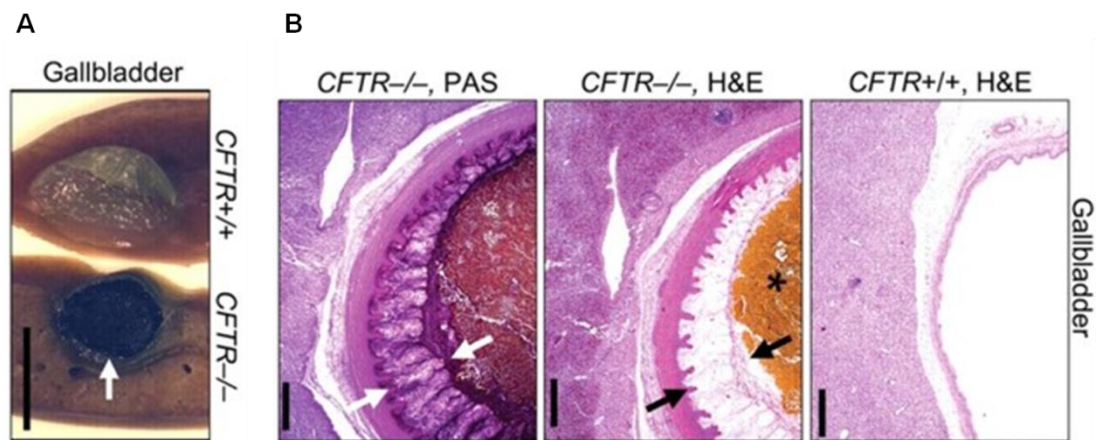


Figure 3.3. The effect of CF disease on the gallbladder. (A) The gallbladder of a healthy (CFTR +/+) and a CF pig (CFTR -/-). The gallbladder is a small organ attached to the liver which acts as a storage for bile. Bile is a fluid produced by the liver which acts as a surfactant allowing the mixing of lipids with water in food. After eating, the gallbladder discharges stored bile into the duodenum (first section of the small intestine) to assist in mixing and digesting food. In (A) after sectioning the CFTR +/+ gallbladder bile drained rapidly. However, after sectioning CFTR -/-, bile did not drain, it was coagulated against the lumen of the gallbladder (indicated by the white arrow). Bar, 0.5 cm. B) H&E (Hematoxylin and Eosin) and PAS (Periodic acid-Schiff) stain of the gallbladder. H&E indicates the location of cells by staining the nucleus dark purple. PAS detects mucus by staining it dark purple. CFTR +/+ H&E show a healthy gallbladder duct. CFTR -/- H&E show the inflammation in the gallbladder duct tissue. The asterisks indicate coagulated bile. Black arrows in CFTR -/-, H&E and white arrows in CFTR -/-, PAS indicate coagulated bile and abnormal mucus

production. Bars, 500 μm . All these figures were obtained from the CF pig model. Adapted from (Rogers, Stoltz, et al., 2008).

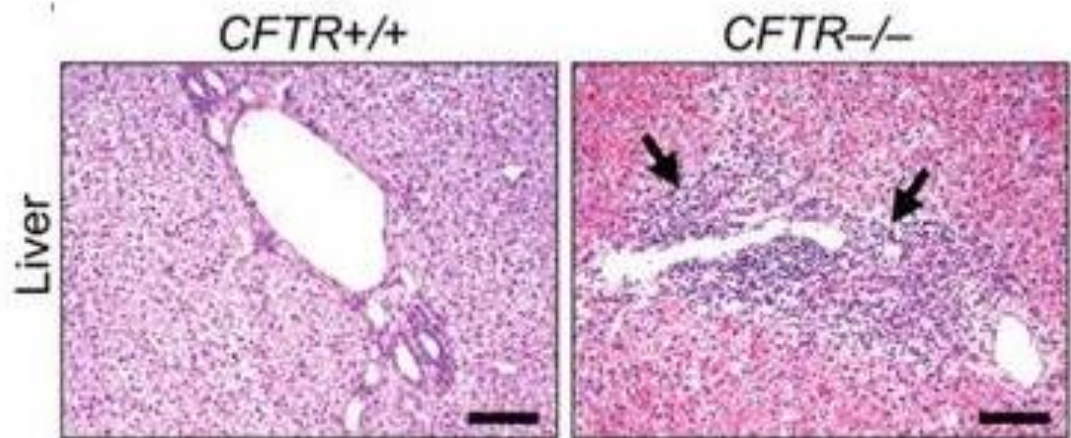


Figure 3.4. The effect of CF disease on the liver. The liver of a healthy (CFTR +/+) and CF pig (CFTR -/-). The figure shows H&E (Hematoxylin and Eosin) staining indicating inflammation and abnormalities in the CFTR-/- liver compared to CFTR +/+. Bars, 100 μm . All these figures were obtained from the CF pig model. Adapted from (Rogers, Stoltz, et al., 2008).

3.1.5. Reproductive system.

Almost all CF males (98 percent) are azoospermic, meaning that they do not have a measurable amount of sperm within their semen (Figure 3.5). Male CF patients typically have bilateral absence of the vas deferens. The body and tail of the epididymides are deformed or absent. The testes may or may not be reduced in size, and the seminal vesicles typically contain various abnormalities. It has been proposed that these abnormalities are caused by a failure of differentiation during the first trimester (Lyon & Bilton, 2002).

Females with CF sometimes find it hard to become pregnant due to the blockage of the cervix by mucus. Patients who decide to have a child must carefully plan out their pregnancy. Women must weigh issues such as a loss of lung function during pregnancy and the toxicity of certain drugs to the fetus. Typically women regain their lost lung function after giving birth, but some women fail to regain their lung function and have a progressive pulmonary decline as a result. Therefore, it is imperative that CF patients talk to their doctors and make the best decision for their individual case as to whether they should become pregnant (Lyon & Bilton, 2002).

3.1.6. Nutrition.

Most CF patients have reduced nutritional status. After birth, CF infants fail to thrive due to fat malabsorption. Late diagnosis with CF can affect a patient's growth due to malabsorption of nutrients specifically fat which persists in 25-50 percent of CF patients, inadequate energy intake, and high energy expenditures due to recurrent pulmonary infections. Once young patients are diagnosed with CF, nutritional treatment is applied to assist absorption and increase dietary intake. The cornerstone treatment for pancreas insufficiency is pancreatic enzyme replacement therapy

(PERT), dietary energy intakes of 120-150% of the Recommended Dietary Allowance (RDA) and the prevention and early treatment of pulmonary infections (Sinaasappel et al., 2002). On average, children with CF grow between the 20th and 30th percentile on the growth chart compared to healthy peers, and decline when pulmonary disease progresses (Haeusler, Frisch, Waldhor, & Gotz, 1994; Stettler et al., 2000). The implementation of neonatal screening for CF may prevent the first decline in nutritional status directly after birth due to the early start of nutritional intervention.

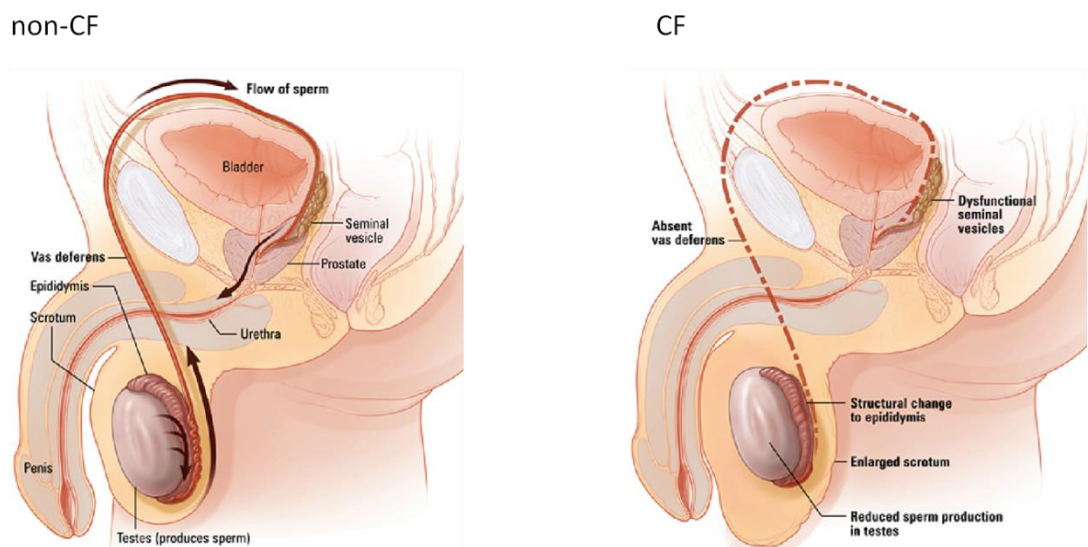


Figure 3.5. Effect of CF disease on the male reproductive system. The figure illustrates bilateral absence of the vas deferens in CF patients compared to healthy non-CF subjects.

Vas deferens is a duct that conveys sperm from the testicles to the urethra. Almost all CF males (98 percent) are azoospermic, meaning that they do not have a measurable amount of sperm within their semen. Adapted from (JohnHopkins, 2014).

3.2. Secondary complications.

3.2.1. Cystic fibrosis related diabetes.

Aside from all the primary complications, CF indirectly causes other disease and secondary complications. One of the most severe secondary complications found with CF is diabetes. CF diabetes is different from type 1 and type 2 diabetes and is known as cystic fibrosis-related diabetes (CFRD). CFRD is normally found within CF patients who have more severe forms of the disease, and is associated with an insufficient pancreatic function leading to an insulin deficiency. Thick sticky mucus in the pancreas blocks the pancreas leading to fibrosis and fatty infiltration which in turn offsets the destruction of the hormone producing areas of the pancreas. As a result, less insulin is produced and released into the blood stream (Kelly & Moran, 2013).

As CF patients age, the normal decline in β -cell function leads to an increase in CFRD. CFRD increases mortality rates in CF patients by about six fold. CFRD is also associated with reduced lung function in CF patients which can begin several years before the patient is diagnosed with CFRD. Another early sign of CFRD is a decrease in body mass index (BMI). Although CFRD is a severe complication associated with CF, improvements in survival have been seen with early diagnosis and treatment. Therefore, now that CFRD is more common and better understood, doctors can screen their patients to catch the onset of diabetes as early as possible, greatly increasing the patient's chance of survival (Kelly & Moran, 2013).

3.2.2. Low bone mineral density.

Low bone mineral density (BMD) was first noted in CF patients in 1979 (Figure 3.6) (Javier & Jacquot, 2011). The absence of CFTR function affects bone properties in several ways. First, insufficient pancreatic activity can lead to malnutrition which causes malabsorption to calcium, vitamin D and vitamin K deficiencies which are all important for maintaining bone structure. Also malnutrition can cause lower BMI, which in turn can reduce BMD. Second, lack of physical and outdoor activity, which can reduce vitamin D levels and reduce bone mass due to reduced loading applied on the bones during physical activity. Third, recurrent infections can lead to muscle and bone resorption. Finally, CF medications can decrease BMD, for example glucocorticoids which are typically used for CF patients to improve lung function (Javier & Jacquot, 2011).

The advance in treatments for CF disease have increased the life expectancy of CF patients. However, reduced BMD increases the risk of fractures in CF patients.

Vertebral fractures are most dominant in CF patients, and females with CF have a greater fracture incidence compared to males with CF. Aside from the severe pain these fractures cause, vertebral fractures can prevent effective treatment of the lung disease associated with CF since treatment induces coughing as a means of breaking up mucus within the lungs (Buntain et al., 2006).

3.2.3. Gastro-intestinal.

As CF patients become older, their risk for gastrointestinal and pancreatic cancers is higher than average (Ooi & Durie, 2012). Several secondary changes in the small intestine, like chronic intestinal inflammation, mucus accumulation, prolonged intestinal transit time and small intestinal bacterial overgrowth are also described in

the CF intestine and may contribute to malnutrition (Bruzzese et al., 2004; Lewindon, Robb, Moore, Davidson, & Martin, 1998; Lisowska, Wojtowicz, & Walkowiak, 2009; Raia et al., 2000; Sbarbati, Bertini, Catassi, Gagliardini, & Osculati, 1998; Smyth, Croft, O'Hea, Marshall, & Ferguson, 2000).

3.2.4. Psychological.

Psychological issues associated with CF not only reduce quality of life, they can also lead to complex social interactions where individuals struggle to explain CF to colleagues and friends, and serious psychiatric disorders are associated with CF. Rates for both major depression and suicide are higher for adult individuals suffering from CF (Vender, 2008). Other secondary complications can include pain such as chest pain and headaches.

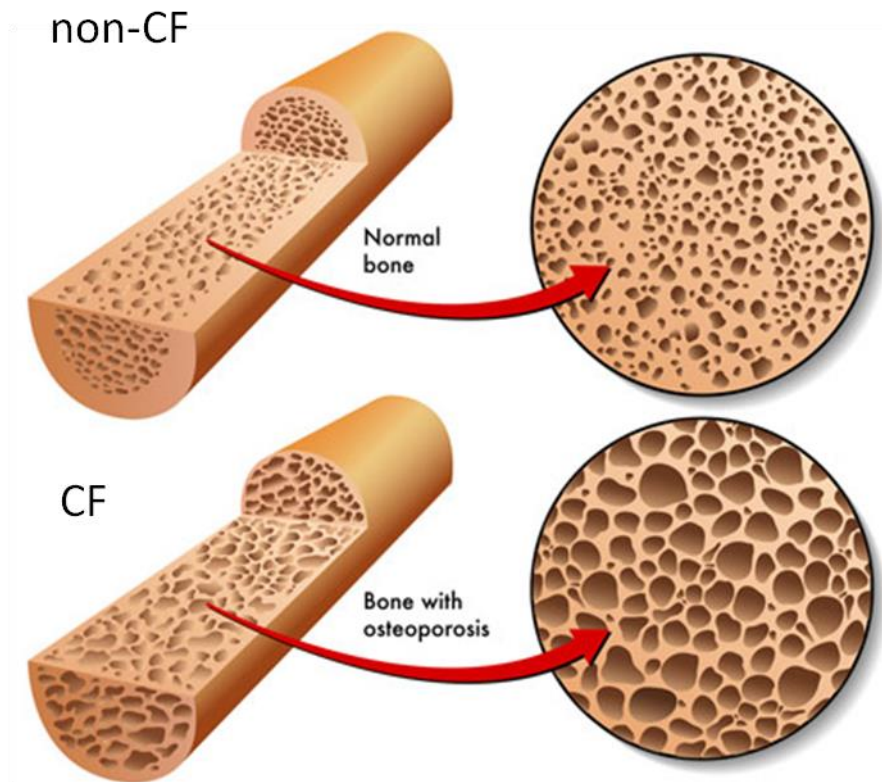


Figure 3.6. Effect of CF disease on bone material density. The figure shows low bone mineral density in CF patients compared to non-CF healthy subjects. Low bone mineral density occurs in over three quarters of CF adults as a consequence of poor absorption of fat, low vitamin D levels, insufficient sunlight exposure insufficient exercise, and delayed onset of puberty. Adapted from (JohnHopkins, 2014).

3.3. Current treatments.

Many treatments for CF have been proposed and implemented over the years. These treatments typically treat the symptoms of CF and differ from patient to patient.

In the last 15 years, many therapeutic approaches have been developed for CF. These have included compounds that increase Cl^- permeability, block epithelial Na^+ channel function, enhance CFTR transfer to the plasma membrane, and deliver a copy of the normal CFTR cDNA to the CF cells using aerosol delivery techniques (Welsh & Ramsey, 1998).

3.3.1. Inhaled treatments.

One of the most common treatments today is inhalation of hypertonic saline through a nebulizer. Hypertonic saline can in-part improve mucociliary clearance. It is hypothesized that inhaling hypertonic saline hydrates the thick mucus layer caused by defective CFTR proteins. Also hypertonic saline induces coughing within patients. Coughing coupled with hydrated mucus can, in part, improve mucociliary clearance by creating a shear force that promotes the removal of mucus within the airways. The increase in mucociliary clearance leads to better lung function within CF patients (Reeves et al., 2012).

Another common inhaled treatment for CF is pulmozyme or dornase alfa.

Pulmozyme was approved in 1994 for use in the treatment of CF (MacConnachie, 1998). This treatment contains an enzyme known as deoxyribonuclease I (DNase I). DNase I removes DNA, which can reduce the viscosity of mucus within CF patients. Due to chronic inflammation within CF lungs, there is an excess of cellular debris. This debris becomes attached to abnormal mucus strings tethered to the submucosal gland and in turn builds up a layer of mucus, cellular debris and bacteria/ pathogens

with a higher viscosity than regular mucus in non-CF patients. Pulmozyme works to reduce viscosity by digesting the extracellular DNA accumulated within the lungs. Similar to hypertonic saline, the loosening of mucus allows for better clearance of the lungs. This leads to an increase in lung function and a decrease in respiratory exacerbations. Moreover unlike hypertonic saline, pulmozyme is also well tolerated in patients, making it an ideal treatment for those with CF (Suri, 2005).

3.3.2. Chest physiotherapy.

Chest physiotherapy for CF patients was first documented in the 1950s and involved pounding on the back of the patient in a head-down position to help clear up the mucus build up. This treatment caused abnormal cardiac rhythms in adults, and due to CF low bone mineral density it could also cause bone fractures. In the 1970s, the flutter valve was introduced which works by increasing resistance to create higher pressure in the airways forcing more air to distal regions (Figure 3.7). The resistance was created by exhaling through a mask mouthpiece, and the increased resistance is thought to break up thick mucus secretions. The positive end expiratory pressure (PEEP) mask has been found to be just as effective as or more effective than conventional chest physiotherapy methods (Pisi & Chetta, 2009).

Currently, the most effective chest physiotherapy method is high-frequency chest compression. This has been shown to increase mucociliary clearance by increasing expiration and creating forces leading to coughing. A device known as the Vest Airway Clearance System was created (Figure 3.8). The Vest works by applying high-frequency oscillations to the patient's chest via an air-pulse-generating compressor. These oscillations help to move mucus secretions from the small airways into larger airways where they are more easily removed by coughing. This treatment is normally well tolerated, but in some patients with more advanced lung

disease, it can cause pain and discomfort. Overall, the Vest is a good alternative to conventional chest physiotherapy methods and has been shown to decrease the rate of decline in pulmonary function over a long period of use (Pisi & Chetta, 2009).



Figure 3.7. Positive End Expiratory Pressure (PEEP) mask. It works by creating higher pressure in the airways forcing more air to distal regions. The resistance is created by exhaling through a mask mouthpiece. The increasing resistance is thought to break up thick mucus secretions. Adapted from (Elettromedicali).



Figure 3.8. High-frequency chest compression vest. This vest uses air pressure and pulses to create compressions on the CF patient's chest. It has been shown to loosen, thin, and increase mucociliary clearance by increasing expiration and creating forces leading to coughing. Adapted from (Respirtech).

3.3.3. Antibiotics.

Prior to the 1940s, lung disease and failure to clear meconium ileus aurous was responsible for the death of many CF patients in their infancy. The main pathogen in CF identified at that time was *S. aureus*. In the 1940s penicillin was discovered, and it became available for injection in 1944. The first use of an aerosolized antibiotic in CF dates back to 1946 (Di & Andersen, 1946). During this time penicillin aerosol had been used for pulmonary diseases like lung abscess (Wolcott & Murphy, 1957) and pneumococcal pneumonia (Kuhn, 2001). Moreover a dry powder inhaler with penicillin for inhalation became available in the late 1940s. It is unclear whether every CF patient had access to this therapy in those days, but aerosol antibiotics have been used extensively in later years (Hodson, Penketh, & Batten, 1981; Kuhn, 2001). In the fifties *P. aeruginosa* was cultured but *S. aureus* was still considered to be the main pathogen. In the early 1970s the first successes of early aggressive antibiotic treatment were documented (Mearns, 1972). It was shown that the mortality rate for children under 5 years of age could be reduced from 14% to 6.5% by early and vigorous anti-staphylococcal treatment. On the other hand, aerosolized penicillins were avoided because of concerns regarding development of hypersensitivity, odour, effect on teeth and greater difficulty in nebulisation (E. Kerem, Conway, Elborn, Heijerman, & Consensus, 2005).

By the late seventies CF was not considered a lethal disease that cannot be treated, but rather a condition that could be controlled with antibiotics. Antibiotics active against *P. aeruginosa* became available: colistimethate sodium (1959), carbenicillin (1967), gentamicin (1968), tobramycin (1971), piperacillin (1982), ceftazidime (1983), aztreonam (1986), ciprofloxacin (1986) and meropenem (1995). Despite

good results, some patients started to relapse between two intravenous courses and aerosolized antibiotics got renewed interest (Hoiby et al., 1977).

Gradually the use of aerosolized antibiotics increased, despite a continuing discussion on the possible increase in antibiotic resistance (Ashby & Stern, 1993). Anti-staphylococcal aerosol treatment had been applied, but it was subsequently shown to have no additional effect over agents administered orally (MacLusky, Levison, Gold, & McLaughlin, 1986; Nolan et al., 1982).

Nowadays, during early lung disease within CF patients, doctors typically prescribe antibiotics to help delay the chronic colonization of pathogens with agents such as colistimethate sodium and tobramycin. Once pathogens have colonized, chronic maintenance antibiotics are given to patients to help slow the decline in pulmonary function. Patients with a chronic *P. aeruginosa* infection benefited from long-term nebulised antibiotics (T. Jensen et al., 1987), and early treatment with aerosolized colistimethate sodium or tobramycin to eradicate *P. aeruginosa* appeared effective too (Frederiksen, Koch, & Hoiby, 1997; Littlewood, Miller, Ghoneim, & Ramsden, 1985; Ratjen, Doring, & Nikolaizik, 2001; Valerius, Koch, & Hoiby, 1991).

Although aerosolized colistimethate sodium has been used for chronic *P. aeruginosa* infection for decades, proper prospective placebo controlled trials are missing. A prospective unblinded study on aerosolized colistimethate sodium and tobramycin showed superiority of tobramycin in improvement of lung function (Adeboyeke, Scott, & Hodson, 2006; Hodson, Gallagher, & Govan, 2002). Efficacy of tobramycin solution for inhalation (TSI) has been studied in a clinical trial (Ramsey et al., 1999). Treatment with tobramycin resulted in an improvement in lung function, a decrease of *P. aeruginosa* density in sputum and a lower risk on hospitalisation.

During times of increased pulmonary symptoms, patients are typically prescribed a more intense antibiotic regimen. Typically, these intense treatments are carried out

through intravenous methods whether they are at a hospital or at home. Less intense antibiotic regimens are typically inhaled during a patient's regular treatment times. Since there are a wide variety of bacterial infections that can take hold in CF patients' lungs, there are also a large number of antibiotics prescribed. Antibiotic treatments are individualized for each patient. There is no clear cut treatment plan for infections within CF patients (Gibson et al., 2003). Although inhaled antibiotics appeared to be relatively safe, in some patients airway narrowing was observed during or shortly after nebulization (Hodson et al., 2002; Ramsey et al., 1999). This side effect might be due to nebulizer mechanical properties or to drug properties.

3.4. Latest breakthrough therapies.

The latest breakthrough for the treatment of CF is VX-770 (Vertex Pharmaceuticals, Cambridge, MA, USA) more commonly known as Kalydeco or ivacaftor. VX-770 is a potentiator meaning that it is a drug that targets CFTR protein channel gating. VX-770 targets the CFTR channel G551D gating mutation to increasing the probability of the CFTR channel to open. It was discovered through a process called high throughput screening. High throughput screening is a relatively new technology in drug discovery. It employs robotics, sophisticated and sensitive sensors, data processing software, and supercomputers to scan a huge number of chemical compounds very quickly to look for molecules that perform a specific function such as control channel gating. When this was employed to screen the G551D cell-culture VX-770 was found to have the ability to affect channel gating. VX-770 was then validated using in-vitro follow up analysis. VX-770 was recently approved by the Food and Drugs Administration for treatment of patients with G551D mutation of CF (Jih & Hwang, 2013). However, its mechanism of action is still not yet known. This has promoted extensive research to find out the safety and effectiveness of this drug

in CF patients with at least one G551D allele. These studies found that patients given VX-770 showed significant improvements in lung function, nasal epithelial cells, and sweat glands compared to patients without the drug. It was determined that VX-770 could be a viable therapeutic treatment for CF patients with the G551D mutation (Accurso et al., 2010). It has also been shown that VX-770 is not a cure for G551D patients, but it offers a significant increase in patients' health and provides hope for all those with or involved with CF (Jih & Hwang, 2013).

Other therapies for the treatment of patient with the deltaF508 mutation are now making their way through trial phases. One of these therapies is VX-809 combined with VX-770. This therapy was recently approved by the FDA. VX-809 is known as a CFTR corrector, and it helps the CFTR protein reach the cell membrane. The VX-770 then works as a potentiator to help keep the CFTR channel open for longer periods of time. In the phase two trial, there was a significant increase in lung function for patients taking the combination of VX-809 and VX-770. The combination of treatments also appears to be well tolerated by patients, with the most severe side effects being pulmonary in nature. (Vertex, 2013).

Another breakthrough therapy undergoing trials for the deltaF508 mutation is the combination of VX-661 and VX-770. This combination therapy just recently finished its phase two study. Like VX-809, VX-661 is a CFTR corrector used to help move the deltaF508 mutated CFTR to the apical membrane. This combination therapy also seems to be well tolerated by patients, with only some mild to moderate pulmonary side effects. The study showed significant decreases in sweat chloride production, which is unusually high in patients with CF. With high enough doses, VX-661 and VX-770 together led to a significant increase in lung function. Along with VX-809 and VX-661, there is still another potential corrector for CFTR being tested.

However, of these three correctors, VX-809 is currently the leader, providing the greatest hope for a radical treatment for those with the deltaF508 mutation (Vertex, 2013).

Currently, there is another potential therapy moving through the trial stages called ataluren. This therapy is effective for patients who have a nonsense mutation in their CFTR gene. Ataluren is a drug that allows for ribosomal readthrough of mRNA molecules that contain premature stop codons. It was determined that ataluren leads to the proper translation of a CFTR protein. Although the trial period was short, there were trends towards higher lung function and a decrease in coughing. These results prove that there could be a clinical benefit of ataluren in individuals with a nonsense mutation in their CFTR gene. Further research is needed to assess the improvement in lung function before this drug will be ready for release to the general CF population. Although it has not been released yet, this is another possible therapy for individuals suffering from CF (Wilschanski et al., 2011).

Another potential therapy that offers the best hope for a life-saving treatment is Gene therapy. Gene therapy works on tackling the root cause of CF, rather than only treating the symptoms. Gene therapy is highly considered as a prospective therapy for a wide range of genetic disorders including acute respiratory distress syndrome (ARDS), cancer, asthma, emphysema, and CF. CF is a desirable candidate for gene therapy treatment because monogenic disorders that currently do not have satisfactory treatment option(Senn, 1998). Although big breakthrough in gene therapy was observed in CF in 1992 (Coutelle, Caplen, Hart, Huxley, & Williamson, 1993; Miller, 1992), the airway innate defence mechanism proved to be challenging. The human airways function as a conductive passage rather than absorptive surface, have led the gene therapy research to develop various viral and non-viral vectors to

deliver a functioning *CFTR* gene. Viral vector have proven to be ineffective in transduction from the airways luminal surface and repeated application was challenging due to lung immune response. However, recent phase 2b trail study from the UK have shown that non-viral vector have worked and lead to a significant increase in patient's FEV1(Alton et al., 2015).

Although our understanding of the causes of the CF disease is increasing every day, our knowledge is still limited in regards to the pathogenesis of lung disease (Quinton, 2008; J.J. Wine, 1999). The knowledge that has been obtained thus far can explain the abnormality in organs such as the sweat gland, the pancreas, and the intestine, but it cannot fully explain the abnormality in the lung. Part of the difficulty in understanding pathogenesis of the CF lung is the lack of knowledge at the organism level and the lack of understanding the early stages in lung disease pathogenesis. To increase our knowledge in this area, an animal or a model system is required.

“Logic takes you from a to b.

imagination takes you

everywhere.”

Albert Einstein

Chapter 4. The respiratory system

4.1. The respiratory system structure and function.

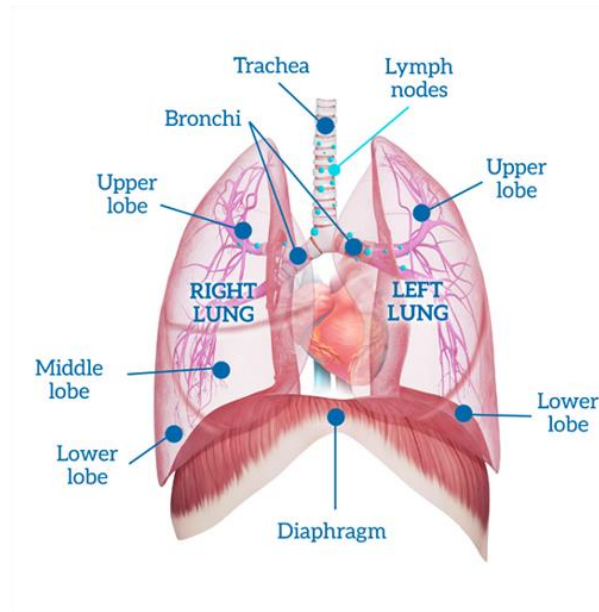
The respiratory system is a complex and versatile multi-organ system. It is designed to perform multiple life necessary functions which include operating as a blood reservoir and filtration system, a cushioned insulator for the heart, as well as facilitating the pH balance of blood. The respiratory system is an integrated system that is composed of the following organs; lungs, the conducting airways, the rib cage, the muscles that control breathing and part of the central nerve system that controls the respiratory muscles (Levitzky, 1995; West, 2012). The most crucial function of the respiratory system is the intake and exchange of oxygen and carbon dioxide between the organism and the environment (West, 2012). For the respiratory system to perform all these functions, a well-coordinated interaction between all the components is required.

The human lung is divided into the left lung and the right lung, where each lung is completely enclosed and further divided by the pleura. The pleura is a membrane layer. The thoracic cavity contains two layers of pleura. The first layer lines the inner surface of the thoracic cavity and it is known as parietal pleura. The other envelops the lungs and is known as the inner pleura or the pulmonary pleura or visceral pleura. The two pleura membrane layers are joined together at their edges and contain a space known as the pleural cavity. The pleural cavity is normally filled with fluid whose pressure is known as the pleural pressure (Hoffman & Ritman, 1985).

The inner pleura divides the lung into five lobes (Figure 5.1.A.). The right lung is divided into the three lobes, right upper lobe (RUL), right middle lobe (RML), and right lower lobe (RLL). The RUL is separated from the RML by a horizontal fissure and the RML is separated from the RLL by an oblique fissure. The left lung is divided into two lobes, the left upper lobe (LUL), and the left lower lobe (LLL), separated by an oblique fissure. Dividing the lung into lobes is essential from a biomechanical point of view since it allows lobes to slide against each other and against the chest wall providing means to reduce lung parenchymal distortion. It also avoids region of high tissue stress in the lung (Rodarte, Hubmayr, Stamenovic, & Walters, 1985).

The lungs are the major organ of the respiratory system that performs a multitude of vital functions every second of our lives. The lung is made up of approximately 10% solid tissue, 10% blood and 80% air (Figure 5.1.B.) (Levitzky, 1995). The two major primary functions of the lung are ventilation and perfusion.

A.



B.

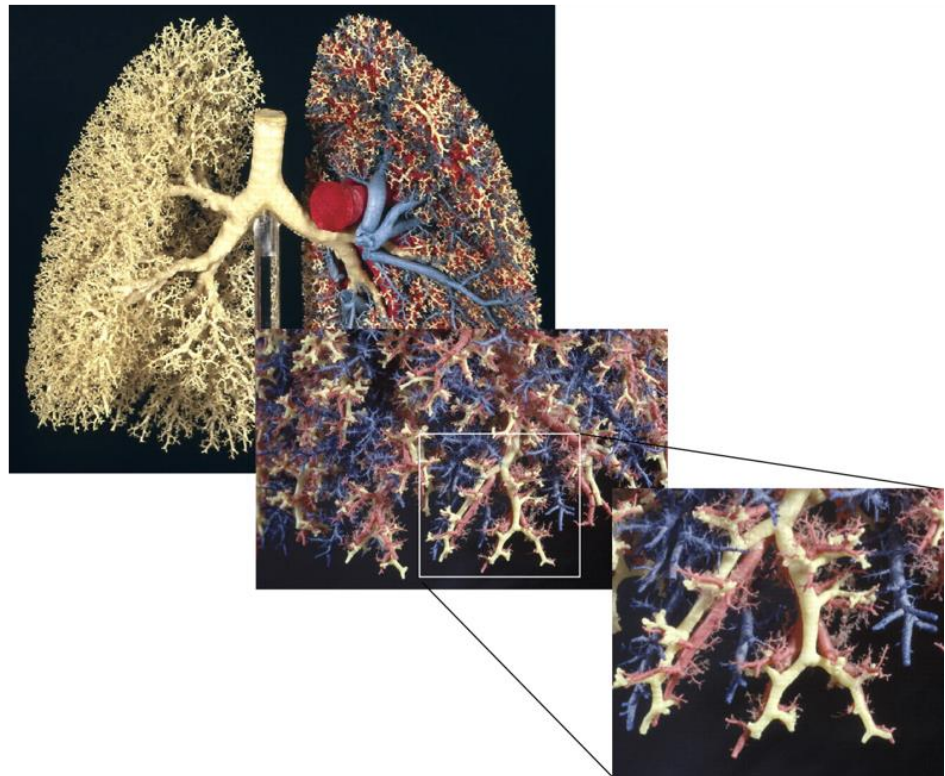


Figure 4.1. Human lung. A. diagram showing all lung lobes positions. Adapted from (LVNG, 2006). B. human lung cast. Left lung: displays the bronchial tree. Right lung: displays arteries shown in red and veins shown in blue. The zoomed in box highlights that the airway and arterial trees mirror each other all of the way out to the terminal branches. Adapted from (Glenny, 2011).

4.2. Ventilation.

Ventilation is the rate at which air enters or leaves the lungs. Under fluid dynamic laws, air flows from regions of higher pressure to regions of lower pressure.

Therefore, a pressure gradient is required between the alveoli and atmosphere for air to flow in and out of the lung (Figure 5.2). Alveoli are small air sacs (approximately 200 μm in diameter) where gas exchange takes place. The atmosphere is connected to the alveoli sacs through a series of branching tubes with progressively decreasing dimensions. There are approximately 300 million alveoli in a healthy human lung.

Alveoli are covered with a dense capillary network with only a single cell layer separating inhaled air and the circulating bloodstream (Figure 5.3) (Levitzky, 1995).

The alveoli expand passively when the chest and diaphragm muscles stretch causing an increase in the area of alveoli and thus a decrease in the pressure. For air to flow from the environment (high pressure) to the passively expanded alveoli (low pressure) it has to pass through two regions of the lung: the conducting and the respiratory regions (West, 2012).

4.2.1. Conducting region.

Air first passes through the nose or the mouth, then through the pharynx, followed by the larynx. These regions are called the upper airways. Air then enters the trachea and tracheobronchial tree, known as the conducting airways. The conducting airways are not involved in gas exchange, but provide the respiratory system with fresh air (West, 2012). The conducting airways divide into generations based upon the airway size and diameter starting from the trachea and the left and right main bronchus (the first generation). These bronchi then divide into the lobar (the second generation) and segmental bronchi (the third generation). The division of bronchioles which comes

after the segmental bronchi continues for 16th generations. With successive divisions the airways become smaller and shorter (Figure 5.4). Although the diameter of the airways decrease with each division, the total cross sectional area increases, causing peripheral resistance to decrease (Levitzky, 1995).

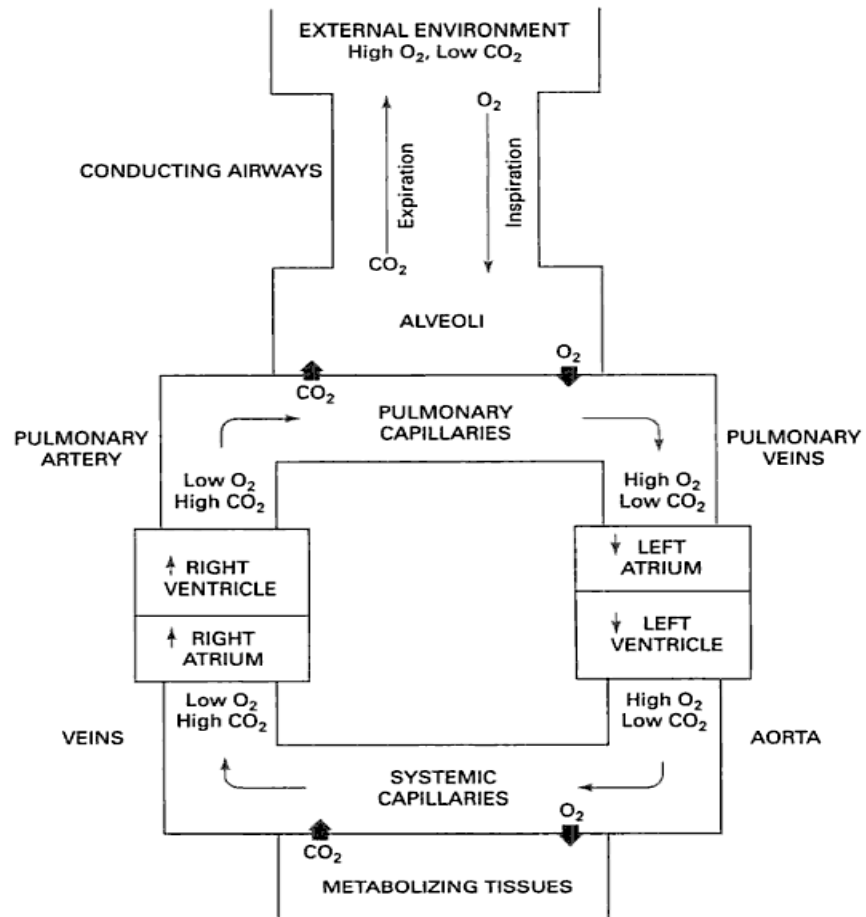


Figure. 4.2. Gas exchange between tissues in the body and the environment. The figure shows the air going through the conducting airways and then to the respiratory airways, the site of gas exchange. Adapted from (Levitzky, 1995).

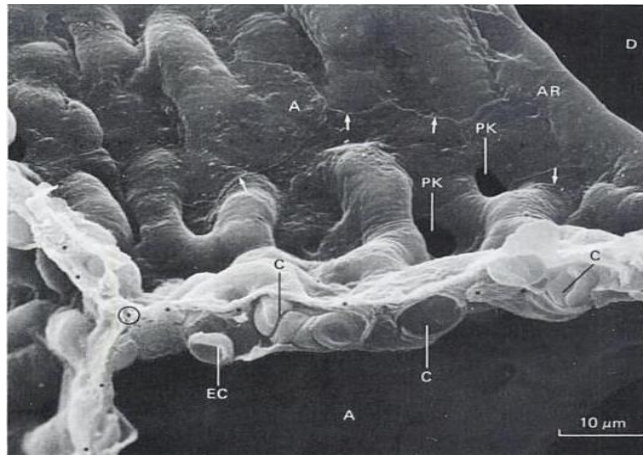


Figure. 4.3. Scanning electron micrograph of the surface and cross section of the alveoli. The image contains three alveoli. A= alveolus; D=alveolar duct; PK= Pores of Kohn; AR= alveolar entrance to duct; *= connective tissue fibers. Adapted from (Weibel, 1973).

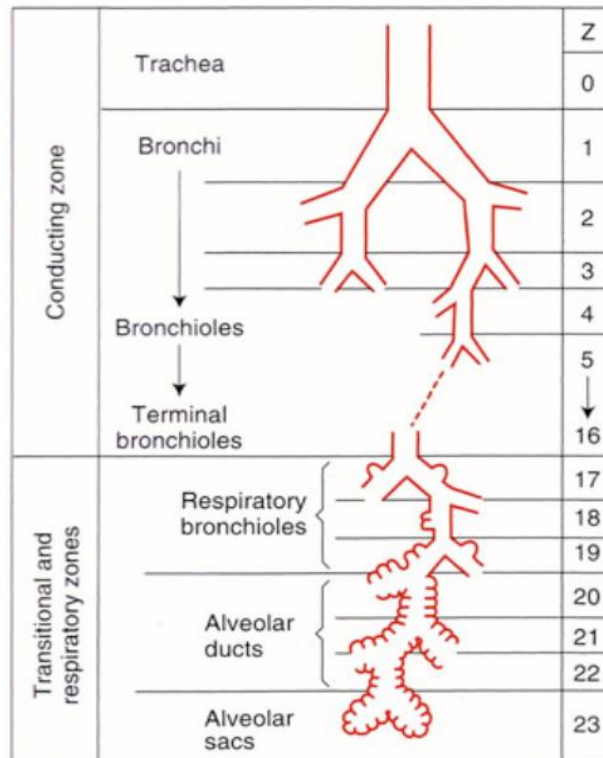


Figure. 4.4. The airway tree structure. The figure depicts the conducting, transitional, and respiratory regions in the lung. Dimensions are approximate. Adapted from (Weibel, 1963).

4.2.2. Transitional and respiratory region.

The terminal bronchioles continue to divide through to the nineteenth generation, however, some changes in the anatomical structure can be seen starting from the seventeenth generation. The bronchioles walls are still lined with cuboidal epithelium and muscles, similar to the conducting airways. Yet bundles of alveoli start to appear on the bronchioles indicating the end of the conducting anatomic dead space region and the start of the transitional region. After the twentieth generation the bronchioles start to divide into small alveolar ducts and alveolar sacs, continuing for the last 3 generations of the lung. The alveolar duct and sacs, which terminate the tracheobronchial tree, are referred to as the respiratory region of the lung (West, 2012).

All of the airways in the respiratory region participate in gas exchange. This significant gas exchange capability is in part attributable to the tremendous total cross-sectional surface area of the alveoli. It is hypothesized that if the alveoli were assumed spherical, the total surface area of the respiratory region would be 85 square meters (Levitzky, 1995).

4.3. Perfusion.

Perfusion is the blood flow through pulmonary capillaries, and gas exchange happens during perfusion (Figure 5.3). With inspiration, air travels down the tracheobronchial tree by bulk flow. As the cross-sectional area increases and the resistance decreases, the air velocity reduces to practically zero at the alveoli (West, 2012). The reduction of the velocity of air allows gas exchange to take place. The exchange of oxygen and carbon dioxide between the air and blood occurs passively, according to their concentration gradients across the alveolar-capillary barrier (West, 2012).

The lung has two blood supply systems, the pulmonary supply, which transports deoxygenated blood from the right atrium of the heart and provides oxygenated blood to the left ventricle, and the bronchial supply, which provides oxygenated blood to the lung tissue (Figure 5.2) (Levitzky, 1995; West, 2012).

4.4. Respiratory cycle.

The inspiration and expiration process of the respiratory cycle is directed by the pressure difference between the atmosphere and the chest. During inspiration, the chest volume increases, the diaphragm contracts and the pressure inside the lung decreases. This causes air to flow from the atmosphere through the airways to the alveoli. During expiration, the lung passively returns to its pre-inspiratory volume because of elasticity. This process forces air to flow out of the lungs and back into the atmosphere (Levitzky, 1995).

The respiratory cycle can fully or partially inflate the lung (Figure 5.5). The volume of inspired or expired air in or out of the lung has been defined as follows:

Tidal volume (TD): the air volume inspired and expired during normal breathing.

The text book value is 500ml for a healthy human adult.

Residual volume (RV): after a maximum expiration, the minimum air left in the lung is called RV.

Vital capacity (VC): the full lung capacity from maximum (fully breathing in) to minimum (fully breathing out- i.e. RV).

Total lung capacity (TLC): Is the total amount of air in the respiratory system after maximum inhalation.

Functional residual capacity (FRC): The amount of air left in the lung after a normal expiration (Levitzky, 1995).

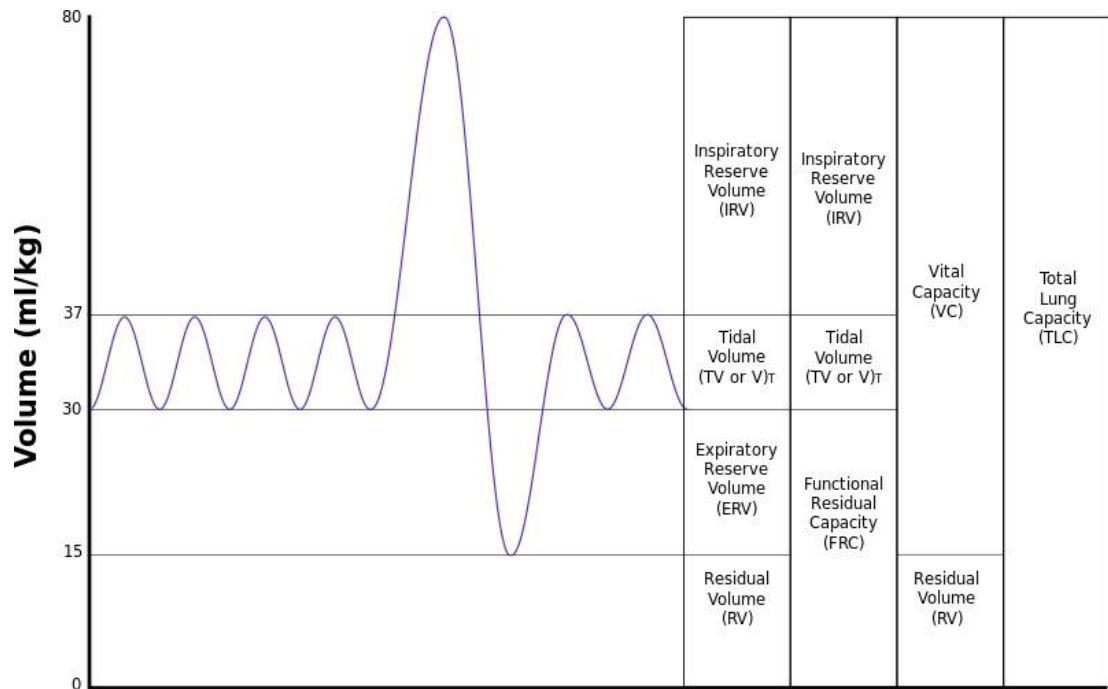


Figure. 4.5. Lung volumes. The figure depicts different lung volumes during the respiratory cycle and their definitions. Dimensions are approximate. Adapted from (Weibel, 1963).

4.5. Methods of quantifying lung structure and function.

There are several methods that have been adapted to quantify CF airways and lung structure and function in vivo including computed tomography (CT), bronchoscopy, magnetic resonance imaging (MRI), optical coherence tomography (OCT), fiberoptic confocal endomicroscopy (FCE) and endobronchial ultrasound (EBU).

Bronchoscopy, OCT, FCE and EBU are some of the techniques currently used to quantify airway diameter and cross-sectional area. These techniques have a lot of potential but also some limitations. Bronchoscopes have a wide angle lens that increases the field of view but cause distance and radial distortion to the image which limits their quantitative capabilities. FCE has a 0.5 mm field of view which will not

provide a representative image of the airway. OCT is an excellent tool but it does not provide any data about the lung parenchyma which is of significant importance analysing lung function. Finally, EBU can only adequately visualize extrathoracic airways due to its large size (H. O. Coxson et al., 2008; Czaja et al., 2007; Flusberg et al., 2005; Masters et al., 2005; McLaughlin et al., 2008; Shaw et al., 2004; Thiberville et al., 2007; Vercauteren, Perchant, Malandain, Pennec, & Ayache, 2006) (Williamson et al., 2009).

The aim of this thesis is to understand the pathogenesis of cystic fibrosis lung disease in the early stages before infection and inflammation. I am interested in dynamic lung function and therefore, I examined the current methods to quantify the pathogenesis of lung disease in cystic fibrosis patients. Dynamic lung function can be quantified by using a breathing apparatus or imaging modality. Breathing apparatus such as spirometry or lung clearance index (LCI) are used in longitudinal analysis to quantify long term lung function and asthma in asthma and CF patients (Wu et al., 2014).

Spirometry is a device used to measure timed inspiratory and expiratory volume, in another word it can measure how quickly the individual's lung can be filled and emptied. Clinically spirometry is used to measure airway function by assess the lungs ability to forcibly expire its vital capacity in a given time. This is also known as airway resistance. Thus spirometry assesses airway resistance(H. M. Cheng, 2015).. Although spirometry is used in several recent studies to assess the progression of lung disease in CF (Davies & Alton, 2009; George et al., 2011; E. Kerem, Reisman, Corey, Canny, & Levison, 1992; Rabe et al., 2007), it is known to be insensitive to small airway disease. Since the small airways (less than 2mm in diameter) have low mean flow rate and low combined resistance (less than 10%) due to its large

combined cross-sectional area (A. Horsley, 2009). Therefore, considerable lung damage can happen in the small airways and the parenchyma before any noticeable change is observed in the spirometry value (Brody et al., 2004). Spirometry results can also be poorly reproducible (Timonen, Randell, Salonen, & Pekkanen, 1997). Spirometry is also very sensitive to age, height, and gender. Therefore it is usually presented as a percent predicted, which means a wide range of spirometry values are considered to be normal which can skew and make spirometry less sensitive. Also the equation that is used to compute the normal percent predicted value changes in late teen, making measurement of rate of decline in early adolescent challenging (Quanjer et al., 1993).

LCI on the other hand, uses inert gas (the gas should neither be absorbed nor excreted by the body to any significant degree) which the patient inhales (washin) until 100% lung saturation is achieved. Then after a few normal successive breath, the peak concentration of the inert gas drops. By quantifying the rate in which peak concentration falls over multiple successive breath (washout) the physician is able to sensitively measure the patient ventilation. In another word, LCI is the measurement of the number of successive breath required to washout a lung saturated with inert gas to predefined end point. LCI increases with increase disease severity (Davies, Cunningham, Alton, & Innes, 2008; A. Horsley, 2009).

LCI is unique in that it's able to follow disease pathogenesis non-invasively with greater sensitivity compared to spirometry (Aurora et al., 2005; Aurora et al., 2004; Gustafsson, Aurora, & Lindblad, 2003; A. R. Horsley et al., 2008). LCI relies on tidal breathing which makes it ideal for all age groups. Also it been demonstrated to be really sensitive to small changes in lung function in CF patients and its results are consistent and are unaffected by gender, weight, or height (because it is derived

using the patient specific FRC) (Davies et al., 2008; A. Horsley, 2009). However, LCI measurement in infants can be challenging requiring extensive technical demand on the LCI apparatus. In addition, the test requires roughly half an hour to complete (both wash-in and washout phase required). A good mouthpiece seal is required which can be challenging to maintain for the duration of the test. Furthermore, LCI is not informative in the local segmental level, it only provide details regarding global lung function. Moreover, for sever CF patients, reoccurring inflammation and infection intervention may open up poorly ventilated lung region leading to worsen LCI. Also until recently all LCI devices where develop in house with no commercial apparatus available and no universal standard of preforming the test or universal protocol of calibration and sensitivity adjustment.

Therefore, to achieve the aim of this study I needed to use an imaging method that provides quantitative data about the lung and the airways at the local and global level. Also that imaging modality needs to be used in a longitudinal analysis allows for estimation of the group or individual baseline lung function and who it changes overtime. This can reduce the effect of potentially confounding stature-related factors (Hankinson, Odenchantz, & Fedan, 1999; Hibbert, Lannigan, Landau, & Phelan, 1989; A. Horsley, 2009; Kristufek, Brezina, Ciutti, Strmen, & Mayer, 1987; Wu et al., 2014).

There a few imaging protocols such as hyperpolarized magnetic resonance imaging (MRI), quantitative computed tomography (QCT), positron emission tomography (PET), or single photon emission CT (SPECT). All of these methods have been previously utilized to quantify the functional defect of the lung and airway structure in CF (D. L. Chen, Atkinson, & Ferkol, 2013; D. L. Chen et al., 2006; D. L. Chen & Kinahan, 2010; Chua et al., 1994; Fain, Schiebler, McCormack, & Parraga, 2010;

Harris & Schuster, 2007; Y. Sun et al., 2011; Tzeng et al., 2007; Wielputz et al., 2013). Although each one of these methods provides a unique quantification of the lung structure and function, over the last 30 years QCT has become one of the most popular tools in lung studies. QCT's popularity is due to its ability to relate detailed airway and lung structure with lung function, it can provide objective phenotype for lung pathology, and it provides a wealth of data at high resolution with low quantitative cost (Aziz et al., 2007; Brody et al., 2004; Busacker et al., 2009; Castro et al., 2011; Echeveste et al., 2005; Folescu et al., 2012; Helbich et al., 1999; Matsuoka et al., 2008; Newman, Lynch, Newman, Ellegood, & Newell, 1994; Wielputz et al., 2013). The main drawback to using MRI or PET is their high scan cost and long scan time compared to CT where chest CT at fixed volume/ pressure takes only 30-40 seconds.

In this thesis, I used QCT for all my investigations. QCT was chosen due to its high spatial resolution, high signal to noise ratio and high acquisition rate. It can provide information about the lung such as: anatomical information about lobes and bronchial tree (Hu, Hoffman, & Reinhardt, 2001; Tschirren, Hoffman, McLennan, & Sonka, 2005; Ukil & Reinhardt, 2009), regional ventilation and perfusion. Moreover all the data are subject specific and use a standardized protocol.

An insight into ventilation in the various regions of the lung is essential for diagnosis and evaluation of pathological conditions. Abnormal regional ventilation can be an indication to abnormal tissue mechanical properties or breathing rate or airway structure or posture.

4.6. Using QCT for studying pulmonary function.

QCT provide a high resolution quantification of the pulmonary function by using image-registration to quantify the changes in intensity between two QCT images obtain at two points in the respiratory cycle (Christensen, Song, Lu, El Naqa, & Low, 2007; Guerrero et al., 2006; Reinhardt et al., 2008). Image registration is an excellent tool for studying regional lung ventilation (Castillo et al., 2009; Kilburn, 1984; Vreman, 2004). In addition, image registration can be used to differentiate between airway and parenchymal phenotypes (Klein, Staring, & Pluim, 2007).

In this study we used image registration to determine the spatial map that matches CT images collected at two lung volumes (TLC and RV) and to estimate regional ventilation and to deform the lung geometry. The outcome of regional ventilation was used to determine subject specific boundary conditions for subsequent computational fluid dynamics analysis (CFD).

In this thesis, I used the mathematical modelling technique CFD to investigate airflow characteristics and particle distribution and deposition non-CF and CF airways. CFD was developed over 50 years ago by engineers and mathematicians to solve heat and mass transfer problems in aeronautics, vehicle aerodynamics, chemical engineering and nuclear design and safety. CFD uses numerical analysis and computational algorithms to study and analyse problems that involve fluid flow. CFD is an alternative to experimental analysis in many areas of fluid dynamics, with its advantage of lower cost and greater flexibility (Bates, 2005). CFD was used in this study because it not only provides accurate predictions for the given boundary conditions, but it also provides potential explanations for the observations. CFD has been used before to study medical phenomena that cannot be tested experimentally. For example, other groups have previously used CFD to find the effect of differences

in patient-specific airway geometry on inhalational therapy in lung disease, such as chronic obstructive pulmonary disease and asthma (L. A. De Backer et al., 2012; Vinchurkar et al., 2012; Vos et al., 2013).

In this thesis, CFD analyses were conducted on QCT airway geometries. I used CFD to investigate the abnormal airway structure in CF and its impact on air velocity, airway resistance, and particle distribution and deposition. The outcome of these analyses could have important implications for targeting drug delivery and explain, in part, the regional distribution of lung disease in CF.

*“The world breaks everyone
and afterward many are
strong in the broken places”*

Ernest Hemingway

Chapter 5. Cell culture and animal models of cystic fibrosis

5.1. Introduction.

In vitro cell culture models and animal models of human disease are critical for understanding the fundamental mechanisms of pathophysiology and developing therapies. CF research has been dominated in the last two decades by the use of in vitro cell culture models and the in vivo CF mouse model. Significant knowledge has been gained from both models. However, both models have several limitations that hinder our understanding of CF disease pathogenesis. These limitations provided the opportunity and the need for the development of additional animal models from different species. In this chapter I will discuss all these models and the CF pig model which is the most relevant to this research.

5.2. CF in vitro cell culture models.

In vitro cell culture methods are very popular because of low cost, ease of production, and the fact that they do not require genetic modification compared to in vivo or ex vivo models. In addition, they do not require submission of animal

protocols or staff experienced in animal handling (Cain, 2013; Nichols, Niles, Vega, & Cortiella, 2013; Vernon, Clark, & Bressler, 2011). In vitro cell culture complexity can vary based on the hypothesis being tested. In vitro culture can be simple (only one or two cell types) or complex (multicellular culture). Both cultures have been used to test and understand the cell-based response, physiological function, pathologic changes, and cell reaction to drugs and toxins (Nichols et al., 2013). In CF, in vitro cell culture has been used to determine the precise nature of CF's ion transport defect. In 1984, through in vitro experiment it was demonstrated that CF eccrine sweat ducts (sweat gland found in virtually all human skin) are impermeable to chloride ions (Bijman & Quinton, 1984). In 1989, through an in vitro technique, the defective gene (*CFTR*) that was suspected to be the cause of CF disease was identified (B. Kerem et al., 1989; Riordan et al., 1989; Rommens et al., 1989). The gene function was confirmed when researchers were able to restore the ability of the CF cell to transport chloride by transferring a normal *CFTR* gene into in vitro epithelia cells of the airway and the pancreas from a CF patient (Drumm et al., 1990; Rich et al., 1990). Currently, in vitro cell culture is being used to test new methods of treating CF disease whether by assisting the channel process or correcting the *CFTR* gene disease causing defect (Chang et al., 2015; Cholon et al., 2014; Cooney, Singh, & Sinn, 2015; Kwilas et al., 2010; Sinha et al., 2015). In vitro cell culture is also used to understand the pathogenesis of the disease (Cain, 2013; Dekkers et al., 2013; Roschetto et al., 2015).

There are two common types of cell cultures: primary and cell lines. Primary cell culture is the culture that comprises of growing cells obtained directly from a subject (human or animal). These cells can be adherent cells (cells that require attachment for growth e.g. lung tissues, kidney, or liver) or suspension cells (cells that does not require attachment for growth e.g. lymphocytes). Primary cells have a shorter

lifespan. Cell lines can be designed to have limited lifespan or to be immortal (transformed under laboratory conditions). These cells can be cultured in submerged conditions or with an air liquid interface (Van Scott, Yankaskas, & Boucher, 1986; Whitcutt, Adler, & Wu, 1988; Wiesel, Gamiel, Vlodaysky, Gay, & Ben-Bassat, 1983).

5.3. CF mouse model.

Although epithelial cell cultures generated from human donors have provided us with valuable information in regards to CF disease, they lack differentiation patterns, the structural complexity of intact organs, and these cells are usually obtained from patients with ongoing lung inflammation and recurrent infections. Therefore, animal models are essential in the study of CF pathogenesis before the onset of infection and inflammation (Scholte et al., 2004). By using an animal model, investigators can track abnormalities at their onset and follow them over time.

Several animal models have been used in CF studies including mice, ferrets, and pigs. The interest in developing a CF animal model began in 1989, following the cloning of the CF gene by Riordan and colleagues (Riordan et al., 1989). This provided the breakthrough for the development of CF mouse strains with various mutations of the *CFTR* gene, just 3 years after the CF gene was found (Grubb & Boucher, 1999; Scholte et al., 2004). Currently, two main CF mice models are in use: *CFTR* nulls and *CFTR* gene specific mutations (Dickinson et al., 2002; O'Neal et al., 1993). These models and several other models that have been developed in the last 20 years have enabled pre-clinical understanding of CF disease pathogenesis, testing of compounds, and mutation-specific therapeutic approaches. However, during their lifespan, CF mice do not develop spontaneous pancreatic or respiratory tract infection typically found in humans with CF (Grubb & Boucher, 1999). Although,

mice can be used as a colonization model by challenging their respiratory system with *P. aeruginosa*, it still does not develop spontaneous infection like that observed in humans (Davidson & Rolfe, 2001). Despite the absence of infection in the CF mice, it has been observed that CF mice do show signs of excessive inflammation (Zahm, 1997), abnormal mucociliary clearance (MCC) (Cowley, Wang, Gosselin, Radzioch, & Eidelman, 1997), an increase in the number of goblet cells (Tarran et al., 2001), a decrease in the nasal airway surface liquid (ASL) height and abnormalities in intracellular nitric oxide synthase expression (Steagall et al., 2000).

It is still unknown why CF mice do not develop lung disease. However, there are multiple hypotheses that are currently being studied. Hypothesis-1, the submucosal glands are abundant in cartilaginous human airways; however, submucosal glands are not frequently present in mice lungs. Knowing that the submucosal gland has an effect in CF pathogenesis suggests that they might play a role in causing differences in the reaction to bacterial pathogens (Engelhardt et al., 1992; Plopper et al., 1983). Hypothesis-2, the mouse airways are covered with Clara cells, in contrast to ciliated cells in human airways (Engelhardt et al., 1992; Pack, Al-Ugaily, & Morris, 1981; Plopper et al., 1983). Hypothesis-3, the difference in the size and surface area between the human and mice airways would most probably affect particle deposition and clearance. Hypothesis-4, the life span of mice is not long enough to express the disease (Grubb, B.R., 1999). Hypothesis-5, absence of lung disease is due to lack of exposure to bacterial pathogens. Therefore, researchers have tried to challenge the CF mouse lung with bacteria such as *S. aureus*, *Haemophilus influenzae*, *P. aeruginosa*, and *Burkholderia cepacia* (Davidson et al., 1995; Kent et al., 1997; Khan et al., 1995; Scholte et al., 2004). The outcome of these studies is variable, as some have observed no difference between CF and non-CF mice; while, others have

observed lung disease characterized by parenchymal interstitial thickening, fibrosis, and inflammation (Kent et al., 1997). Although CF mice challenged with the above bacteria have shown signs of infection and inflammation, the pathology is different from human CF lung disease. For example, the histological studies showed that the mice lungs infected with *P. aeruginosa* show lymphoid hyperplasia, while in CF humans the lungs show neutrophil-dominated inflammation (Khan et al., 1995).

5.4. CF ferret model.

Most (90%) morbidity and mortality in CF is caused by repeated lung inflammation and infection (Boucher et al., 1997; Lands et al., 1992; Marcotte et al., 1986). The absence of lung abnormalities in CF mouse models has driven the need to develop an animal model with greater similarity in lung anatomy and biology to humans (Tebbutt, Wardle, Hill, & Harris, 1995; Zhu, Dor, & Cooper, 2007). One of these models that were recently developed is the CF ferret model (X. Sun et al., 2010).

CF ferrets has been developed using targeting with adeno-associated virus (rAAV). The virus introduced a stop codon and a neomycin cassette into exon 10 of the *CFTR* gene. This was done in ferret primary fibroblast cells (X. Sun et al., 2010). Through this process heterozygote (*CFTR*^{+/-}, the ferret has one functioning gene and one non-function disease causing gene) breeder pairs were developed. Similar to mice, there was no parental lethality associated with the heterozygote *CFTR* deficiency in CF ferrets (X. Sun et al., 2010).

At birth, CF ferrets failed to thrive compared to their wild type and heterozygous litter mates. 75% of the CF ferrets died in the first 36-48 hours due to meconium ileus, intestinal perforation and sepsis (when a infection occurs and the body develops an over-whelming immune response, releasing chemicals into the blood

stream triggering inflammation in multiple organs and damaging them). The remaining CF ferrets (25%) that passed stool, died in the first week of life due to malabsorption of nutrients from food and lung infection (X. Sun et al., 2010).

After birth, CF ferrets showed similar pathology to that observed in humans with CF (Oppenheimer & Esterly, 1973, 1975; X. Sun et al., 2010). First, in the pancreas, CF ferrets showed mild pancreatic disease similar to that found in humans with CF. CF ferrets' exocrine acinar ducts were swollen with inspissated secretions (thickened dehydrated secretion). This made CF ferrets an excellent model for CF related diabetes (CFRD), since they develop exocrine and endocrine pancreatic disease during the first few month of life. The CF ferret model has demonstrated that early pancreatic endocrine defects lead to hyper-secretion of insulin that was improperly regulated by glucose. As the CF ferrets age, they start to suffer from spontaneous hyperglycemia, glucose intolerance, and pancreatic destruction. All of these findings are associated with pancreatic destruction (Olivier et al., 2012; X. Sun et al., 2010).

Second, in the liver, CF ferrets demonstrated significant bile plugging compared to non-CF ferrets (Olivier et al., 2012; X. Sun et al., 2010). Newborn CF ferrets also had elevated plasma alanine aminotransferase and bilirubin levels (method used to test liver health by its ability to process old red blood cells and catalyze reaction) similar to those observed in CF infants suggesting early liver disease (X. Sun et al., 2010). Third, in the gallbladders, CF ferrets develop moderate lesions which include biliary cirrhosis, ductal hyperplasia, steatosis, and fibrosis. Surprisingly, CF ferrets have normal gallbladder at birth despite absence of cAMP-mediated current (Fisher et al., 2013).

Fourth, in the lungs, similar to humans, CF ferrets develop spontaneous lung infection. This includes mucous filled airways with alveolar sparing, atelectasis, and

air-trapping (X. Sun et al., 2010). At birth, CF ferrets demonstrates an abnormally elevated inflammation response compared to humans with CF. The outcome of a proteomics analysis on sterile caesarean-sectioned and natural-born ferrets compared to non-CF suggests that altered lung immunity may begin before birth. This may, in part, prime the lung for hyper-inflammation after the first bacteria exposure during birth and lead to rapid onset of lung infection (X. Sun et al., 2010). Therefore, CF ferrets require multiple antibiotics from birth to allow for a slow progress lung disease study, which might not be ideal for studying the early pathogenesis of CF lung disease.

5.5. CF pig model.

The absence of lung disease in the mouse model and the abnormally elevated inflammation response in the ferrets' respiratory system presented the need for a new CF animal model. The interest was high in finding an animal model that shared many anatomical, histological, biochemical, and physiological features with human lungs. Several animal models were considered for these studies. However, it can be observed that pigs share many anatomical, histological, biochemical, and physiological features with humans (Tebbutt et al., 1995; Zhu et al., 2007). The reproductive characteristics of pigs are also very favourable for development as a research model, pigs have a short gestational period, reach sexual maturity quickly, and produce 24 to 36 offspring per year when compared to the other animals (Tebbutt et al., 1995; Zhu et al., 2007). In addition, the pig is an excellent model for cardiovascular disease, obesity, diabetes, alcoholism, hypertension, cutaneous pharmacology and toxicology, and injury repair. In the same vein, pigs are being developed as a source of organs for xenotransplantation to humans (Zhu et al., 2007). Although pig airways are monopodial (multi daughter airways branches out of the

parent main branch at bud points along the length of the parent branch. The parent main branch extends to the apex of the lung. Also diameter of the parent branch and daughter branches decreases with at each bud point) and human airways are bipodial (Dichotomous, The tip of the parent branch divides to generate two almost equivalent daughter branches, daughter branches usually shorter than parent branch), the porcine bronchi show similar patterns of branching and histology, their percentages of submucosal gland in the airways and glycoprotein synthesis are similar to human airways, and both human and pigs have a similar respiratory immune system (Padst, 1994).

Development of a gene targeted CF pig model was not an easy process. Until 2008, gene targeted mammalian models of human genetic disease have not been reported in any species other than mice (Rogers, Hao, et al., 2008; Rogers, Stoltz, et al., 2008). The development of somatic cell nuclear transfer (SCNT) a laboratory technique for creating a cloned embryo using an ovum with a donor nucleus, and nucleus injection, has provided a pathway for the production of cloned sheep and numerous other animal species (Cibelli et al., 1998; Rogers, Hao, et al., 2008; Wilmut, Schnieke, McWhir, Kind, & Campbell, 1997). However, these techniques have many limitations. The homologous recombination using promoter-trap strategy in somatic cells results in low gene targeting efficiencies (Williams et al., 2003). Delivering a target vector through electroporation and lipid mediated transfection, which can deliver the target to high percentage of cells, results in random non-homologous integration (Vasquez, Marburger, Intody, & Wilson, 2001). Moreover, nuclear microinjection, which delivers the target vector directly to the nucleus, is not sufficient to deliver the target to large numbers of cells in a timely manner. These limitations decreased the success rate in creating a targeted gene mammal other than

the mouse, and works as a barrier to the development of other human genetic disease animal models (Thomas, Folger, & Capecchi, 1986).

Several different gene targeting approaches and techniques were used to disrupt *CFTR* in pig fibroblasts, but the most effective approach utilized a recombinant adeno-associated virus (rAAV1) as a vector to deliver a genetic construct targeting the *CFTR* gene. After creating SCNT embryos using male fetal fibroblasts, the embryos were transferred to surrogate females. *CFTR*-null heterozygotes were born and then mated to produce *CFTR*-null homozygotes. A similar strategy was also used to develop *CFTR*- Δ F508 homozygous pigs.

At birth, CF pigs have intestinal lesions, exocrine pancreatic destruction, gallbladder abnormalities, and early focal biliary cirrhosis. These findings are similar to those observed in humans with CF (Stoltz et al., 2010). Following surgical correction of the meconium ileus, CF pigs spontaneously develop lung disease within the first few months of life. In addition, studies in newborn CF pigs have now shown that a bacterial eradication defect exists in the CF pig lung as early as 8-12 hours after birth. In addition, when the newborn CF pig airway structure was compared with non-CF pigs, it was observed that CF airways are less circular, have smaller diameters, have irregular appearing cartilage rings, and contain abnormal appearing smooth muscle (Meyerholz et al., 2010). Furthermore, similar findings (smaller and irregular shaped airways in human CF infants and young children) have also been reported (Meyerholz et al., 2010). The irregularity and abnormality in the airway structure of newborn CF pig and human lungs raises an important question: how does the CF airway structure affect disease pathogenesis. Specifically, does it affect particle/bacterial deposition and clearance in the CF airways?

5.6. Conclusions.

In the previous chapters I highlighted that CF disease affects multiple organs in the human body, however most morbidity and mortality in CF is caused by progressive lung disease (Boucher et al., 1997; Lands et al., 1992; Marcotte et al., 1986). The aim of this thesis is to better understand the pathogenesis of CF lung disease. It was also highlighted in the previous chapter and in this chapter that there is a need to understand the early development of the CF lung prior to infection and inflammation. These studies are currently not possible in newborn humans with CF.

In this chapter I discussed all the models available to study the early stages of the disease. I found that in vitro models will not be suitable for this study due to the lack of structural complexity. In addition, the mouse model is not suitable due to the absence of lung disease (Tebbutt et al., 1995; Zhu et al., 2007). In addition, the CF ferret had an abnormally elevated early inflammation response in the respiratory system which is not ideal for our case (X. Sun et al., 2010). On the other hand, the CF pig model developed spontaneous lung disease within the first few months of life similar to that observed to humans and it has been a good model for studying early lung disease pathogenesis (Adam et al., 2013; Hoegger, Awadalla, et al., 2014; Hoegger, Fischer, et al., 2014; Meyerholz et al., 2010). I selected the pig model as the ideal model to investigate the effect of early airway structural abnormalities, observed in humans and pigs with CF, on disease pathogenesis.

It is important to note that there are various differences between all the current CF models. These differences in the severity of various aspects of CF organ disease in the mouse, pig and ferret models have revealed and will continue to elucidate new biologic discoveries about CFTR's role in organ physiology and how dysfunction of these processes leads to disease in humans. Comparing the differences and

similarities among these animal models will greatly enhance our understanding of the disease and accelerate the development of a cure for CF. It is also important to emphasize that differences among species in their ability to model CF will likely help to educate the field on what factors influence phenotypic variability seen in CF patients.

*“You must do things you
think you cannot do.”*

Eleanor Roosevelt

Chapter 6. Early airway structural changes in cystic fibrosis pigs as a determinant of particle distribution and deposition

6.1. Introduction.

Cystic fibrosis (CF) is caused by loss of cystic fibrosis transmembrane conductance regulator (CFTR) function and results in morbidity and mortality due to progressive lung disease (Quinton, 1990; Rowe, Miller, & Sorscher, 2005; Welsh M.J., 1996).

While significant efforts have identified a key role for infection and inflammation in CF airway disease, relatively little is understood regarding the early events in airway disease pathogenesis.

Our research group recently developed a porcine model of CF that mimics the phenotype of human CF lung disease, including bacterial infection susceptibility, inflammation, mucus accumulation, airway wall remodelling, and airway obstruction (Ostedgaard et al., 2011; Rogers, Hao, et al., 2008; Rogers, Stoltz, et al., 2008; Stoltz et al., 2010). An unexpected finding in the CF porcine model was that, at birth, prior to the onset of infection and inflammation, the CF airways displayed structural

abnormalities. These included a reduced calibre, a less circular shape, irregular-appearing cartilage rings, and abnormal-appearing airway smooth muscle bundles (Meyerholz et al., 2010). Similar observations have been reported in CF mice; and structural abnormalities have also been observed in infants and young children with CF (Bonvin et al., 2008; Meyerholz et al., 2010).

These observations raised the possibility that early airway structural abnormalities may be important in CF lung disease pathogenesis. The aim of this study is to quantify the effect of airway structural abnormalities on the global and local lung function. In this study, I used the mathematical modelling technique computational fluid dynamics (CFD) to investigate airflow characteristics and virtual particle distribution and deposition in newborn non-CF and CF pig airways. The outcome of these analyses could have important implications for targeting drug delivery and explain, in part, the regional distribution of lung disease in CF.

6.2. Methods.

6.2.1. CT imaging.

All animal studies were approved by the University of Iowa Animal Care and Use Committee. I used five non-CF (*CFTR* +/+, birth weight 1.1 ± 0.1 kg, tracheal cross-sectional area 17.9 ± 1.2 mm²) and five CF pigs (*CFTR* -/-, 1.2 ± 0.1 kg, tracheal cross-sectional area 9.9 ± 0.3 mm²) in this study. These pigs were anesthetized initially with intramuscular ketamine (20 mg/kg) and xylazine (2 mg/kg) and maintained with intravenous propofol. Pigs underwent tracheostomy with a 2.0-mm inner diameter endotracheal tube. I used succinylcholine to prevent spontaneous breathing during imaging. All imaging was performed on a dual-source CT scanner (Somatom Definition Flash: Siemens Medical Systems, Erlangen, Germany). Airway geometries were obtained from chest CT imaging performed during a breath hold at a fixed airway pressure of 20 cmH₂O.

Recent studies have shown that the upper airways are primarily responsible for laryngeal jet turbulence, which can affect airflow patterns in the lower airways (Alipour & Scherer, 2006; Brouns, Verbanck, & Lacor, 2007; Y. Choi & Wroblewski, 1998; C. L. Lin, Tawhai, McLennan, & Hoffman, 2007; Miyawaki, 2013; Yin, Choi, Hoffman, Tawhai, & Lin, 2013). However, in order to obtain the intra-thoracic airway geometry at fixed pressure, the pigs had to have a tracheostomy prior to undergoing a chest CT scan. This eliminated our ability to image the larynx from these animals. Therefore, for most pigs used in this study, prior to tracheostomy, I obtained a CT scan of the laryngeal/upper trachea area and added these regions for each animal to our computational model. At the start of the study a pair of non-CF and CF pigs were not scanned prior to tracheostomy. Thus I used the

larynx from scans of non-intubated non-CF and CF pigs that had similar upper tracheal cross-sectional areas.

6.2.2. Image analysis.

The larynx and intra-thoracic airways were segmented using Amira software (Visage Imaging, San Diego, CA), the average tracheal cross-sectional areas measured, and smoothed using the weighted Laplacian smoothing (Magics, Materialise, Ann Arbor, MI). The smoothed larynx geometry was merged with the fixed pressure intra-thoracic airway tree using the Boolean unite operation (Magics). This operation was performed on both non-CF and CF airways creating full non-CF and CF airway geometries, including both the larynx and intra-thoracic airways. The terminal branches of the smoothed airway tree were trimmed to ensure that their cross-sectional surfaces were near perpendicular to the centreline. The pig lung includes the left cranial (LCr) and caudal (LCa) lobes, and on the right the cranial (RCr), middle (RM), accessory (RAc), and caudal (RCa) lobes (Figure 6.1A). The main airways to all of these lobes were included in the non-CF and CF reconstructed airway geometries. The 3D airway tree reconstruction provided a realistic representation of both the porcine larynx and tracheobronchial tree (Figures 6.1A and 6.2A). For subglottic area measurements, CT image datasets were imported into Pulmonary Workstation 2.0 (VIDA Diagnostics, Iowa City, IA) and airway area measurements were obtained both at the smallest cross-sectional area in the subglottic region for each animal and at a fixed distance of 4.5 mm below the glottic opening.

The smoothed surface geometry of the airway tree was then meshed (by discretization of the airway tree from a continuous domain into a set of discrete sub-domains called elements) using Gambit software (Fluent, Lebanon, NH). To verify

that the solutions were independent of the mesh size, two unstructured mesh densities were generated and are referred to as the original and refined mesh. The original mesh consisted of $343,027 \pm 54,696$ nodes and $2,111,000 \pm 254,735$ tetrahedral elements. The refined mesh consisted of $1,281,000 \pm 131,796$ nodes and $7,416,000 \pm 842,812$ tetrahedral elements. A grid sensitivity test was then performed. Unless otherwise noted, all of the results presented are based on the refined mesh data, since this provides greater resolution for the analysis of the virtual particle trajectory pattern.

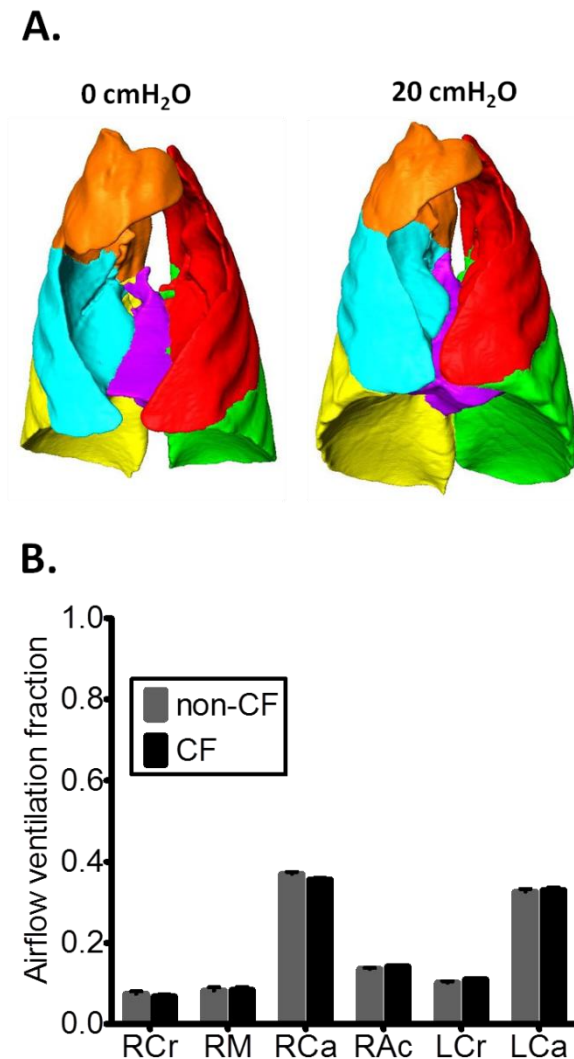


Figure 6.1. Lung structure and lobar airflow ventilation fraction acquired using computed tomography at 0 and 20 cm H₂O. (A) Front view of non-CF lung at 0 and 20 cmH₂O. The color codes indicate each individual lobe in the pig lung. Gold-right cranial (RCr), blue-right middle (RM), purple-right accessory (RAc), yellow-right caudal (RCa), red-left cranial (LCr), and green-left caudal (RCa). (B) Airflow ventilation fraction to each lobe in newborn non-CF and CF pigs (n = 5 for each genotype).

6.2.3. Computational fluid dynamics solver.

The airflow predictions were based on solution of the filtered continuity (eq. 6.1) and Navier-Stokes (eq. 6.2) equations of incompressible flow using an in-house large eddy simulation (LES).

$$\frac{\partial u_i}{\partial x_i} = 0 \quad (6.1)$$

$$\frac{\partial u_i}{\partial t} + u_j \frac{\partial u_i}{\partial x_j} = -\frac{1}{\rho} \frac{\partial P}{\partial x_i} + \nu \frac{\partial^2 u_i}{\partial x_j \partial x_j} \quad (6.2)$$

where u_i is the velocity component in the i direction, P is the pressure, ρ is the fluid density, ν is the kinematic viscosity, and ν_T is the subgrid-scale (SGS) turbulent eddy viscosity. The continuity equation was enforced by solving a pressure-Poisson equation.

The Vreman (Vreman, 2004) SGS model was implemented to yield $\nu_T=0$ for laminar flows (J. Choi, Tawhai, Hoffman, & Lin, 2009). As ρ is a constant, it can be factored into the pressure gradient and combined with P . For these simulations, ν is set to $1.7 \times 10^{-5} \text{ m}^2 \text{ s}^{-1}$ at ambient conditions. The governing equations were discretized using a characteristic Galerkin approximation together with a fractional four step algorithm that featured second-order accuracy in both time and space (C. L. L. Lin, H.; Lee, T.; Weber, L.J., 2005). The solver has been verified for flows under various conditions (J. Choi et al., 2009; Kumar, Tawhai, Hoffman, & Lin, 2009; C. L. Lin et al., 2007; Xia, Tawhai, Hoffman, & Lin, 2010).

I considered airflow at peak inspiration. Therefore, a parabolic velocity profile with a constant rate of 15 ml s^{-1} (Mortola, 1984) was imposed at the airway inlet. To employ physiologically consistent boundary conditions at the peripheral airway

segments, regional ventilation was assessed by measuring the increase in volume in each lung lobe for each pig from 0 to 20 cmH₂O. Flow rate at each boundary outlet was measured by quantifying the airflow ventilation fraction to each lobe (Figures 6.1A and 6.1B). If more than one airway in the segmented geometry supplied a lobe (e.g., the right and left caudal lobes), the airflow ventilation fraction to this lobe was divided between these airways based on their outlet diameter. For example, if in our geometry the lobe is supplied by two airways and the outlet diameter for the first airway is double the outlet diameter of the second, then the first airway outlet ventilation fraction would be double that of the second. Reynolds number (Re) was 102.00 ± 0.83 in the CF trachea and 73.43 ± 4.70 in the non-CF trachea ($p < 0.001$) (Miyawaki, Tawhai, Hoffman, & Lin, 2012). For lobar Reynolds and particle Stokes number calculations, I used the mean airflow velocity and cross-sectional area at the inlet of the airway supplying each lobe.

6.2.4. Lagrangian particle tracking algorithm.

The CFD simulations were then used to predict particle trajectories. For this study, spherical virtual particles were used with a density of water (1000 kg/m³) and ranged in size from 1- μ m to 10- μ m in diameter. Particle trajectory was computed using a Lagrangian tracking algorithm (Faiyazuddin et al., 2013). In general, particle distribution and deposition are dependent on the virtual particle size, air velocity, and particle inertia. Since I studied the transport of relatively large virtual particles and the air velocity in the model was constant over time, particle transport was based primarily on drag force and deposition was mainly due to impaction. Therefore, the Brownian motion associated with diffusion of the virtual particles was not considered in the algorithm. The governing equation used to predict particle transport is:

$$\frac{dv_{pi}}{dt} = f_{Di} + \frac{r_p - r_f}{r_p} g_i \quad (6.3)$$

where v_{pi} is the i-component particle velocity, g_i is the i-component of the gravitational acceleration, ρ_p is the particle density and was set to equal water density, ρ_f is the density of the air in which the particle travels, and f_{Di} is the particle drag force per unit mass. The drag force per unit mass (f_{Di}) was computed as:

$$f_{Di} = \frac{U_l}{Stk \cdot D_l} (v_{fi} - v_{pi}) \quad (6.4)$$

where v_{fi} is the fluid velocity interpolated from the fluid velocity field (u_i) at the particle location, U_l and D_l are the respective local velocity and length scales, and Stk is the Stokes number defined as:

$$Stk = \frac{U_l r_p d^2}{18mD_l} C_C \quad (6.5)$$

where d is the diameter of a particle and C_C is the Cunningham slip correction factor. Stokes number is typically characterized as a ratio of the particle stopping distance to the characteristic dimension of an obstacle (Longest & Hindle, 2012). Particles with a small Stokes number ($\ll 1$) follow streamlines, while particles with a large Stokes number (~ 1) deviate from curved streamlines.

At the start of every simulation, particles were initialized as a cylindrical bolus consisting of 10,000 spherical virtual particles located at the proximal larynx. All of the particles were distributed in a constant concentration (Faiyazuddin et al., 2013). Particles can exist in one of three states: moving, deposited, or escaped. To indicate the states of the particles as they travelled through the airway tree, I used three colour codes. The colour black indicated that the particle was moving through the airway.

Once a particle impacted the airway surface the color changed to red, indicating that the particle had been deposited. Particles were recognized as deposited if the shortest distance from the particle's centre of mass to the airway wall was less than the particle's radius. Particles were allowed to move all of the way to the lower tips of the computational airway tree if they were not deposited. Under these conditions, if a particle reached the airway tip without depositing, the particle was considered as escaped and its colour changed to blue. If a particle remained moving at the end of the simulation, without depositing or escaping, the colour of the particle remained black. The total simulation time was 400 ms and the time step used for the Lagrangian tracking of the particles was 1.65×10^{-6} s, below which there is no real improvement upon the simulation. Since I used a steady-state simulation with a fixed aspiratory flow rate and flow is essentially in the laminar regime in both non-CF and CF airways, a time-dependent fluid field was not required. Particle ventilation fraction was determined for the right lung (particles entering the right mainstem bronchus), left lung (particles entering the left mainstem bronchus), and right cranial lobe (particles entering the right cranial lobe bronchus) divided by the total number of particles entering the right mainstem, left mainstem, and right cranial lobe bronchi. I separated the right cranial lobe from the "right lung" since the right cranial lobe bronchus branches from the trachea and not the right mainstem bronchus.

6.2.5. Statistical analysis.

Data are presented as mean \pm standard error of the mean (SEM). For statistical analyses between groups, Student's t or Mann-Whitney tests were used. Differences were considered statistically significant at $P < 0.05$.

6.3. Results.

6.3.1. Airway structure in newborn non-CF and CF pigs.

First, I compared the airway structures from five non-CF and five CF newborn pigs. Similar to our prior observations (Meyerholz et al., 2010), the CF airways had a reduced lumen calibre (Figures 6.2A and 6.2B). Specifically, for the airway geometries used in the current study, the non-CF tracheal cross-sectional area was $17.9 \pm 1.2 \text{ mm}^2$ compared to the CF tracheal cross-sectional area of $9.9 \pm 0.3 \text{ mm}^2$ ($p < 0.001$). These measurements are consistent with our previously published findings [tracheal cross-sectional area $15.3 \pm 0.6 \text{ mm}^2$ for non-CF and $8.4 \pm 0.4 \text{ mm}^2$ for CF newborn pigs (Meyerholz et al., 2010)]. When I measured the subglottic area at a fixed distance below the glottis (4.5 mm), CF was smaller than non-CF (Figure 6.2B). However, when I measured the smallest cross-sectional airway area in this region, which was the glottic opening (above the fixed distance measurement), I found no difference between non-CF and CF (5.8 ± 0.6 vs. $5.6 \pm 0.5 \text{ mm}^2$, respectively). The right and left mainstem bronchi areas were also reduced in size relative to non-CF (Figure 6.2B).

6.3.2. Airflow characteristics in non-CF and CF airways.

The main aim of this study was to compare particle behaviour in newborn CF pig airways to non-CF. Therefore, I first used CFD to simulate airflow. Although the general outcomes of the simulation were predictable (e.g., smaller sized airways in CF lead to greater airflow velocity), I observed that non-CF:CF differences in airway structure as well as variations in subject-specific airway geometries had significant effects on airflow patterns and secondary flow which altered particle distribution and deposition patterns.

First, I examined airway pressure. While the pressure along the non-CF airway tree remained relatively constant, the narrower CF airway structure caused a greater pressure drop from the larynx to the lower airways (Figures 6.2A and 6.2C). For example, in the CF left mainstem bronchus the pressure was -21.00 ± 2.20 Pa compared to -10.35 ± 2.10 Pa in non-CF relative to laryngeal pressure (Figure 6.2C).

CFD modelling of air velocity revealed a number of differences between non-CF and CF. When a vertical plane of the air velocity contour was examined, a higher velocity was observed in the CF laryngeal region (1.28 ± 0.06 m.s⁻¹) compared to non-CF (0.92 ± 0.18 m.s⁻¹) (Figures 6.2A and 6.2D). I also observed the formation of an airflow jet in the glottic area in both non-CF and CF pigs. This jet develops as airflow rapidly accelerates through this narrowed region. Although the airflow velocity at the laryngeal region was higher in CF than non-CF it was not statistically significant. However, the average air velocity in the CF airway geometry was significantly greater than the average velocity in the non-CF airway geometry (1.57 ± 0.06 m.s⁻¹ vs. 0.84 ± 0.12 m.s⁻¹, $p < 0.002$). Finally, the increased velocity profile in the CF airway extended down to the carina region and the mainstem bronchi. Since airway resistance is dependent on both pressure difference and the volume flow rate, I examined the resistance in both non-CF and CF airways. I found that the resistance was significantly higher in CF compared to non-CF airways (Figure 6.2E). These findings collectively suggest that the narrowed airways in CF uniquely change airflow characteristics.

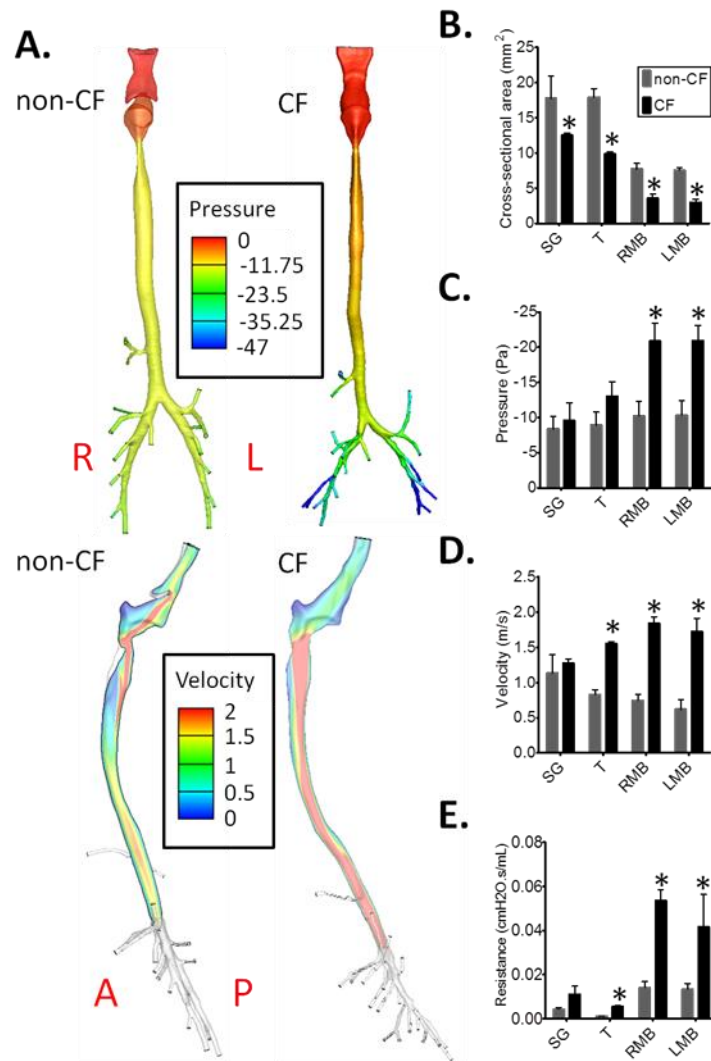


Figure 6.2. Computational fluid dynamic modeling of air pressure and velocity in newborn non-CF and CF porcine airways. (A) Air pressure (Pa) and velocity (m/s) in non-CF and CF airways. (B) The cross-sectional area in the subglottis (SG), the average along the tracheal (T), the right mainstem bronchus (RMB), and left mainstem bronchus (LMB) in non-CF and CF. (C) The pressure drop at the SG, T, RMB, and LMB in non-CF and CF. (D) The average air velocity at the SG, T, RMB, and LMB in non-CF and CF. (E) The average airway resistance in the area of the SG, T, RMB, and LMB in non-CF and CF. Data for B-E were obtained from horizontal slices extracted from the 3D airway geometry, perpendicular to the centreline using Tecplot. R denotes right side, L denotes left side, A denotes anterior, and P denotes posterior. * denotes statistical significance between non-CF and CF data ($p < 0.05$) ($n = 5$ for each genotype).

6.3.3. Effect of CF airway structural abnormalities on particle distribution and deposition patterns.

Particle distribution of 1, 5, and 10- μm particles in both non-CF and CF airway models was investigated. Figure 6.3 shows the distribution pattern for 10- μm particles at 50 and 400 ms in non-CF and CF airways. In the non-CF airway at $t = 50$ ms, most particles were in the glottic region and proximal trachea with minimal particle deposition (less than 50 out of 10,000). At $t = 400$ ms, I observed that particles in the trachea tended to deposit along the anterior surface of the airway tree. This was observed in three out of five non-CF pigs. In the other two non-CF pigs, I observed circumferential deposition around the trachea. In the CF airway at $t = 50$ ms, particles were travelling at a higher velocity compared to non-CF pigs. The higher particle velocity led to significantly higher deposition rate in CF airways at $t = 50$ ms (more than 200 out of 10,000). By $t = 400$ ms in the CF airway, most of the particles were either deposited or escaped from the computational domain (Figure 6.3). In contrast to the majority of the non-CF airways, particles deposited on both the anterior and posterior airway surfaces in all of the CF pig tracheas (Figure 6.3B). These differences in particle deposition patterns in both non-CF and CF pigs were caused by structural features in the individual tracheal geometries (Figure 6.4). Proximal to the tracheal bronchus, the porcine trachea angles posteriorly. I found that the steepness of this angle determined whether particles preferentially deposited on the anterior tracheal surface or not. In non-CF pig tracheas that exhibited anterior particle deposition, this tracheal angle was greater than in pigs with more uniform particle deposition patterns (anterior deposition alone 174.0 ± 0.7 degrees vs. 165.6 ± 1.2 degrees for tracheas with more uniform deposition, $p < 0.05$). The combination of glottic constriction followed by the steeper tracheal angle induces a centrifugal force

that skews the axial velocity and leads to the formation of secondary flow (Figure 6.4, upper panels). The skewed axial velocity near the anterior wall increases the likelihood of the particles travelling in that zone; thereby impacting and depositing along the anterior tracheal wall. In contrast, in two of the non-CF tracheas and all of the CF tracheas the axial velocity did not favour the anterior or posterior walls leading to more even particle deposition along the tracheal surface.

In general, particle ventilation fraction to the right and left lung was similar between genotypes except for 10- μm particles, in which more particles travelled to the right lung (excluding the right cranial lobe) instead of the left lung in CF (Table 6.1).

Interestingly, this asymmetry in particle ventilation occurred despite similar airflow ventilation to the right and left mainstem bronchi between non-CF and CF (Figure 6.1B). Particle Stokes number in the trachea was significantly different for 1- μm , 5- μm , and 10- μm particles (Table 6.1). However, in CF I only observed greater particle ventilation to the right lung (excluding the right cranial lobe) for 10- μm particles.

These data demonstrate that, in the newborn CF pig trachea, the particle ventilation fraction does not equal the airflow ventilation fraction when the particle Stokes number is greater than approximately 0.3 (Table 6.1). Interestingly, Darquenne et al. reported that when Stokes number was greater than 0.01 particle transport and airflow ventilation fraction were not equal in human airways (Darquenne, van Ertbruggen, & Prisk, 2011). Differences in absolute Stokes values could be related to variations in porcine vs. human airway geometries, the airway inlet flow rates, or modelling technique employed.

CFD modelling also predicted that deposition efficiency was greater in CF compared to non-CF for 5 and 10- μm particles (Figure 6.5). These differences were most significant in the airways included in the geometry supplying the right accessory,

right caudal, left cranial and left caudal lobes (Figure 6.6). Collectively these results demonstrate that as particle size increases, particle deposition is greater in CF than non-CF airways. Moreover, there are regional differences in particle ventilation and deposition between non-CF and CF.

Particle size	Left mainstem bronchus		Right mainstem bronchus		Right cranial bronchus		Tracheal Stokes number	
	non-CF	CF	non-CF	CF	non-CF	CF	non-CF	CF
1 μm	0.42	0.51	0.49	0.42	0.09	0.07	0.0009	0.0021
	0.41	0.43	0.51	0.49	0.08	0.08	0.0006	0.0022
	0.43	0.39	0.52	0.54	0.05	0.07	0.0010	0.0021
	0.43	0.45	0.49	0.47	0.08	0.08	0.0004	0.0067
	0.42	0.47	0.50	0.52	0.08	0.01	0.0011	0.0032
	0.43 \pm 0.01	0.44 \pm 0.02	0.50 \pm 0.01	0.48 \pm 0.02	0.08 \pm 0.01	0.06 \pm 0.01	0.0008 \pm 0.0001	0.003 \pm 0.0008[#]
5 μm	0.40	0.52	0.50	0.40	0.1	0.08	0.0225	0.0824
	0.43	0.45	0.49	0.48	0.08	0.07	0.0145	0.0721
	0.40	0.38	0.55	0.56	0.05	0.06	0.0256	0.1161
	0.41	0.40	0.48	0.54	0.11	0.06	0.0109	0.0702
	0.39	0.42	0.52	0.52	0.09	0.06	0.0184	0.2453
	0.41 \pm 0.01	0.44 \pm 0.03	0.51 \pm 0.01	0.49 \pm 0.03	0.09 \pm 0.01	0.06 \pm 0.01	0.018 \pm 0.003	0.117 \pm 0.033[#]
10 μm	0.46	0.35	0.40	0.61	0.14	0.04	0.0736	0.3299
	0.44	0.28	0.43	0.56	0.13	0.16	0.0901	0.2885
	0.35	0.30	0.56	0.67	0.09	0.03	0.0579	0.4645
	0.35	0.26	0.57	0.71	0.08	0.03	0.1023	0.2807
	0.35	0.28	0.48	0.68	0.17	0.04	0.0436	0.2813
	0.40 \pm 0.02	0.30 \pm 0.02[#]	0.49 \pm 0.04	0.63 \pm 0.03[#]	0.12 \pm 0.02	0.06 \pm 0.03	0.073 \pm 0.011	0.329 \pm 0.035[#]

Table 6.1. Particle ventilation fraction in non-CF and CF airways. The particle ventilation fraction and particle Stokes number in the trachea for each corresponding animal are shown.

Particle ventilation fraction was determined for the right lung (particles entering the right mainstem bronchus), left lung (particles entering the left mainstem bronchus), and right cranial lobe (particles entering the right cranial lobe bronchus) divided by the total number of particles entering the right mainstem, left mainstem, and right cranial lobe bronchi. I separated the right cranial lobe from the “right lung” since the right cranial lobe bronchus branches from the trachea and not the right mainstem bronchus. Each line represents data from a pair of non-CF and CF pigs. Mean \pm SEM for the group are in bold. #denotes statistical significance between non-CF and CF data ($p < 0.05$).

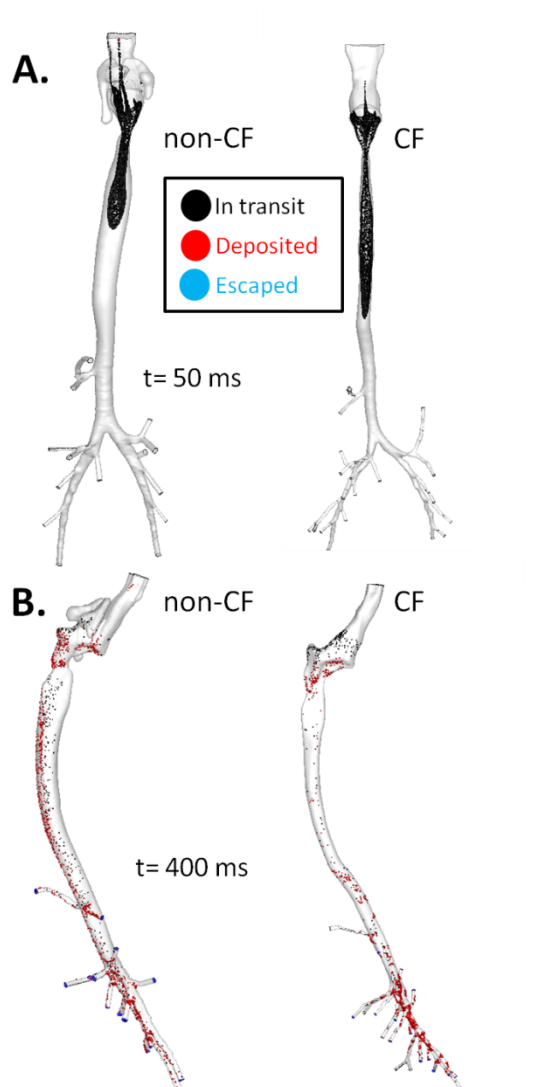


Figure 6.3. Particle distribution and deposition in non-CF and CF airways. 10- μm particle flow path and deposition pattern at 50 and 400 ms in non-CF and CF airways. Particle colour denotes particle states (black = in-transit, red = deposited, blue = escaped).

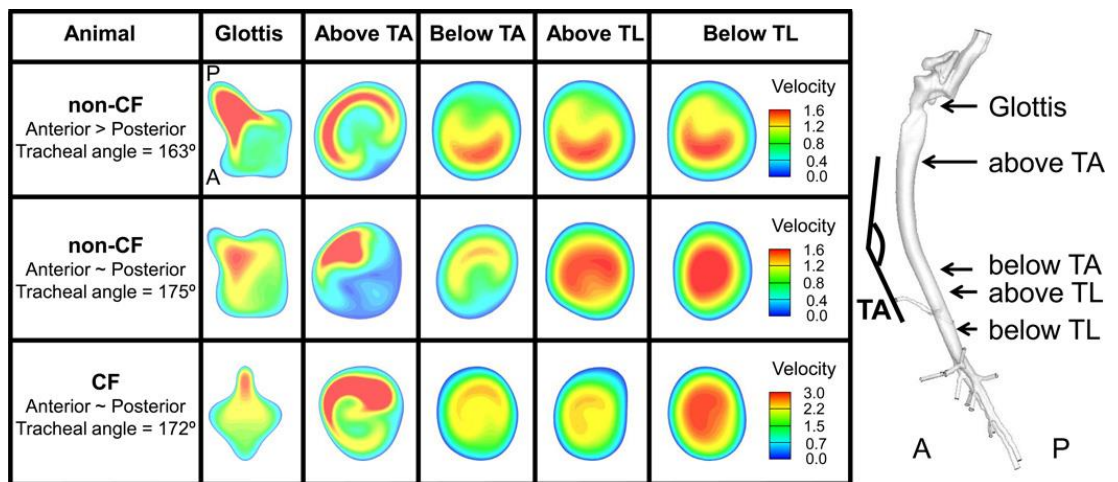


Figure 6.4. CFD prediction of airflow characteristics in non-CF and CF trachea. Shown are tracheal cross-sections at 5 different levels: glottis, above the tracheal angle (above TA), below the tracheal angle (below TA), above the tracheal lobe (above TL), and below the tracheal lobe (below TL). Top panel shows data from a representative non-CF trachea where greater anterior particle deposition was observed. Middle and lower panels show data from a representative non-CF trachea (middle panel) and CF trachea (lower panel) where more circumferential particle deposition was observed. The velocity profile ($\text{m}\cdot\text{s}^{-1}$) at each level is shown. A denotes anterior, and P denotes posterior. TA denotes tracheal angle.

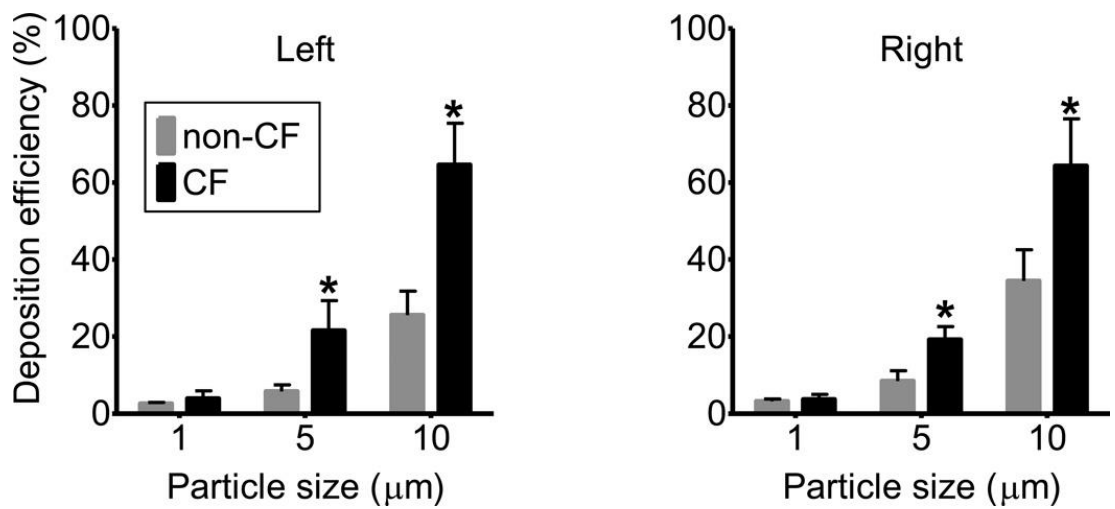


Figure 6.5. The effects of increasing particle size on deposition efficiency for the left and right lung. Particle deposition efficiency was defined as the number of particles depositing in the right (excluding the right cranial lobe since the right cranial lobe bronchus branches from the trachea) or left lung divided by the number of particles that entered the right or left lung, respectively. * denotes statistical significance between non-CF and CF data ($p < 0.05$) ($n = 5$ for each genotype).

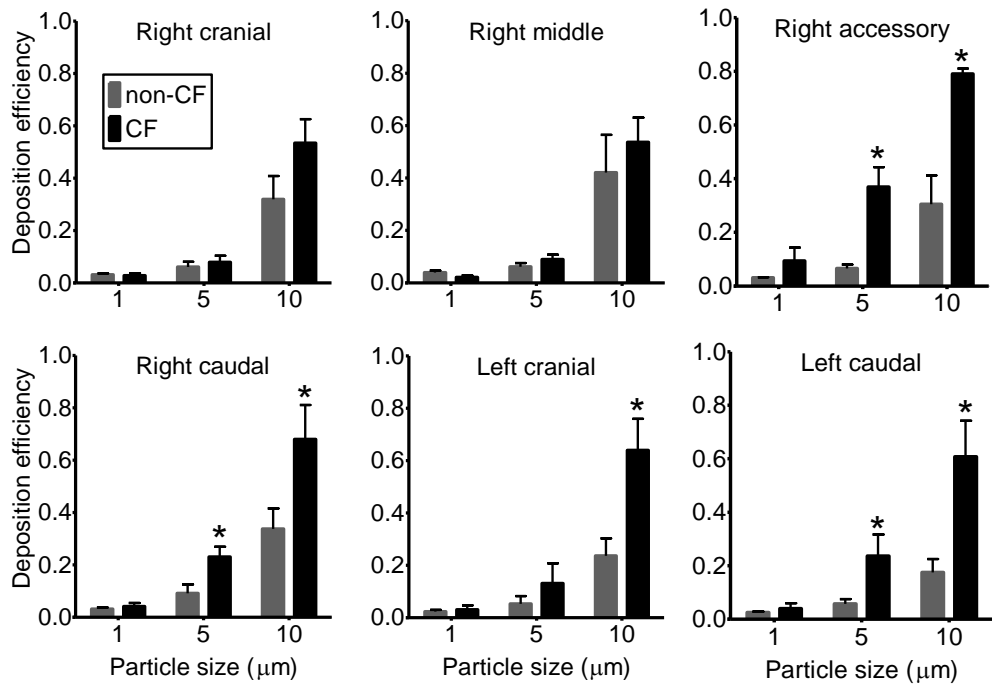


Figure 6.6. Particle deposition efficiency *f* for lobar airways in non-CF and CF airway geometries. Shown are the effects of increasing particle size on particle deposition efficiency for lobar airways included in non-CF and CF airway geometries. Particle deposition efficiency was defined as the number of particles depositing in a specific lobar airway divided by the number of particles that entered that lobar airway. * denotes statistical significance between non-CF and CF data ($p < 0.05$) ($n = 5$ for each genotype).

6.3.4. Factors that cause higher particle deposition in the CF airway.

I observed that the CF airway had a greater efficiency of particle deposition (Figures 6.5 and 6.6). With increasing particle size, the Stokes number increased in both non-CF and CF airways (Table 6.2). Compared to non-CF, I found a significantly greater Stokes number at the inlet of the airways supplying the right middle, right accessory, right caudal, left cranial, and left caudal lobes which could account for the greater particle deposition in these CF airways (Table 6.2). Particle Stokes number at the inlet of the airway supplying the right middle lobe was also increased despite no increase in particle deposition in this airway. The lack of an increase in particle deposition in the CF right middle lobe airway is in part due to a low Reynolds number (Table 6.2). Therefore, the reduced airway diameter and increased air velocity in the CF airways increases the likelihood that particles will deviate off the streamline and deposit on the airway surface.

Lobes	Particle Stokes Number				Reynolds number	
	5 μ m		10 μ m		non-CF	CF
	non-CF	CF	non-CF	CF		
Right Cranial	0.036 \pm 0.007	0.037 \pm 0.004	0.142 \pm 0.030	0.147 \pm 0.018	62.0 \pm 8.3	63.5 \pm 4.6
Right Middle	0.035 \pm 0.008	0.078 \pm 0.014 [#]	0.140 \pm 0.031	0.316 \pm 0.057 [#]	64.5 \pm 6.2	87.4 \pm 8.8
Right Accessory	0.038 \pm 0.006	0.073 \pm 0.014 [#]	0.152 \pm 0.024	0.295 \pm 0.054 [#]	45.1 \pm 2.7	61.7 \pm 4.5 [#]
Right Caudal	0.018 \pm 0.003	0.117 \pm 0.033 [#]	0.073 \pm 0.011	0.469 \pm 0.132 [#]	144.3 \pm 6.4	276.5 \pm 35.1 [#]
Left Cranial	0.028 \pm 0.004	0.082 \pm 0.022 [#]	0.111 \pm 0.015	0.327 \pm 0.089 [#]	65.8 \pm 6.0	103.3 \pm 8.7 [#]
Left Caudal	0.017 \pm 0.003	0.064 \pm 0.011 [#]	0.069 \pm 0.013	0.255 \pm 0.044 [#]	131.7 \pm 8.6	225.0 \pm 13.1 [#]

Table 6.2. Particle Stokes number and Reynolds number at the airway inlet of each individual lobe in non-CF and CF newborn pigs. #denotes statistical significance between non-CF and CF data ($p < 0.05$) ($n = 5$ for each genotype).

6.3.5. Enhanced particle ventilation to the right CF lung.

I next used our CFD predictions to understand why 10- μm particles preferentially travelled to the right lung in CF despite equal airflow ventilation to both the right and left lungs. Particle trajectory is controlled by both drag and body force (eq. 6.3). Body force is dependent on gravity; however our initial studies (data not shown) demonstrated that gravity produced a minimal affect on particle deposition and distribution in both non-CF and CF. These findings led us to exclude gravity from simulations and thus ignore the effect of body force on particle trajectory. Therefore, I only focused on drag, which opposes particle motion (eq. 6.4) (K. Hussain, Hussain, Mansoor, & Briddon, 2011). Drag is dependent on particle size, inertia, Stokes number, and velocity (eqs. 6.3 and 6.4).

I investigated how particle, airway, and airflow characteristics integrate to cause more particles to deviate to the right lung in CF. In general, 10- μm particles in CF had a higher inertia, larger Stokes number, and greater velocity than in non-CF. Analysing particle trajectory over time, I found that larger particles followed the secondary flow in the CF airways (Figures 6.7A and 6.7B). Secondary flow developed, in part, due to a greater glottic constriction ratio (subglottic area/tracheal area) (in CF 1.36 ± 0.04 vs. 0.99 ± 0.11 in non-CF, $p < 0.05$). The effect of the glottic constriction ratio can be observed in Figure 6.4 where the subglottic narrowing skews axial velocity towards the right side of the trachea causing secondary flow development in this region. This high velocity zone extended into the CF right mainstem bronchus ($1.51 \pm 0.05 \text{ m}\cdot\text{s}^{-1}$ in the right vs. $1.12 \pm 0.07 \text{ m}\cdot\text{s}^{-1}$ in the left mainstem bronchus, $p < 0.05$) and particles were preferentially directed towards the right leading to higher particle ventilation to the right lung at the level of the mainstem carina bifurcation (Figures 6.4 and 6.7C). This right-left asymmetry in

particle distribution was further enhanced by a steeper branching angle of bifurcation for the right mainstem bronchus in CF (Figures 6.8A and 6.8B). Figure 6.8C shows the formation of the particle bolus while entering the right and left mainstem bronchi and highlights the preferential distribution of particles to the right lung in CF.

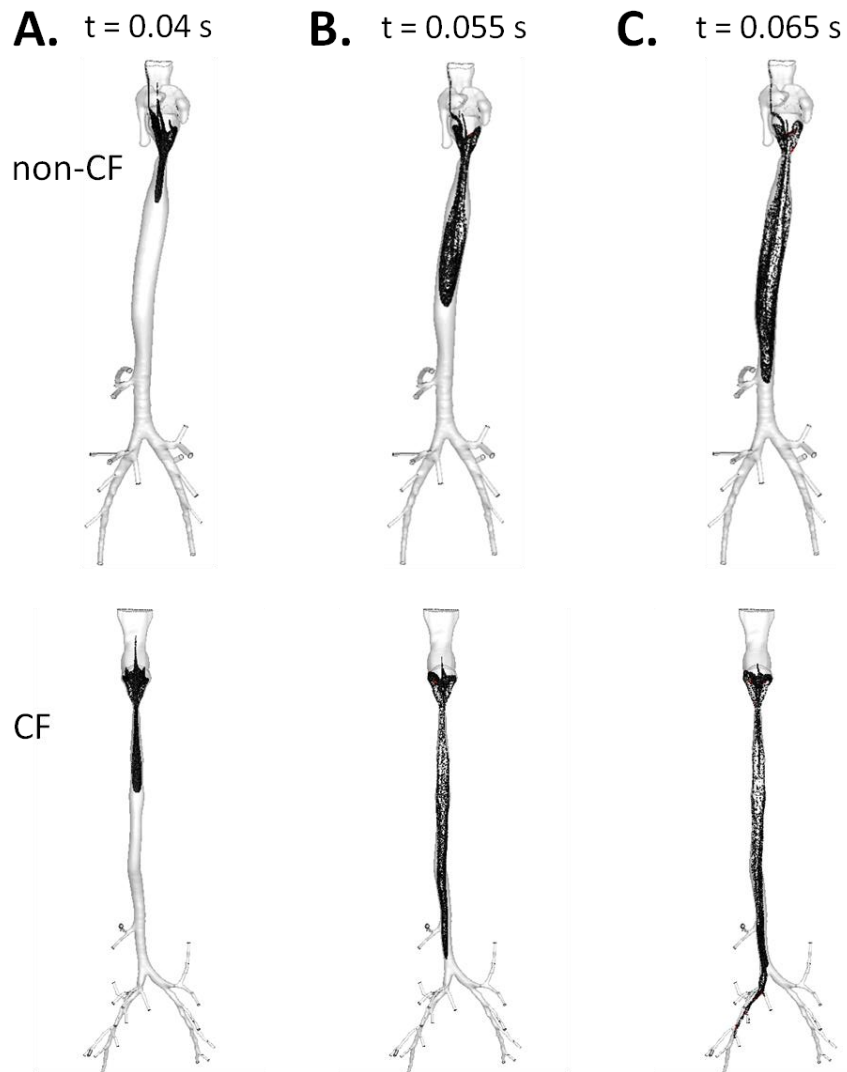


Figure 6.7. 10- μm particle trajectory in newborn non-CF and CF porcine airways. (A) Particle trajectory in non-CF and CF airways at 0.04 s. Note the formation of a fork shape at the front tip of the particle bolus in CF indicating that the particles follow a secondary flow. (B) Particle trajectory in non-CF and CF airway at 0.055 s. Note the particles tend to travel near the right side of the trachea. (C) Particle trajectory in non-CF and CF airways at 0.065 s. The particles are coloured based upon their status - black = in-transit and red = deposited.

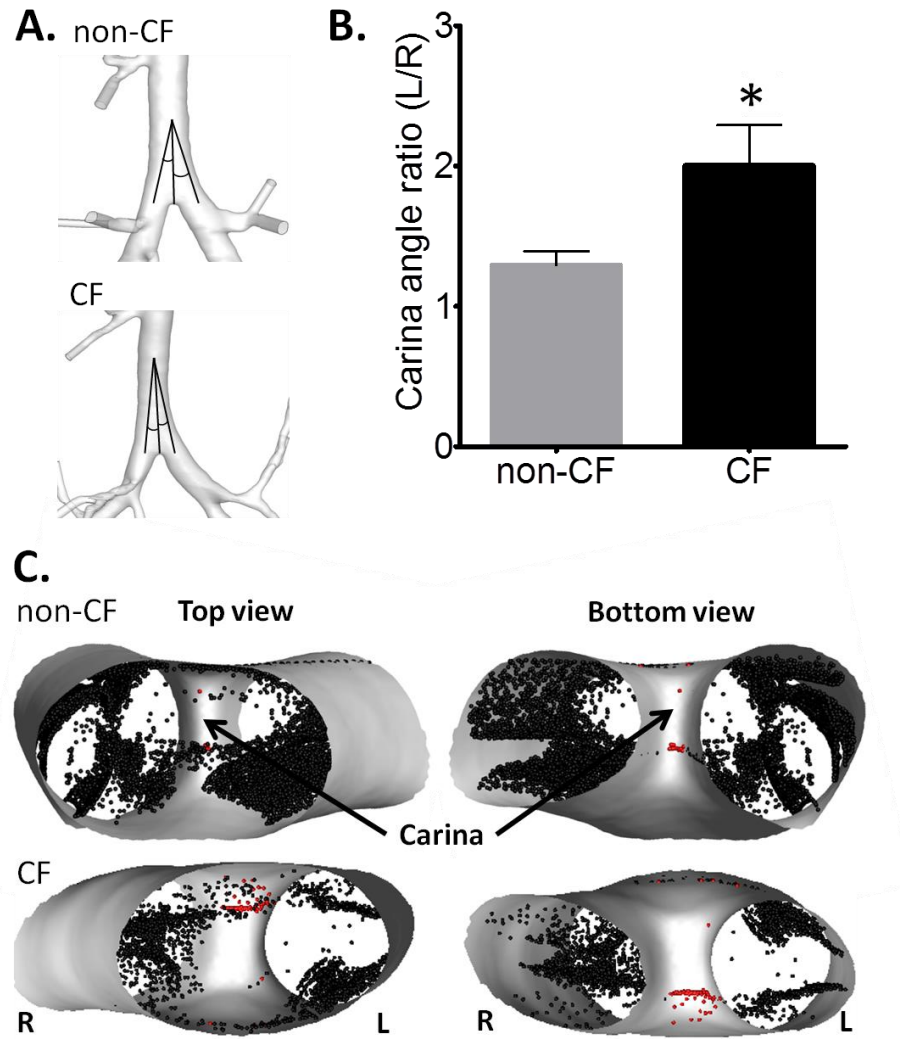


Figure 6.8. The effect of the carina bifurcation angle relative to the trachea on particle ventilation to the right and left lung. (A) Visual comparison between non-CF and CF carina position, and bifurcation angle to right and left main stem bronchus relative to the trachea. (B) The bifurcation angle ratio of the carina relative to the trachea. Note the carina angle ratio was computed by dividing the angle of the left mainstem bronchus by right mainstem bronchus. * denotes statistical significance between non-CF and CF data ($p < 0.05$) ($n = 5$ for each genotype). (C) The formation of the particle bolus while entering the right and left mainstem bronchi. The particles are coloured based upon their status - black = in-transit and red = deposited. R denotes right side and L denotes left side.

6.4. Discussion.

This work aimed to study numerically the effect of airway structural abnormalities on airflow characteristics and aerosol particle distribution and deposition patterns in newborn CF pigs. The CFD model predicted that CF airways have a higher air velocity and pressure drop compared to non-CF airways. The higher air velocity increased particle deposition in CF. Moreover, I found that particles larger than 5- μm preferentially distributed to the right lung in CF due to the skewed axial velocity and formation of secondary flow in the trachea. Thus, our computational model shows that the irregular airway structure in CF has a significant effect on the airflow pattern and subsequently on particle distribution and deposition.

Several of our findings provide potential explanations for the observation of enhanced particle ventilation to the right lung. First, the higher air velocity in the CF airway caused particles to travel faster in the trachea. Second, the particle Stokes number was higher in CF airways, suggesting that these particles would not follow the airflow streamline and their transport would be dependent on their inertia impaction. Third, the irregular structure (glottis constriction ratio, tracheal angle, carina angle) of the CF airways drove particles to travel near the wall due to secondary flow. Finally, as the particles travelled near the wall, particle velocity decreased and a greater number of particles followed the airflow streamline to the right lung at the level of the carina bifurcation.

Our study has several advantages and caveats. Advantages include: 1) A numerical model was used because it not only provides accurate predictions for the given boundary conditions, but it also provides potential explanations for the observations.

2) The findings of this study are likely generalisable to newborn CF pig airways

since I were able to perform CFD analysis on a number of subjects. 3) I were able to perform CFD modelling on airway trees from newborn CF pigs, thereby studying the primary effect of congenital airway narrowing in CF and eliminating secondary effects from infection, inflammation, and mucus obstruction. While our findings are consistent with recent experimental and stochastic aerosol studies (Brown & Bennett, 2004; Brown, Zeman, & Bennett, 2001; K. Hussain et al., 2011; M. Hussain, Renate, & Werner, 2011; Martonen, 1993; Sturm, 2011; Sturm & Hofmann, 2006), several caveats exist. 1) The airway geometry was assumed to be rigid in this study.

Although physiologically the airway structure is deformable, this study only predicts the flow at peak inspiration. Therefore, having a deformable model is much more computationally expensive since I predict the flow at fixed pressure. 2) Our CFD analyses are based upon newborn airway trees that might differ with growth, increasing airway size, and disease progression. Future studies using airway geometries from older CF pigs will likely be informative. 3) It is possible that mesh size influences results of airway and particle behaviour. To test the influence of mesh size I conducted a grid sensitivity test on a pair of non-CF and CF pigs (approximately two million versus ten million elements). I found that particle deposition, tracheal airflow velocity, and pressure drop were similar for the two mesh sizes studied [particle deposition efficiency for 10- μm particles in the trachea: 14% vs. 15% (non-CF) and 37% vs. 35% (CF); tracheal airflow velocity: 0.82 $\text{m}\cdot\text{s}^{-1}$ vs. 0.89 $\text{m}\cdot\text{s}^{-1}$ (non-CF) and 1.53 $\text{m}\cdot\text{s}^{-1}$ vs. 1.49 $\text{m}\cdot\text{s}^{-1}$ (CF); pressure drop: 8.4 Pa vs. 7.3 Pa (non-CF) and 12.5 Pa vs. 13.2 Pa, refined mesh vs. original mesh respectively]. These findings suggest that the observed differences in particle distribution and airflow characteristics are independent of mesh size. Importantly, prior studies have reported good agreement between particle deposition model predictions and measured data, suggesting that our predictions are likely valid

(Hofmann, Sturm, Fleming, Conway, & Bolt, 2005; Lambert, O'Shaughnessy, Tawhai, Hoffman, & Lin, 2011; Miyawaki et al., 2012). 4) Although beyond the scope of the current study, future simulations with transient pulsatile flows will be important to conduct since differences in predicted particle distribution and deposition might be expected to occur when studied under transient flow versus steady-state conditions (current study).

What is the significance of our findings? First, many CFD and CT-based airway geometry studies of airflow and aerosols (therapeutic or pollutant) are based on airway geometries from healthy subjects or used non-physiological based boundary conditions, which may not provide an accurate description of aerosol behaviour in diseased airways. Results from our study show that I was able to make predictions on realistic non-CF and CF airway geometries, and that important differences exist dependent upon congenital airway abnormalities. More recently, other groups have used a similar approach to ours (functional imaging based computational fluid dynamics with the same type of boundary conditions) to find the effect of differences in patient-specific airway geometry on inhalational therapy in lung disease, such as chronic obstructive pulmonary disease and asthma (L. A. De Backer et al., 2012; Vinchurkar et al., 2012; Vos et al., 2013). Second, many therapeutics for CF airway disease are delivered by inhalation. A better understanding of the CF airway and how airway size and shape influences particle/aerosol deposition and distribution in the lung is critical for targeted delivery of aerosolized treatments to people with irregular airway morphology. Development of submicron particle technology for therapeutic aerosols could be particularly important for lung diseases in which airway narrowing exists, either from a congenital etiology or due to disease progression such as in asthma or CF where mucus accumulation, airway wall thickening, or airway constriction leads to airway narrowing (Faiyazuddin et al., 2013; C. L. L. Lin, H.;

Lee, T.; Weber, L.J., 2005; Longest & Hindle, 2012; Tian, 2011). In the setting of airway narrowing in CF, improved drug delivery and deposition to the small airways is more likely to occur with submicron particles. By performing CFD analyses on human- and disease-specific airway geometries, more efficient and better targeting of inhaled therapies may be achieved (Byron et al., 2010; Corley et al., 2012; L. A. De Backer et al., 2012; Ma & Lutchen, 2009; Vinchurkar et al., 2012; Vos et al., 2013). Third, our comparison of airflow characteristics and particle distribution and deposition pattern in non-CF and CF airways has significant implications for understanding disease pathogenesis in the CF lung.

How do these findings help us better understand the pathogenesis of CF airway disease? First, when bacteria are inhaled into the lung, the airway surface has antimicrobial factors that destroy invading microorganisms. However, both humans and newborn pigs with CF have an impaired ability to kill these inhaled bacteria (Pezzulo et al., 2012; Rowe et al., 2005; Stoltz et al., 2010). I hypothesize, based upon results from the current study, that early in CF a significantly greater fraction of inhaled particulate matter and microbes will deposit in the CF airways. This increased microbe deposition on the CF airway surface, combined with the impaired ability to kill bacteria, could overwhelm the airway host defences and be an important determinant of early CF lung disease. Although no studies have specifically examined this question in early CF, both modelling predictions and experimental results show regional differences in particle deposition in the adult CF lung (Brown & Bennett, 2004; Brown et al., 2001). These findings could correlate to greater bacterial deposition on the airway surface. Furthermore, with disease progression airway lumen obstruction occurs in CF secondary to mucus accumulation and this airway narrowing might be expected to cause similar effects and/or worsen the congenital abnormalities (Sturm, 2011). It will be interesting in

future studies to determine if particle deposition patterns obtained from newborn CF airway geometries predict the sites of airway disease development later in CF. These studies would be difficult to perform in humans, but feasible in the CF pig model.

Second, there is increasing evidence that human CF lung disease, including airflow obstruction, is present earlier than originally thought; even within months after birth (Hoo et al., 2012; Mott et al., 2013; Sly et al., 2009). However, technical and ethical constraints limit our ability to investigate the human lung at even earlier time points. Our CFD data predict an increased airway resistance (the presence of airflow obstruction) in CF pigs on the day that they are born. Since our research group previously reported that the CF pig airways lack infection, inflammation, or mucus accumulation at birth (Stoltz et al., 2010), our findings suggest that, in CF, airflow obstruction can occur in the absence of airway inflammation or mucus build-up. These findings have important implications for the timing and type of therapeutics used to treat early CF lung disease. Third, in humans, CF-related lung disease has a known proclivity for the right lung (Brody et al., 2004; Davis et al., 2007; Maffessanti, Candusso, Brizzi, & Piovesana, 1996; Mott et al., 2013; Santis, Hodson, & Strickland, 1991). The reason(s) for this right-sided predominance is unknown. Potential explanations have included a higher rate of micro aspiration/reflux into the right mainstem bronchus or preferential mucus accumulation and/or impaired mucus removal from the right lung. Alternatively, our modelling data support the idea that secondary flow in the CF airways promotes greater particle ventilation and deposition to the right lung in newborn CF pigs. If a greater number of inhaled particles and bacteria land in the right lung, then this could potentially explain higher rates and more severe disease in the right lung in CF.

6.5. Conclusion.

In conclusion, our results suggest that early structural abnormalities in the newborn CF airway might contribute to the pathogenesis of CF lung disease and may be a significant determinant of the regional distribution of CF lung disease. Moreover, these findings could have important implications for the development of inhaled therapeutics in CF.

*“If nature were not
beautiful, it would not be
worth studying it, and life
would not be worth living”*

Henry Poincare

Chapter 7. Computational fluid dynamics modelling of airflow and particle deposition in older cystic fibrosis pigs

7.1. Introduction.

Cystic fibrosis (CF) is the most common life-shortening recessively inherited disease. It is caused by loss of cystic fibrosis transmembrane conductance regulator (CFTR) function and results in defective lung host defence which is the primary cause for morbidity and mortality due to progressive lung disease (Quinton, 1990; Rowe et al., 2005; Welsh M.J., 1996). While significant efforts have identified a key role for infection and inflammation in CF airway disease, relatively little is understood regarding the early events in airway disease pathogenesis.

Recent development of a porcine CF model that mimics the phenotype of human CF lung disease have provided us with the opportunity to investigate the disease in its early stages (Awadalla et al., 2014). The pig model mimics bacterial infection susceptibility, inflammation, mucus accumulation, airway wall remodelling, and airway obstruction in humans with CF (Ostedgaard et al., 2011; Rogers, Hao, et al.,

2008; Rogers, Stoltz, et al., 2008; Stoltz et al., 2010). An unexpected finding in the CF porcine model was that, at birth, prior to the onset of infection and inflammation, the CF airways displayed structural abnormalities. These included a reduced calibre, a less circular shape, irregular-appearing cartilage rings, and abnormal-appearing airway smooth muscle bundles (Meyerholz et al., 2010). Similar observations have been reported in CF mice; and structural abnormalities have also been observed in infants and young children with CF (Bonvin et al., 2008; Meyerholz et al., 2010). These findings have prompted further research in this area. A recent study using mathematical modelling predicted that these airway abnormalities in newborn CF pigs have a direct impact on particle behaviour. Particles larger than 5- μm were predicted to ventilate more to the right lung compared to the left in CF, despite equal ventilation to the right and left in CF pigs. Moreover, higher deposition in the lower right lobe was observed compared to the upper right in CF pigs. In addition the deposition efficiency in CF pig's lower lobe was greater compared to non-CF (Awadalla et al., 2014).

As CF pigs age, malnutrition due to CF pancreatic and gastrointestinal disease slows the pigs growth rate leading to persistently smaller airways in CF, which is also observed in young children with CF (Haeusler et al., 1994; Stettler et al., 2000). Since the CF airways have reduced bacterial killing abilities and abnormal mucus properties (Hoegger, Fischer, et al., 2014; Pezzulo et al., 2012). Within weeks from birth, airway infection and inflammation takes place in CF pigs. This would likely lead to further remodelling to the irregular CF airways structure due to the mucus plugging and presence of infection and inflammation.

In this study, I used the mathematical modelling technique computational fluid dynamics (CFD) to investigate airflow characteristics and particle distribution and

deposition in three week old non-CF and CF pig airways. CFD analyses were conducted on multi-detector row computed tomography (MDCT) airway geometries. I then used in-house computer programs to predict how the abnormal structure of the CF airway impacts air velocity, airway resistance, and particle distribution and deposition. The outcome of these analyses could have important implications for targeting drug delivery and explain, in part, the regional distribution of lung disease in CF.

7.2. Methods.

7.2.1. CT imaging.

All animal studies were approved by the University of Iowa Animal Care and Use Committee. I used five non-CF at three weeks of age (*CFTR* +/+ , birth weight 10.8 ± 1.1 kg, tracheal cross-sectional area 63.4 ± 8.4 mm²), and five CF pigs at three weeks of age (*CFTR* -/-, 7.1 ± 1.5 kg, tracheal cross-sectional area 23.9 ± 4.5 mm²) in this study. These pigs were anesthetized initially with intramuscular ketamine (20 mg/kg) and xylazine (2 mg/kg) and maintained with intravenous propofol. Pigs were intubated for the studies with a 4-mm inner diameter endotracheal tube. I used succinylcholine to prevent spontaneous breathing during imaging. All imaging was performed on a dual-source CT scanner (Somatom Definition Flash: Siemens Medical Systems, Erlangen, Germany). Airway geometries were obtained from chest CT imaging performed during a breath hold at a fixed airway pressure of 20 cmH₂O.

Recent studies have shown that the upper airways are primarily responsible for laryngeal jet turbulence, which can affect airflow patterns in the lower airways (Alipour & Scherer, 2006; Brouns et al., 2007; Y. Choi & Wroblewski, 1998; C. L. Lin et al., 2007; Miyawaki, 2013; Yin et al., 2013). However, in order to obtain the intra-thoracic airway geometry at fixed pressure, the pigs were intubated prior to a chest CT scan. However, I have been fortunate to have obtained a CT scan of the laryngeal/upper trachea prior to the intubation. These laryngeal/upper trachea scans were not obtained under fixed pressure and the glottis opening ratio (ratio between glottis constriction cross-sectional area and tracheal cross-sectional area) was not the same in all pigs scanned. Since I am interested in examining the effect of the

structural abnormality in CF the intra-thoracic airway and the scope of this study cannot cover the laryngeal/upper trachea, I had to keep the cross-sectional area of laryngeal/upper trachea consistent in all pigs included in this study with respect to genotype. Meaning I measured the averaged laryngeal/upper trachea cross-sectional areas in non-CF and CF. Then I adjusted the cross-sectional area of each animal's laryngeal/upper trachea with respect to their genotype. This adjustment in the cross-sectional area was conducted on the 3D geometry of laryngeal/upper trachea obtained from segmenting (tracing) the airways in the laryngeal/upper trachea CT scan data. This allowed us to keep the effect of laryngeal/upper trachea region consistent between animals with respect to genotype.

Since the laryngeal/upper trachea was scanned prior to intra-thoracic airways, I had to obtain a 3D geometry from each scan (by tracing the airways in CT data) then attach the geometries together creating one airway that includes both laryngeal/upper trachea and intra-thoracic airways. To ensure that the angle of attachment is consistent in each genotype to the average tracheal angle in that genotype, I measured the angle of the trachea from the glottis to the carina in non-CF and CF scan prior to tracheostomy. Then I averaged the angle in non-CF and CF respectively. This gave us a specific angle on which the trachea should be attached in non-CF and CF to represent a physiologically correct tracheal angle. The larynx and intra-thoracic airways were segmented using Amira software (Visage Imaging, San Diego, CA), the average tracheal cross-sectional areas measured, and smoothed using the weighted Laplacian smoothing (Magics, Materialise, Ann Arbor, MI). The smoothed larynx geometry was merged with the fixed pressure intra-thoracic airway tree using the Boolean unite operation (Magics). This operation was performed on both non-CF and CF airways creating full non-CF and CF airway geometries, including both the larynx and intra-thoracic airways.

For the CFD modelling, I simulated airflow at the peak of tidal volume inspiratory cycle. Tidal volume is dependent on the weight (Serpa Neto et al., 2012). I found that the pig's weight at three weeks of age is heterogeneous with respect to genotype. Thus is not physiologically correct to assume the same tidal volume on both genotypes. Therefore I had to calculate the average tidal volume for non-CF pig and CF pigs. The three week old CF pigs have lower weight and lung size (approx 40 percent smaller) compared to non-CF pig. I measured tidal volume using the relationship between tidal volume and the pig's weight (8mL/kg). I then used the tidal volume to measure the flow rate for each pig by assuming that both non-CF and CF pigs have the same respiratory rate (Greve, 2012).

To employ physiologically consistent boundary conditions at the peripheral airway segments, regional ventilation was assessed by measuring the increase in volume in each lung lobe from 0 to 20 cmH₂O. Flow rate at each boundary outlet was measured by quantifying the airflow ventilation fraction to each lobe (Figures 7.1A and 7.1B). The program then divides the flow rate at each terminal branch by flow rate at the inlet, and the outcome is the fraction of air being ventilated at the boundary outlet.

For subglottis area measurements, CT image datasets were imported into Pulmonary Workstation 2.0 (VIDA Diagnostics, Iowa City, IA) and airway area measurements were obtained 7 mm below the glottic opening. To summarize three programs were used, Amira to segment the airways, Magics to smooth the airways and prepare the airway geometry for CFD study, and Pulmonary Workstation 2.0 to verify Amira's measurements.

7.2.2. Image analysis.

I used Amira software which is a semi-automated airway and lung segmentation software. The software outputs three dimensional (3D) airways geometry at 20 cmH₂O (Awadalla et al., 2014). The geometry is then smoothed on Magics software, and the terminal branches are trimmed to ensure that their cross-sectional surfaces were near perpendicular to the centreline.

The smoothed surface geometry of the airway tree was then meshed (by discretization of the airway tree from a continuous domain into a set of discrete sub-domains called elements) using Gambit software (Fluent, Lebanon, NH). To verify that the solutions were independent of the mesh size, two unstructured mesh densities were generated and are referred to as the original and refined mesh. The original mesh consisted of 524,327 nodes and 3,286,412 tetrahedral elements. The refined mesh consisted of 1,137,168 nodes and 8,632,215 tetrahedral elements. A grid sensitivity test was then performed. Unless otherwise noted, all of the results presented are based on the refined mesh data, since this provides greater resolution for the analysis of the particle trajectory pattern.

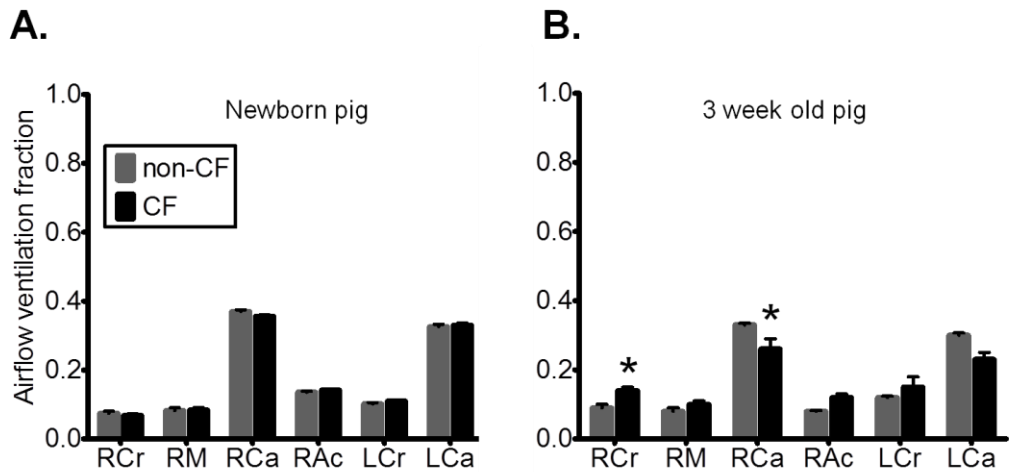


Figure 7.1. Lobar airflow ventilation fraction as the lung expands from 0 to 20 cm H₂O in non-CF and CF pigs at two time point birth and 3 weeks after. (A) Airflow ventilation fraction to each lobe in newborn non-CF and CF pigs (n = 5 for each genotype). RCr denotes right cranial, RM denotes right middle, RAc denotes right accessory, RCa denotes right caudal, LCr denotes left cranial, LCa denotes left caudal. (B) Airflow ventilation fraction to each lobe in 3 week old non-CF and CF pigs (n = 5 for each genotype). * denotes statistical significance.

7.2.3. Computational fluid dynamics solver.

The same method in [Chapter 6.2.3](#) was used in this study.

7.2.4. Lagrangian particle tracking algorithm.

The same method in [Chapter 6.2.4](#) was used in this study. However, a small modification was made. Considering that the flow is Turbulent in non-CF and CF pig's airways, full time dependent fluid field was used in the simulation. In this study I used constant flow at the inlet the simulation time was 2.5 seconds in which the flow takes 1 second to fully develop. The data files obtained every 0.006 of a second in the last second of the simulation is then used to provide a time dependent particle flow data.

7.2.5. Statistical analysis.

Data are presented as mean \pm standard error of the mean (SEM). For statistical analyses between groups, Student's t or Mann-Whitney tests were used. Differences were considered statistically significant at $P < 0.05$.

7.3. Results.

7.3.1. Demographics, lung, airways characteristics in newborn and three week old non-CF and CF pigs.

I studied CF pig airways three weeks after birth. First, I decided to investigate the demographics of three week old non-CF and CF pigs and then compare it to the newborn pig's demographic data. Newborn CF pigs have the same size and body weight compared to non-CF (Table. 7.1). However, only three weeks after birth I observed statistically significant differences in CF pig size and weight compared to non-CF. CF pigs weighed about three Kg less, and their femur length was also reduced (non-CF 66.0 ± 2.6 vs. CF 55.5 ± 1.5 mm, $P < 0.05$) (Table. 7.2).

Second, I analysed lung properties of three week old non-CF and CF pigs at two different lung pressures (0 cmH₂O vs. 20 cmH₂O) and compared it to newborn. In newborn CF pigs, at both pressures, there were no statistically significant differences in lung volume or in radiographic density of the computed x-ray tomography of the pig's lung quantified by Hounsfield unit scale (Table. 7.1). Three weeks after birth, at both pressures, I observed that CF pigs had smaller lung volume which was statistically different when compared to non-CF pigs (Table. 7.2). Also the increase in the volume going from 0 cmH₂O to 20 cmH₂O in three week old CF pigs was significantly greater compared to non CF (in non-CF 386.6 ± 46.5 vs. in CF 231.9 ± 25.4 cm³, $P < 0.05$). A difference was also observed in the Hounsfield units increase from 0 cmH₂O to 20 cmH₂O (in non-CF -333.3 ± 10.0 vs. in CF -290.6 ± 10.2 , $P < 0.05$).

Third, I studied the expansion of each lobe in the lung in relation to the whole lung when the pressure was increased from 0 cmH₂O to 20 cmH₂O in newborn and three

week old non-CF and CF pigs. In newborn CF pigs, I found no statistical significance in each lobe expansion ratio compared to non-CF. However, by three weeks of age I observed an increased volume expansion ratio in the upper lobes and a decreased volume expansion ratio in the lower lobes. This was statistically significant in the right lung (Figure. 7.1). Interestingly, in newborn CF pigs I previously reported, significantly greater particle ventilation to the right lung and significantly greater deposition in the right lower lung (Awadalla et al., 2014).

Fourth, I measured and compared the major airways diameter, perimeter and cross-sectional area (CSA) between newborn and three week old non-CF and CF pigs. In newborn and three week old CF pigs, the airway major, minor, equivalent diameter, CSA, and perimeter of the trachea was statistically smaller when compared to non-CF at zero centimetres of water to twenty five centimetre of water pressure (Average trachea perimeter at newborn, at 0 cmH₂O, non-CF 11.8 ± 0.6 vs. CF 9.3 ± 0.6 , at 20 cmH₂O, non-CF 13.6 ± 0.4 vs. CF 9.9 ± 0.3 mm, $P < 0.05$) (Average trachea perimeter at three weeks of age, at 0 cmH₂O, non-CF 24.9 ± 0.3 vs. CF 13.3 ± 0.7 , at 20 cmH₂O, non-CF 31.6 ± 0.6 vs. CF 17.2 ± 0.7 mm, $P < 0.05$) (Table. 7.1 and 7.2) (Figure. 7.2). Also, the ratio of increase of the trachea's major, minor, and equivalent diameter, CSA, and perimeter with increasing the pressure from 0 cmH₂O to 20 cmH₂O was statistically significant in newborn and three week old CF pigs when compared to non-CF. In addition, I observed smaller airway CSA in all of the major airways including the subgottic region and right and left mainstem bronchus in CF compared to non-CF, both at newborn and three week old time point (Figure. 7.2) (Awadalla et al., 2014).

CF pig growth is retarded compared to non-CF, which is was also observed in young children with CF (Haeusler et al., 1994; Stettler et al., 2000). This, in part, explains

the smaller lung volume found in the three week old CF pigs compared to non-CF. Therefore it is expected, due to the absence of lung volume difference at birth and its presence at three weeks of age, that the fold difference between non-CF and CF will increase at three weeks after birth compared to a day after birth. To explain this further, if I subtract the trachea CSA for each individual non-CF pig from the average trachea CSA in CF pigs the fold difference going to be higher as pigs get older due to their slowed growth. However, we may inquire if this increase in fold difference is significant at three weeks of age compared to newborn pig. I found that this difference was significant at three weeks of age compared to newborn pigs (newborn 1.9 ± 0.1 vs. three weeks old 3.3 ± 0.2 fold, $P < 0.05$).

Thus far, I found that at birth, non-CF and CF pigs have similar weight, lung size and similar distribution of air to each lobe. However, CF pig airways are significantly smaller compared to non-CF. In contrast, at three weeks of age, CF pigs have lower body weight, smaller lung size, different air distribution to each lobe and smaller airways compared to non-CF. These findings suggest that airflow characteristics and particle deposition and distribution will be likely different between newborn and older non-CF and CF pigs.

		Non-CF	CF
Demographic	Sample size	5	5
	Age, days	0	0
	Weight	1.1 ± 0.1	1.3 ± 0.1
0 cmH ₂ O	Lung volume	55.8 ± 4.2	51.2 ± 4.9
	Average Hounsfield units value	-599.0 ± 11.6	-582.8 ± 24.8
	Trachea major diameter	3.9 ± 0.2	3.2 ± 0.1 #
	Trachea minor diameter	3.6 ± 0.2	2.7 ± 0.1 #
20 cmH ₂ O	Lung volume	121.0 ± 11.1	114.8 ± 12.5
	Average Hounsfield units value	-803.4 ± 4.0	-789 ± 5.9
	Trachea major diameter	4.5 ± 0.1	3.4 ± 0.1 #
	Trachea minor diameter	4.0 ± 0.1	2.9 ± 0.1 #

Table 7.1. The demographical and physiological data from all the newborn non-CF and CF pigs selected for the study of lung structure and function. Age units is in days. Weight in kilograms (kg). Lung volume in millilitres (mL). Trachea major and minor diameter in millimetre (mm). The physiological data represents the lung at two inflation position 0 cmH₂O and 20 cmH₂O. # denotes statistical significance between non-CF and CF ($p < 0.05$).

		Non-CF	CF
Demographic	Sample size	4	5
	Age, days	27 ± 1.4	23.2 ± 0.8
	Weight	10.6 ± 0.5	7.1 ± 0.7 #
0 cmH ₂ O	Lung volume	320.1 ± 19.2	194.4 ± 17.4 #
	Average Hounsfield units value	-376.6 ± 29.2	-428.4 ± 24.4
	Trachea major diameter	8.9 ± 0.4	4.7 ± 0.3 #
	Trachea minor diameter	6.7 ± 0.4	3.6 ± 0.1 #
20 cmH ₂ O	Lung volume	706.7 ± 71.2	426.4 ± 41.0 #
	Average Hounsfield units value	-710.9 ± 28.2	-719.1 ± 16.5
	Trachea major diameter	10.7 ± 0.2	5.8 ± 0.2 #
	Trachea minor diameter	9.6 ± 0.3	5.1 ± 0.2 #

Table 7.2. The demographical and physiological data from all the 3 week old non-CF and CF pigs selected for the study of lung structure and function. Age units is in days. Weight in kilograms (kg). Lung volume in millilitres (mL). Trachea major and minor diameter in millimetre (mm). The physiological data represents the lung at two inflation position 0 cmH₂O and 20 cmH₂O. # denotes statistical significance between non-CF and CF ($p < 0.05$).

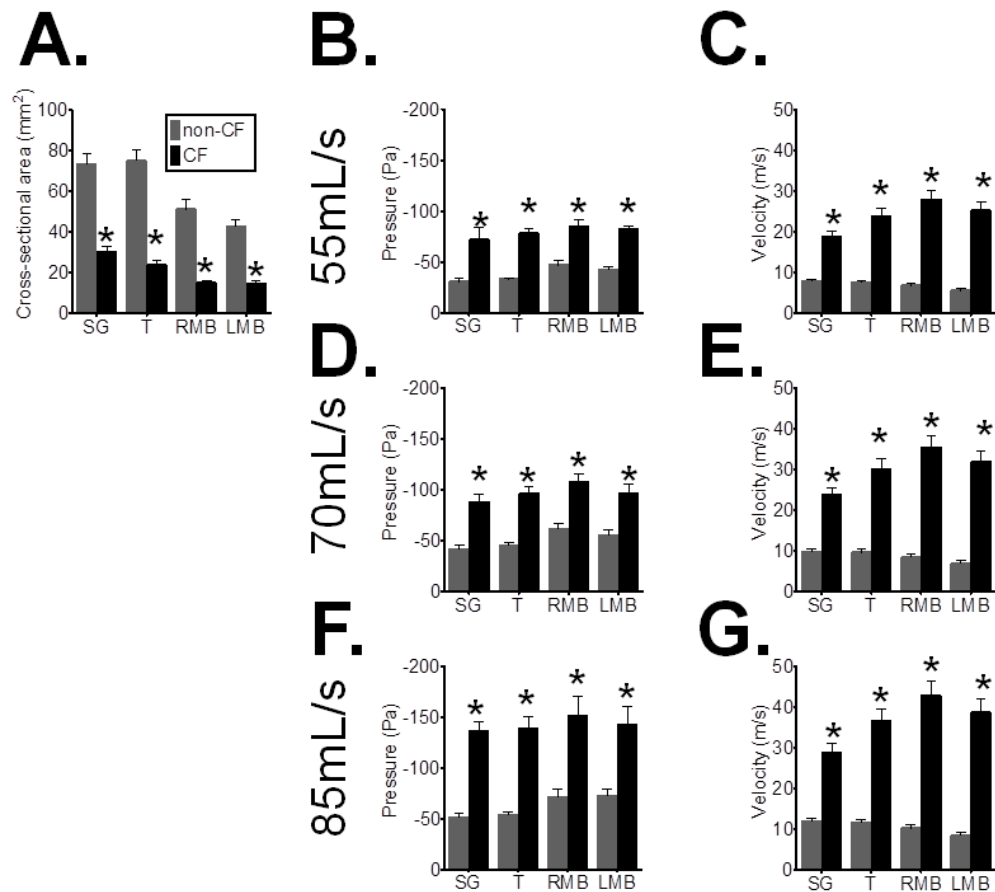


Figure 7.2. Airway cross-sectional area, air pressure, and velocity obtained from computational fluid dynamics modelling of three week old non-CF and CF porcine airways. (A) The cross-sectional area in the subglottis (SG), the average along the tracheal (T), the right mainstem bronchus (RMB), and left mainstem bronchus (LMB) in non-CF and CF. (B) The pressure drop at the SG, T, RMB, and LMB in non-CF and CF with inhalation flow rate of 55 ml/s. (C) The average air velocity at the SG, T, RMB, and LMB in non-CF and CF with inhalation flow rate of 55 ml/s. (D) The pressure drop at the SG, T, RMB, and LMB in non-CF and CF with inhalation flow rate of 70 ml/s. (E) The average air velocity at the SG, T, RMB, and LMB in non-CF and CF with inhalation flow rate of 70 ml/s. (F) The pressure drop at the SG, T, RMB, and LMB in non-CF and CF with inhalation flow rate of 85 ml/s. (G) The average air velocity at the SG, T, RMB, and LMB in non-CF and CF with inhalation flow rate of 85 ml/s. * denotes statistical significance.

7.3.2. Airflow characteristics in three week old non-CF and CF pig airways.

The striking differences in lung volume, lobar air distribution, and airway size and prompted us to further study the effect of all these factors on airflow characteristics in non-CF and CF three week old pigs. I used CFD to study airflow characteristics in these pigs. Our goal was to study airflow and particle distribution at peak tidal volume inspiration. However, the three week old CF pigs have lower weight and lung volume compared to non-CF, therefore using the same flow rate was not appropriate. I computed the tidal volume for both non-CF and CF pigs using the relationship between tidal volume and body weight (8 millilitres per kilograms) (Serpa Neto et al., 2012). I used a respiratory rate of 20 breaths per minute. Therefore, each breath takes roughly 3 seconds and thus, if I assume that the inspiration: expiration ratio is 1:2, the inspiration takes roughly 1 second. Hence, the non-CF and CF pig will inhale its tidal volume in approximately 1 second.

Based on the tidal volume weight relationship, the non-CF pig average inspiratory flow is roughly eighty-five millilitre per second and the CF pig inspiratory flow is approximately fifty-five millilitre per second. Comparing the outcome of the simulation at two different flow rates for each genotype can be confusing. Therefore, I simulated airflow for each genotype at fifty-five (the predicted flow rate for CF), seventy (average of the predicted non-CF and CF flow rate), and eighty-five (the predicted flow rate for non-CF) millilitres per second.

After running the simulation, I analysed airflow pressure drop and airflow velocity in the airway of three week old non-CF and CF pigs and compared it to the newborn non-CF and CF pig data. In newborn pigs, in regards to pressure drop no statistical

difference was observed in the subglottis and trachea (Awadalla et al., 2014).

However, for the three week old pigs, I found that the pressure drop is higher in the CF subglottic region and trachea compared to non-CF at all flow rates studied (Figure. 7.2). Even when comparing the two genotypes using weight representative flow rates, 85ml/s in non-CF and 55ml/s in CF, I found that the pressure drop in the subglottic region and trachea was still statistically significant. The increased pressure drop was also observed in the next three airway generations analysed. This increased pressure drop is due to two factors. First, the CF subglottis and trachea CSA are smaller compared to non-CF, and the fold difference between non-CF and CF airway CSA in three week old pigs is 1.1 ± 0.1 fold greater in subglottis and 1.4 ± 0.4 fold greater in trachea compared to newborn (P value less than 0.05). Second, the glottis constriction ratio (subglottis cross-sectional area divided by trachea cross-sectional area) causes a greater pressure drop leading, in part, to elevated pressure drop in CF.

Next I inspected the airflow velocity in non-CF and CF three week old pigs. I found that, as would be predicted due to decreased airway cross-sectional area in CF, airflow in CF airways was statistically greater compared to non-CF at all flow rates and in almost all of the major airways supplying each lobe (LMB, RMB, UR, MR, LR, UL,LL airways) (Figure. 7.2). Although, this difference was predictable when comparing each genotype at the same flow rate, this difference persisted when the two genotypes were compared using weight representative flow rates (85ml/s in non-CF and 55ml/s in CF). For example, in the trachea, using weight representative flow rates, the airflow velocity in non-CF was 11.6 ± 0.9 compared to 23.7 ± 2.0 in CF ($P < 0.05$). In another major airway, for example supplying right cranial lobe, using weight representative flow rates, the airflow velocity in non-CF was 4.9 ± 0.4 compared to 17.9 ± 1.5 in CF ($P < 0.05$).

It is important to note that although the velocity is statistically higher in the trachea of the three week old CF pig compared to non-CF at weight representative flow rates, the Reynolds number is not statistically different. This means that when I compare 85ml/s in non-CF to 55ml/s in CF, I'm indeed comparing at controlled Reynolds number.

It might be argued that I should have conducted the comparative simulation between non-CF and CF pigs by controlling velocity in the trachea (controlled velocity means the airflow velocity in the trachea is not statistically different when I compare non-CF and CF) rather than Reynolds number. However, in the case of controlled trachea velocity the flow rate in CF will be half the current predicted flow rate value which was calculated at the peak of tidal volume inspiration. It is important to note that even at half tidal volume in CF the airflow velocity in the airway supplying the right cranial lobe will still be statistically higher in CF compared to non-CF (in non-CF 4.9 ± 0.4 vs. in CF 7.0 ± 0.6 , $P < 0.05$). I chose to control the Reynolds number since it provides the most physiologically accurate description for this current study.

7.3.3. Particle distribution and deposition patterns in non-CF and CF three week old pigs.

Through our analysis of three week old CF airways, in comparison to non-CF, I have observed that CF pigs have smaller lung volume, lobar air distribution, and airway size compared to non-CF. Moreover, our CFD analysis have also indicated that even if I use genotype and weight specific flow rates and control for Reynolds number I still observe higher airflow, pressure drop, and airflow resistance in three week old CF pigs. Also, the higher airflow velocity and smaller diameter in CF is an indicator

for a high Stokes number. All of these findings suggested that particle behaviour in the airways of three week old CF pigs would be different than non-CF.

After running the particle simulation; in all our subjects, I computed lobar particle ventilation fraction. Lobar particle ventilation fraction is the number of particles that entered a specific lobe over the total number of particles that entered all of the lobes in lung. Particle ventilation fraction does not consider the particles that are deposited or suspended in the trachea or the subglottis. After analysing particle ventilation fraction I observed that at all flow rates there is an upward trend in particle ventilation in the upper and right middle lobes in CF, and downward trend in lower lobes in CF compared to non-CF. There are some variations, but overall was the trend. This preferential pattern of more particles going to right cranial lobe was statistically significant for particles larger than 1- μm (Figure. 7.3).

I further investigated the pattern in CF and I divided the particle ventilation fraction to the upper lobes (U), by the particle ventilation fraction to the middle lobes (M) and lower lobes (L). In 3 week old, I found that significantly greater number of particles (larger than 5- μm) go to the upper in CF compared to non-CF at all flow rate studied (Figure. 7.4).

Moreover, the trend for more particles to go to the upper lobe in CF persisted when I compared particle ventilation at weight based flow rates. I observed that, in three week old CF pigs, particles larger than 1- μm tend to travel to the upper lobes. I also observed that in the right cranial lobe the particle ventilation fraction was statistically larger in CF compared to non-CF for particles larger than 1- μm at weight based flow rates (Figure. 7.5).

I next investigated lobar particle deposition efficiency. Lobar particle deposition efficiency represents the number of particles that were deposited in a specific lobe

over the number of particles that entered that lobe. As expected with high air velocity and high Stokes number in the trachea (Table. 7.3), particle deposition was greater in CF compared to non-CF under most condition studied (Figure. 7.6). These findings predict that a greater number of particles that enters a specific lobe in CF will get deposited.

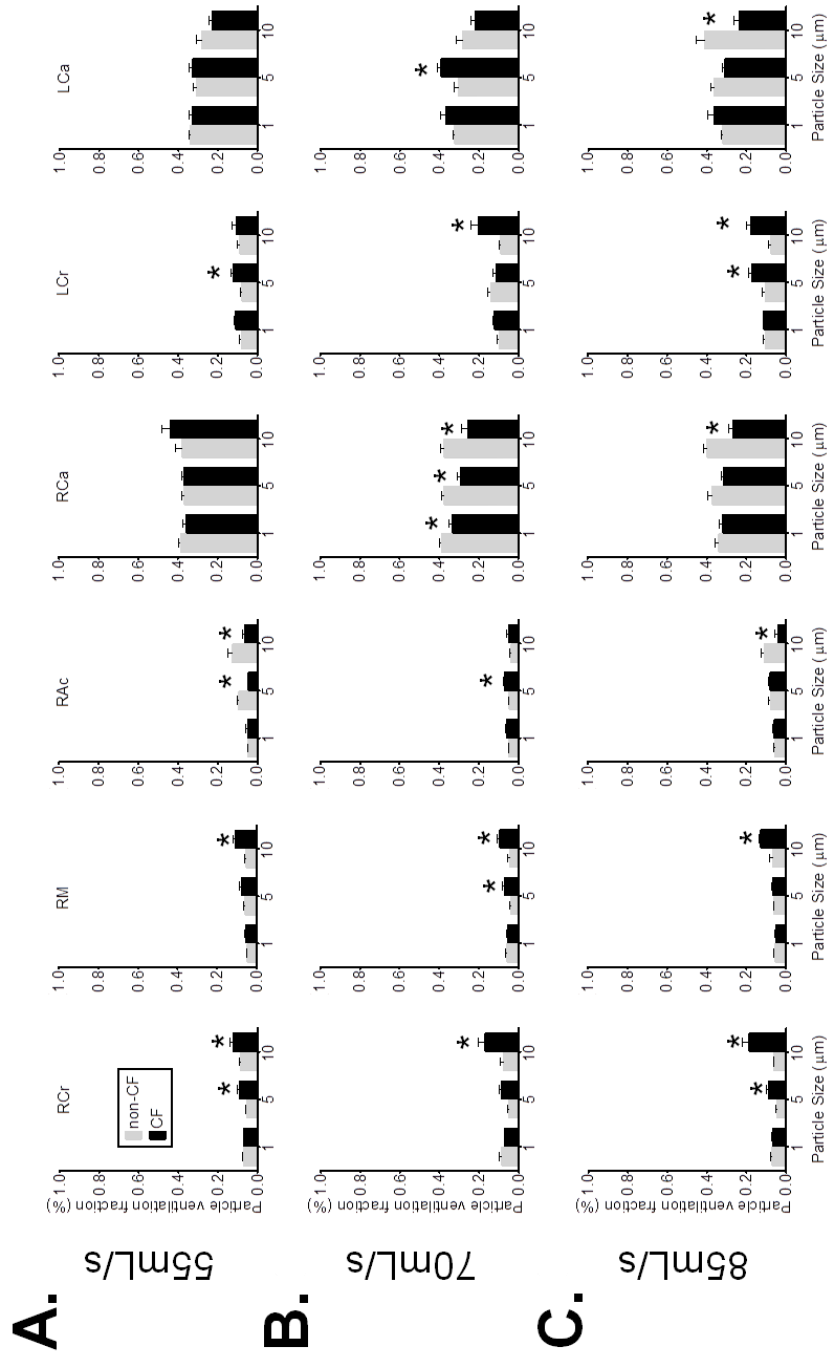


Figure 7.3. Particle ventilation fraction in 3 week old non-CF and CF lung lobes at three different inhalation flow rate. (A) Particle ventilation fraction in all lung lobes at inhalation flow rate of 55mL/s. RCr denotes right cranial, RM denotes right middle, RAc denotes right accessory, RCa denotes right caudal, LCr denotes left cranial, LCa denotes left caudal. (B) Particle ventilation fraction in all lung lobes at inhalation flow rate of 70 mL/s. (C) Particle ventilation fraction in all lung lobes at inhalation flow rate of 85 mL/s. * denotes statistical significance.

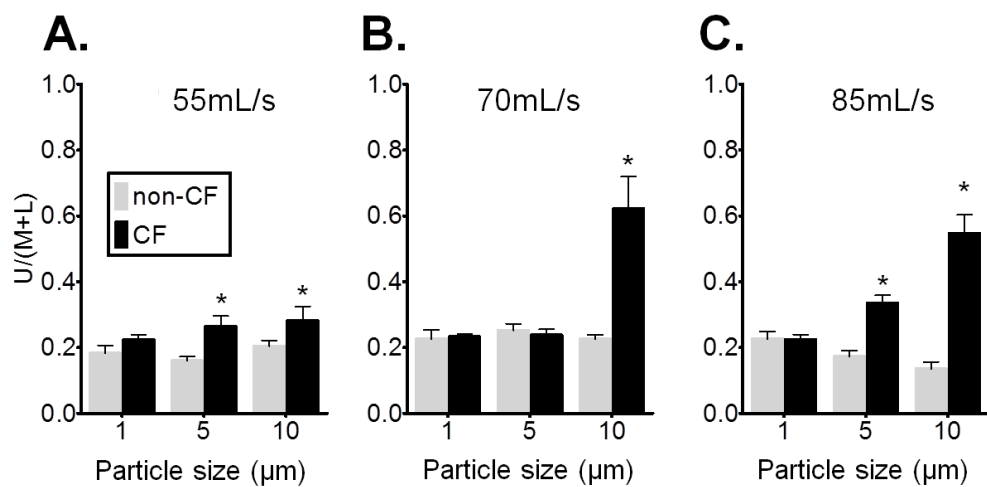


Figure 7.4. The relationship between particle ventilation fraction to the upper lobes vs. the middle and lower lobes for three week old non-CF and CF pigs. For all three graphs, in the y-axis, U denotes upper lobes which consists of right cranial (RCr), right middle (RM), and left cranial (LCr). M denotes middle lobe which consists of right accessory (RAc). L denotes lower lobes which consist of right caudal (RCa) and left caudal (LCa). (A) The relationship between particle ventilation fraction in upper lung lobes vs. the middle and lower lung lobes at inhalation flow rate of 55mL/s. (B) The relationship between particle ventilation fraction in upper lung lobes vs. the middle and lower lung lobes at inhalation flow rate of 70mL/s. (C) The relationship between particle ventilation fraction in upper lung lobes vs. the middle and lower lung lobes at inhalation flow rate of 85mL/s. * denotes statistical significance.

85mfr in non-CF vs. 55mfr in CF

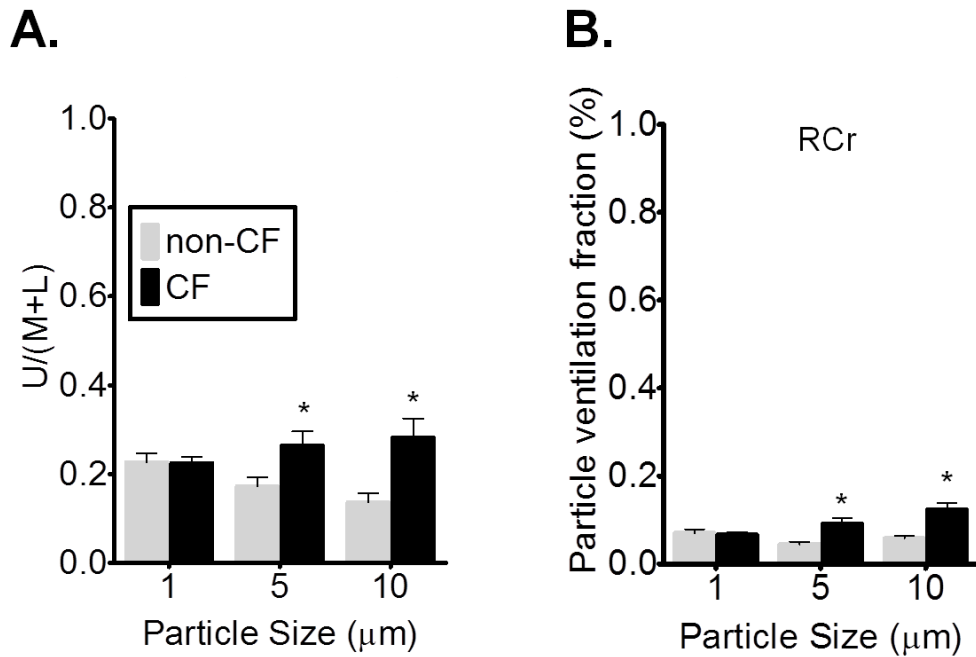


Figure 7.5. The relationship between particle ventilation fraction to the upper lobes vs. the middle and lower lobes for three week old non-CF and CF pigs at each genotype physiological flow rate. (A) The relationship between particle ventilation fraction in upper lung lobes vs. the middle and lower lung lobes. Non-CF inhalation flow rate of 85mL/s. CF inhalation flow rate of 55mL/s. In the y-axis, U denotes upper lobes which consists of right cranial (RCr), right middle (RM), and left cranial (LCr). M denotes middle lobe which consists of right accessory (RAc). L denotes lower lobes which consist of right caudal (RCa) and left caudal (LCa). (B) Particle ventilation fraction in the right cranial lobe. RCr denotes right cranial. Non-CF inhalation flow rate of 85mL/s. CF inhalation flow rate of 55mL/s. * denotes statistical significance.

Particle size	55 mL/s		70 mL/s		85 mL/s	
	non-CF	CF	non-CF	CF	non-CF	CF
1 μm	0.001 \pm 2.8E-5	0.007 \pm 27.1E-5 #*	0.003 \pm 7.7E-5	0.015 \pm 60.0E-5 #	0.004 \pm 11.1E-5	0.034 \pm 0.001 #
5 μm	0.028 \pm 70.5E-5	0.165 \pm 0.007 #*	0.079 \pm 0.002	0.384 \pm 0.016 #	0.112 \pm 0.003	0.847 \pm 0.035 #
10 μm	0.114 \pm 0.003	0.661 \pm 0.027 #*	0.315 \pm 0.008	1.535 \pm 0.063 #	0.448 \pm 0.011	3.389 \pm 0.139 #

Table 7.3. Particle Stokes number in the trachea for 3 week old non-CF and CF pigs at three different inspirational flow rates. mL/s denotes the flow rate unites millilitres per second. 55 mL/s denotes the value of the inhalation flow rate in non-CF and CF. 70 mL/s denotes the value of the inhalation flow rate in non-CF and CF. 85 mL/s denotes the value of the inhalation flow rate in non-CF and CF. * denotes statistical significance between non-CF inhalation flow rate of 85mL/s and CF inhalation flow rate of 55mL/s ($p < 0.05$). # denotes statistical significance between non-CF and CF at the same inhalation flow rate ($p < 0.05$).

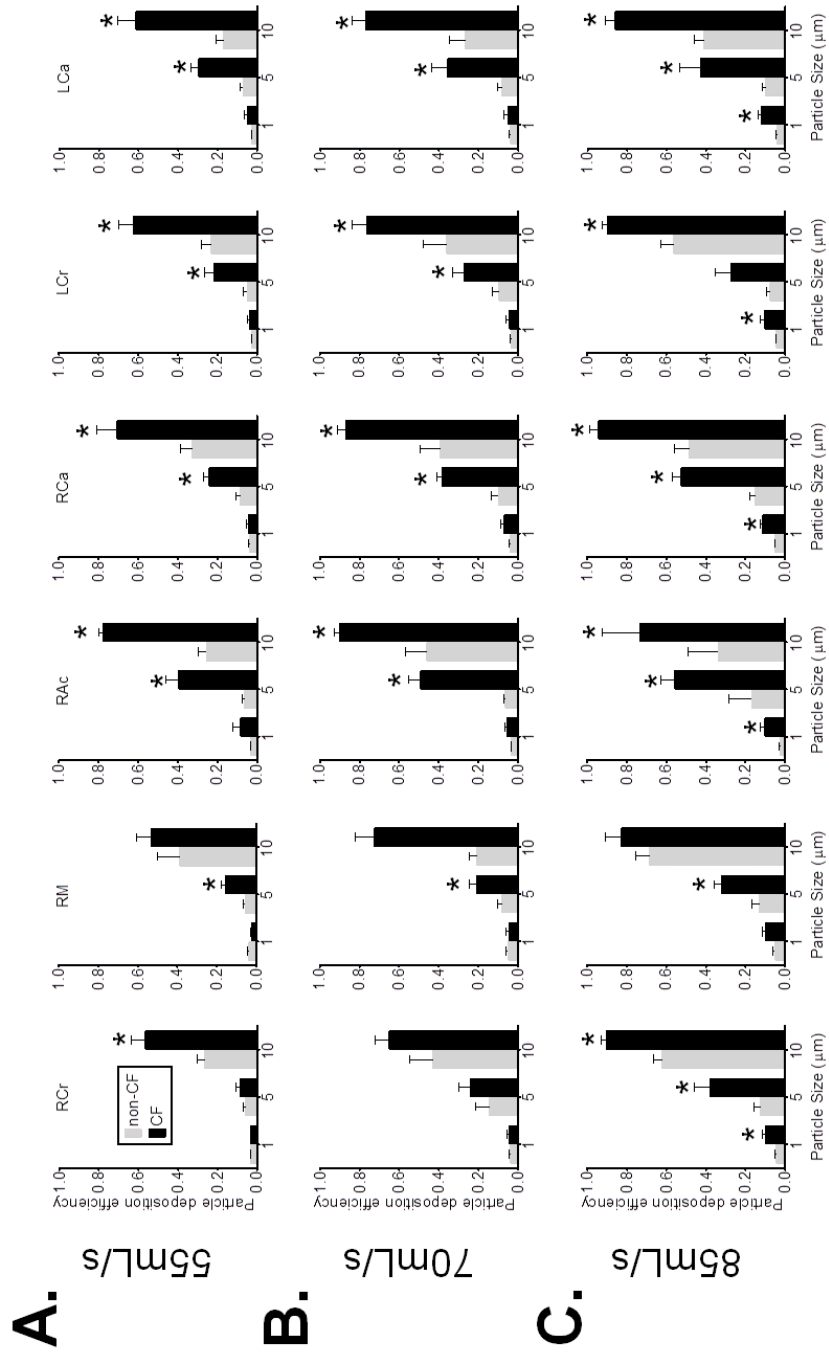


Figure 7.6. Particle deposition efficiency in 3 week old non-CF and CF lung lobes at three different inhalation flow rate. (A) Particle deposition efficiency in all lung lobes at inhalation flow rate of 55mL/s. RCr denotes right cranial, RM denotes right middle, RAc denotes right accessory, RCa denotes right caudal, LCr denotes left cranial, LCa denotes left caudal. (B) Particle deposition efficiency in all lung lobes at inhalation flow rate of 70 mL/s. (C) Particle deposition efficiency in all lung lobes at inhalation flow rate of 85 mL/s. * denotes statistical significance.

7.3.4. Factors that lead to enhanced particle ventilation to the CF upper lobes.

Three week old CF pigs have statistically different lung and airways characteristics compared to non-CF. In addition, CFD analysis predicted that the airflow and particle deposition and distribution characteristics are statistically different between non-CF and CF. CFD analysis also predicted that particle flow to the upper lobes in CF was greater compared to non-CF. For example, particle ventilation and deposition in the right cranial lobe for particles larger than 1- μm is greater under all flow rates in CF compared to non-CF.

Increased particle ventilation can be due to direct or indirect factors. Direct factors are dependent on the governing equation of particle flow and the flow rate distribution to each lobe (boundary conditions). Indirect factors are dependent on airway structural properties such as the angle of the parent branch airway and/or the angle of the daughter branch airway at the bifurcation point.

The governing equation for particle flow in our model indicates that there are three factors controlling particle behaviour. To understand the increased particle ventilation to the upper lobes in CF, I focused on the right cranial lobe. First, airway size has a major effect on particle behaviour. I measured the CSA of the airways supplying the upper lobe. I found that, in three week old CF pigs, the airways are smaller in CF compared to non-CF. For example, the cross sectional area of the airway supplying the right cranial lobe in CF is fivefold smaller compared to non-CF (non-CF 16.3 ± 2.8 vs. CF 3.3 ± 0.3 mm, $P < 0.05$). Another important value that controls particle trajectory is the ratio between the parent and daughter branch CSA (e.g. trachea CSA vs. the CSA of the airway supplying right cranial lobe). I found

that the ratio is smaller in CF compared to non-CF, which indicates that the constriction ratio was higher causing higher airflow velocity and great resistance (e.g. Resistance in right cranial lobe in non-CF 0.21 ± 0.01 vs. CF 0.13 ± 0.01 Pa/l, $P < 0.05$). Second, air velocity in the upper airways can increase particle ventilation to these airways. I found that in CF pigs the velocity was greater in all the upper airway branches. For example, in the airway supplying the right cranial lobe the airflow velocity was significantly higher even when weight based flow rates were considered (Figure. 7.7). Third, higher pressure drop ratio in a specific area in the airway can lead to higher particle ventilation to that area. This is because the drag equation used to simulate particle flow in our model is pressure dependent. The small constriction ratio between the parent and child branch in CF, and the higher velocity in the right cranial lobe lead to greater pressure drop in the right cranial lobe in CF compared to non-CF.

The next dependent factor that affects particle behaviour is flow rate at each lobe. I found that the flow rates to the upper lobes in three week old CF pigs are large compared to non-CF (Figure. 7.1). This increase in the flow rate is statistically significant at the right cranial lobe where I observed greater particle ventilation.

However, I also found that although the flow rate at the left cranial lobe was greater in CF compared to non-CF it was not statistically different. Despite that, the particle ventilation fraction to the left cranial lobe is higher in CF compared to non-CF. This can be, in part, due to other factors such as airway constriction ratio, airway angle, high pressure drop, high velocity, and high Stokes number.

In addition to the dependent factors that can influence particle trajectory there are a few independent factors that might aid in increasing particle ventilation to the upper lobes in CF compared to non-CF. These factors are mostly structural. First, I looked

at relative particle location in the airway as they move through the trachea. I found that due to the trachea structure (e.g. the curvature of the trachea in pigs) and particle properties (the particle density and weight) about forty percent of particles entering the lungs tended to cluster near the anterior surface of the airway attributable to centrifugal force (Awadalla et al., 2014). This clustering near the wall was also observed in newborn pigs, where it imposed a greater effect due to the relatively low Reynolds number in newborn CF pigs (Awadalla et al., 2014). Since the angle of the trachea is important in determining the particle distribution in the airway (Awadalla et al., 2014), I measured the tracheal angle in non-CF and CF. I found that the tracheal angle in three week old CF pigs was steeper compared to non-CF (Figure. 7.8A). The steeper angle of CF trachea increases particle density near the anterior wall in CF compared to non-CF. This increase in particle density leads to a higher particle ventilation to the upper lobes. Since the particles are clustered near the anterior wall of trachea, I investigated the angle of bifurcation to the airway supplying the right cranial lobe. I found that, in three week old CF pigs, the right cranial lobe airway is tilted towards the anterior region of the trachea at an angle that is larger in CF compared to non-CF (Figure. 7.8B).

To summarize, from our data I speculate that as particles leave the glottis and enter the trachea they are well mixed due to the glottis constriction and the high Reynolds number in both non-CF and CF airways. As the particles move down the curved non-CF and CF trachea, they cluster near the anterior wall of the airway. However, due to the steeper angle of the CF trachea the particle density near the anterior wall increases in CF compared to non-CF. The high Reynolds number in both non-CF and CF (>1000) causes secondary flow in both non-CF and CF airways. In CF, the particles clustered near the right anterior wall face a larger pressure difference at the

right cranial lobe airway entrance, leading to higher particle ventilation to the right cranial lobe.

Another interesting observation was the increased particle deposition in the CF compared to non-CF. This is due to many factors such as higher airflow velocity in CF airways at all flow rates and weight based flow rates. This leads to higher particle velocity in CF and increases the chance of deposition due to impaction. The higher particle velocity in CF leads to higher Stokes number, which indicates that particle momentum is going to be the dominant force on particle trajectory and not airflow pattern. Under the same flow rate, Stokes number is dependent on the airway size, velocity in the airway, and particle diameter. I found that the Stokes number is significantly greater in the CF trachea (~ 5.6 fold greater compared to non-CF) (Table. 7.3). However, the Stokes number in CF airway supplying the right cranial lobe was 12 fold higher compared to non-CF at the same flow rate. Even under weight specific flow rates, Stokes number was 8 fold greater compared to non-CF. This means that the likelihood of the fast moving particles in CF to impact the wall and deposit (due to their own momentum) is significantly higher compared to non-CF. This suggest that during the time of the simulation if more particles are going to a specific lobe (e.g. right cranial lobe) in CF compared to non-CF (where particle deposition efficiency is greater), most of these particles are depositing in airways considered in our model rather than staying suspended as in the case in non-CF (Figure. 7.6).

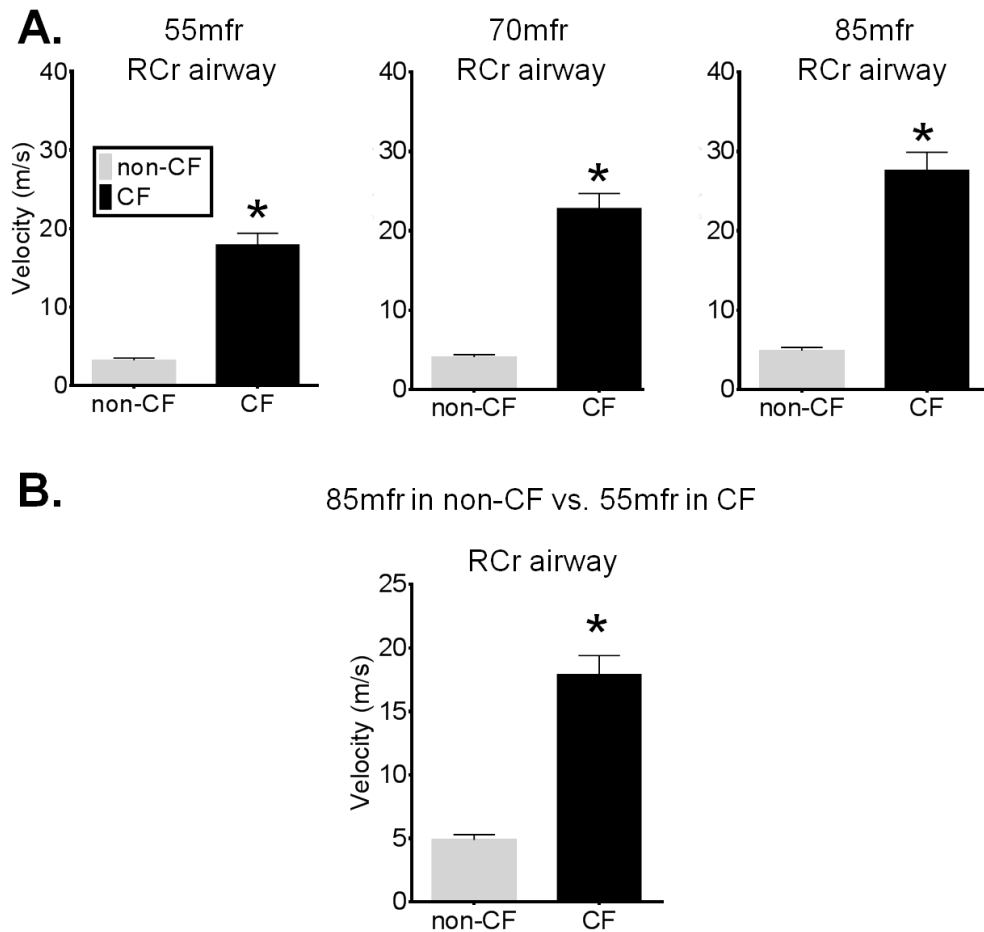


Figure 7.7. Air velocity in the right cranial airway at three different inhalation flow rates. (A) Air velocity at the right cranial (RCr) airway at a inhalation flow rate of 55, 70, 85 ml/s. (B) Air velocity at the right cranial (RCr) airway at each genotype physiological flow rate. Non-CF inhalation flow rate of 85mL/s. CF inhalation flow rate of 55mL/s. * denotes statistical significance.

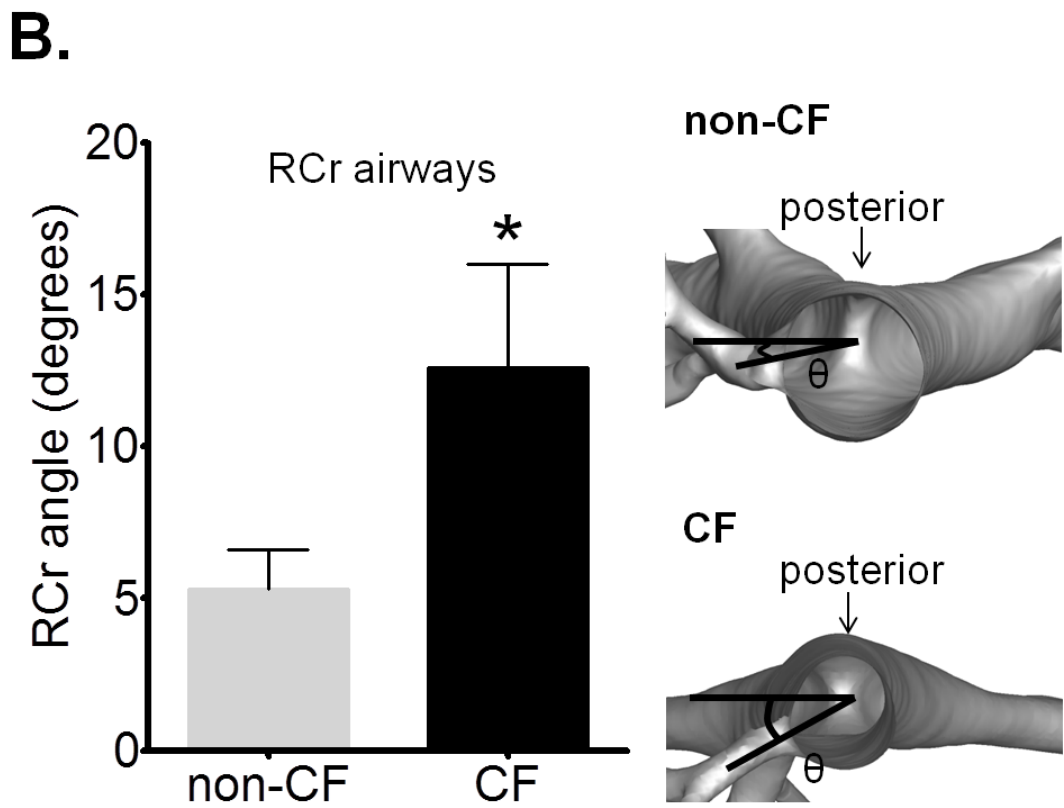
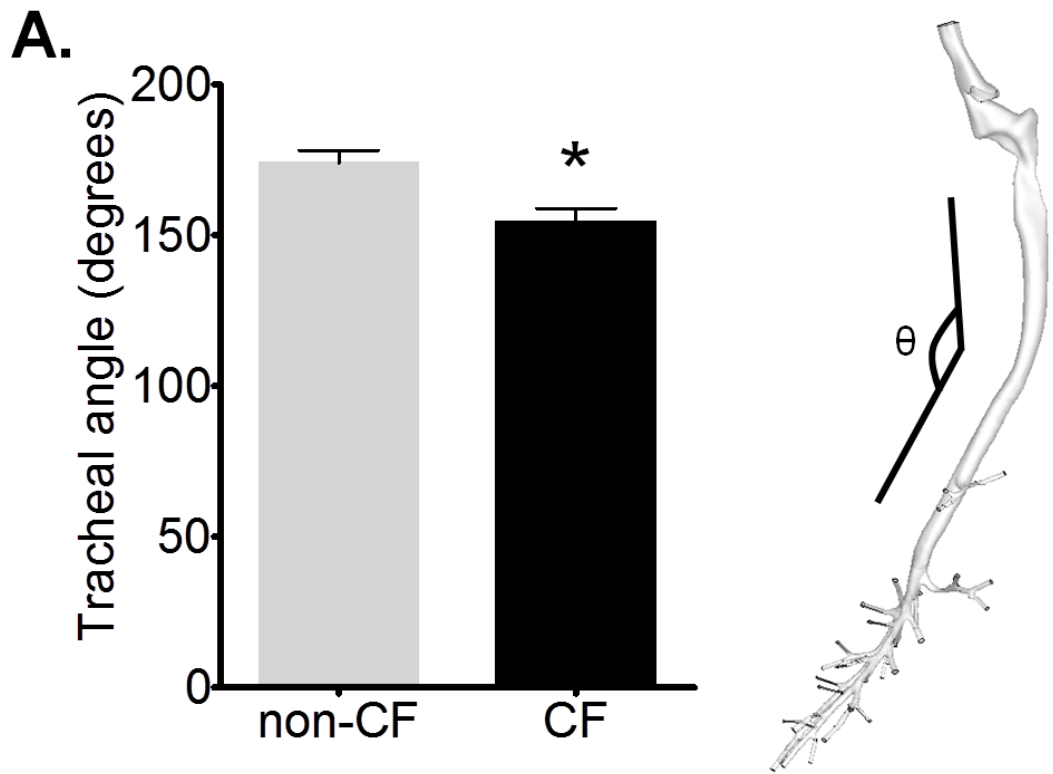


Figure 7.8. Tracheal angle and right cranial lobe airway bifurcation angle. (A) Left panel: comparing non-CF and CF tracheal angle. Right panel: diagram demonstration the location the tracheal angle was measured. (B) Left panel: Comparing non-CF and CF right cranial (RCr) lobe airway bifurcation angle. This angle was measured in relation to the straight line connecting the centres of the right and left main bronchus at the carina bifurcation point. Right panel: diagram demonstration the location and method the right cranial bifurcation angle was measured. Arrow denotes the posterior region of the airway. * denotes statistical significance ($p < 0.05$).

7.4. Discussion.

Cystic fibrosis is the most common lethal recessively inherited disease. The primary cause of morbidity and mortality in CF is due to progressive lung disease (Quinton, 1990; Rowe et al., 2014; Welsh M.J., 1996). The pathogenesis of cystic fibrosis in its early stages is not yet understood. Computed x-ray tomography (CT) have been previously performed on infants and children with CF at two lung pressures 0 cmH₂O and 20 cmH₂O (Mott et al., 2012; Sly et al., 2009; Stick et al., 2009). However, some of these studies would either consist of three thin-slices during inspiration or expiration scan or about twenty slices using volumetric technique (Mott et al., 2013; Sly et al., 2009; Stick et al., 2009). Although this technique is used to maximize the information obtained with minimal radiation exposure to infants and young children, it limits the number of airways that can be evaluated. Moreover, if the airway on the CT slices was scanned at the bifurcation point this would lead to overestimation of the size of the bronchus lumen. Therefore, to understand the lung's structure and function in the early stages of CF disease I needed an animal model. With this animal model I can obtain a high resolution volumetric CT scan with more than 300 slices at two pressures 0 cmH₂O and 20 cmH₂O. This provides a more detailed analysis of the lung's structure and function in the early stages of CF and also it allow us to compare our findings to non-CF too.

A porcine model of CF (*CFTR*^{-/-} pigs) was recently generated. Unexpectedly, at birth CF pigs displayed airway structural abnormalities. These include airways that are reduced in calibre and less circular. Also, it was observed that the cartilage rings are irregularly shape and the smooth muscles bundles are abnormal (Meyerholz et al., 2010; Ostedgaard et al., 2011; Ramsey et al., 2011; Rogers, Hao, et al., 2008; Stoltz et al., 2010). Furthermore, recent studies have revealed that newborn CF pigs have

reduced bacterial killing and abnormal mucus properties (Hoegger, Awadalla, et al., 2014; Pezzulo et al., 2012). Mathematical modelling of airflow and particle behaviour in newborn pig airways have revealed that in CF the pressure drop and airflow velocity were greater compared to non-CF. Also the computational model predicted greater particle ventilation to the right lung due to higher airflow velocity, the presence of secondary flow and skewed axial velocity due to the subglottic narrowing. Moreover, a higher deposition in the lower right lobe was also reported (Awadalla et al., 2014). It was also reported in the literature that newborn pigs have a reduced bacteria killing ability and impaired mucociliary transport (Haeusler et al., 1994; Hoegger, Fischer, et al., 2014; Pezzulo et al., 2012; Stettler et al., 2000). As these pigs get older, all these factors present in the lungs of CF pigs at birth can affect the lung development and worsen the airway abnormalities.

The aim of this study was to examine airflow properties and particle behaviour in newborn and three week old non-CF and CF pigs. First, I examined the pigs weight and size, and I found that CF pigs weigh 3kg less and their femur is about ten millimetres less compared to non-CF. Also three week old CF pigs have smaller lung volume at both lung pressures, 0 cmH₂O and 20 cmH₂O, and their lung expiration ratio was decreased compared to non-CF pigs. In addition, when I examined their lobar ventilation I found that in three week old CF pigs the expansion ratio in the upper lobes was increased and in the lower lobes decreased in comparison to non-CF pigs. Moreover, I found that the major, minor, equivalent diameter, CSA, and perimeter are smaller in CF compared to non-CF. I also found that the fold difference between the non-CF and CF airway diameter, CSA, and perimeter at three weeks of age to be statistically larger compared to newborn. These striking differences have encouraged us to further study airflow and particle behaviour in three week old non-CF and CF pigs.

I used CFD modelling to predict airflow and particle behaviour in five non-CF and five CF three week old pigs. I found that when comparing non-CF to CF at equal flow rates and at weight specific flow rates the CF pigs had higher pressure drop and air velocity compared to non-CF. This was due to the glottis constriction ratio and that the trachea in CF was three fold smaller compared to non-CF. The increased air velocity in CF was predicted by our model in all the airways supplying all the lung lobes even when I compared the two genotypes at flow rates based on their body weight.

Next, I simulated particle behaviour in non-CF and CF three week old pigs. In CF pigs, I observed that there was an upward trend in particle ventilation fraction to the upper lobes with increasing particle size. In addition I have also observed a downward trend in particle ventilation fraction to lower lobes with increasing particle size. This upward trend was still observed when I compared non-CF and CF particle ventilation at flow rates based on their weight. I have also observed higher particle deposition in CF compared to non-CF. Although, higher particle deposition is predictable since the air velocity is higher and the airway CSA is smaller in CF, the data provided valuable information. These data show that during the time of the simulation (one second) more particle travel to the upper airways and deposited on the airway wall (in our geometry I included the first three monopodial generations).

With the above findings, I can provide a potential explanation for enhanced particle ventilation to the right cranial lobe. As particles leave the glottis in non-CF and CF they are well mixed. As these particles enter the trachea, the high Reynolds number (above 1000 in both genotypes) maintains the even particle distribution across the tracheal cross-section. The angle of the trachea curvature forces the particles to move towards the anterior wall due to centrifugal force. The angle of the trachea curvature

can have a significant effect on the density of particles near the anterior wall. I found that the angle of the trachea was statistically steeper in CF compared to non-CF and caused more particles toward the high pressure drop of the right cranial lobe airway bifurcation which is located on the anterior wall at a bifurcation angle that is greater in CF compared to non-CF.

This study has several advantages and caveats. Advantages include: 1) This is the first study to use CFD and CT-based airway geometry in a longitudinal analysis of cystic fibrosis disease. 2) This study compared CF pig airway and lung structure and function before and after the onset of inflammation and infection in CF pigs (newborn vs. 3 weeks of age), thereby studying the primary and secondary effects of congenital airway narrowing in CF. 3) This provided not only observation of what happens to airway structure and function after the onset of the disease but it also provides an potential explanation for why it happens. While our findings are consistent with recent experimental and stochastic aerosol studies (Brown & Bennett, 2004; Brown et al., 2001), several caveats exist. 1) To calculate the tidal volume for each pig I used the relationship between tidal volume and body weight for tidal volume in humans. I do not know if the same relationship applies for both pigs and humans. Moreover, I do not know if the same relationship would apply to both non-CF and CF. In human infants and adults, tidal volume was not different between non-CF and CF (Colasanti, Morris, Madgwick, Sutton, & Williams, 2004; Ranganathan et al., 2003). I attempted to measure tidal volume in non-CF and CF pigs, under light or moderate sedation, but the results were too variable and unable to be used for the current studies. Future studies could include accurate measurements of tidal volume in non-CF and CF pigs, but would likely require a large sample size of both non-CF and CF animals. For this study, I chose to use the same predicted tidal volume relationship for both non-CF and CF pigs to standardize the analysis. 2) I used the

same respiratory rate for both non-CF and CF pigs. Human infants and adults studies have found that the respiratory rate is higher in CF compared to non-CF (Colasanti et al., 2004; Ranganathan et al., 2003). Since beginning this work, our group has found that the respiratory rate between newborn non-CF and CF pigs is the same. For the current studies, I chose to use the same respiratory rate for both non-CF and CF analyses to maintain consistency. 3) I have assumed that the inspiration expiration ratio is 1:2 in both non-CF and CF pigs. I know that in humans the typical ratio is also 1:2. Whether the same relationship is true in non-CF and CF pigs is unknown. However, for the purposes of the modelling simulation I assumed this to be the case. Based upon the known pathophysiology of CF lung disease, it seems reasonable to assume that the inspiratory phase (the component of the respiratory cycle that I modelled) would be similar between non-CF and CF animals. 4) When comparing non-CF and CF three week old pigs at the same flow rate the Reynolds number was statistically higher in CF compared to non-CF. Usually in comparative CFD studies the Reynolds number is maintained relatively constant. In our study, CF pig airways are 3-fold smaller compared to non-CF. Therefore, when comparing at the same flow rate Reynolds number will always be different. However, when I compared both genotypes using flow rates based on the pigs' body weight, I found that the Reynolds number in the trachea was almost equal with no statistical difference between non-CF and CF pigs. 5) I simulated airflow at peak of inspiration cycle. Modelling the full inspiratory cycle would provide us with more information on the effect of airway abnormalities on the whole respiratory cycle. However, it would be computationally expensive to conduct this kind of study on five subjects in each genotype. Also particle simulation will increase in complexity and would require a more time dependent flow field which is computationally expensive. In addition, I do not know the flow-volume relationship throughout tidal volume inspiration and expiration in

non-CF and CF three week old pigs. Therefore, simulating at the peak of inspiration was appropriate for this study. It is important to note that in this study I simulated the airflow and particle distribution in each pig at three different flow rates. This should provide insight into airflow and particle behaviour at different points in the respiratory cycle. 6) I used rigid airway geometry in this study. Due to our lack of knowledge about the airway tissue properties in non-CF and CF pigs, I were not able to model a physiologically deformable airway structure. Also conducting a deformable simulation on a sample size of ten is computationally expensive. In addition, this study only predicts the flow at peak of tidal volume inspiration. Therefore, having a deformable model would not be computationally efficient since I predict the flow at fixed pressure. 7) It is possible that mesh size influences results of airway and particle behaviour. To test the influence of mesh size I conducted a grid sensitivity test on a pair of non-CF and CF pigs. I found that air velocity, and pressure drop for the two mesh sizes were approximately the same (data not shown). These findings suggest that the observed differences in particle distribution and airflow characteristics are independent of mesh size. Importantly, prior studies have reported good agreement between particle deposition model predictions and measured data, suggesting that our predictions are likely valid (Hofmann et al., 2005; Lambert et al., 2011; Miyawaki et al., 2012).

What are the implications of our findings? First, this study is novel in providing longitudinal analysis of the effect of airway size, shape, lung morphologies on airflow pattern and particle behaviour in non-CF and CF pigs at birth and three weeks of age. At birth, abnormal CF airways and lung morphology led to higher particle ventilation to the right lung and higher particle deposition in the right lower lobe. Three weeks after birth, I found that in CF pigs, airflow volume fraction to the lower lobes had decreased and airflow volume fraction to the upper lobes increased.

These findings, in part, caused an increase in particle ventilation to the right cranial lobe. This has significant implications for understanding disease pathogenesis in the CF lung and its progress from birth to later time points. Second, many therapeutics for CF airway disease are delivered by inhalation. A better understanding of the CF airway and how airway size and shape influences particle/aerosol deposition and distribution in the lung is critical for targeted delivery of aerosolized treatments to people with irregular airway morphology. By performing CFD analyses on human- and disease-specific airway geometries, more efficient and better targeting of inhaled therapies may be achieved. Furthermore, our modelling techniques are directly translatable to human studies.

In humans, CF-related lung disease has a known proclivity for the upper lung zones (Gurney, Habbe, & Hicklin, 1997; Kennedy, Morice, Jimenez, & Eapen, 2007; Li et al., 2012; Rogers, Stoltz, et al., 2008), and in older CF pigs I tend to observe lung disease more frequently in the right cranial lobe (Rogers, Stoltz, et al., 2008; Stoltz et al., 2010) (Figure. 7.9). Moreover, other pulmonary diseases have a predilection for the upper lung regions including tuberculosis, silicosis, hypersensitivity pneumonitis, and pneumoconioses. The underlying etiology for these regional differences is unknown, but ventilation and perfusion irregularities are most often implicated (Gurney & Schroeder, 1988). However, in the upright position greater ventilation occurs in the bases than the apices of the normal lung and more particles are deposited in the dependent lung zones (Bennett, Messina, & Smaldone, 1985; Subramaniam, Asgharian, Freijer, Miller, & Anjilvel, 2003). Might congenital airway abnormalities be important in determining regional ventilation in CF airways affecting disease pathogenesis and account for the upper lobe predilection for CF disease?

Both humans and newborn pigs with CF have a host defence defect against inhaled bacteria, and impaired mucociliary transport (Hoegger, Fischer, et al., 2014; Pezzulo et al., 2012; Stoltz et al., 2010). I hypothesize that in newborn CF pigs a greater fraction of inhaled particulate matter and microbes reaches the lower lung zone causing infection and inflammation in that region. With time (2- 3 weeks), there was higher airflow volume ventilation in CF upper lobes compared to non-CF at three weeks of age. The higher airflow ventilation combined with abnormal airway and lung morphology increases the airflow velocity, particle ventilation and deposition in the upper lobes. This upper lung particle ventilation predilection, combined with the CF host defence defect and impaired mucociliary clearance, might then cause greater lung disease in the right cranial lobe rather than lower lung regions. Although no studies have specifically examined this question in CF, both modelling predictions and experimental results show greater airway particle deposition in the apical lung regions of adults with CF (Brown & Bennett, 2004; Brown et al., 2001). Furthermore, airway lumen obstruction in CF secondary to mucus accumulation might be expected to cause similar effects and/or worsen the congenital abnormalities (Sturm, 2011).

A.
Human CF lung



B.
Porcine CF lung



Figure 7.9. A slice of a computed x-ray tomography representing upper lung lobe disease in humans and porcine with CF. In a computed x-ray tomography image air appear black, tissue appear gray, and bone appear white. If a huge portion of the lung appears light gray, it is an indication of lobe disease or collapse. (A) Upper lobe disease in a human CF patient. (B) Upper lobe disease in the right cranial lobe (RCr) in a year old CF pig. Arrow denotes the location of the upper lobe and the disease.

7.5. Conclusion.

In conclusion, our results suggest that both airway structural abnormalities and differences in lobar airflow distribution in three week old CF pigs contribute to the pathogenesis of CF lung disease and may be a significant determinant of the future of regional distribution of CF lung disease. Moreover, these findings might have important implications for the development of inhaled therapeutics in CF.

“The present is theirs; the future, for which I really worked, is mine.”

Nikola Tesla

Chapter 8. Analysing the global and local lung structure and function in adult human CF lungs

8.1. Introduction.

In the previous two chapters, I investigated the early stages of the cystic fibrosis disease in the porcine CF model. In this chapter, I will use similar methodologies to investigate lung disease pathogenesis in adult human patients. I will investigate the global and local lung structure and function. I will see if there is similarity between lung abnormality investigated in the CF animal model and disease pathogenesis in adult human with CF. Also I will investigate the effects of CF disease severity on local and global lung functions. As mentioned in the previous chapters, CF is a genetic disease caused by mutations in the *CFTR* gene. The *CFTR* gene encodes a protein which is expressed in the apical membrane of conductance epithelial cells. CFTR protein has multiple activities that are required for epithelia cells to function correctly. Many mutations in the *CFTR* gene result in abnormalities in epithelial cell chloride and bicarbonate ion transport function (Matsui et al., 1998; Stutts, 1999; Welsh M.J., 1996).

CF is a recessive genetic disease where mutations on both *CFTR* alleles will lead to abnormal *CFTR* channel function. Approximately, one in 25 people carry one of over 1,500 disease causing mutations which act to reduce either the number or functionality of *CFTR* channels at the epithelia cell surface (Strom et al., 2004). The World Health Organization estimates that 1 in 2000-3000 European newborns, in Australia 1 in 2800 and in the United States 1 in 3500 are born with homozygote defective genes (Stoltz et al., 2010; Welsh M.J., 1996). Defective *CFTR* channels result in abnormal sweat electrolytes, sino-pulmonary disease, male infertility, and pancreatic exocrine insufficiency in up to ninety five percent of patients (Stutts, 1999; Welsh M.J., 1996).

CF disease phenotype can be caused by over 1500 different mutations in the *CFTR* gene (Spicuzza et al., 2012). These mutations can be divided into six classes (defective protein synthesis, abnormal processing and trafficking, defective regulation, decreased conductance, reduced synthesis and trafficking and decreased stability). The most common mutation in *CFTR* is caused by the deletion of three base pairs, which results in loss of a phenylalanine residue at amino acid position 508. This mutation is called delta phe508 ($\Delta F508$), and accounts for ~ 70% of the *CFTR* mutations in North America (S. H. Cheng et al., 1990; Denning et al., 1992; Du et al., 2005; Lukacs & Verkman, 2012). The second most common CF mutation is G542X. G542X mutation is considered a nonsense mutation, since no protein is produced in this mutation due to the presence of a premature stop codon instead of glycine residue at position 542 in the *CFTR* amino acid. The stop codon triggers the ribosome to stop the translation prematurely before any protein is produced (Bedwell et al., 1997; Castaldo et al., 1997). The third most common CF mutation is G551D. It is the most prevalent gating mutation (Sermet-Gaudelus, 2013). In this mutation the glycine residue at position 551 of the *CFTR* amino acid is replaced by an aspartate

residue which is a negatively charged amino acid. This change in the amino acid has a significant effect on CFTR channel efficiency specifically at ATP-binding site 2. Unlike the other severe mutations, G551D exhibits normal synthesis, trafficking, processing, and membrane stability. Although G551D R domain can be phosphorylated normally, the channel activation time by cAMP is greatly reduced with increased closing time (Bompadre et al., 2007; Xu et al., 2014).

The CF phenotype that causes most of the morbidity and mortality is respiratory disease. Respiratory disease in CF is challenging to define and understand due to patient exposure to a multitude of endogenous and exogenous factors that leads to complex multistage disease pathogenesis. This, in part, is the reason lung disease is the primary target for considerable research to understand CF pathogenesis and treatment (Zielenski, 2000).

Pathogenesis and treatment of respiratory disease in the third most common CF mutation, G551D, has received a lot of research interest in the last few years due to development of a new drug that potentiates the channel function (Barry et al., 2014; Bompadre, Li, & Hwang, 2008; Char et al., 2014; Comer et al., 2009; Ramsey et al., 2011; Rowe et al., 2014; Van Goor et al., 2009; Wainwright, 2014). The new drug is known as VX-770, ivacaftor (Kalydeco, Vertex Pharmaceuticals) (Cuthbert, 2011; Neuberger, Burton, Clark, & Van Goor, 2011; Rogan et al., 2011; Van Goor et al., 2009; Van Goor et al., 2006). CF patients with the G551D mutation showed increase in Force Expiratory Volume in one second (FEV1), increased weight gain, and increased body mass index (BMI). Also, a reduction in sweat chloride was observed (Davis et al., 2007; Ramsey et al., 2011). Several studies have been conducted to provide an understanding on the abnormalities in G551D CF patient lung function and on the method in which ivacaftor improves lung function abnormalities (Van

Goor et al., 2009). However, our understanding of global and local lung function in G551D CF patients before treatment is limited. I had the unique opportunity to study controlled ventilation volume CT scans from a cohort of CF subjects with the G551D mutation. The aim of this study is to understand the effect of G551D CF disease on global and local lung structure and function compared to normal non-diseased subjects. Also, since lung disease severity heterogeneity exists in all CF patients even in among patients of the same genotype (e.g. in homozygote CF patients, some develop severe lung disease in their childhood, others can reach adulthood with normal lung function), the second aim of this study is understand the effect of lung disease severity on a global and local lung function of G551D CF patients compared to healthy subjects (Cutting, 2010; E. Kerem et al., 1990; Knowles & Drumm, 2012).

The two aims of this study were achieved by examining the lung structure and function using quantitative computed tomography (QCT) lung scans obtained from CF patients with the G551D mutation and comparing the finding to scans obtained from normal non-disease subject. The lung structure and function were assessed by analysing the properties of the lung at the global and the local segmental scale.

Global lung analysis included analysing PFT-based variables and a single volume scan obtained from QCT. The local segmental lung analysis included analysing CT scans at lobar level, using image registration to quantify volume expansion and deformation at the segmental level. Finally I used CFD to correlate the effect of global and local variables on lung ventilation and deposition of inhaled particles. The effect of lung disease severity was also investigated. Understanding the effect of each one of these variables locally and their interplay globally may shed light on the pathophysiology of CF lung disease.

8.2. Methods.

8.2.1. Human subject data sets.

Non-CF and CF subjects were used in this study (Table 8.1.). CT images were obtained from each subject. The CT images of non-CF subjects and CF subjects were acquired at University of Iowa Hospitals and Clinics (Iowa City, USA) and St. Vincent University Hospital (Dublin, Ireland), respectively (Table 8.2.). The associated human studies along with the imaging protocol were approved by the Institutional Review Boards. CT images were gathered during coached breath-holds which were practised before image acquisition. CT scans were obtained at two breath holds, first at end inspiration (inspiratory, TLC scan) which is the maximum a patient can breathe in. The second breath hold scan was at end expiration (expiratory, RV scan) which is the point at the end of a full expiratory maneuver. Both breath hold scans were obtained in the supine position.

The scans were then processed using the Apollo software (VIDA Diagnostics, Coralville, Iowa). Apollo software is approved by the FDA to provide a quantitative support in lung analysis. The software offers a simple but powerful tool that provides airway measurement and lung parenchyma analysis by lobes using automatic lung densitometry tool (H.O. Coxson, 2012). I used the airways and parenchyma data provided by Apollo to compare airway and lung structure at both global and local segmental levels between our two groups (CF and normal non-diseased subjects). For airway measurements, I used averaged values extracted by Apollo from the middle region (30% - 70%) of the airway segment.

	No. (% male)	Age	Weight	Height	BMI
Healthy non-CF	8(37%)	22.5 ± 0.7	59.3 ± 3.3	168.6 ± 2.5	20.8 ± 0.8
CF patients	12(25%)	30.6 ± 2.8*	59.6 ± 2.8	164.3 ± 1.8	21.8 ± 0.6

Table 8.1. The demographical data from all the subjects selected for lung structure and function of CF patients compared to healthy non-CF subjects study. Age units is in years. Weight in kilograms (kg). Height in centimetre (cm). BMI is body mass index which is a ratio between weight and height. BMI = Weight/(height*height).

	Ireland	Iowa
Subject type	G551D CF patients	non-CF
Scanner	GE medical system	SIEMENS
Model	Discovery CT750 HD	Sensation 64
Slice thickness	0.625 mm	0.75 mm
Kernel	B30f	B30f
Voxel dimension	0.5469* 0.5469* 0.5 mm	0.5469* 0.5469* 0.7 mm
Tube voltage [Kvolt]	120	120

Table 8.2. The scanner and scanning protocol used for both non-CF and G551D CF patients. Two different scanners were used to scan each group of patients. The same coached breath-holds at TLC and RV in the supine position were used on both groups. The slice thickness is smaller in the CF data. However, the slice thickness in both data sets are below 0.8 mm which is the quantitative computed tomography threshold. Slice thickness and voxel dimensions are in millimetre (mm). Tube voltage is measured in kilovolts (Kvolt).

8.2.2. Image analysis.

Apollo only provides static quantitative information about the static lung structure and function of the lung. Therefore, to better understand lung kinematics I used an image registration to provide quantitative information about the dynamic translation of the lung air and tissue volume between different inflation levels (S. Choi et al., 2013; Murphy et al., 2011; Song, 2010). Image registration is a process to determine the optimal spatial map or warping function to minimize a dissimilarity measure (known as the cost function c) between two images obtained with different modalities. In this study, I used the sum of square tissue volume difference (SSTVD) to determine the cost function C :

$$C = \sum_{\mathbf{x} \in \Omega} (V_{tissue}^{ref}(\mathbf{x}) - V_{tissue}^f(T(\mathbf{x})))^2 \quad (8.1)$$

$V_{tissue}^{ref}(\mathbf{x})$ is the local tissue volume in the TLC scan (reference image), while $V_{tissue}^f(T(\mathbf{x}))$ is the local tissue volume in the RV scan (floating image). $T(\mathbf{x})$, is the warping function which uses a B-spline transformation technique to map a local volume at location \mathbf{x} in the RV scan to the corresponding location in the TLC scan (Y. L. Choi, S., 2000; Y. Yin, E. A. Hoffman, & C. L. Lin, 2009). In another word, $T(\mathbf{x})$ is a warping function that describes a transformation of the local point \mathbf{x} at TLC to corresponding location at RV.

I used image registration to quantify the effect of dynamical translation from the RV volume to the TLC volume on the local and segmental air volume change, the ratio of change in air and tissue volume and finally the degree of variability in air and tissue volume deformation. Then I compared the output of the image registration for the two groups CF and normal non-diseased subjects.

With the aid of the warping function $T(\mathbf{x})$ the air volume change and the lung deformation were evaluated. Since air and tissue volume in the lung CT images can be quantified by the image voxel intensity/ density, I used the intensity/ density based image registration method (S. Choi et al., 2013; Yin, Choi, Hoffman, Tawhai, & Lin, 2010; Y. Yin, E. A. Hoffman, & C.-L. Lin, 2009). Using this method, I first evaluated the tissue and air fraction as follow:

$$\beta_{tissue}(x) = \frac{I(x) - HU_{air}}{HU_{tissue} - HU_{air}} \quad (8.2)$$

$$\beta_{air}(x) = \frac{HU_{tissue} - I(x)}{HU_{tissue} - HU_{air}} \quad (8.3)$$

$\beta_{tissue}(\mathbf{x})$ is the tissue fraction, while $\beta_{air}(\mathbf{x})$ is air fraction, $I(\mathbf{x})$ is the Hounsfield unit (CT density) of the voxel, HU_{air} is the air Hounsfield unit of air and HU_{tissue} is the Hounsfield unit for tissue. HU_{air} and HU_{tissue} were set to -1000 and 55, respectively (Youbing Yin et al., 2009; Y. Yin et al., 2009). The local tissue volume $V_{tissue}(\mathbf{x})$ and air volume $V_{air}(\mathbf{x})$ can be calculated by multiplying the local volume $v(\mathbf{x})$ by the tissue and air fractions, respectively.

With regard to the floating image, the corresponding local volume for the RV scan to the local volume $v^{ref}(\mathbf{x})$ at TLC scan is $v^f(T(\mathbf{x}))$ which can be calculated after the warping function $T(\mathbf{x})$ is identified.

$$v^f(T(\mathbf{x})) = \frac{v^{ref}(\mathbf{x})}{J} \quad (8.4)$$

J is the determinant of Jacobian matrix. At RV scan, the air fraction $\beta_{air}^f(\mathbf{T}(\mathbf{x}))$ is obtained by CT intensity value $I(\mathbf{T}(\mathbf{x}))$ (Equation 6-3). Therefore the air volume is

$$V_{air}^f(\mathbf{T}(\mathbf{x})) = v^f(\mathbf{T}(\mathbf{x})) \beta_{air}^f(\mathbf{T}(\mathbf{x})) \quad (8.5)$$

Thus the regional air volume change ΔV_{air} between TLC and RV is calculated in the segmental scale as follows (Yin et al., 2010):

$$\Delta V_{air}(\mathbf{x}) = V_{air}^{ref}(\mathbf{x}) - V_{air}^f(\mathbf{T}(\mathbf{x})) \quad (8.6)$$

Next I determined the ratio of volume change (also known as the Jacobian or J) and the degree of deformation heterogeneity (also known as anisotropic deformation index or ADI) on the voxel level as the lung volume expands from RV to TLC. The Jacobian and ADI are calculated using eigenvalues determined by the deformation gradient tensor which accounts for the direction of deformation, the orthogonal rotation and stretch tensor.

$$J = \lambda_1 \lambda_2 \lambda_3 \quad (8.7)$$

$$ADI = \sqrt{\left(\frac{\lambda_1 - \lambda_2}{\lambda_2}\right)^2 + \left(\frac{\lambda_2 - \lambda_3}{\lambda_3}\right)^2} \quad (8.8)$$

λ are the eigenvalues representing the principal strain (maximum and minimum strain) along the principal direction of deformed lung tissue element from RV to TLC, where $\lambda_1 > \lambda_2 > \lambda_3 > 0$.

Since Jacobian is a ratio of volume increase from RV to TLC, a Jacobian value of one indicates no change in volume, a Jacobian value that is bigger than 1 indicates the ratio of expansion and a value less than 1 indicates shrinking. The Jacobian is different from ΔV_{air} , since it measures the ratio of both air and tissue volume

expansion and its values are interpolated given that they were obtained by 1st order derivative of warping function. On the other hand, ΔV_{air} , provides an actual volume change not a ratio and it provides discrete field data that are sensitive to the local CT intensity/ density.

Similar to Jacobian, ADI was also obtained by 1st order derivative of warping function to quantify the preferential deformation of the local volume. However, it is independent from the Jacobian (Amelon et al., 2011). ADI is an indicator to the degree of non-uniform expansion of the volume. If the volume uniformly expands in all directions (isotropically) where $\lambda_1=\lambda_2=\lambda_3$, ADI would be equal to zero given by equation 6-7. If the value of ADI is bigger than zero then this indicates a heterogeneous (anisotropic) expansion. ADI only provides the degree of anisotropy not the direction.

8.2.3. Air trapping.

Usually in air trapping analysis a voxel is regarded as an air-trapped voxel if the Hounsfield Unit of the voxel at RV is below -856 (Busacker et al., 2009; Castro et al., 2011). However, in our study the CT scans for healthy and CF subjects are obtained from different centres. Therefore a different method of measuring air trapping was required, since the threshold approach can be sensitive to scanner differences and scanner calibration methods to correct for beam hardening and scatter. Accordingly, I used a fraction-threshold-based method developed by Choi et al. (S. Choi et al., 2013) using fixed air fraction (β_{air}) calculated by equation 8.3 to compute the adjusted thresholds ($I_{threshold}$).

$$I_{threshold} = \beta_{air\ threshold} HU_{air} + (1 - \beta_{air\ threshold}) HU_{tissue} \quad (8.9)$$

HU_{air} is the Hounsfield unit for air and it is subject specific (extracted from the trachea CT density). Therefore, the effect of different scanner calibration or data obtained from different centres is minimized. HU_{air} is measured by eroding airway mask by using a binary filter to exclude partial volume of higher CT density near the airway lumen wall. The median of the remaining voxels in the eroded airways was used as HU_{air} of the specific subject. $\beta_{air\ threshold}$ is the threshold level for HU_{air} (air fraction) to identify trapped voxel usually set to 0.9. HU_{tissue} is the Hounsfield unit for tissue and it was set to 55. This new measure is referred to as the “fraction-based” air-trapping metric (S. Choi et al., 2013). A voxel is regarded as air-trapped if its density (I) in the CT scan is below the adjusted threshold level ($I_{threshold}$).

8.2.4. Structural variables.

I needed a method to accurately measure and compare structural variables between different lung inflation levels and also between different groups. I used methods developed by Choi S. et al. to measure lumen area, airway hydraulic diameter, airway bifurcation angle, diameter, and circularity (S. Choi et al., 2013). The airway bifurcation angle was computed by using the subject specific airway skeleton(1D) obtained with Apollo and I extracted the one dimensional (1D) airway tree. The angle of a segment is computed by measuring the angle between the two daughter branches of the corresponding branch (the tracheal angle is the angle between the right and left main stem bronchus). This angle was measured as follows:

$$Bifurcation\ angle = \cos^{-1} \left(\frac{d1 \cdot d2}{|d1||d2|} \right) \tag{8.10}$$

d1 is the directional vector of the 1D tree vector of the airway first daughter branch, while d2 is the directional vector of the 1D tree vector of the airway second daughter branch.

The average luminal diameter (D_{avg}) was calculated by:

$$D_{avg} = \sqrt{\frac{4 * CSA_{lumen}}{\pi}} \quad (8.11)$$

The circularity Cr and hydraulic diameter (diameter of noncircular tubes) was computed to assess the analysis of change in airway properties in CF and normal subjects.

$$Cr = \frac{\text{Perimeter of an area equivalent circle}}{\text{Perimeter of a luminal area}} = \frac{\pi D_{avg}}{Pe} \quad (8.12)$$

$$D_h = \frac{4 * CSA_{lumen}}{Pe} \quad (8.13)$$

8.2.5. Flow parameters.

The airway tree of each patient analysed consisted of at least 45 branches. Analysing the pressure drop between all subjects studied by manually measuring the pressure in each airway is time consuming. Therefore, I adapted Choi S. et al. method and used the following equation to measure the pressure drop in each airway segment.

$$\Delta p = f \frac{L}{D_h} \frac{\rho U^2}{2} + K \frac{\rho U^2}{2}$$

(8.14)

f is the frictional coefficient, L is the length of the segment, ρ is the air density, U is the mean velocity, and K denotes coefficient of minor loss. The equation above accounts for both major and minor loss in pressure. The term on the right side of the equation accounts for variation in pressure due to variation in circularity or hydraulic diameter. However, the term on the left accounts for variation in pressure due to angle of branching or abnormal heterogeneous airway shape.

8.2.6. Construction of the 3-D Hybrid CL-CT-based model.

CT based geometries have been used previously in subject specific CFD studies (J. Choi et al., 2009; Finlay, 2001; Lambert et al., 2011; Lippmann, Yeates, & Albert, 1980; Miyawaki et al., 2012). However, CT based models have several limitations. First, it is time consuming to construct and requires numerous pre- and post-process algorithms. Second, due to beam hardening and scatter the surface of the geometry is usually uneven and it needs to be smoothed leading to problems with the surface mesh structure. Third, the geometry needs to be manually split to segments to study regional ventilation. Finally cross-sections need to be created between the different branches if secondary flow investigation or regional aerosol ventilation is required in the study (Lambert et al., 2011; Miyawaki et al., 2012). Therefore, I used a modified centreline (CL) based model using CT image to construct the hybrid centreline computed tomography (CLCT) based model. CL-based models are constructed with circular and straight cylindrical structures. The cylindrical structure can be symmetrical or asymmetrical following Weibel's model or a 1D tree obtained for a human CT (G. S. I. Kim, A.J., 1989; Schmidt et al., 2004; Spencer, Schroeter, &

Martonen, 2001). I used subject specific CT skeleton data obtained from Apollo that contains the airway length, cross-sectional area (CSA) and angle to create a CL model. It is important to note that this is a state of the art CL model developed by Miyawaki, S. et al. 2013. The CL model can predict trifurcation shape and type. This CL model was then fitted to the CT geometry by first fitting all of the skeletons. Then I fitted the ring nodes on the airway surface of the centreline model to the surface of the CT model (Miyawaki et al., 2012). To ensure the correct fitting of each branch in the CL model I divided the CL skeleton into sub-branches where the aspect ratio is close to one. The aspect ratio is defined as the ratio of length to diameter. Any noise in the CT geometry produced by beam hardening or scattering was detected by DBSCAN (Density Based Spatial Clustering of Applications with Noise) and was ignored during the fitting process (Ester, 1996; Miyawaki, 2013). This produced a CL-CT model with curved CL and circular cross-section.

8.2.7. Geometric laryngeal model.

Recent studies have shown that the upper airways are primarily responsible for laryngeal jet turbulence, which can affect airflow patterns in the lower airways (Alipour & Scherer, 2006; Brouns et al., 2007; Y. Choi & Wroblewski, 1998; C. L. Lin et al., 2007; Miyawaki et al., 2012; Yin et al., 2013). However, to reduce radiation exposure, most chest CT scans do not include the laryngeal region. Therefore, I generated an artificial subject specific glottis construction based on information from the literature (K. H. Cheng, Cheng, Yeh, & Swift, 1997) and CT scans from healthy subjects. The artificial glottis was created for each subject by empirically determining five parameters. First, I needed to determine the location of the glottis or the distance from the glottis to the carina. This distance was determined using CT scans of healthy subjects and data from the literature (J. Choi et al., 2009). Second, I needed to determine the hydraulic diameter of the glottis. This was

empirically determined by plotting the hydraulic diameter distribution around the larynx using CTs of healthy subjects and data from the literature (K. H. Cheng et al., 1997). Third, I needed to determine the hydraulic diameter above the glottis. Fourth, I need to determine the length of the larynx above the glottis. Finally, I needed to determine the length of the larynx below the glottis. The last two variables were empirically determined by manually fitting the cubic Hermite spline curve (Fernandez, Mithraratne, Thrupp, Tawhai, & Hunter, 2004) on the diameter distribution obtained in the second step and verified using CT scans of healthy subjects and data from the literature (K. H. Cheng et al., 1997). All of these five parameters were then normalized by the diameter of the trachea. These steps allowed the production of subject specific glottis constriction.

8.2.8. CFD mesh generation and boundary conditions.

The CFD mesh was automatically generated using Gmsh (Geuzaine, 2009). I used uniform grid distribution across the tracheal cross-sectional area, since Reynolds number in the trachea is in the range between 1500 and 2000. When the program selects the mesh size for the trachea it accounts for the viscous sub-layer of the trachea, where the flow is most turbulent. The program selects the optimum size mesh, at which any reduction in the size would not improve the prediction of flow field or particle distribution and deposition. I used the flow rate in each branch to determine the branch mesh size Δ_b relative to the trachea.

$$\Delta_b = \min \left(\Delta_t \sqrt{\frac{D_b^3}{r_{Q,b} D_t^3}}, \frac{D_b}{6} \right)$$

(8.15)

Δ_t is the mesh size in the trachea, D_t is the trachea diameter, D_b is the branch diameter, and $r_{Q,b}$ is the flow rate ratio between the branch to trachea (Miyawaki, 2013). Equation 8-14, ensures the accuracy of the mesh selected by certifying the mesh determined relative to the trachea is smaller than one sixth the diameter of the branch. Thereby ensuring that no matter how small the branch is there will be at least six elements in it.

The accuracy and density of the mesh size is dependent on the flow rate ratio between the branch and the trachea. The flow rate in each branch was determined by using the image registration data (Yin et al., 2010). The image registration then uses a volume filling method to bridge the existing three dimensional (3D) CL-CT conductive airway geometry, I segmented using Apollo, to the lung parenchyma. This involves construction of a 1D tree from the end branches of the CL-CT geometry to each voxel in the lung's parenchyma. Then image registration assesses air volume change in the parenchyma at the voxel level between RV and TLC. These data are then interpolated through the 1D tree branches from the voxels at the lung's parenchyma to the end branches of the 3D CL-CT model (Fuld et al., 2008; Miyawaki et al., 2012; Yin et al., 2010) .

The meshed CL-CT geometry was then divided into multiple volumes based on branching of the airway (e.g. the trachea, right main stem bronchus, and left main stem bronchus are three distinct separate volumes). The boundary condition was then applied to all of the volume branches. Separating each airway branch into a distinct volume assists in the analysis of airflow data and particle distribution and deposition. The resulting CFD mesh for the whole geometric model consists of boundary and volume meshes for each branch.

Our model does not include the oral cavity. However the oral cavity is responsible for production of homogeneous isotropic turbulence above the glottis constriction (J. Choi et al., 2009). This turbulence affects the characteristics of the laryngeal jet below the glottis constriction, and in the trachea. Unlike the glottis constriction, the structure details and measurement of the extrathoracic airway are not well reported in the literature. Therefore, I introduced homogeneous isotropic turbulence at the inlet of the geometry above the glottis using the synthetic eddy method (Jarrin, 2009; Miyawaki, 2013). This method reproduces turbulence that has correlation with time and space. It only requires data regarding the intensity and length scale of the homogenous isotropic turbulence and it will synthetically produce extrathoracic turbulence at the inlet surface. I used data reported in the literature obtained from healthy subjects for the turbulent intensity of 0.29 and turbulent length scale of 8.0 mm (J. Choi et al., 2009; Miyawaki et al., 2012).

8.2.9. Computational fluid dynamics solver.

The same method in [Chapter 6.2.3](#) was used in this study.

8.2.10. Lagrangian particle tracking algorithm.

The same method in [Chapter 7.2.4](#) was used in this study.

8.2.11. Statistical analysis.

Data are presented as mean \pm standard error of the mean (SEM). For statistical analyses between groups, Student's t or Mann-Whitney tests were used. Differences were considered statistically significant at $P < 0.05$.

8.3. Results.

This study had two major aims. First, I investigated the global and local lung function in CF patients compared to healthy subjects. Second, I divided the CF patients I studied in the first aim into two groups: mild and severe. I then investigated the global and local lung function in each group and observed which one had a major effect on the data. I also compared the outcome of each CF group to the data from healthy subjects. Therefore, the results are divided into two sections. First, I analysed the CF lung structure and function compared to healthy subjects. Second, I investigated the effect of disease severity in CF patients on lung structure and function compared to healthy subjects. I have been fortunate to have access to CT scan datasets from CF subjects with the G551D mutation. Therefore this study was performed in that patient population.

8.3.1. CF lung structure and function.

8.3.1.1. Demographics.

The non-CF and CF subjects selected for this study had the same weight, height, body mass index (BMI) and similar gender ratio when compared statistically (under forty percent male) (Table. 8.1). Although the age difference between the two groups (normal and G551D CF patients) was statistically different, it was not considered to be an affecting factor since both groups are adults and in their twenties/ thirties and the two groups were site-matched. For the normal patients, coached pulmonary function tests (PFTs) and CT images were acquired at the University of Iowa. For CF patients, both PFTs data and CT images were obtained in St. Vincent University Hospital (Dublin, Ireland). The CT images were obtained during a coached breath-hold at end full inspiration and end expiration in the supine position. The end-

inspiratory and end-expiratory, for scans will be referred to as TLC and RV respectively, for simplicity. Similar scanner settings were used for both the normal healthy subjects and CF patients (Table. 8.2).

I next assessed the global predicted pulmonary function in normal and in CF subjects. I used the percent predicted values instead of the observed values (value actually measured by the spirometre) because the predicted value accounts for the gender, race, height, and age differences between patients. The pulmonary function was assessed by examining the forced expiratory data to predict the change in airway resistance. This measurement is called forced expiratory lung volume (FVC). FVC is the maximum volume of air a patient is able to expire with maximum effort, following an inspiration with maximum effort to reach total lung capacity (TLC) volume (Levitzky, 1995; University, 2014; Widmaier, 2011).

8.3.1.2. PFTs.

First I examined force expiratory volume in one second (FEV1). I found that G551D CF patients had statistically lower FEV1 compared to normal subjects (Figure 8.1A). I also found that forced (mid) expiratory flow rate (FEF25-75%) was statistically lower in CF patients compared to normal subjects (Figure 8.1C). Although, it is argued that FEF is effort based and it does not provide reliable quantitative data (Levitzky, 1995; Quanjer, Weiner, Pretto, Brazzale, & Boros, 2014), it is still important in general assessment of small airway disease. Therefore, although I cannot use FEF25-75% to quantify small airway disease, I can use it as an indicator of the presence of small airway disease in CF patients. I also examined force vital capacity (FVC) and FEV1/FVC (Figure 8.1B & 8.1D). I found that although both FVC and FEV1/FVC were lower than normal, the values in CF were not statistically significant when compared to normal.

To summarize, I found that G551D CF patient had FEV1, FEF25-75%, FVC and FEV1/FVC that is lower than normal. The FEV1 and FEF25-75% data were statistically lower in CF compared to normal subjects. This is an indicator that CF patients suffer from an obstructive airway disease caused in-part by abnormalities in the small airways. However, using the PFTs alone I'm unable to identify the abnormality in the small airways or its effect on the local lung resistance and function.

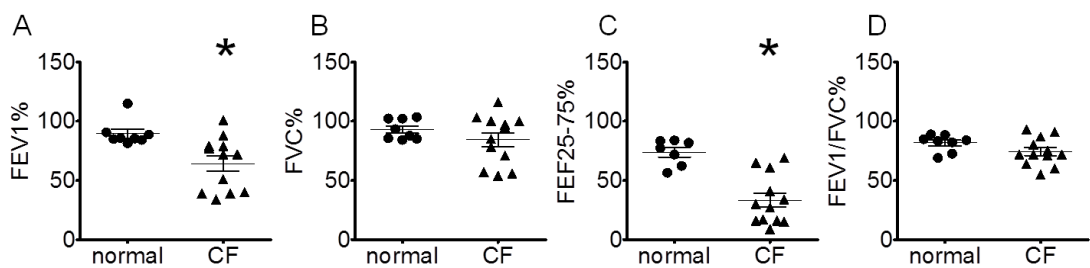


Figure 8.1. Comparing global lung function between healthy non-CF subjects and CF patients using PFTs. (A) FEV1% is forced expiratory volume in one second. (B) FVC% is forced vital capacity. (C) FEF 25-75% is forced (mid) expiratory flow rate. (D) FEV1/FVC % is the ratio between FEV1 and FVC. * denotes statistical significance ($P < 0.05$). Black filled circle (normal, on the x-axis) denote each individual healthy non-CF patients. Black filled triangle denote each individual CF patient.

8.3.1.3. Fixed lung volume analysis.

I next examined the total lung capacity at both RV and TLC in CF and normal patients using CT scan data. I found that G551D CF patients had higher average RV lung volume and lower average TLC lung volume compared to normal. However, these global differences were not statistically significant (Figure 8.2A). I next examined local volume changes by quantifying the normalized lobar lung volume at RV and TLC. I normalized the lobar volume by the total lung volume at TLC for each patient. I found that the average RV volume was higher in all the lung lobes in CF compared to normal. This increase in RV volume was statistically different in both the upper and lower right lobe (Figure 8.2B). I also examined the normalized TLC volume and I found no statistical difference in all lung lobes in CF compared to normal (Figure 8.2C). Next I assessed the change in volume in CF compared to normal. I found that CF patients had lower volume change in all lung lobes compared to normal. This decrease in volume change is statistically significant in the upper right lobe (Figure 8.2D). This decrease in volume is predictable since the normalized RV volume is greater and the TLC volume is the same in CF compared to normal subjects. The increase in RV volume can be due to tissue inflammation or air trapping due small airway collapse (Figure 8.2E). I quantified the tissue volume and I found no difference between normal and CF patients. I next quantified air trapping, and I found that average air trapping was greater (~ 60% greater) in all lung lobes and the whole lung in CF compared to normal. The increase in local air trapping was statistically significant in the upper right and left lung compared to normal. Moreover, the global air trapping was statistically greater in CF compared to normal (Figure 8.2F).

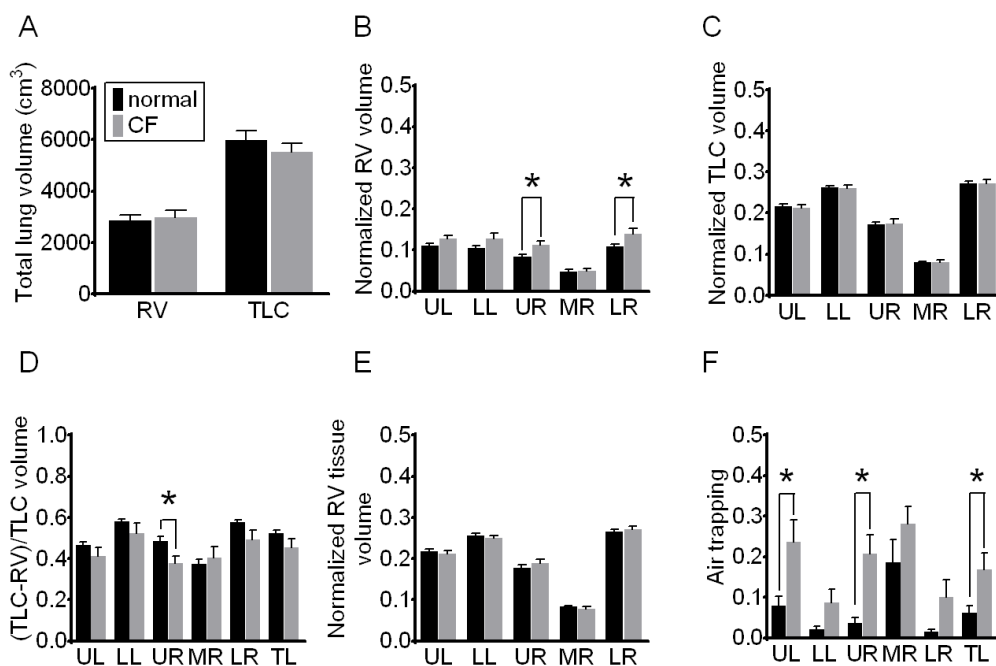


Figure 8.2. Supine computed tomography fixed volume global and local values. (A)

Total lung volume (global) at residual volume (RV) and total lung capacity (TLC). Normal denote non-CF patients. CF denotes CF patients. (B) Lobar lung volume at RV normalized by total lung volume at TLC for each individual patient's lobe. UL denotes upper left lung lobe. LL denotes lower left lung lobe. UR denotes upper right lung lobe. MR denotes middle right lung lobe. LR denotes lower right lung lobe. * denotes statistical significance ($P < 0.05$).

(C) Lobar lung volume at TLC normalized by total lung volume at TLC for each individual patient's lobe. (D) Lobar lung compliance measures the dynamic change in lobe volume from TLC to RV normalized by the lobe volume for each individual patient total lung volume at TLC. (E) Tissue density at the RV scan. Tissue density is defined as any voxel with a Hounsfield unit greater than -55. (F) Lobar air trapping. TL denotes total lung.

8.3.1.4. Image registration.

I next used image registration to examine the changes in the dynamic lung properties. The warped image generated by the image registration code was used to quantify the change in the lung shape. I found that CF lungs had a statistically longer depth (distance from the ventral to dorsal side of the lung). In addition, CF lungs had a statistically shorter height (distance from the apical to basal side of the lung). No statistical difference was observed in the width (lateral distance from the right to the left side of the lung) (Figure 8.3A). The differences found in depth and height of the lung leads to the CF abnormal lung shape. I quantified the lung shape from the lateral view by dividing the height of the lung by its depth (Z/Y). If the outcome of the Z/Y is equal to one this means that the lung occupies a square like-shape. I found that Z/Y was statistically smaller in CF patients compared to normal, meaning that the CF lung is more square-like compared to normal subjects (Figure 8.3B). I next examined the lung shape from the front view (Z/X) and I found that in this view the lungs are also more square-like. Z/X in CF was statistically lower compared to normal. This indicates that the global dynamic change in lung shape in CF is statistically different compared to normal healthy subjects.

I next examined the change in volume expansion ratio from RV to TLC or Jacobian of each lung lobe in CF patients compared to normal subjects. I found that all the lung lobes in CF patients expand less compared to normal control subjects. This decrease in expansion ratio in CF was statistically significant in the upper and lower right lobe compared to normal (Figure 8.3C). I next quantified the anisotropic deformation index (ADI), which is the non-uniform deformation of the lung tissues. I found that the tissue deformed less in all lung lobes in CF patients compared to normal. This decrease in ADI was statistically significant in the upper right, upper

left lobe and in the lower right lobe (Figure 8.3D). The decrease in the volume expansion and ADI in CF patients is in part due to the higher air trapping in CF which increases the RV volume.

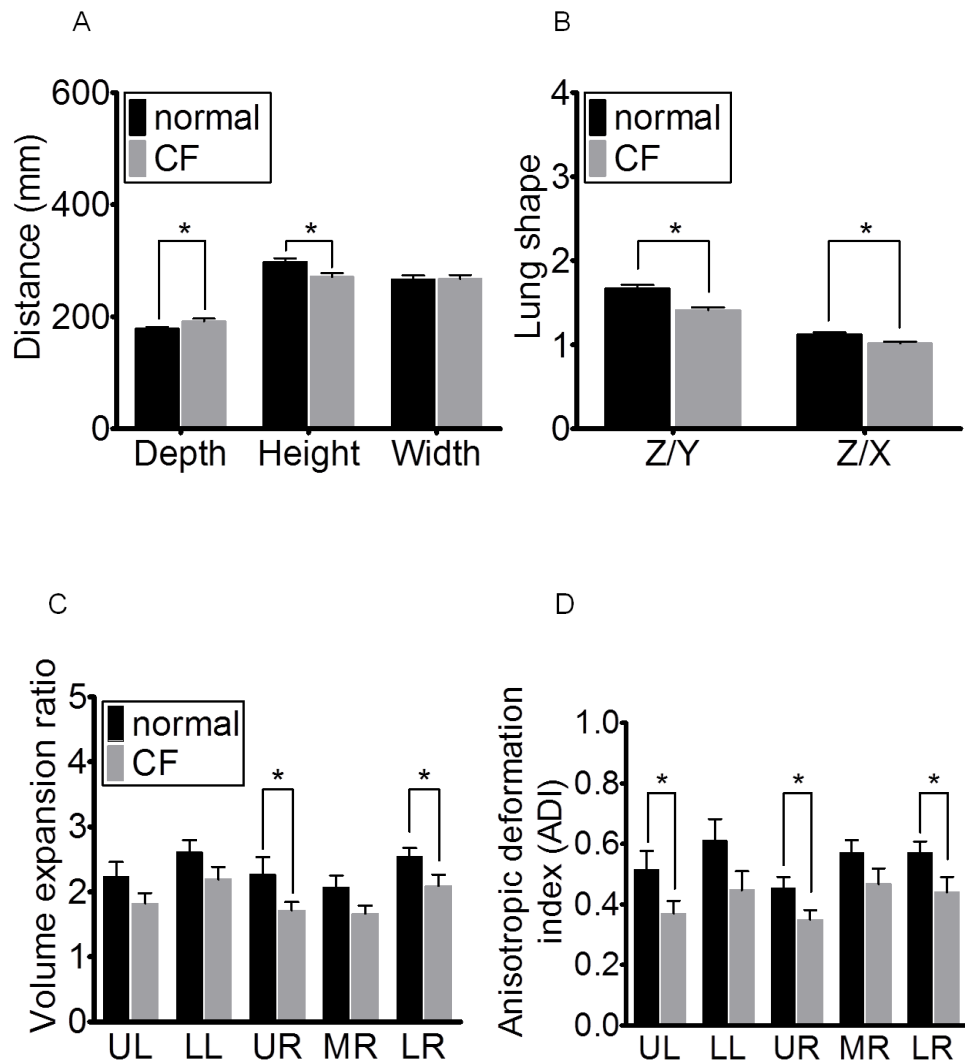


Figure 8.3. The effect of lung expansion from RV to TLC on total lung dimensions, shape, volume expansion and tissue deformation in non-CF and CF. (A) Total lung dimensions: the depth (the distance from the ventral to the dorsal side), the height (the distance from the apical to the basal side), and the width (distance from the left to the right lateral side). Normal denote non-CF patients. CF denotes CF patients. * denotes statistical significance ($P < 0.05$). (B) Lung shape defined as height (Z) over depth (Y) and height (Z) over width (X). (C) The ratio of lobar air and tissue volume change as the lung expands from RV to TLC. (D) The non-symmetrical deformation in the tissue ratio also know as anisotropic deformation index (ADI).

8.3.1.5. The effect of abnormal local lung function on particle ventilation and deposition.

I selected three representative subjects from each group (normal and CF) for CFD analysis. The normal representative subjects for the CFD analysis were selected based on having no statistical difference in lung volume and air trapping compared to all the non-CF subjects used in this study (Figure 8.4A-D). The three CF subjects selected had the highest air trapping percentage globally in the whole lung and locally in all lung lobes (Figure 8.4E). The representative subjects had similar RV and TLC volume globally in the whole lung and locally in all the lung lobes compared to all CF subjects in the study (Figure 8.4F- 8.4K).

I investigated the particle ventilation fraction in selected representative normal and CF patients. I found that for all particle sizes studied CF patient tended to have greater particle ventilation to the upper lobes (left and right) as well as the right lower lobe, with these differences being most statistically significant for the right upper lobe (Table 8.3). I also quantified the number of particles deposited in the airways considered in the airway geometry. I found that in CF patients, particle deposition efficiency was higher than normal healthy subjects for all particle sizes studied in all lung lobes, except the lower left lobe. This increase in particle deposition in CF patient was statistically significant in the right upper lobes (Table 8.4).

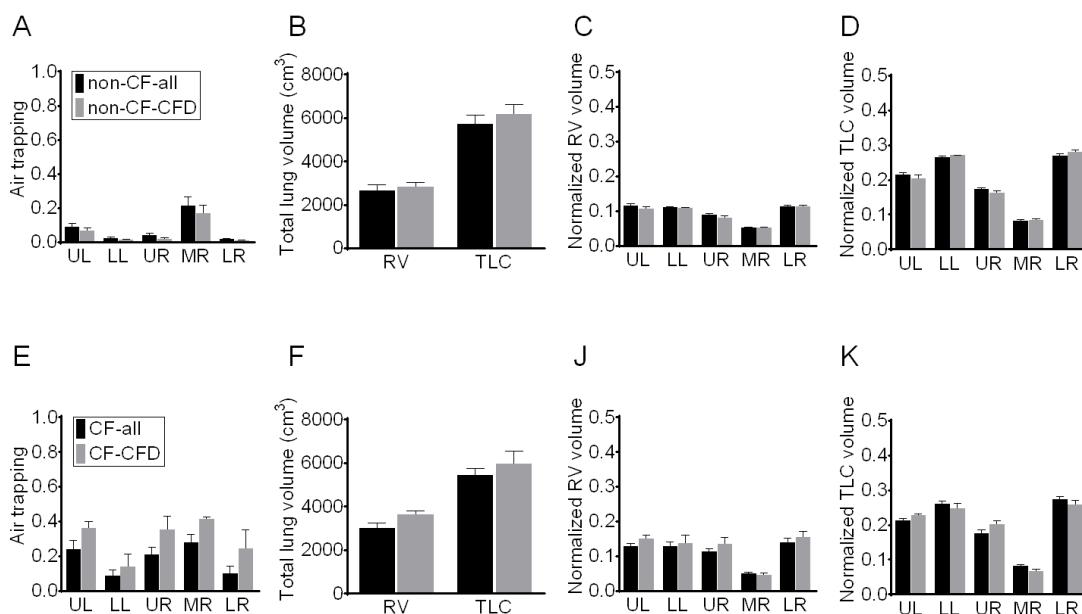


Figure 8.4. Selecting three representative CF patients for computational fluid

dynamics (CFD) study based on maximum air trapping in all lobes. (A) Air trapping in all healthy normal subjects (non-CF-all) compared to the selected representative healthy normal subjects for CFD study (non-CF-CFD). UL denotes upper left lung lobe. LL denotes lower left lung lobe. UR denote upper right lung lobe. MR denotes middle right lung lobe. LR denotes lower right lung lobe. (B) Total lung volume in all healthy normal subjects compared to the selected representative non-CF-CFD. RV denotes residual lung volume. TLC denotes total lung capacity. (C) Lobar RV volume normalized in all non-CF-all compared to the selected representative non-CF-CFD patients. Each lobe at RV was normalized by total lung volume at TLC from each individual patient. (D) Lobar TLC volume normalized in all non-CF-all compared to the selected representative non-CF-CFD patients. Each lobe at TLC was normalized by the total lung volume at TLC from each individual patient. (E) Air trapping in all CF patients (CF-all) compared to the selected representative CF patients for CFD study (CF-CFD). (F) Total lung volume in all CF patients compared to the selected representative CF-CFD patient. (J) Lobar RV volume normalized in all CF patients compared to the selected representative CF-CFD patients. (K) Lobar TLC volume normalized in all CF patients compared to the selected representative CF-CFD patients.

Particle size	genotype	UL	LL	UR	MR	LR
0.5 μm	Normal	0.15 \pm 0.05	0.45 \pm 0.11	0.10 \pm 0.02	0.04 \pm 0.01	0.15 \pm 0.04
	CF	0.22 \pm 0.03	0.30 \pm 0.02	0.17 \pm 0.02 *	0.05 \pm 0.01	0.20 \pm 0.01
1 μm	Normal	0.15 \pm 0.06	0.45 \pm 0.10	0.10 \pm 0.02	0.04 \pm 0.01	0.15 \pm 0.04
	CF	0.22 \pm 0.03	0.30 \pm 0.02	0.17 \pm 0.02 *	0.05 \pm 0.01	0.20 \pm 0.01

Table 8.3. Particle ventilation fraction for CF patients compared to healthy non-CF subjects. Ventilation fraction is the number of particles that entered a specific lobe divide by the total number of particles that entered all the lobes. Two particle sizes were considered in the study 0.5 μm and 1 μm . UL denotes upper left lung lobe. LL denotes lower left lung lobe. UR denotes upper right lung lobe. MR denotes middle right lung lobe. LR denotes lower right lung lobe. * denotes statistical significance ($P < 0.05$). \pm denotes standard error.

Particle size	Genotype	UL	LL	UR	MR	LR
0.5 μm	Normal	0.012 \pm 0.002	0.021 \pm 0.007	0.005 \pm 0.001	0.002 \pm 0.001	0.012 \pm 0.005
	CF	0.018 \pm 0.005	0.018 \pm 0.004	0.009 \pm 0.001 *	0.004 \pm 0.001	0.020 \pm 0.003
1 μm	Normal	0.013 \pm 0.003	0.020 \pm 0.006	0.005 \pm 0.001	0.002 \pm 0.001	0.013 \pm 0.004
	CF	0.019 \pm 0.004	0.019 \pm 0.002	0.010 \pm 0.001 *	0.003 \pm 0.001	0.020 \pm 0.003

Table 8.4. Particle deposition efficiency for CF patients compared to healthy non-CF subjects. Deposition efficiency is the number of particles that deposited in a specific lobe divided by the total number that entered that same lobe. Two particle sizes were considered in the study 0.5 μm and 1 μm . UL denotes upper left lung lobe. LL denotes lower left lung lobe. UR denotes upper right lung lobe. MR denotes middle right lung lobe. LR denotes lower right lung lobe. * denotes statistical significance ($P < 0.05$). \pm denotes standard error.

8.3.1.6. Airway and lung properties in the CF lung that lead to increased particle ventilation and deposition in the right upper lobe.

I found that the mass flow rate to the upper lobes is statistically increased in CF compared to normal (Figure 8.5A). I then examined the airway cross-sectional area, pressure drop and resistance in the airway branch supplying the right upper lobe (RUL airway). I found that the average airway cross sectional area of the RUL airway for the subjects selected was smaller in CF patients compared to normal (Figure 8.5B). This decrease in area, in the CFD analysis although not statistically significant did increase the pressure drop and resistance in the RUL airway (Figure 8.5C & 8.5D). I have also found the airflow velocity was statistically higher in the RUL airway in CF compared to normal (Figure 8.5E). Due to the higher pressure drop and lower and higher velocity more particles enter the right upper lobes in CF compared to normal.

I also observed that the mass flow rate was greater in left upper lobe in CF patients. However, the CFD model did not predict increased particle ventilation to the left upper lobe. This is, in part, due to the greater cross-sectional area of the airway supplying the upper left lobe (LUL airway) in CF compared to normal (normal: $45.2 \pm 5.5 \text{ mm}^2$, CF: $48.8 \pm 7.5 \text{ mm}^2$, $P = 0.7$). Therefore, both the airflow velocity and pressure drop were not statistically significant in CF compared to normal (airflow velocity, normal: 0.8 ± 0.1 , CF: 1.5 ± 0.3 , $P = 0.1$; pressure drop, normal: $0.3 \pm 0.1 \text{ Pa}$, CF: 0.7 ± 0.2 , $P = 0.2$). The higher average pressure drop and velocity values in CF patients lead to increased particle ventilation to the upper left lobe compared to normal (Table 8.3). However, the difference failed to be significant in part due to less

significant changes in the airflow velocity and pressure drop in the LUL airway in CF patients compared to normal subjects.

The increased deposition in the RUL airways was due, in part, to the greater airflow velocity, greater turbulent kinetic energy and greater Stokes number in the CF RUL airway compared to normal subjects (Figure 8.6).

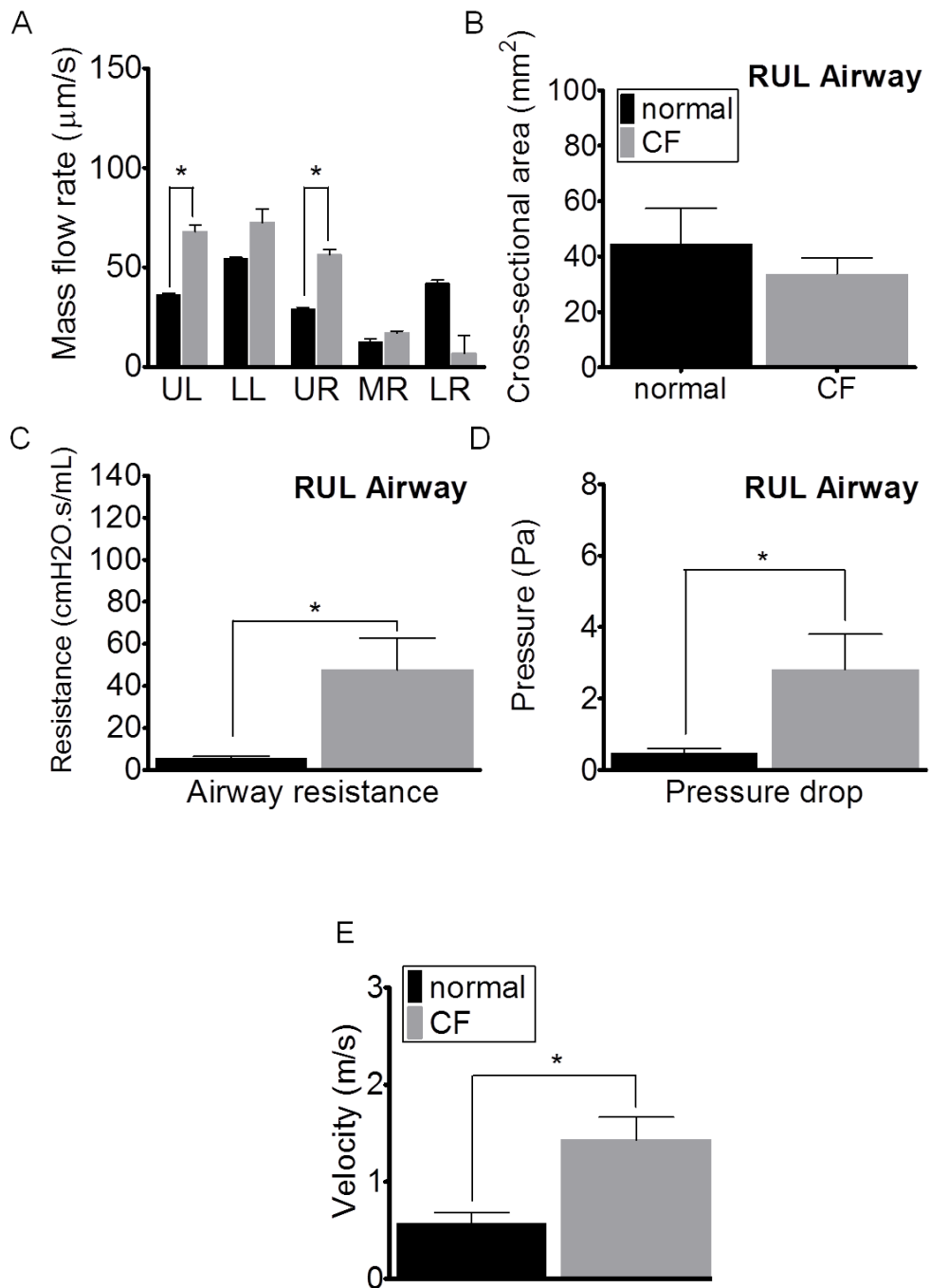


Figure 8.5. Factors that lead to increase particle ventilation into the right upper lobe. (A) Mass flow rate at the airway supplying right upper lobe (RUL Airway) in healthy non-CF subjects and CF patient. Normal denotes healthy non-CF subjects. CF denotes CF patients. UL denotes upper left lung lobe. LL denotes lower left lung lobe. UR denotes upper right lung lobe. MR denotes middle right lung lobe. LR denotes lower right lung lobe. * denotes statistical significance ($P < 0.05$). (B) Cross-sectional area of the RUL airway. (C) Airway resistance at the RUL airway. (D) Pressure drop at the RUL airway. (E) Airflow velocity at the RUL airway.

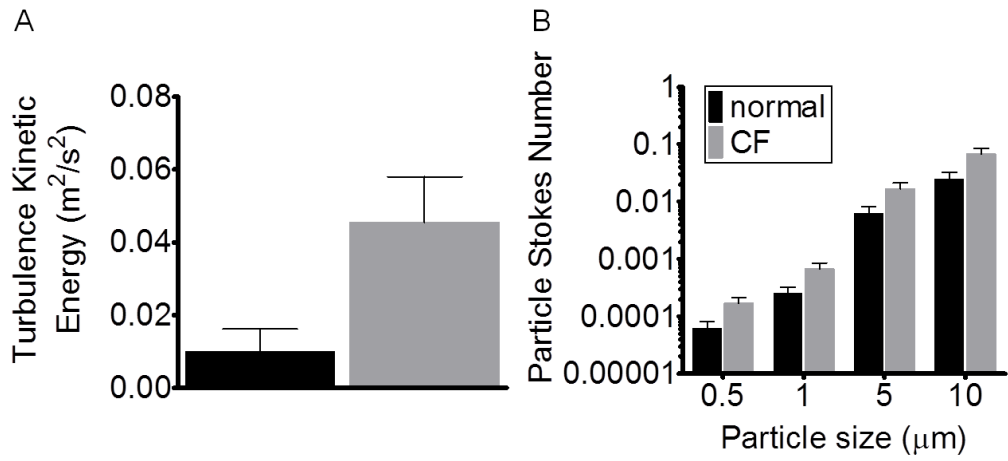


Figure 8.6. Factors that lead to increase particle deposition into the airways considered in right upper lobe. (A) Turbulent kinetic energy at the airway supplying right upper lobe (RUL airway) in healthy non-CF subject and CF patient. Normal denotes healthy non-CF subject. CF denotes CF patient. (B) Particle Stokes number in a log scale. Stokes number indicates the ability of the particle to deviate from the stream line due to its speed or mass. Particle sizes considered varied from 0.5 to 10 µm.

8.3.2. The effect of disease severity in CF patients on lung structure and function.

8.3.2.1. Demographics.

Same subjects examined in the previous section were further divided in two groups to investigate the effects of disease severity. I had 8 normal subjects, and I divided our CF subjects into two groups: “mild” and “severe” based on FEV1 of greater than (mild) or less than (severe) 55%. I had 6 mild G551D cystic fibrosis (CF) patients with FEV1 > 55%, and 3 severe G551D CF patients with FEV1 < 55%. All of the CF severe subjects had the same weight, height, body mass index (BMI) and similar gender ratio around 34% male compared to mild and normal healthy subjects (Table. 8.5).

	No. (% male)	Age	Weight	Height	BMI
Normal	8(37%)	22.5 ± 0.7	59.3 ± 3.3	168.6 ± 2.5	20.8 ± 0.8
CF-H	6(33%)	29.7 ± 1.9	59.3 ± 4.8	164.5 ± 2.8	21.7 ± 1.1
CF-L	3(33%)	26.3 ± 2.3	56.7 ± 6.7	165 ± 4.2	20.7 ± 1.4

Table 8.5. The demographical data from all the subjects selected for the effect of disease severity study. Disease severity was determined by FEV1 value. 8 non-CF subjects, 6 mild G551D cystic fibrosis (CF) patients with FEV1 > 55%, and 3 severe G551D CF patients with FEV1 < 55%. Age units is in years. Weight in kilograms (kg). Height in centimetre (cm). BMI is body mass index which is a ratio between weight and height. BMI = Weight/(height*height). CF-L denotes patients with low FEV1 (FEV1% < 55%). CF-H denotes patients with high FEV1 (FEV1% > 55%).

8.3.2.2. PFTs.

I first examined the difference in the global lung function in the three groups (normal, mild CF patients, and severe CF patients) using PFTs. I quantified the average FEV1 value for the normal subjects, mild CF, and severe CF patients. I found that severe CF patients had an average FEV1 value of 43% compared to 70% in the mild CF patients and 85% in the normal subjects (Figure. 8.7). As expected, FEV1 was statistically lower when the severe CF patients were compared to the normal subjects (Figure. 8.7). Although the average value of mild CF patients' FEV1% was lower compared to normal subjects, there was no statistical difference between mild CF patients and normal subjects. I next examined FVC. I found that FVC in severe patients was lower compared to mild CF patients and normal subjects. There was no statistical difference between mild CF patients and normal subjects (Figure. 8.7). However, I found that FEF25-75% value was statistically lower in both severe and mild CF patients, compared to normal. FEF25-75% was also statistically lower in severe CF patients compared to mild CF patients. Finally, I examined FEV1/FVC%. I found that FEV1/FVC% was statistically lower in severe patients compared to mild patients and normal subjects. Despite that the average value of FEV1/FVC% in mild CF patients was lower compared to normal subjects, the difference was not statistically significant (Figure. 8.7).

These PFTs findings suggest that severe CF patients have more severe obstructive lung disease indicated by lower FEV1%, FVC% and FEV1/FVC%. FEF25-75% was also lower in severe CF patients compared to both normal and mild CF patients. This is an indicator of severe small airway disease. Although, it is argued that FEF is effort based and it does not provide reliable quantitative data (Levitzky, 1995; Quanjer et al., 2014), it is still important in general assessment of small airway disease. Therefore, although I cannot use FEF25-75% to quantify small airway

disease, I can use it as an indicator of the presence of small airway disease in CF patient.

In mild CF patients FEV1 and FEV1/FVC were lower than normal but not statistically different. Moreover, FVC in mild CF patients was almost equal to normal. This is an indicator of a mild obstructive airway disease, and since FEF25-75% is statistically lower in mild CF patients compared to normal I can speculate that this obstruction is caused by small airway abnormalities.

However, using PFT values alone, I'm unable to demonstrate how disease severity indicated by FEV1 values will affect the global and local segmental lung function and structure. Moreover, obstructive disease can be caused by bronchial smooth muscle contraction, inflammation and swelling of bronchial mucosa, hypertrophy and hyperplasia of bronchial glands, excessive mucus plugging, tumours and trauma, or destruction of lung tissue and loss of elasticity (Voelkel, 2008). Using PFTs alone will not provide any information in regards to the underlying causes of the obstructive disease.

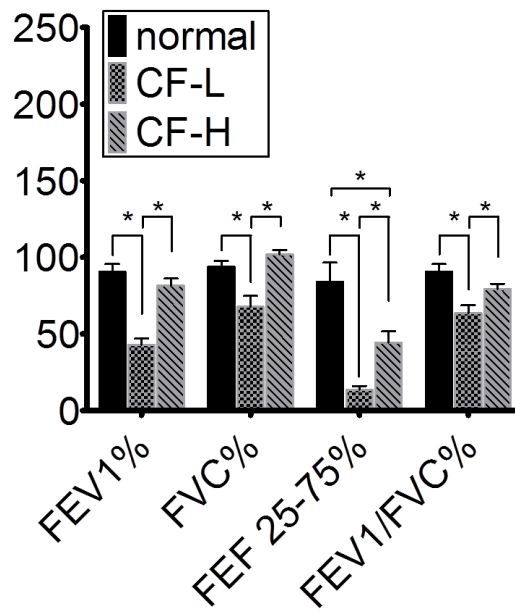


Figure 8.7. Comparing global lung function between non-CF, mild CF patients, and severe CF patients using predicted PFTs. FEV1% is force expiratory volume in one second. FVC is forced vital capacity. FEF 25-75% is forced (mid) expiratory flow rate. FEV1/FVC % is the ratio between FEV1 and FVC. * denotes statistical significance ($P < 0.05$). Normal denotes non-CF patients. CF-L denotes patients with low FEV1 ($FEV1\% < 55\%$). CF-H denotes patients with high FEV1 ($FEV1\% > 55\%$).

8.3.2.3. Fixed volume lung analysis.

To further understand global and local lung function in mild and severe CF patients, I next investigated the total and lobar lung volume at RV and TLC and the change in lung volume from RV to TLC. First I examined the total lung volume at RV and TLC. I found that severe CF patients had greater RV volumes compared to normal subjects and mild patients. In mild patients the average RV volume was actually lower than normal subjects. However no statistical difference was observed between mild CF patients and normal subjects. I found no statistical difference in TLC volume when comparing normal subject, mild CF patients, and severe CF patients (Figure. 8.8A).

Next I examined the lobar volume difference at RV and TLC. I found that severe patients had statistically higher RV volume in all lobes compared to normal except in the right middle lobe where no difference was observed. In addition RV volume in severe patients was also statistically greater compared to mild CF patients except in the right middle and lower lobe where no statistical difference in the volume was observed. In mild CF patients, I observed no statistical difference in RV volume compared to normal patients (Figure. 8.8B). For lobar TLC volumes, I found no statistical difference between normal subjects, mild CF patients, and severe CF patients (Figure. 8.8C).

I next analyzed the change in global and lobar volume from RV to TLC. I found that severe patients had statistically smaller volume change in all lobes compared to normal and mild patients. No statistical difference was observed in lobar lung volume change between normal and mild CF patients (Figure. 8.8D).

The higher RV can, in part, explain the statistically lower FVC values in severe CF patients. A common cause for increase a RV volume is air trapping. I quantified the air trapping in the global and local lobar level in the normal subjects, mild CF subjects, and the severe CF subjects. I found that in all the lungs lobes, except for middle and lower right lobe, air trapping was statistically higher in severe CF patients compared to both normal subjects and mild CF patients. In mild CF patients, the average value of air trapping was larger in the upper right and left lobe and lower right lobe compared to normal subjects. However, the increase in air trapping value in mild patients was only statistically significant in the upper right lobe compared to normal subjects (Figure. 8.8E).

I next examined the airway size, shape, and function. I first investigated the airway size at TLC. I found that severe CF patients' airway cross-sectional area at TLC was smaller compared to mild CF patients and normal subjects. This decrease in cross-sectional area in severe CF patients was statistically significant for all the airways with a diameter smaller than 7.5 mm compared to normal subjects. In addition, the decrease in severe CF patients' airway cross-sectional area was statistically significant for airways with diameter ranging from 4.5 to 9 mm compared to mild patients. No statistical difference in airway cross-sectional area was observed between normal and CF subject with mild disease (Figure. 8.9A).

Next I quantified the airway cross-sectional area at the RV. I found no difference in RV airway cross-sectional area between that the severe CF patients, mild CF patients, and normal subjects. Except for airways smaller than 4.5mm in diameter where the severe patients had larger airway cross-sectional area compared to mild CF patients. It is important to note that in severe CF patients, at both RV and TLC, for airways with a diameter larger than 9 mm (Trachea, RMB, BronInt, LMB, LLB6) the

average airway cross-sectional area tended to be larger compared to normal and mild CF patients (Figure. 8.9B).

I also assessed airway distensibility. Airways distensibility was measured by subtracting the airway diameter at TLC from the airway diameter at RV, then dividing the outcome by the airway diameter at TLC. I found that in all subjects studied (severe CF patients, mild CF patients, and normal subjects) airway distensibility increased with the decrease of the airway diameter. I also found that the airway distensibility was decreased in severe CF patients compared to mild patients and normal subjects. This decrease was statistically significant in severe patients for airways with a diameter smaller than 7.5 mm and larger than 9 mm compared to normal and mild CF patients. The absence of a significant difference for airways with a diameter between 7.5 and 9 mm is due to our small sample size. I found no statistical difference in airway cross sectional area at RV and TLC and airway distensibility between normal subjects and mild CF patients (Figure. 8.9A-C).

To conclude, I found that severe CF patients had higher air trapping in all lung lobes except for the right middle and lower lobe. The increased air trapping led to a larger RV volume in severe CF patients in all lobes except right middle and lower lobes. This was associated with decreased air volume change in severe patients in all lobes. Interestingly, I found that the decrease in air volume change in all G551D CF patients (severe and mild patients combined) in the upper right lobe might be, in part, due to the combined increase in air trapping in the right upper lobe in both mild and severe patients (Figure. 8.8E & 8.8D).

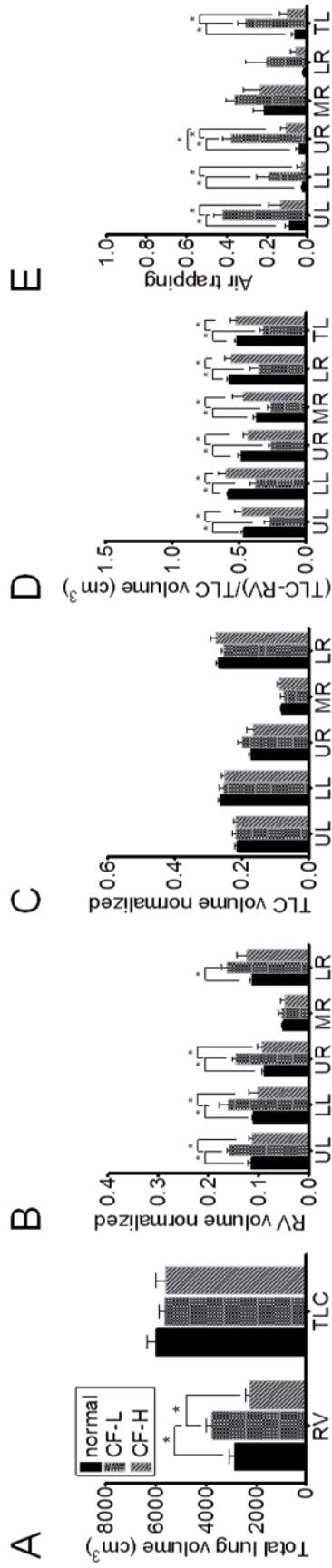


Figure 8.8. Supine computed tomography fixed volume global and local value. (A) Total lung volume (global) at residual volume (RV) and total lung capacity (TLC). Normal denote non-CF patients. CF-L denotes patients with low FEV1 (FEV1% < 55%). CF-H denotes patients with high FEV1 (FEV1% > 55%). * denotes statistical significance (P < 0.05). (B) Lobar lung volume at RV normalized by total lung volume at TLC for each individual patient's lobe. UL denotes upper left lung lobe. LL denotes lower left lung lobe. UR denotes upper right lung lobe. MR denotes middle right lung lobe. LR denotes lower right lung lobe. (C) Lobar lung volume at TLC normalized by total lung volume at TLC for each individual patient's lobe. (D) Lobar lung compliance, measures the dynamic change in lobe volume from TLC to RV normalized by the lobe volume for each individual patient total lung volume at TLC. (E) Lobar air trapping.

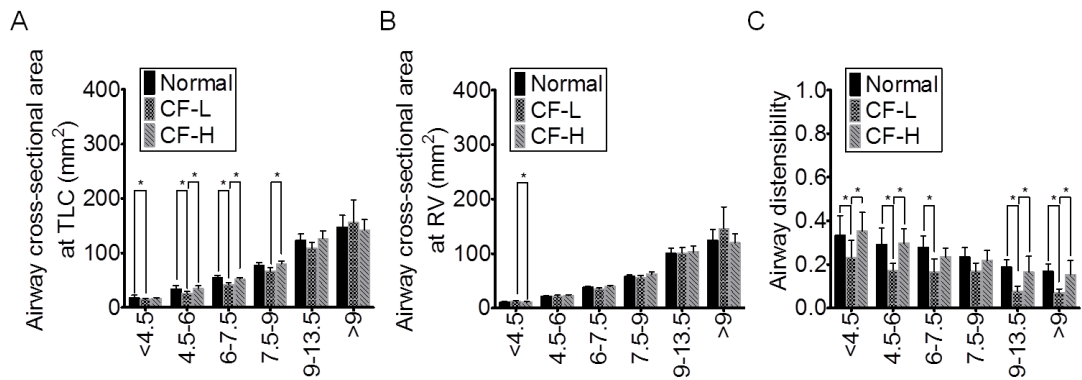


Figure 8.9. Static and dynamic airway values. All the airways measured were grouped based on their diameter at TLC (less than 4.5 mm, between 4.5 to 6, between 6 to 7.5, between 7.5 to 9, between 9 to 13.5, and finally larger than 13.5 mm). Airway diameter at total lung capacity (TLC) was picked since it is more stable and less based on patient effort. (A) Airway cross-sectional area at TLC (static). Normal denoted non-CF patients. CF-L denotes patients with low FEV1 (FEV1% < 55%). CF-H denotes patients with high FEV1 (FEV1% > 55%). * denotes statistical significance (P < 0.05). (B) Airway cross-sectional area at residual volume (RV) (static). (C) Airway distensibility (dynamic). The change in airway area from TLC to RV normalized by airway area at TLC.

8.3.2.4. Image registration.

I used image registration to predict the dynamic properties of the lung as it expands from RV to TLC. I first examined the total lung shape by examining the depth (the distance from the ventral to the dorsal side), height (the distance from the apical to the basal side), and the width (distance from the left to the right lateral side). I found that the depth of the lung was statistically larger in both mild and severe patients compared to normal subjects. Also I found that the lung height of both the severe and mild CF patients was smaller compared to normal subjects. Finally, I found that the width was only statistically greater in mild patients but not severe compared to normal subjects. No statistical difference was found in the depth, height, and width between the severe patients and the mild patients (Figure. 8.10A).

I next quantified the lung shape by dividing the height by the depth (Z/Y) and the height by the width (Z/X). I found that Z/Y was statistically smaller in both mild and severe patients compared to normal. I also found that Z/X was only statistically smaller in mild patients compared to normal. I found no statistical difference between severe and mild patients (Figure. 8.10B).

I next analysed lobar air volume change. I found that severe CF patients had statistically lower air volume change in all lung lobes compared to normal subjects and mild CF patients (Figure. 8.11A). Next I examined the expiration ratio of the lung volume (tissue and air). This ratio is also known as the Jacobian (J). I found that severe CF patients had a statistically lower J compared to normal subjects and mild CF subjects (Figure. 8.11B). Finally I examined the anisotropic deformation index, which indicates the ratio of tissue deformation. I found that severe CF patients' tissue deform less compared to mild CF patients and normal subjects (Figure. 8.11C). In addition, I found no statistical difference in air volume change, lung volume

expansion ratio, and deformation index in mild patients compared to normal subjects (Figure. 8.11).

These results further illustrate the effect of greater RV volume in severe CF patients due to increased air trapping in all lung lobes. The greater air trapping in severe patients leads to lower air volume change, Jacobian and tissue deformation ratio. Interestingly, in mild patients the air volume change, Jacobian and tissue deformation ratio were not statistically different compared to normal patients. In addition, the normalized lobar lung volume at RV and TLC was also not statistically different compared to normal. However, the change in lung shape from RV to TLC in the front view (Z/X) and the side view (Z/Y) was statistically smaller in mild CF patients compared to normal. Also, I found that mild CF patients had greater air trapping in all lobes. However, it was only statistically greater in the right upper lobe. This indicates that, in mild G551D CF patients, the increase in lobar air trapping might, in part, change the shape of the lung statistically without changing the lung volume very significantly.

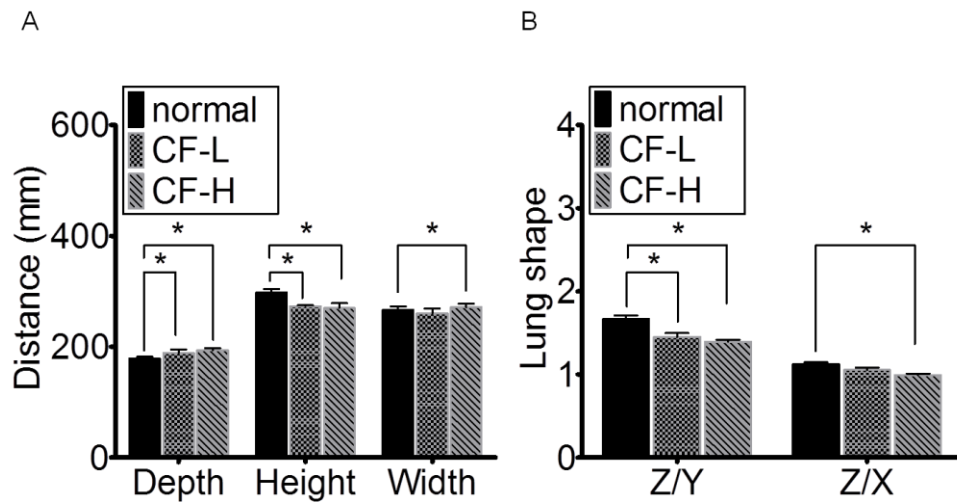


Figure 8.10. Comparing total lung dimensions and shape between non-CF, mild CF patients, and severe CF patients. (A) Total lung dimensions: the depth (the distance from the ventral to the dorsal side), the height (the distance from the apical to the basal side), and the width (distance from the left to the right lateral side). Normal denotes non-CF patients. CF-L denotes patients with low FEV1 (FEV1% < 55%). CF-H denotes patients with high FEV1 (FEV1% > 55%). * denotes statistical significance (P < 0.05). (B) Lung shape defined as height (Z) over depth (Y) and height (Z) over width (X).

Figure 8.11. Comparing dynamic volume and tissue properties between non-CF, mild CF patients and severe CF patients. (A) The change in lobar air volume as each lobe expands from residual volume (RV) to total lung capacity (TLC). Normal denotes non-CF patients. CF-L denotes patients with low FEV1 (FEV1% < 55%). CF-H denotes patients with high FEV1 (FEV1% > 55%). * denotes statistical significance (P < 0.05). UL denotes upper left lung lobe. LL denotes lower left lung lobe. UR denotes upper right lung lobe. MR denotes middle right lung lobe. LR denotes lower right lung lobe. Total denotes all lung lobes. (B) The ratio of lobar air and tissue volume change as the lung expands from RV to TLC. (C) The non-symmetrical deformation in the tissue ratio also known as anisotropic deformation index (ADI).

8.3.2.5. The effect of disease severity on local and segmental airflow ventilation and tissue deformation.

The lobar image registration data does not provide enough information in regards to the change in the dynamic lung function from the dorsal to ventral region or left to right lateral region. Therefore I analysed the dynamic lung function by examining slices obtain from the lung CT scans at a similar depth ratio. Conducting and displaying the outcome of this analysis in all patients included in the study is too time intensive. Therefore, I picked one representative severe CF patient, mild CF patient, and normal subject. I previously observed that the air trapping in both the mild and severe patients was only statistically greater in the right upper lobe compared to normal (Figure. 8.8E). Therefore, the representative healthy normal subject, severe patient, and mild CF patient were selected based on the highest air trapping in the upper right lobe (Figure. 8.12A - 8.12C). I found that the representative subjects in each group had similar total lung and lobar volumes at RV and TLC compared to the group they are representing (Figure. 8.12D - 8.12L).

Using these representative subjects, I first examined air volume change in vertical lung slices extracted at a lateral depth of 15, 30, 70, and 85% of the normal subject's , mild CF patient's and severe CF patient's lung. I found that the mild CF patient had lower air volume change in the apical region of the lung compared to the normal subject. However, the air volume change in the basal dorsal region of the lung in the mild patient was almost normal. In the severe patient, I observed over all lower air volume change and I also observed that the lung was hyper-inflated due to greater air trapping. I still observed higher air volume change in the severe CF patient's basal dorsal region compared to the apical region. However, this increase in air volume change is lower than both the normal subject and the mild patient (Figure. 8.13A).

This decrease in air volume change globally and locally in the representative severe CF patient is actually significant when I examine the whole severe CF group studied compared to mild CF patients and normal subjects (Figure. 8.13A).

Next, I examined air volume change in horizontal lung slices extracted at 20, 40, 60, and 80% of the height of the normal subject's, mild CF patient's and severe CF patient's lung. I found that mild patients had less air volume change in the left apical compared to the right apical lobe. Also, I observed greater air volume change in the dorsal region in the mild patient starting from the 40% slice and going to the basal region of the lung. In the severe patient, I observed lower overall ventilation to the entire lung region. The ventilation was specifically lower in the ventral top 60 percent of the lung (Figure. 8.13B).

In addition, I examined the Jacobian, which is the whole lung volume expansion ratio. I found higher Jacobian in the dorsal basal region of the normal lung. In the mild patient, the Jacobian value was lower in the dorsal basal region of the lung compared to the normal subject. In the severe patient I observed almost no change in the Jacobian in the dorsal region of the lung (Figure. 8.13C & 8.13D). This decrease in Jacobian value observed in the representative severe is significant when I examine the whole severe CF group studied compared to mild CF patients and normal subjects (Figure. 8.11B).

Finally, I examined the anisotropic deformation index. In this analysis, the value of zero (indicated by the deep blue colour) means there is no deformation in lung tissue as lung volume increases from RV to TLC. I found only few spots of deep blue in the normal patient. In the mild patient, I observed more deep blue spots in the right and left central region of the lung (Figure. 8.13E & 8.13F). This abnormal deformation found in the representative mild CF patient did not have a significant effect on the

deformation value in the whole mild CF group studied (Figure. 8.11C). In the severe patient, I observed more deep blue spots in all lung regions. This decrease in tissue deformation ratio observed in the representative severe is significant when I examine the whole severe CF group studied compared to mild CF patients and normal subjects (Figure. 8.11C).

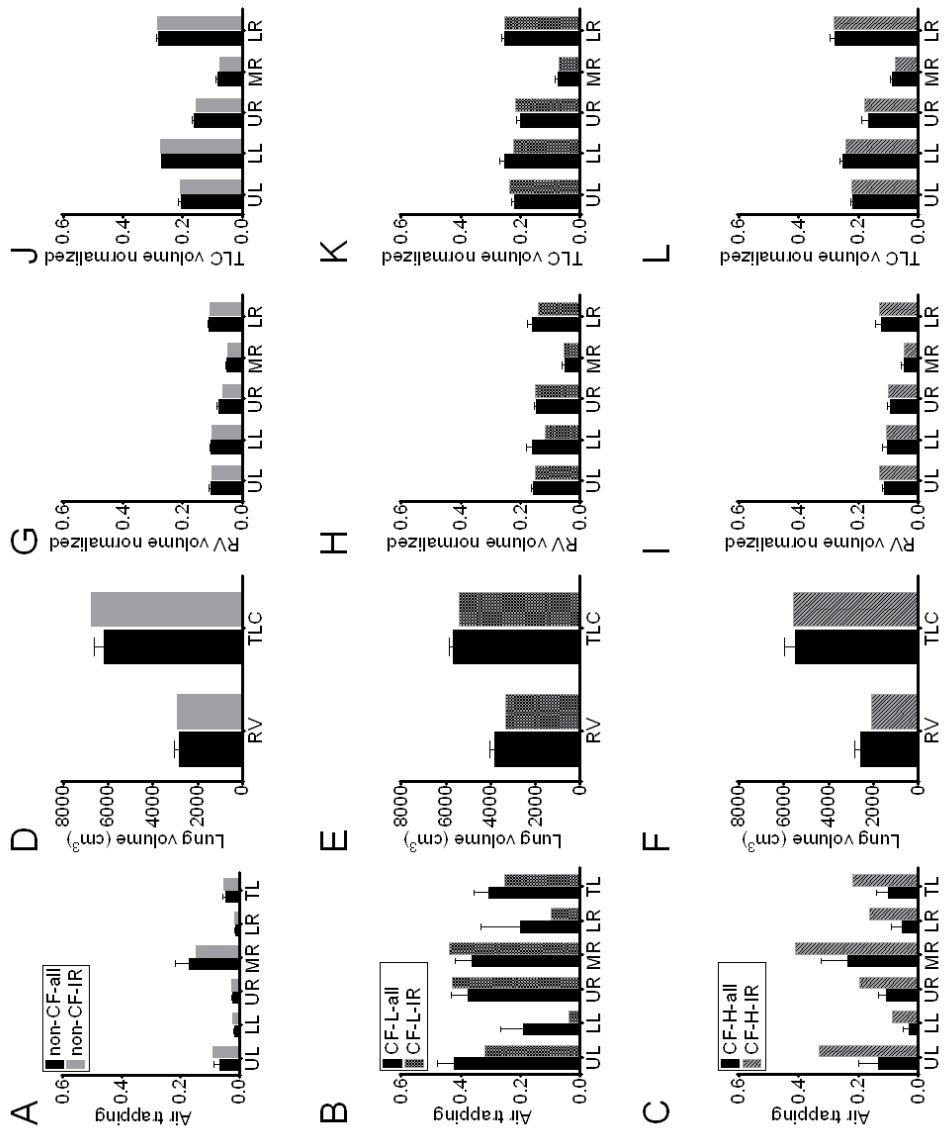
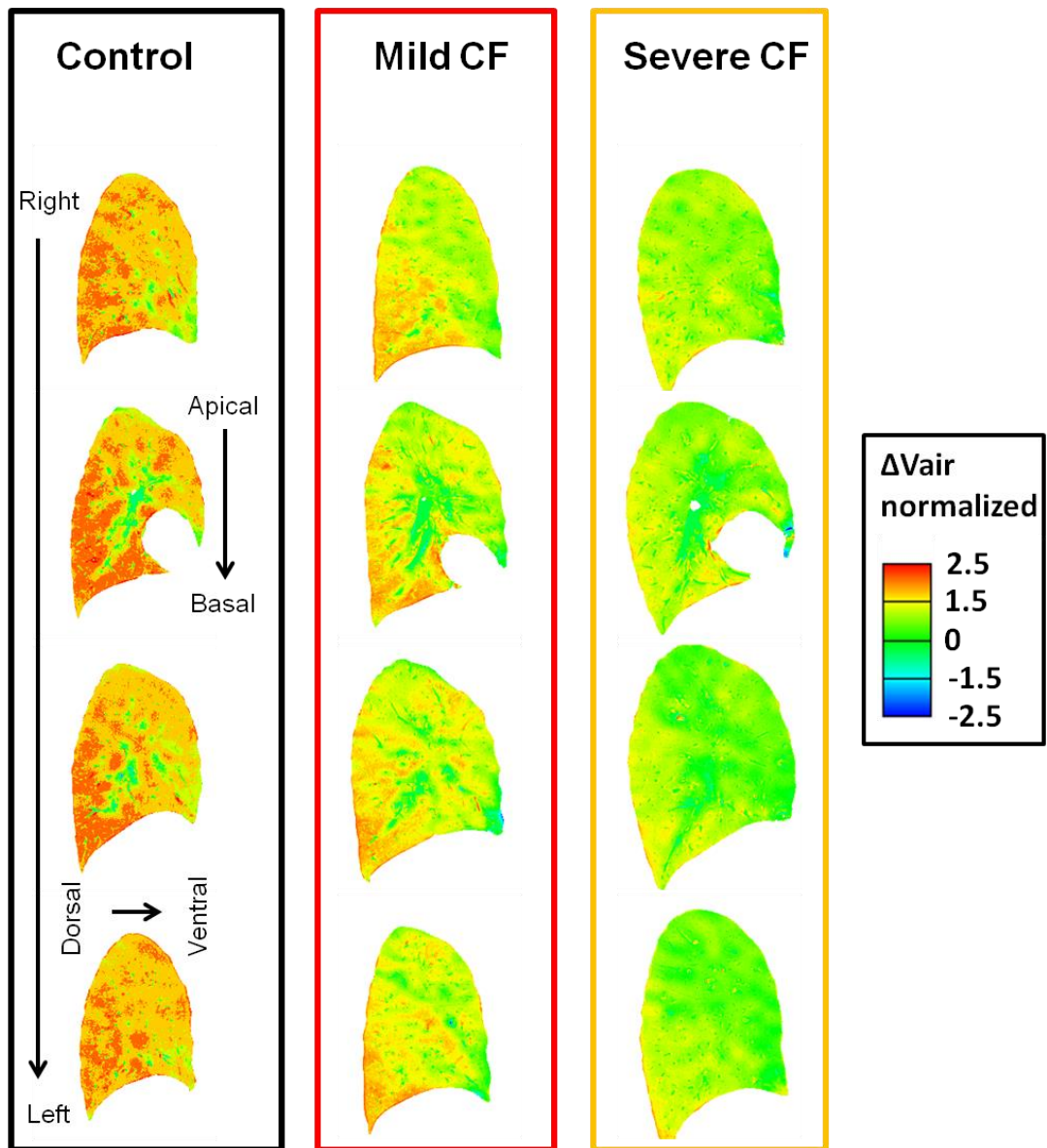
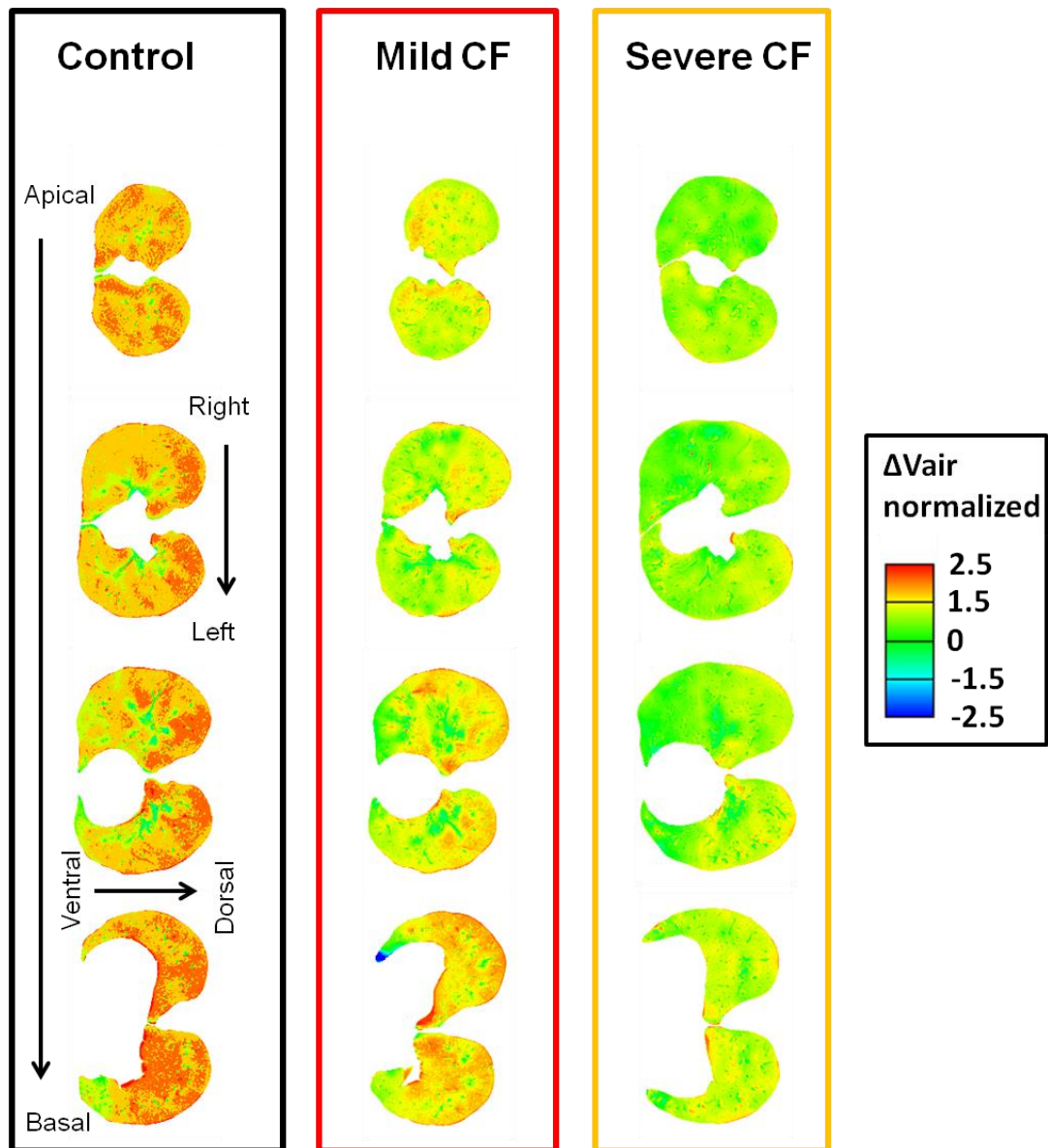


Figure 8.12. Selecting one representative severe CF patient and mild CF patient based on maximum air trapping in the upper lobe. (A) Air trapping in all healthy normal subjects (non-CF-all) patients compared to the selected representative healthy normal subject (non-CF-IR). UL denotes upper left lung lobe. LL denotes lower left lung lobe. UR denotes upper right lung lobe. MR denotes middle right lung lobe. LR denotes lower right lung lobe. TL denotes all lung lobes. (B) Air trapping in all severe (CF-L-all) patients compared to the selected representative severe patient (CF-L-IR). (C) Air trapping in all mild patients (CF-H-all) compared to the selected representative mild patient (CF-H-IR). (D) Total lung volume in all healthy normal subjects compared to the selected representative healthy normal subject. RV denotes lung residual volume. TLC denotes total lung capacity. (E) Total lung volume in all severe patients compared to the selected representative severe patient. (F) Total lung volume in all mild patients compared to the selected representative mild patient. (G) Lobar RV volume normalized in all healthy normal subjects compared to the selected representative healthy normal subject. Each lobe at RV was normalized by total lung volume at TLC from each individual patient. (H) Lobar RV volume normalized in all severe patients compared to the selected representative severe patient. (I) Lobar RV volume normalized in all mild patients compared to the selected representative mild patient. (J) Lobar TLC volume normalized in all healthy normal subjects compared to the selected representative healthy normal subject. Each lobe at TLC was normalized by the total lung volume at TLC from each individual patient. (K) Lobar TLC volume normalized in all severe patients compared to the selected representative severe patient. (L) Lobar TLC volume normalized in all mild patients compared to the selected representative mild patient.

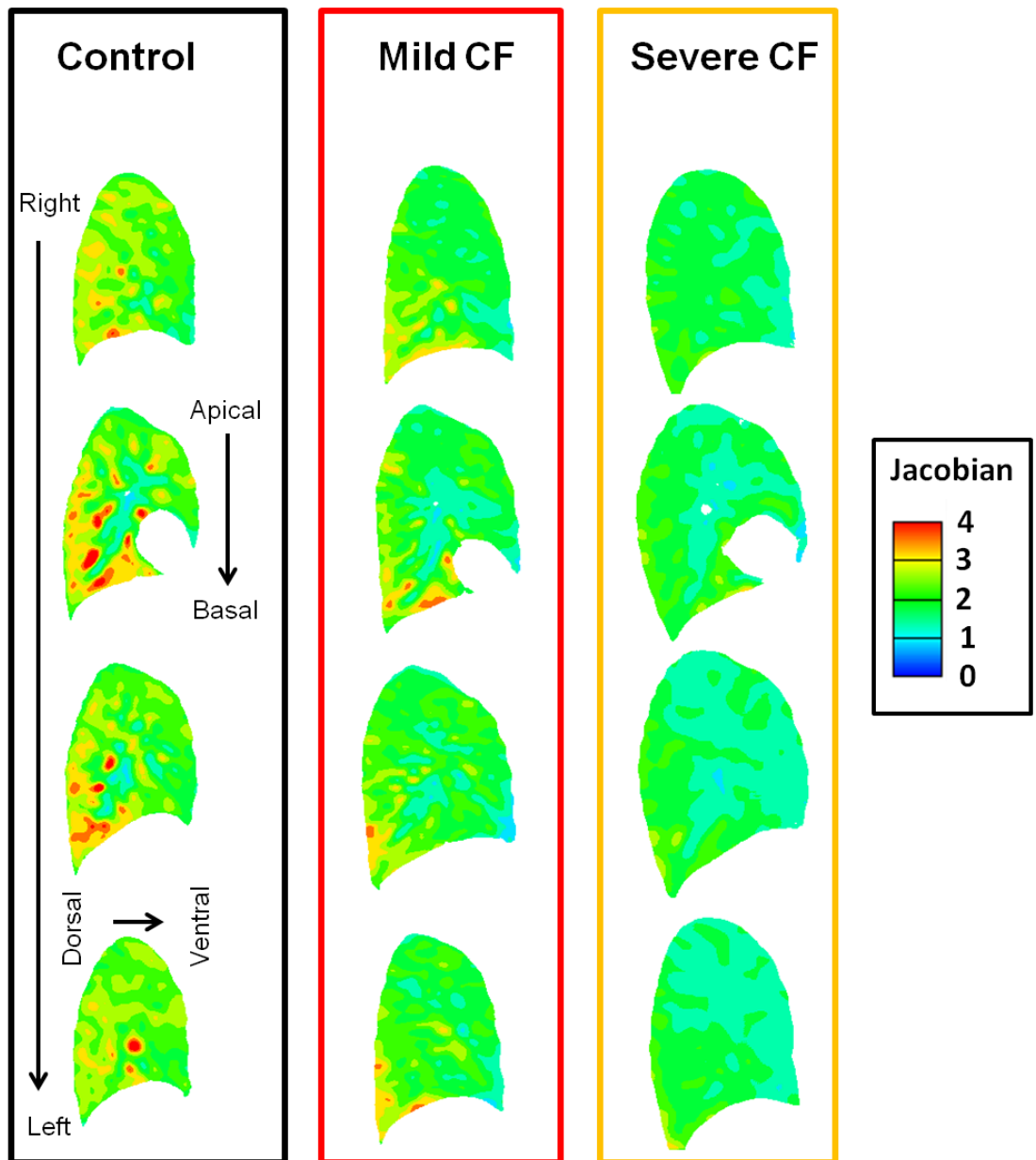
A.



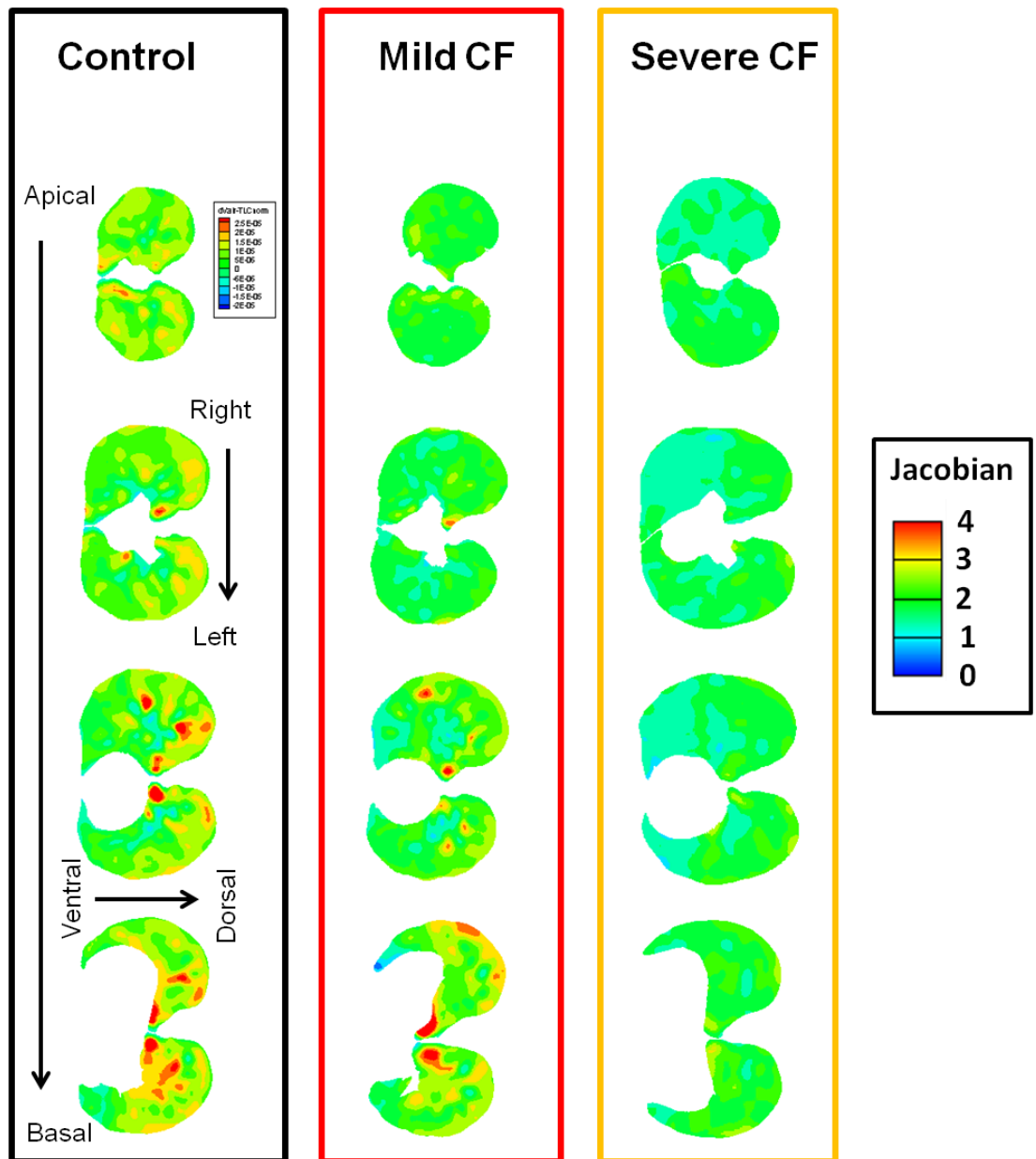
B.



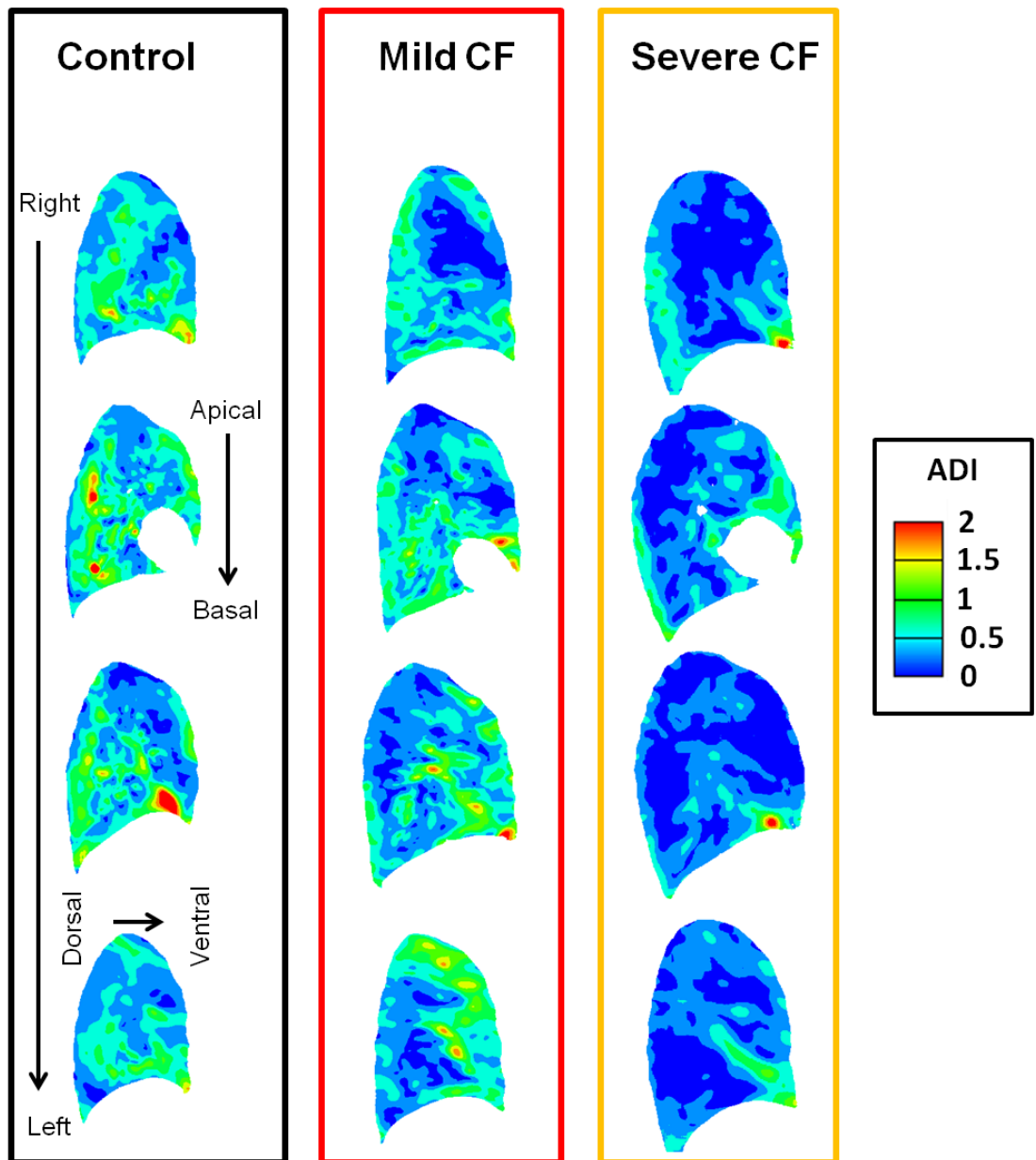
C.



D.



E.



F.

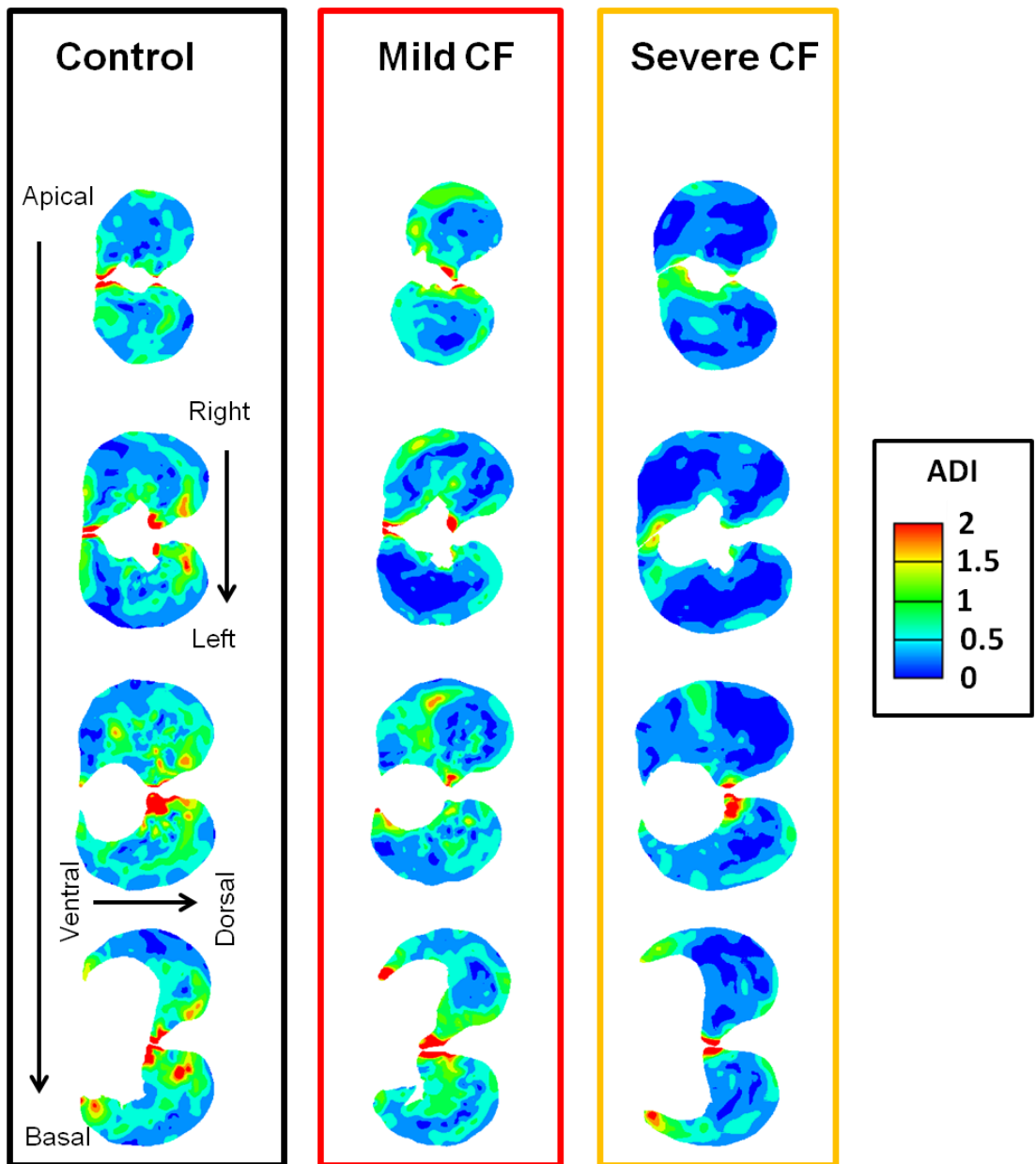


Figure 8.13. Comparing dynamic volume and tissue properties between a representative non-CF subject, mild CF patient and severe CF patient using extracted vertical and horizontal slices. (A) Vertical lung slices representing air volume change, extracted at a lateral depth of 15, 30, 70, and 85% of the non-CF subject's (control, black box), mild CF patient's (mild CF, red box) and severe CF patient's (severe CF, orange box) lung. Air volume change from residual volume (RV) to total lung capacity (TLC) is represented by a heat map. Red denotes high volume change. Blue denotes low volume change. (B) Horizontal lung slices representing air volume change, extracted at 20, 40, 60, and 80% of the height of the non-CF subject's, mild CF patient's, and severe CF patient's lung. (C) Vertical lung slices representing the ratio of air volume change (Jacobian), extracted at lateral depth of 15, 30, 70, and 85% of the non-CF subject's, mild CF patient's and severe CF patient's lung. The ratio of air volume change from residual volume (RV) to total lung capacity (TLC) is represented by a heat map. Red denotes high ratio of volume change. Blue denotes low ratio of volume change. (D) Horizontal lung slices representing ratio of air volume change (Jacobian), extracted at 20, 40, 60, and 80% of the height of the non-CF subject's, mild CF patient's, and severe CF patient's lung. (E) Vertical lung slices representing the ratio of non-uniform tissue deformation of anisotropic deformation index (ADI), extracted at a lateral depth of 15, 30, 70, and 85% of the non-CF subject's, mild CF patient's and severe CF patient's lung. The ADI from residual volume (RV) to total lung capacity (TLC) is represented by a heat map. Red denotes high ADI. Blue denotes low ADI. (F) Horizontal lung slices representing ADI, extracted at 20, 40, 60, and 80% of the height of the non-CF subject's, mild CF patient's, and severe CF patient's lung.

8.4. Discussion.

The aim of this thesis is to understand the pathogenesis of CF lung disease. CF is a multi-organ disease. I studied the lung because most of the morbidity and mortality in CF is due to lung disease (Boucher et al., 1997; Lands et al., 1992; Marcotte et al., 1986). Lung disease severity in CF is influenced by both genetic and non-genetic factors (Collaco, Blackman, McGready, Naughton, & Cutting, 2010; Corey, McLaughlin, Williams, & Levison, 1988; Merlo & Boyle, 2003; Nixon et al., 2001). By understanding the contribution of these factors we can learn more about the pathogenesis and treatment of CF lung disease (Zielenski, 2000).

Through investigating the first aim of this chapter, I found that CF patients had greater air trapping, smaller lung volumes, decreased air volume expansion, and less lung tissue deformation compared to non-CF subjects. I have also found that for particles 0.5- μm and 1- μm , particle ventilation fraction and deposition efficiency were greater in the right upper lobe of CF patients. This is, in part, due to the abnormal airway shape and size in the right upper lobe which increases the pressure drop and the airflow velocity in the airways supplying the right upper lobe in CF patients. Moreover, through investigating the second aim, I found heterogeneity in the FEV1% value in these patients, where FEV1% ranged from 38% to 100% in the CF cohort. I divided the 8 CF subjects studied in the first aim of this chapter into two groups: mild CF patient with FEV1% greater than 55% and severe CF patients with FEV1% less than 55%. The threshold of 55% was selected based on previous FEV1 criteria (boundaries) used to identify patients as mild or severe to enrol them in a gene modifier study (Kulich et al., 2005). The mild group included 5 CF patients and the severe group included 3 CF patients. I found that severe CF patients had greater air trapping, greater expiratory volume, reduced air volume expansion, and reduced

tissue deformation compared to mild CF patients and non-CF subjects. However, in mild patients I did not observe any differences in these measures compared to normal healthy subjects, except for air trapping in the right upper lobe where it was greater in mild CF patients compared to normal healthy subjects. I also observed decreased compliance in the right upper lobe in mild patients. Interestingly, although no statistical difference was found in mild patients' lobar lung volumes, the lung shape was different from the front and side view compared to normal healthy subjects. The mild CF lung was more square-like compared to non-CF lungs. Air trapping in the upper lobes might in part play a role in the abnormal lung shape.

Our study has several advantages and caveats. Advantages include: 1) I used subjects scanned under the same breath hold protocol and with similar scanner settings. 2) I was able to use the same subjects to study both aims of this chapter by dividing the subjects used in the first aim into mild and severe patients. This provided an example of the effect of using patients with different disease severity in a study, which is observed in several publications (Davies et al., 2013; De Boeck et al., 2014; Quon et al., 2015; Sheikh et al., 2015a, 2015b). 3) I was able to investigate the relation between PFT data, CT data, and image registration in mild and severe CF subjects compared to healthy non-CF subjects. 4) I provided an actual value for disease severity in each lobe in individual patients using CT density compared to healthy subjects. 5) I was able to account for multi-centre scanner calibration differences between subjects when measuring air trapping by normalizing the air in lung by the air value in the mid-section of the trachea for each individual subject. 6) I obtained and analysed volumetric, whole lung CT scans at RV and TLC, which is rare in CF related studies. Most published work in CF has focused on single-slice analysis (Quon et al., 2015; Saynor, Barker, Oades, & Williams, 2014; Sheikh et al., 2015a, 2015b). Several caveats do exist. 1) The lung volumes obtained from the CT

data were smaller since the patients were supine and not upright and the lung air volume is affected more by patient body posture, dead space, and gas in abdomen. 2) I used coached breath hold methods to obtain TLC and RV CT data instead of spirometry-gated data acquisition. However the methodology was consistent between subjects and groups. 3) I had a small sample size of seven non-CF healthy subjects and eight CF subjects for this study (5 mild patients and 3 severe patients). Despite this low number of subjects, I were able to make several significant conclusions. 4) I did not have big enough sample size to study the effect of gender differences on disease severity. 5) The non-CF subjects were slightly younger than the CF subjects. However, both groups were adult and in the age range between 20 and 30. Importantly, the subjects were site-matched by using same demographics and CT protocol. 6) B-spline cubic interpolation of the Jacobian and ADI provides a smoothed displacement field which can smooth important details in these data. Moreover, it causes high discontinuity near lobar edges and the diaphragm. 7) The error in registration value is usually higher near the diaphragm which might increase the value of air volume exchange in that region. 8) I used FEV1% to define disease severity. FEV1% is commonly used to monitor lung function, describe disease severity and indicate survival rate in CF and chronic obstructive lung disease (COPD) patients (Davies & Alton, 2009; George et al., 2011; E. Kerem et al., 1992; Rabe et al., 2007). However, physicians use FEV1% to make clinical decisions about changing or intensifying treatment and quantifying the deterioration or improvement in global lung function (Konstan, Morgan, et al., 2007; Konstan, Schluchter, Xue, & Davis, 2007; Ramsey et al., 1993). Therefore, heterogeneity in FEV1% value in CF patients included in this study indicates heterogeneity in the disease severity in these patients.

This study has several implications. First, it provides a novel way of understanding and analysing the pathogenesis of CF disease. I'm aware of no studies that have investigated CF lung structure function using similar methods.

Second, our findings show that increased particle ventilation and deposition to the right upper lobe that was observed in adult CF patients (Chapter 8) and 3 week old CF pigs (Chapter 7), but not newborn CF pig (Chapter 6), is a secondary effect that develops with time and disease progression. I did not observe higher particle ventilation to the right upper lobe in newborn CF pigs, but at 3 weeks after birth CF pigs started to have reduced particle ventilation to the lower lobes and increased particle ventilation to the right upper lobe, compared non-CF. This increased ventilation to the right upper lobe can be also observed in adult humans with CF included in this study as well as in the literature (Beddy, Babar, & Devaraj, 2011; Dasenbrook et al., 2013; Echeveste et al., 2005; Li et al., 2012; Olivier et al., 2012; Trotman-Dickenson, 2014). Furthermore, our observation of the abnormal increase in particle ventilation to the right lung in newborn CF pigs compared to non-CF is also the same lung region where early disease is observed in CF children younger than 6 years old (with no upper lobe preference) (Mott et al., 2013). Interestingly, as children get older there tends to have predilection for the upper lung to be affected more, which correlates to the increased ventilation to the upper right lobe in 3 week old pigs compared to non-CF (Dasenbrook et al., 2013; Li et al., 2012; Rossi & Owens, 2005). Therefore, these findings suggest that the upper lobe disease predominance might be a secondary effect of *CFTR* abnormalities and abnormal airway structure features.

Third, these data also suggest that upper lobe disease predominance might be somewhat independent of disease severity. For example, I observed greater air

trapping in the right upper lobe of both mild and severe CF patients. However, the air trapping was greater in the more severe patients suggesting that disease progression does worsen these changes with time.

Fourth, the methods used in this study can in the future provide a tool for physician to use to predict accurately disease location, intensity, and type using image registration and hopefully predict best and optimal way to deliver treatment (inhalation technique, speed, and inhaler design) to the patient using CFD-obtained data.

Fifth, there is a new drug that was recently developed that directly targets and improves the primary cause of the CF disease by enhancing the function of the mutated CFTR channel. The drug is called ivacaftor and it is currently approved primarily for patients with G551D CFTR mutation (Cuthbert, 2011; Neuberger et al., 2011; Rogan et al., 2011; Van Goor et al., 2009; Verkman & Galietta, 2009). The development and approval of ivacaftor have increased the interest in studying the global and local lung function in G551D CF patients before and after the start of ivacaftor treatment (Deeks, 2013; Kotha & Clancy, 2013; Quon et al., 2015; Rowe et al., 2014; Saynor et al., 2014). However, these studies have only used PFTs to quantify the global lung function (Davies et al., 2013; Kotha & Clancy, 2013; Rowe et al., 2014; Sheikh et al., 2015b). In addition, other studies have used a few slices of CT scans to demonstrate but not quantify local improvement in lung function (Hoare et al., 2014; Quon et al., 2015; Saynor et al., 2014; Sheikh et al., 2015a, 2015b). Moreover, even in the publications that describe the G551D CF patients phenotype before the start of ivacaftor treatment little is mentioned about their local lung function and global lung shape and structure (Comer et al., 2009; Deeks, 2013; Mickle & Cutting, 2000).

Sixth, by using patient specific airway geometries derived from chest CT scan datasets, more optimal delivery of drugs via the aerosol route may be able to be achieved. This could represent a form of “personalized medicine”. A current limitation of many drugs delivered via the aerosol route is that a large fraction of the drug does not reach the diseased regions. With new knowledge gained from CT datasets it might be possible to optimize aerosol/particle properties to target different regions of the lung. Moreover, with time and disease progression additional optimization of drug properties could occur tailored to the structural changes that occur in the lung. Finally, understanding the global and local lung function in G551D CF patients before and after ivacaftor treatment and how it may affect particle and aerosol distribution and deposition is highly important for target aerosol delivery.

In summary, I investigated the global and local lung structure and function of adult G551D CF patients compared to normal subjects. As expected, I found that CF patients had lower FEV1 and FEF25-75% compared to normal. This is global indicator of obstructive lung disease and may be caused by small airways disease. Next I examined the lung volume at TLC and RV. I found that CF patient had elevated RV volume in the right upper and lower lobe compared to normal healthy subjects. The elevated volume at RV was, in part, due to increased air trapping. The air trapping was greater in CF upper lobes. This air trapping in CF was associated with reduced volume expansion ratio and tissue deformation in the CF lung compared to normal. I next picked three representative subjects from each group (normal and CF) to study particle distribution and deposition. I found that particle ventilation to the right upper lobe was elevated in CF patients. This was, in part, due to a smaller RUL airway in CF that led to increased pressure drop, resistance and airflow velocity. The increased velocity, pressure drop, and mass flow rate increased

particle ventilation to the right upper lobe. I also observed increased particle deposition in the right upper lobe. This was due, in part, to increased turbulent kinetic energy and Stokes number in the CF right upper lobe.

8.5. Conclusion.

In conclusion, by assessing both the global and local lung function in CF, I found that G551D CF patients had higher air trapping, lower volume expansion and lower tissue deformation in their upper lobes. Moreover, our findings suggest that the combination of air trapping, smaller airways, and higher respiratory rate in CF patients promotes higher particle ventilation to the right upper lobe in CF. Moreover, these findings might have important implications for better understanding the pathogenesis of CF airway disease and the development of inhaled therapeutics in CF.

*“I don’t think I’ll ever get
over the wow feeling that
engulfs me now I have
healthy lungs and I can lead
a normal life”*

Holly van Geffen,

Cystic fibrosis patient

Chapter 9. Summary and concluding remarks

9.1. Summary.

In the preceding chapters I discussed the framework I set up to investigate the pathogenesis of cystic fibrosis (CF) lung disease. I was interested in examining the CF lung structure and function at three time points: birth, early development, and adulthood. Through this study I was able to develop an understanding of the effect of early CF lung structure and function on lung disease pathogenesis in CF later in the patient’s life. It’s important to note that lung disease is the main cause of morbidity and mortality in 90% of CF patients (Boucher et al., 1997; Lands et al., 1992; Marcotte et al., 1986).

In the current chapter, I discuss the outcome of our study at each time point starting from birth until adulthood. I also examined the implications of our findings and reviewed possible future work. Finally, I provided the reader with the most recent update on Holly’s (the CF patient introduced in the first chapter) story.

9.2. Pathogenesis of CF lung disease.

9.2.1. CF lung abnormalities at birth.

In Chapter 6, I studied the effect of lung structural and functional abnormalities on airflow characteristics and aerosol particle distribution and deposition patterns in newborn CF pigs. I chose the pig model because these studies would be difficult to perform in newborn humans. Although, computed x-ray tomography (CT) has been previously performed on infants and children with CF (Mott et al., 2012; Sly et al., 2009; Stick et al., 2009), these studies consist of only a few CT slices making them unsuitable for quantitative analysis (Mott et al., 2012; Sly et al., 2009; Stick et al., 2009). I used a numerical model based on CFD in this study because it not only provides accurate predictions for the given boundary conditions, but it also provides potential explanations for the observations. The CFD simulation was applied on airway CT-based models obtained from the CF pig. The CFD model predicted that CF airways have a higher air velocity and pressure drop compared to non-CF airways. The higher air velocity increased particle deposition in CF. Moreover, I found that particles larger than 5- μm preferentially distributed to the right lung in CF due to the skewed axial velocity and formation of secondary flow in the trachea. Thus, our computational model shows that the irregular airway structure in CF has a significant effect on the airflow pattern and subsequently on particle distribution and deposition. The findings of this study are likely generalisable to newborn CF pig airways since I was able to perform CFD analysis on a number of subjects. By performing this study at birth I was able to investigate the primary effect of congenital airway narrowing in CF and eliminating secondary effects from infection, inflammation, and mucus obstruction.

9.2.2. CF lung abnormalities three weeks after birth.

In Chapter 7, I examined the effect of three week old non-CF and CF pig lung structure and function on airflow properties and particle behaviour. This is the first study to use CFD and CT-based airway geometry in a longitudinal analysis of CF disease. In this study I first examined the pigs' weight and size, and I found that CF pigs weigh less and their femur size is significantly smaller compared to non-CF. Also three week old CF pigs have smaller lung volume at lung pressures of 0 cmH₂O and 25 cmH₂O, and their lung expiration ratio was decreased compared to non-CF pigs. In addition, when I examined their lobar ventilation I found that in three week old CF pigs the expansion ratio in the upper lobes was increased and in the lower lobes decreased in comparison to non-CF pigs. Moreover, I found that the major, minor, equivalent diameter, CSA, and perimeter are smaller in CF compared to non-CF. Next, I simulated particle behaviour in non-CF and CF three week old pigs. I found that particle ventilation fraction to the upper lobes was significantly greater in CF compared to non-CF pig. I have also observed higher particle deposition in CF compared to non-CF. The outcome of this study might, in part, suggest that upper lung disease predominance in CF human and pig model is related to congenital or early structural airway changes.

9.2.3. CF lung abnormalities at adulthood.

In chapter 8, I investigated the effect of CF lung disease on the structure and function of adult patient lungs. I used non-CF and CF adult human CT scans obtained under the same breath hold protocol and with similar scanner settings. I investigated the relationship between pulmonary function test data, CT data, and image registration in non-CF and CF subjects. I first examined the difference between non-CF and CF

human lung structure and function. I found that CF patients had greater air trapping, smaller lung volumes, decreased air volume expansion, and less lung tissue deformation compared to non-CF subjects. I accounted for multi-centre scanner calibration differences between subjects when measuring air trapping by normalizing the air in the lung by the air value in the mid-section of the trachea for each individual subject. Next I examined the effect of CF structural abnormalities on inhaled particle distribution and deposition. I found that particle ventilation fraction and deposition efficiency were greater in the right upper lobe of CF patients. This is, in part, due to the abnormal airway shape and size in the right upper lobe which increases the pressure drop and the airflow velocity in the airways supplying the right upper lobe in CF patients.

I next investigated the effect of disease severity on lung structure and function in adult patients with CF. I was able to use the same subjects. I divided the subjects used previously into mild and severe patients. I found that severe CF patients had greater air trapping, greater expiratory volume, reduced air volume expansion, and reduced tissue deformation compared to mild CF patients and non-CF subjects. However, in mild CF patients I did not observe any differences in these measures compared to normal healthy subjects, except for air trapping in the right upper lobe where it was greater in mild CF patients compared to normal healthy subjects. I also observed decreased compliance in the right upper lobe in mild patients. Interestingly, although no statistical difference was found in mild CF patients' lobar lung volumes, the lung shape was different from the front and side view compared to normal healthy subjects. The mild CF lung was more square-like compared to non-CF lungs. Air trapping in the upper lobes might in part play a role in the abnormal lung shape. This study is unique since I analysed volumetric, whole lung CT scans at RV and TLC, which is rare in CF related studies. Most published work in CF has focused on

single-slice analysis (Quon et al., 2015; Saynor et al., 2014; Sheikh et al., 2015a, 2015b).

9.3. Implications.

1. This study provided a novel way of understanding and analysing the pathogenesis of CF disease. I'm aware of no studies that have investigated CF lung structure function using similar methods. I used realistic non-CF and CF airway geometries and conducted a longitudinal analysis of the effect of CF disease on the lung structure and function. I found that congenital airway structural abnormalities have a significant effect on lung function locally and globally. More recently, other groups have used a similar approach to ours (functional imaging based computational fluid dynamics with the same type of boundary conditions) to find the effect of differences in patient-specific airway geometry on inhalational therapy in lung disease, such as chronic obstructive pulmonary disease and asthma (L. A. De Backer et al., 2012; Vinchurkar et al., 2012; Vos et al., 2013).

2. This study provided a better understanding of the development defect in CF airway structure through a longitudinal analysis. It also investigated the influences of particle/aerosol deposition and distribution in the lung which is critical for targeted delivery of aerosolized treatments to people with irregular airway morphology. In the setting of airway narrowing in CF, improved drug delivery and deposition to the small airways is more likely to occur with submicron particles. By performing CFD analyses on human with disease-specific airway geometries, more efficient and better targeting of inhaled therapies may be achieved (Byron et al., 2010; Corley et al., 2012; L. A. De Backer et al., 2012; Ma & Lutchen, 2009; Vinchurkar et al., 2012; Vos et al., 2013). Furthermore, our modelling techniques are directly translatable to human studies.

3. The outcomes of this thesis suggest that congenital airway abnormalities are important in determining regional ventilation in CF airways affecting disease pathogenesis and account for the upper lobe predilection for CF disease. This is a very significant finding since other pulmonary diseases have a predilection for the upper lung regions including tuberculosis, silicosis, hypersensitivity pneumonitis, and pneumoconioses. The underlying aetiology for these regional differences is unknown, but ventilation and perfusion irregularities are most often implicated (Gurney & Schroeder, 1988).

4. The technique used in this study is novel in the investigation of CF lung disease pathogenesis and therefore might in-part assist in diagnosis of lung disease, airway abnormality, and aerosol distribution and deposition. However, this technique is not yet ready for “prime time” patient diagnosis. Therefore, for this technique to be ready for CF patient diagnosis a larger sample size and further verification with PET-CT, Fluoroscopy-CT, and SPECT-CT scans would be required. Although, this technique is novel in CF research, it has been used previously in research studies regarding COPD and asthma (Burrowes, 2014; S. Choi et al., 2015; S. Choi, Hoffman, Wenzel, Castro, & Lin, 2014; S. Choi et al., 2013; J. W. De Backer et al., 2008; L. A. De Backer et al., 2012; Luo, Liu, & Yang, 2007). Using image registration and CFD is also available in commercial product Fluidda (Fluidda, Kontich, Belgium) however this product tend to use a uniform pressure boundary condition which is not quite physiologically accurate (FLuidda, 2016). Therefore, I can conclude that the technique used in this study is currently commercially available and has been implemented in COPD and asthma research. However, it's have not been used in CF previously. Image registration have been shown to be significantly superior to other volume analysis methods specifically in 4D longitudinal studies with CT (Varadhan, Karangelis, Krishnan, & Hui, 2013; Vickress, Battista, Barnett, Morgan, & Yartsev,

2016; Yamamoto et al., 2011). The accuracy and sensitivity of this technique of picking up subtle change in CF lung structure and function depends mostly on the quality of the CT data and the resolution (size of the voxel) (Hekmatian, Jafari-Pozve, & Khorrami, 2014). Currently, the highest resolution in commercially available CT is 41 μm (HRpQCT Xtreme II) (Manske, Zhu, Sandino, & Boyd, 2015). Therefore this technique can pick up subtle changes down to 41 μm , and it can analyse the effect of these changes on the structure and function. However, it is important to note that currently this CT (HRpQCT Xtreme II) can only be used on limbs. Therefore the current resolution limit is 0.4 mm in lungs.

5. Moreover, the outcome of this thesis in adult CF patients suggests that upper lobe disease predominance might be somewhat independent of disease severity.

9.4. Future directions.

1. In this study I investigated the change in lung structure and function at the peak of inspiration (TLC in humans, or 25 cmH₂O in the pig model) to peak expiration (RV in humans, or 0 cmH₂O in the pig model). This analysis is limited in its interpretation since I'm analysing maximum volume to minimum volume. The data that I'm fortunate to have did not include tidal volume CT scan. Therefore, tidal volume analysis was not possible. However, in future studies I can use technologies such as 4Dx x-ray (4Dx, 2014) to obtain real time images of a breathing lung. Investigating breathing lung can have significant implications in understanding how bacteria deposit while normally breathing, understanding tissue characteristics, investigating lobar friction, producing accurate tidal boundary conditions for CFD, and investigating friction between the chest wall, diaphragm and the lungs during normal breathing.

2. The methods used in this study can in the future provide a tool for physicians to use to accurately predict accurately disease location, intensity, and type using image registration and hopefully predict the optimal way to deliver treatment (inhalation technique, speed, and inhaler design) to the patient using CFD-obtained data.

3. There is a new drug that was recently developed that directly targets and improves the primary cause of the CF disease by enhancing the function of the mutated CFTR channel. The drug is called ivacaftor and it is currently approved primarily for patients with G551D CFTR mutation (Cuthbert, 2011; Neuberger et al., 2011; Rogan et al., 2011; Van Goor et al., 2009; Van Goor et al., 2006). The methods presented in this thesis can be used to test the efficiency of drugs such as ivacaftor in improving the lung structural and functional defect. Moreover, this study can be used to explore new methods to target delivery of these drugs to the area of disease.

4. In this thesis I used patient specific airway geometries. These geometries were derived from chest CT scan datasets, and can be used to determine the most optimal delivery route for therapeutic aerosol or gene vectors for gene therapy for the individual patient. This represents a form of “personalized medicine”. A current limitation of many drugs delivered via the aerosol route is that a large fraction of the drug does not reach the diseased regions. With new knowledge gained from CT datasets it might be possible to optimize aerosol/particle properties to target different regions of the lung. Moreover, with time and disease progression additional optimization of drug properties could occur tailored to the structural changes that occur in the lung.

9.5. Final remarks and conclusion.

In the beginning of this thesis I introduced the reader to Holly's story. I personally followed Holly's story throughout my PhD. Holly was at the end-stage of cystic fibrosis lung disease. Only 30% of her lung was functioning and the doctor predicted that she only had 18 months to live. Holly was only 21 years old at the time. Holly was on the double lung transplant list, having waited for a whole year and taken a cocktail of antibiotics especially designed for her to be well enough to get onto the list. Once on the list, Holly had to decide what donor lung she would deem acceptable. "You are asked at the start of this process to tick boxes for lungs you will and will not receive, with factors like age, smoking, cancer, drugs and promiscuous sexual behaviour. I just said I would receive anything they deemed suitable; I knew they want it to be a success and you can't get lungs brand-new off the shelf" Holly says (Collins, 2015).

After another year waiting on the lung transplant list and two false alarms of donors lungs being available, Holly finally got the call for a lung transplant in February this year (2015). The operation took 7 hours. Cystic fibrosis lungs are renowned for being difficult to remove. The surgeons had to carefully scrape out the scar tissues from her chest cavity to ensure no cross contamination.

The surgery was successful; however there were several complications after the surgery. First, Holly developed surgical emphysema few days after. "My body was filling with air, all in my face and neck and shoulders. When you touch my skin it cracked and popped. It got so bad I could barely open my eyes" Holly says (Figure 9.1.) (Collins, 2015).

Eight days after the surgery Holly's oxygen saturation level dropped dramatically. Holly was put on CPAP machine, which forces air into her lungs. Holly described the experience as terrifying. "I have cystic fibrosis- I know what it is to struggle to breathe, but it had never been like this. My heart was beating so fast it felt as though it would explode. I just laid there thinking, what have I done?"

Two weeks after the transplant, Holly developed acute kidney failure. This caused her breathing to become increasingly erratic. Holly was put on haemodialysis to save her kidneys.

Thankfully that was the last of the complications. Almost two months after the surgery Holly was discharged from the hospital. Holly still needs to take a daily cocktail of anti-rejection drugs and antibiotics. However she lives a pretty active life now (Figure 9.2.): she competes in cycling and running events; she recently climbed Mount Tryfan in Snowdonia. For the first time Holly was able to participate in the general election. "It's the simple things" Holly says (Collins, 2015).

Holly is currently living a healthier life. However it is important to note this is not the case for every CF lung transplant patient. Emma, Holly's friend, passed away two years ago from CF lung complications before she could get on the list. Another friend who got her call to the list in December died in April. A third friend who had her transplant for a year passed away from lung complications in June. Others have had their transplant for 20 years now with no complications (Collins, 2015).

In this thesis, I investigated the pathogenesis of CF shortly after birth and in adulthood. This study used both a pig model and humans with CF. It used both experimental and computational analysis to assess the pathogenesis of CF disease and its effect on both global and local lung function. With the current methodology used, I can in the future personalize the treatment of CF using mathematical

modelling and target diseased areas before it is too late. So Holly and many other CF patients will be able to live a healthier life.

“Being an organ donor is the most selfless, heroic thing you can do. Whoever they are, they are not going to see the benefit of their action; not only has my world been transformed, but the lives of my friends and family, too. The domino effect of happiness is humongous and I cannot begin to describe how grateful I am” Holly van Geffen (Collins, 2015).



Figure 9.1. A picture of Holly van Geffen suffering from surgical emphysema. Adapted from (Collins, 2015).



Figure 9.2. A picture of Holly van Geffen on the left next to her parents Nick and Jayne. The picture was taken during the transplant games this year. Adapted from (Collins, 2015).

References

- 4Dx. (2014). 4Dx. Retrieved from <http://4dx.com/tech>
- (UNOS), U. N. f. O. S. (2014). double lung transplant cost. Retrieved from <http://www.transplantliving.org/before-the-transplant/financing-a-transplant/the-costs/>
- Accurso, F. J., Rowe, S. M., Clancy, J. P., Boyle, M. P., Dunitz, J. M., Durie, P. R., . . . Ramsey, B. W. (2010). Effect of VX-770 in persons with cystic fibrosis and the G551D-CFTR mutation. *N Engl J Med*, 363(21), 1991-2003. doi:10.1056/NEJMoa0909825
- Adam, R. J., Michalski, A. S., Bauer, C., Abou Alaiwa, M. H., Gross, T. J., Awadalla, M. S., . . . Stoltz, D. A. (2013). Air trapping and airflow obstruction in newborn cystic fibrosis piglets. *Am J Respir Crit Care Med*, 188(12), 1434-1441. doi:10.1164/rccm.201307-1268OC
- Adeboyeke, D., Scott, S., & Hodson, M. E. (2006). Open follow-up study of tobramycin nebuliser solution and colistin in patients with cystic fibrosis. *J Cyst Fibros*, 5(4), 261-263. doi:10.1016/j.jcf.2006.05.009
- Alipour, F., & Scherer, R. C. (2006). Characterizing glottal jet turbulence. *J Acoust Soc Am*, 119(2), 1063-1073. Retrieved from <http://www.ncbi.nlm.nih.gov/pubmed/16521768>
- Alton, E. W., Armstrong, D. K., Ashby, D., Bayfield, K. J., Bilton, D., Bloomfield, E. V., . . . Consortium, U. K. C. F. G. T. (2015). Repeated nebulisation of non-viral CFTR gene therapy in patients with cystic fibrosis: a randomised, double-blind, placebo-controlled, phase 2b trial. *Lancet Respir Med*, 3(9), 684-691. doi:10.1016/S2213-2600(15)00245-3

Amelon, R., Cao, K., Ding, K., Christensen, G. E., Reinhardt, J. M., & Raghavan, M. L. (2011). Three-dimensional characterization of regional lung deformation. *J Biomech*, *44*(13), 2489-2495. doi:10.1016/j.jbiomech.2011.06.009

Andersen D.H. (1938). Cystic fibrosis of the pancreas and its relations to celiac disease: A clinical and pathological study. *Am J Dis Child*, *56*, 344-399.

Ashby, B. L., & Stern, D. H. (1993). Aerosolized tobramycin in patients with cystic fibrosis. *N Engl J Med*, *329*(22), 1659-1660. doi:10.1056/NEJM199311253292218

Augarten, A., Ben Tov, A., Madgar, I., Barak, A., Akons, H., Laufer, J., . . . Yahav, Y. (2008). The changing face of the exocrine pancreas in cystic fibrosis: the correlation between pancreatic status, pancreatitis and cystic fibrosis genotype. *Eur J Gastroenterol Hepatol*, *20*(3), 164-168. doi:10.1097/MEG.0b013e3282f36d04

Aurora, P., Bush, A., Gustafsson, P., Oliver, C., Wallis, C., Price, J., . . . London Cystic Fibrosis, C. (2005). Multiple-breath washout as a marker of lung disease in preschool children with cystic fibrosis. *Am J Respir Crit Care Med*, *171*(3), 249-256. doi:10.1164/rccm.200407-895OC

Aurora, P., Gustafsson, P., Bush, A., Lindblad, A., Oliver, C., Wallis, C. E., & Stocks, J. (2004). Multiple breath inert gas washout as a measure of ventilation distribution in children with cystic fibrosis. *Thorax*, *59*(12), 1068-1073. doi:10.1136/thx.2004.022590

Awadalla, M., Miyawaki, S., Abou Alaiwa, M. H., Adam, R. J., Bouzek, D. C., Michalski, A. S., . . . Stoltz, D. A. (2014). Early airway structural

changes in cystic fibrosis pigs as a determinant of particle distribution and deposition. *Ann Biomed Eng*, 42(4), 915-927.

doi:10.1007/s10439-013-0955-7

Aziz, Z. A., Davies, J. C., Alton, E. W., Wells, A. U., Geddes, D. M., & Hansell, D. M. (2007). Computed tomography and cystic fibrosis: promises and problems. *Thorax*, 62(2), 181-186.

doi:10.1136/thx.2005.054379

Baker, J. M., Hudson, R. P., Kanelis, V., Choy, W. Y., Thibodeau, P. H., Thomas, P. J., & Forman-Kay, J. D. (2007). CFTR regulatory region interacts with NBD1 predominantly via multiple transient helices. *Nat Struct Mol Biol*, 14(8), 738-745. doi:10.1038/nsmb1278

Barry, P. J., Plant, B. J., Nair, A., Bicknell, S., Simmonds, N. J., Bell, N. J., . . . Horsley, A. R. (2014). Effects of ivacaftor in patients with cystic fibrosis who carry the G551D mutation and have severe lung disease. *Chest*, 146(1), 152-158. doi:10.1378/chest.13-2397

Bartlett, J. R., Friedman, K. J., Ling, S. C., Pace, R. G., Bell, S. C., Bourke, B., . . . Gene Modifier Study, G. (2009). Genetic modifiers of liver disease in cystic fibrosis. *JAMA*, 302(10), 1076-1083.

doi:10.1001/jama.2009.1295

Bates, P. D. L., S.N.; Ferguson, R.I. (2005). *Computational fluid dynamics: application and environmental hydraulics*. West Sussex, England: John Wiley.

Beddy, P., Babar, J., & Devaraj, A. (2011). A practical approach to cystic lung disease on HRCT. *Insights Imaging*, 2(1), 1-7. doi:10.1007/s13244-010-0050-7

- Bedwell, D. M., Kaenjak, A., Benos, D. J., Bebok, Z., Bubien, J. K., Hong, J., . . . Sorscher, E. J. (1997). Suppression of a CFTR premature stop mutation in a bronchial epithelial cell line. *Nat Med*, 3(11), 1280-1284. Retrieved from <http://www.ncbi.nlm.nih.gov/pubmed/9359706>
- Bennett, W. D., Messina, M. S., & Smaldone, G. C. (1985). Effect of exercise on deposition and subsequent retention of inhaled particles. *J Appl Physiol* (1985), 59(4), 1046-1054. Retrieved from <http://www.ncbi.nlm.nih.gov/pubmed/4055585>
- Bijman, J., & Quinton, P. M. (1984). Apparent absence of cystic fibrosis sweat factor on ion-selective and transport properties of the perfused human sweat duct. *Pediatr Res*, 18(12), 1292-1296. Retrieved from <http://www.ncbi.nlm.nih.gov/pubmed/6522143>
- Bompadre, S. G., Li, M., & Hwang, T. C. (2008). Mechanism of G551D-CFTR (cystic fibrosis transmembrane conductance regulator) potentiation by a high affinity ATP analog. *J Biol Chem*, 283(9), 5364-5369. doi:10.1074/jbc.M709417200
- Bompadre, S. G., Sohma, Y., Li, M., & Hwang, T. C. (2007). G551D and G1349D, two CF-associated mutations in the signature sequences of CFTR, exhibit distinct gating defects. *J Gen Physiol*, 129(4), 285-298. doi:10.1085/jgp.200609667
- Bonvin, E., Le Rouzic, P., Bernaudin, J. F., Cottart, C. H., Vandebrouck, C., Crie, A., . . . Bonora, M. (2008). Congenital tracheal malformation in cystic fibrosis transmembrane conductance regulator-deficient mice. *J Physiol*, 586(13), 3231-3243. doi:10.1113/jphysiol.2008.150763
- Borowitz, D., Durie, P. R., Clarke, L. L., Werlin, S. L., Taylor, C. J., Semler, J., . . . Heubi, J. (2005). Gastrointestinal outcomes and confounders in

cystic fibrosis. *J Pediatr Gastroenterol Nutr*, 41(3), 273-285. Retrieved from <http://www.ncbi.nlm.nih.gov/pubmed/16131979>

Boucher, G. P., Lands, L. C., Hay, J. A., & Hornby, L. (1997). Activity levels and the relationship to lung function and nutritional status in children with cystic fibrosis. *Am J Phys Med Rehabil*, 76(4), 311-315.

Retrieved from <http://www.ncbi.nlm.nih.gov/pubmed/9267191>

Brody, A. S., Klein, J. S., Molina, P. L., Quan, J., Bean, J. A., & Wilmott, R. W. (2004). High-resolution computed tomography in young patients with cystic fibrosis: distribution of abnormalities and correlation with pulmonary function tests. *J Pediatr*, 145(1), 32-38.

doi:10.1016/j.jpeds.2004.02.038

Brouns, M., Verbanck, S., & Lacor, C. (2007). Influence of glottic aperture on the tracheal flow. *J Biomech*, 40(1), 165-172.

doi:10.1016/j.jbiomech.2005.10.033

Brown, J. S., & Bennett, W. D. (2004). Deposition of coarse particles in cystic fibrosis: model predictions versus experimental results. *J Aerosol Med*, 17(3), 239-248. Retrieved from

<http://www.ncbi.nlm.nih.gov/pubmed/15625816>

Brown, J. S., Zeman, K. L., & Bennett, W. D. (2001). Regional deposition of coarse particles and ventilation distribution in healthy subjects and patients with cystic fibrosis. *J Aerosol Med*, 14(4), 443-454.

doi:10.1089/08942680152744659

Bruzzese, E., Raia, V., Gaudiello, G., Polito, G., Buccigrossi, V., Formicola, V., & Guarino, A. (2004). Intestinal inflammation is a frequent feature of cystic fibrosis and is reduced by probiotic administration. *Aliment*

Pharmacol Ther, 20(7), 813-819. doi:10.1111/j.1365-2036.2004.02174.x

- Buntain, H. M., Schluter, P. J., Bell, S. C., Greer, R. M., Wong, J. C., Batch, J., . . . Wainwright, C. E. (2006). Controlled longitudinal study of bone mass accrual in children and adolescents with cystic fibrosis. *Thorax*, 61(2), 146-154. doi:10.1136/thx.2005.046516
- Burrowes, K. S. (2014). Computational modeling of the obstructive lung diseases asthma and COPD. *Journal of Translational Medicine*, 12(Suppl 2), S5. doi:10.1186/1479-5879-12-S2-S5
- Busacker, A., Newell, J. D., Jr., Keefe, T., Hoffman, E. A., Granroth, J. C., Castro, M., . . . Wenzel, S. (2009). A multivariate analysis of risk factors for the air-trapping asthmatic phenotype as measured by quantitative CT analysis. *Chest*, 135(1), 48-56. doi:10.1378/chest.08-0049
- Byron, P. R., Hindle, M., Lange, C. F., Longest, P. W., McRobbie, D., Oldham, M. J., . . . Finlay, W. H. (2010). In vivo-in vitro correlations: predicting pulmonary drug deposition from pharmaceutical aerosols. *J Aerosol Med Pulm Drug Deliv*, 23 Suppl 2, S59-69. doi:10.1089/jamp.2010.0846
- Cain, C. (2013). Personalizing cystic fibrosis in vitro. *SciBX*, 6(23). Retrieved from <http://www.nature.com/scibx/journal/v6/n23/full/scibx.2013.564.html>
- Castaldo, G., Rippa, E., Salvatore, D., Sibillo, R., Raia, V., de Ritis, G., & Salvatore, F. (1997). Severe liver impairment in a cystic fibrosis-affected child homozygous for the G542X mutation. *Am J Med Genet*,

69(2), 155-158. Retrieved from

<http://www.ncbi.nlm.nih.gov/pubmed/9056552>

- Castillo, R., Castillo, E., Guerra, R., Johnson, V. E., McPhail, T., Garg, A. K., & Guerrero, T. (2009). A framework for evaluation of deformable image registration spatial accuracy using large landmark point sets. *Phys Med Biol*, *54*(7), 1849-1870. doi:10.1088/0031-9155/54/7/001
- Castro, M., Fain, S. B., Hoffman, E. A., Gierada, D. S., Erzurum, S. C., Wenzel, S., . . . Blood Institute's Severe Asthma Research, P. (2011). Lung imaging in asthmatic patients: the picture is clearer. *J Allergy Clin Immunol*, *128*(3), 467-478. doi:10.1016/j.jaci.2011.04.051
- Chang, E. H., Tang, X. X., Shah, V. S., Launspach, J. L., Ernst, S. E., Hilkin, B., . . . Zabner, J. (2015). Medical reversal of chronic sinusitis in a cystic fibrosis patient with ivacaftor. *Int Forum Allergy Rhinol*, *5*(2), 178-181. doi:10.1002/alr.21440
- Char, J. E., Wolfe, M. H., Cho, H. J., Park, I. H., Jeong, J. H., Frisbee, E., . . . Wine, J. J. (2014). A little CFTR goes a long way: CFTR-dependent sweat secretion from G551D and R117H-5T cystic fibrosis subjects taking ivacaftor. *PLoS One*, *9*(2), e88564. doi:10.1371/journal.pone.0088564
- Chen, D. L., Atkinson, J. J., & Ferkol, T. W. (2013). FDG PET imaging in cystic fibrosis. *Semin Nucl Med*, *43*(6), 412-419. doi:10.1053/j.semnuclmed.2013.06.002
- Chen, D. L., Ferkol, T. W., Mintun, M. A., Pittman, J. E., Rosenbluth, D. B., & Schuster, D. P. (2006). Quantifying pulmonary inflammation in cystic fibrosis with positron emission tomography. *Am J Respir Crit Care Med*, *173*(12), 1363-1369. doi:10.1164/rccm.200506-934OC

- Chen, D. L., & Kinahan, P. E. (2010). Multimodality molecular imaging of the lung. *J Magn Reson Imaging*, 32(6), 1409-1420.
doi:10.1002/jmri.22385
- Chen, J. H., Stoltz, D. A., Karp, P. H., Ernst, S. E., Pezzulo, A. A., Moninger, T. O., . . . Welsh, M. J. (2010). Loss of anion transport without increased sodium absorption characterizes newborn porcine cystic fibrosis airway epithelia. *Cell*, 143(6), 911-923.
doi:10.1016/j.cell.2010.11.029
- Cheng, H. M. (2015). *Physiology Question-Based Learning* (Vol. 6). Switzerland: Springer International.
- Cheng, K., Ashby, D., & Smyth, R. (2000). Ursodeoxycholic acid for cystic fibrosis-related liver disease. *Cochrane Database Syst Rev*(2), CD000222. doi:10.1002/14651858.CD000222
- Cheng, K. H., Cheng, Y. S., Yeh, H. C., & Swift, D. L. (1997). Measurements of airway dimensions and calculation of mass transfer characteristics of the human oral passage. *J Biomech Eng*, 119(4), 476-482.
Retrieved from <http://www.ncbi.nlm.nih.gov/pubmed/9407288>
- Cheng, S. H., Gregory, R. J., Marshall, J., Paul, S., Souza, D. W., White, G. A., . . . Smith, A. E. (1990). Defective intracellular transport and processing of CFTR is the molecular basis of most cystic fibrosis. *Cell*, 63(4), 827-834. Retrieved from
<http://www.ncbi.nlm.nih.gov/pubmed/1699669>
- Cheung, J. C., & Deber, C. M. (2008). Misfolding of the cystic fibrosis transmembrane conductance regulator and disease. *Biochemistry*, 47(6), 1465-1473. doi:10.1021/bi702209s

- Choi, J., Tawhai, M. H., Hoffman, E. A., & Lin, C. L. (2009). On intra- and intersubject variabilities of airflow in the human lungs. *Phys Fluids (1994)*, *21*(10), 101901. doi:10.1063/1.3247170
- Choi, S., Hoffman, E. A., Wenzel, S. E., Castro, M., Fain, S. B., Jarjour, N. N., . . . Lin, C. L. (2015). Quantitative assessment of multiscale structural and functional alterations in asthmatic populations. *J Appl Physiol (1985)*, *118*(10), 1286-1298. doi:10.1152/jappphysiol.01094.2014
- Choi, S., Hoffman, E. A., Wenzel, S. E., Castro, M., & Lin, C. L. (2014). Improved CT-based estimate of pulmonary gas trapping accounting for scanner and lung-volume variations in a multicenter asthmatic study. *J Appl Physiol (1985)*, *117*(6), 593-603. doi:10.1152/jappphysiol.00280.2014
- Choi, S., Hoffman, E. A., Wenzel, S. E., Tawhai, M. H., Yin, Y., Castro, M., & Lin, C. L. (2013). Registration-based assessment of regional lung function via volumetric CT images of normal subjects vs. severe asthmatics. *J Appl Physiol (1985)*, *115*(5), 730-742. doi:10.1152/jappphysiol.00113.2013
- Choi, Y., & Wroblewski, D. E. (1998). Characteristics of glottis-induced turbulence in oscillatory flow: an empirical investigation. *J Biomech Eng*, *120*(2), 217-226. Retrieved from <http://www.ncbi.nlm.nih.gov/pubmed/10412383>
- Choi, Y. L., S. (2000). Injectivity conditions of 2D and 3D uniform cubic B-spline functions. *Graph Models*, *62*(6), 16.
- Cholon, D. M., Quinney, N. L., Fulcher, M. L., Esther, C. R., Jr., Das, J., Dokholyan, N. V., . . . Gentsch, M. (2014). Potentiator ivacaftor

abrogates pharmacological correction of DeltaF508 CFTR in cystic fibrosis. *Sci Transl Med*, 6(246), 246ra296.

doi:10.1126/scitranslmed.3008680

Christensen, G. E., Song, J. H., Lu, W., El Naqa, I., & Low, D. A. (2007).

Tracking lung tissue motion and expansion/compression with inverse consistent image registration and spirometry. *Med Phys*, 34(6), 2155-2163. Retrieved from <http://www.ncbi.nlm.nih.gov/pubmed/17654918>

Chua, H. L., Collis, G. G., Newbury, A. M., Chan, K., Bower, G. D., Sly, P. D., & Le Souef, P. N. (1994). The influence of age on aerosol deposition in children with cystic fibrosis. *Eur Respir J*, 7(12), 2185-2191.

Retrieved from <http://www.ncbi.nlm.nih.gov/pubmed/7713202>

Cibelli, J. B., Stice, S. L., Golueke, P. J., Kane, J. J., Jerry, J., Blackwell, C., . . . Robl, J. M. (1998). Cloned transgenic calves produced from nonquiescent fetal fibroblasts. *Science*, 280(5367), 1256-1258.

Retrieved from <http://www.ncbi.nlm.nih.gov/pubmed/9596577>

Cohn, J. A., Strong, T. V., Picciotto, M. R., Nairn, A. C., Collins, F. S., & Fitz, J. G. (1993). Localization of the cystic fibrosis transmembrane conductance regulator in human bile duct epithelial cells.

Gastroenterology, 105(6), 1857-1864. Retrieved from

<http://www.ncbi.nlm.nih.gov/pubmed/7504645>

Colasanti, R. L., Morris, M. J., Madgwick, R. G., Sutton, L., & Williams, E. M. (2004). Analysis of tidal breathing profiles in cystic fibrosis and COPD. *Chest*, 125(3), 901-908. Retrieved from

<http://www.ncbi.nlm.nih.gov/pubmed/15006948>

Collaco, J. M., Blackman, S. M., McGready, J., Naughton, K. M., & Cutting, G. R. (2010). Quantification of the relative contribution of

environmental and genetic factors to variation in cystic fibrosis lung function. *J Pediatr*, 157(5), 802-807 e801-803.

doi:10.1016/j.jpeds.2010.05.018

Collaco, J. M., & Cutting, G. R. (2008). Update on gene modifiers in cystic fibrosis. *Curr Opin Pulm Med*, 14(6), 559-566.

doi:10.1097/MCP.0b013e3283121cdc

Collin, G. (2013). The big interview: The moving story of Holly's battle with cystic fibrosis. Retrieved from <http://www.leicestermercury.co.uk/BIG-INTERVIEW-moving-story-Holly-8217-s-battle/story-20169152-detail/story.html>

Collins, G. (2015). Being an organ donor is the most selfless, heroic thing you can do. I'm forever grateful. Retrieved from

<http://www.leicestermercury.co.uk/Holly-van-Geffen/story-27621866-detail/story.html>

Colombo, C., & Battezzati, P. M. (2004). Liver involvement in cystic fibrosis: primary organ damage or innocent bystander? *J Hepatol*, 41(6), 1041-1044. doi:10.1016/j.jhep.2004.10.002

Colombo, C., Battezzati, P. M., Crosignani, A., Morabito, A., Costantini, D., Padoan, R., & Giunta, A. (2002). Liver disease in cystic fibrosis: A prospective study on incidence, risk factors, and outcome.

Hepatology, 36(6), 1374-1382. doi:10.1053/jhep.2002.37136

Comer, D. M., Ennis, M., McDowell, C., Beattie, D., Rendall, J., Hall, V., & Elborn, J. S. (2009). Clinical phenotype of cystic fibrosis patients with the G551D mutation. *QJM*, 102(11), 793-798.

doi:10.1093/qjmed/hcp120

- Cooney, A. L., Singh, B. K., & Sinn, P. L. (2015). Hybrid nonviral/viral vector systems for improved piggyBac DNA transposon in vivo delivery. *Mol Ther*, 23(4), 667-674. doi:10.1038/mt.2014.254
- Corey, M., McLaughlin, F. J., Williams, M., & Levison, H. (1988). A comparison of survival, growth, and pulmonary function in patients with cystic fibrosis in Boston and Toronto. *J Clin Epidemiol*, 41(6), 583-591. Retrieved from <http://www.ncbi.nlm.nih.gov/pubmed/3260274>
- Corley, R. A., Kabilan, S., Kuprat, A. P., Carson, J. P., Minard, K. R., Jacob, R. E., . . . Einstein, D. R. (2012). Comparative computational modeling of airflows and vapor dosimetry in the respiratory tracts of rat, monkey, and human. *Toxicol Sci*, 128(2), 500-516. doi:10.1093/toxsci/kfs168
- Couper, R. T., Corey, M., Moore, D. J., Fisher, L. J., Forstner, G. G., & Durie, P. R. (1992). Decline of exocrine pancreatic function in cystic fibrosis patients with pancreatic sufficiency. *Pediatr Res*, 32(2), 179-182. doi:10.1203/00006450-199208000-00011
- Coutelle, C., Caplen, N., Hart, S., Huxley, C., & Williamson, R. (1993). Gene therapy for cystic fibrosis. *Arch Dis Child*, 68(4), 437-440. Retrieved from <http://www.ncbi.nlm.nih.gov/pubmed/8503661>
- Cowley, E. A., Wang, C. G., Gosselin, D., Radzioch, D., & Eidelman, D. H. (1997). Mucociliary clearance in cystic fibrosis knockout mice infected with *Pseudomonas aeruginosa*. *Eur Respir J*, 10(10), 2312-2318. Retrieved from <http://www.ncbi.nlm.nih.gov/pubmed/9387959>
- Coxson, H. O. (2012). Lung parenchyma density and airway wall thickness in airway diseases. *Breathe*, 9, 8.

- Coxson, H. O., Quiney, B., Sin, D. D., Xing, L., McWilliams, A. M., Mayo, J. R., & Lam, S. (2008). Airway wall thickness assessed using computed tomography and optical coherence tomography. *Am J Respir Crit Care Med*, 177(11), 1201-1206. doi:10.1164/rccm.200712-1776OC
- Csanady, L. (2013). CFTR's degenerate nucleotide binding site 1 probably moves during channel gating. Retrieved from <http://www.physoc.org/proceedings/abstract/Proc%2037th%20IUPSS>
[A30](#)
- Cuthbert, A. W. (2011). New horizons in the treatment of cystic fibrosis. *Br J Pharmacol*, 163(1), 173-183. doi:10.1111/j.1476-5381.2010.01137.x
- Cutting, G. R. (2005). Modifier genetics: cystic fibrosis. *Annu Rev Genomics Hum Genet*, 6, 237-260.
doi:10.1146/annurev.genom.6.080604.162254
- Cutting, G. R. (2010). Modifier genes in Mendelian disorders: the example of cystic fibrosis. *Ann N Y Acad Sci*, 1214, 57-69. doi:10.1111/j.1749-6632.2010.05879.x
- Czaja, P., Soja, J., Grzanka, P., Cmiel, A., Szczeklik, A., & Sladek, K. (2007). Assessment of airway caliber in quantitative videobronchoscopy. *Respiration*, 74(4), 432-438. doi:10.1159/000097993
- Darquenne, C., van Ertbruggen, C., & Prisk, G. K. (2011). Convective flow dominates aerosol delivery to the lung segments. *J Appl Physiol* (1985), 111(1), 48-54. doi:10.1152/jappphysiol.00796.2010
- Dasenbrook, E. C., Lu, L., Donnola, S., Weaver, D. E., Gulani, V., Jakob, P. M., . . . Flask, C. A. (2013). Normalized T1 magnetic resonance imaging for assessment of regional lung function in adult cystic fibrosis

patients--a cross-sectional study. *PLoS One*, 8(9), e73286.

doi:10.1371/journal.pone.0073286

Davidson, D. J., Dorin, J. R., McLachlan, G., Ranaldi, V., Lamb, D., Doherty,

C., . . . Porteous, D. J. (1995). Lung disease in the cystic fibrosis

mouse exposed to bacterial pathogens. *Nat Genet*, 9(4), 351-357.

doi:10.1038/ng0495-351

Davidson, D. J., & Rolfe, M. (2001). Mouse models of cystic fibrosis. *Trends*

Genet, 17(10), S29-37. Retrieved from

<http://www.ncbi.nlm.nih.gov/pubmed/11585674>

Davies, J. C., & Alton, E. W. (2009). Monitoring respiratory disease severity

in cystic fibrosis. *Respir Care*, 54(5), 606-617. Retrieved from

<http://www.ncbi.nlm.nih.gov/pubmed/19393105>

Davies, J. C., Cunningham, S., Alton, E. W., & Innes, J. A. (2008). Lung

clearance index in CF: a sensitive marker of lung disease severity.

Thorax, 63(2), 96-97. doi:10.1136/thx.2007.082768

Davies, J. C., Wainwright, C. E., Canny, G. J., Chilvers, M. A., Howenstine,

M. S., Munck, A., . . . Group, V. X. S. (2013). Efficacy and safety of

ivacaftor in patients aged 6 to 11 years with cystic fibrosis with a

G551D mutation. *Am J Respir Crit Care Med*, 187(11), 1219-1225.

doi:10.1164/rccm.201301-0153OC

Davis, S. D., Fordham, L. A., Brody, A. S., Noah, T. L., Retsch-Bogart, G. Z.,

Qaqish, B. F., . . . Leigh, M. W. (2007). Computed tomography reflects

lower airway inflammation and tracks changes in early cystic fibrosis.

Am J Respir Crit Care Med, 175(9), 943-950.

doi:10.1164/rccm.200603-343OC

- De Backer, J. W., Vos, W. G., Gorle, C. D., Germonpre, P., Partoens, B., Wuyts, F. L., . . . De Backer, W. (2008). Flow analyses in the lower airways: patient-specific model and boundary conditions. *Med Eng Phys*, 30(7), 872-879. doi:10.1016/j.medengphy.2007.11.002
- De Backer, L. A., Vos, W., De Backer, J., Van Holsbeke, C., Vinchurkar, S., & De Backer, W. (2012). The acute effect of budesonide/formoterol in COPD: a multi-slice computed tomography and lung function study. *Eur Respir J*, 40(2), 298-305. doi:10.1183/09031936.00072511
- De Boeck, K., Munck, A., Walker, S., Faro, A., Hiatt, P., Gilmartin, G., & Higgins, M. (2014). Efficacy and safety of ivacaftor in patients with cystic fibrosis and a non-G551D gating mutation. *J Cyst Fibros*, 13(6), 674-680. doi:10.1016/j.jcf.2014.09.005
- Deeks, E. D. (2013). Ivacaftor: a review of its use in patients with cystic fibrosis. *Drugs*, 73(14), 1595-1604. doi:10.1007/s40265-013-0115-2
- Dekkers, J. F., Wiegerinck, C. L., de Jonge, H. R., Bronsveld, I., Janssens, H. M., de Winter-de Groot, K. M., . . . Beekman, J. M. (2013). A functional CFTR assay using primary cystic fibrosis intestinal organoids. *Nat Med*, 19(7), 939-945. doi:10.1038/nm.3201
- Denning, G. M., Anderson, M. P., Amara, J. F., Marshall, J., Smith, A. E., & Welsh, M. J. (1992). Processing of mutant cystic fibrosis transmembrane conductance regulator is temperature-sensitive. *Nature*, 358(6389), 761-764. doi:10.1038/358761a0
- Di, S. A. P. E., & Andersen, D. H. (1946). Celiac syndrome; chemotherapy in infections of the respiratory tract associated with cystic fibrosis of the pancreas; observations with penicillin and drugs of the sulfonamide

- group, with special reference to penicillin aerosol. *Am J Dis Child*, 72, 17-61. Retrieved from <http://www.ncbi.nlm.nih.gov/pubmed/20994054>
- Dickinson, P., Smith, S. N., Webb, S., Kilanowski, F. M., Campbell, I. J., Taylor, M. S., . . . Dorin, J. R. (2002). The severe G480C cystic fibrosis mutation, when replicated in the mouse, demonstrates mistrafficking, normal survival and organ-specific bioelectrics. *Hum Mol Genet*, 11(3), 243-251. Retrieved from <http://www.ncbi.nlm.nih.gov/pubmed/11823443>
- Drumm, M. L., Pope, H. A., Cliff, W. H., Rommens, J. M., Marvin, S. A., Tsui, L. C., . . . Wilson, J. M. (1990). Correction of the cystic fibrosis defect in vitro by retrovirus-mediated gene transfer. *Cell*, 62(6), 1227-1233. Retrieved from <http://www.ncbi.nlm.nih.gov/pubmed/1698126>
- Du, K., Sharma, M., & Lukacs, G. L. (2005). The DeltaF508 cystic fibrosis mutation impairs domain-domain interactions and arrests post-translational folding of CFTR. *Nat Struct Mol Biol*, 12(1), 17-25. doi:10.1038/nsmb882
- Echeveste, J., Fernandez-Velilla, M., Torres, M. I., Pardo, M., Berrocal, T., & Martin-Hervas, C. (2005). [Cystic diseases of the lung: high-resolution computed tomography findings]. *Arch Bronconeumol*, 41(1), 42-49. Retrieved from <http://www.ncbi.nlm.nih.gov/pubmed/15676135>
- Elettromedicali. PEP Mask. Retrieved from <http://www.elettromedicali.it/it/shop/respirazione-aerosol-cpap/distanziatori-incentivatori/p747-vitapep-per-mask-con-1-maschera-adulti>
- Engelhardt, J. F., Yankaskas, J. R., Ernst, S. A., Yang, Y., Marino, C. R., Boucher, R. C., . . . Wilson, J. M. (1992). Submucosal glands are the

predominant site of CFTR expression in the human bronchus. *Nat Genet*, 2(3), 240-248. doi:10.1038/ng1192-240

Ester, M. K., H.P.; Sander, J.; Xu, X. (1996). *Proceedings of the 2nd International Conference of Knowledge Discovery and Data Mining*. Menlo Park, California: AAAI Press.

Fain, S., Schiebler, M. L., McCormack, D. G., & Parraga, G. (2010). Imaging of lung function using hyperpolarized helium-3 magnetic resonance imaging: Review of current and emerging translational methods and applications. *J Magn Reson Imaging*, 32(6), 1398-1408. doi:10.1002/jmri.22375

Faiyazuddin, M., Mujahid, M., Hussain, T., Siddiqui, H. H., Bhatnagar, A., Khar, R. K., & Ahmad, F. J. (2013). Aerodynamics and deposition effects of inhaled submicron drug aerosol in airway diseases. *Recent Pat Inflamm Allergy Drug Discov*, 7(1), 49-61. Retrieved from <http://www.ncbi.nlm.nih.gov/pubmed/22663775>

Fernandez, J. W., Mithraratne, P., Thrupp, S. F., Tawhai, M. H., & Hunter, P. J. (2004). Anatomically based geometric modelling of the musculo-skeletal system and other organs. *Biomech Model Mechanobiol*, 2(3), 139-155. doi:10.1007/s10237-003-0036-1

Finlay, W. H. (2001). *The mechanics of inhaled pharmaceutical aerosols: An introduction*. Academic (1st edition ed.).

Fisher, J. T., Tyler, S. R., Zhang, Y., Lee, B. J., Liu, X., Sun, X., . . .

Engelhardt, J. F. (2013). Bioelectric characterization of epithelia from neonatal CFTR knockout ferrets. *Am J Respir Cell Mol Biol*, 49(5), 837-844. doi:10.1165/rcmb.2012-0433OC

- FLuidda. (2016). FRI Technology. *FRI Technology*. Retrieved from <http://www.fluidda.com/fri-technology/>
- Flusberg, B. A., Cocker, E. D., Piyawattanametha, W., Jung, J. C., Cheung, E. L., & Schnitzer, M. J. (2005). Fiber-optic fluorescence imaging. *Nat Methods*, 2(12), 941-950. doi:10.1038/nmeth820
- Folescu, T. W., Marques Ede, A., Boechat, M. C., Daltro, P., Higa, L. Y., & Cohen, R. W. (2012). High-resolution computed tomography scores in cystic fibrosis patients colonized with *Pseudomonas aeruginosa* or *Staphylococcus aureus*. *J Bras Pneumol*, 38(1), 41-49. Retrieved from <http://www.ncbi.nlm.nih.gov/pubmed/22407039>
- Frederiksen, B., Koch, C., & Hoiby, N. (1997). Antibiotic treatment of initial colonization with *Pseudomonas aeruginosa* postpones chronic infection and prevents deterioration of pulmonary function in cystic fibrosis. *Pediatr Pulmonol*, 23(5), 330-335. Retrieved from <http://www.ncbi.nlm.nih.gov/pubmed/9168506>
- Fuld, M. K., Easley, R. B., Saba, O. I., Chon, D., Reinhardt, J. M., Hoffman, E. A., & Simon, B. A. (2008). CT-measured regional specific volume change reflects regional ventilation in supine sheep. *J Appl Physiol* (1985), 104(4), 1177-1184. doi:10.1152/jappphysiol.00212.2007
- Gadsby, D. C., Vergani, P., & Csanady, L. (2006). The ABC protein turned chloride channel whose failure causes cystic fibrosis. *Nature*, 440(7083), 477-483. doi:10.1038/nature04712
- Garcia, M. A., Yang, N., & Quinton, P. M. (2009). Normal mouse intestinal mucus release requires cystic fibrosis transmembrane regulator-dependent bicarbonate secretion. *J Clin Invest*, 119(9), 2613-2622. doi:10.1172/JCI38662

- Gautam, V., Singhal, L., & Ray, P. (2011). Burkholderia cepacia complex: beyond pseudomonas and acinetobacter. *Indian J Med Microbiol*, 29(1), 4-12. doi:10.4103/0255-0857.76516
- Gelman, M. S., & Kopito, R. R. (2003). Cystic fibrosis: premature degradation of mutant proteins as a molecular disease mechanism. *Methods Mol Biol*, 232, 27-37. doi:10.1385/1-59259-394-1:27
- George, P. M., Banya, W., Pareek, N., Bilton, D., Cullinan, P., Hodson, M. E., & Simmonds, N. J. (2011). Improved survival at low lung function in cystic fibrosis: cohort study from 1990 to 2007. *BMJ*, 342, d1008. doi:10.1136/bmj.d1008
- Geuzaine, C. (2009). Gmsh: A 3-D finite element mesh generator with built-in pre- and post-processing facilities. *International Journal for Numerical Methods in Engineering*, 79(11), 19.
- Gibson, R. L., Burns, J. L., & Ramsey, B. W. (2003). Pathophysiology and management of pulmonary infections in cystic fibrosis. *Am J Respir Crit Care Med*, 168(8), 918-951. doi:10.1164/rccm.200304-505SO
- Glenny, R. W. (2011). Emergence of matched airway and vascular trees from fractal rules. *J Appl Physiol (1985)*, 110(4), 1119-1129. doi:10.1152/japplphysiol.01293.2010
- Gorter, R. R., Karimi, A., Sleeboom, C., Kneepkens, C. M., & Heij, H. A. (2010). Clinical and genetic characteristics of meconium ileus in newborns with and without cystic fibrosis. *J Pediatr Gastroenterol Nutr*, 50(5), 569-572. doi:10.1097/MPG.0b013e3181bb3427
- Goss, C. H., & Muhlebach, M. S. (2011). Review: Staphylococcus aureus and MRSA in cystic fibrosis. *J Cyst Fibros*, 10(5), 298-306. doi:10.1016/j.jcf.2011.06.002

- Greve, J. H. (2012). *Diseases of Swine* (J. J. Z. L. A. K. A. R. K. J. S. a. G. E. Stevenson Ed. 10th edition ed.). West Sussex UK: Wiley.
- Grubb, B. R., & Boucher, R. C. (1999). Pathophysiology of gene-targeted mouse models for cystic fibrosis. *Physiol Rev*, 79(1 Suppl), S193-214. Retrieved from <http://www.ncbi.nlm.nih.gov/pubmed/9922382>
- Guerrero, T., Sanders, K., Castillo, E., Zhang, Y., Bidaut, L., Pan, T., & Komaki, R. (2006). Dynamic ventilation imaging from four-dimensional computed tomography. *Phys Med Biol*, 51(4), 777-791. doi:10.1088/0031-9155/51/4/002
- Gurney, J. W., Habbe, T. G., & Hicklin, J. (1997). Distribution of disease in cystic fibrosis: correlation with pulmonary function. *Chest*, 112(2), 357-362. Retrieved from <http://www.ncbi.nlm.nih.gov/pubmed/9266869>
- Gurney, J. W., & Schroeder, B. A. (1988). Upper lobe lung disease: physiologic correlates. Review. *Radiology*, 167(2), 359-366. doi:10.1148/radiology.167.2.3282257
- Gustafsson, P. M., Aurora, P., & Lindblad, A. (2003). Evaluation of ventilation maldistribution as an early indicator of lung disease in children with cystic fibrosis. *Eur Respir J*, 22(6), 972-979. Retrieved from <http://www.ncbi.nlm.nih.gov/pubmed/14680088>
- Haeusler, G., Frisch, H., Waldhor, T., & Gotz, M. (1994). Perspectives of longitudinal growth in cystic fibrosis from birth to adult age. *Eur J Pediatr*, 153(3), 158-163. Retrieved from <http://www.ncbi.nlm.nih.gov/pubmed/8181496>
- Hamosh, A., King, T. M., Rosenstein, B. J., Corey, M., Levison, H., Durie, P., . . . et al. (1992). Cystic fibrosis patients bearing both the common missense mutation Gly----Asp at codon 551 and the delta F508

mutation are clinically indistinguishable from delta F508 homozygotes, except for decreased risk of meconium ileus. *Am J Hum Genet*, 51(2), 245-250. Retrieved from

<http://www.ncbi.nlm.nih.gov/pubmed/1379413>

Hankinson, J. L., Odencrantz, J. R., & Fedan, K. B. (1999). Spirometric reference values from a sample of the general U.S. population. *Am J Respir Crit Care Med*, 159(1), 179-187.

doi:10.1164/ajrccm.159.1.9712108

Harris, R. S., & Schuster, D. P. (2007). Visualizing lung function with positron emission tomography. *J Appl Physiol* (1985), 102(1), 448-458.

doi:10.1152/jappphysiol.00763.2006

Hekmatian, E., Jafari-Pozve, N., & Khorrami, L. (2014). The effect of voxel size on the measurement of mandibular thickness in cone-beam computed tomography. *Dent Res J (Isfahan)*, 11(5), 544-548.

Retrieved from <http://www.ncbi.nlm.nih.gov/pubmed/25426143>

Helbich, T. H., Heinz-Peer, G., Eichler, I., Wunderbaldinger, P., Gotz, M., Wojnarowski, C., . . . Herold, C. J. (1999). Cystic fibrosis: CT assessment of lung involvement in children and adults. *Radiology*, 213(2), 537-544. doi:10.1148/radiology.213.2.r99nv04537

Herrmann, U., Dockter, G., & Lammert, F. (2010). Cystic fibrosis-associated liver disease. *Best Pract Res Clin Gastroenterol*, 24(5), 585-592.

doi:10.1016/j.bpg.2010.08.003

Hibbert, M. E., Lannigan, A., Landau, L. I., & Phelan, P. D. (1989). Lung function values from a longitudinal study of healthy children and adolescents. *Pediatr Pulmonol*, 7(2), 101-109. Retrieved from

<http://www.ncbi.nlm.nih.gov/pubmed/2797918>

- Hoare, S., McEvoy, S., McCarthy, C. J., Kilcoyne, A., Brady, D., Gibney, B., . . . Dodd, J. D. (2014). Ivacaftor imaging response in cystic fibrosis. *Am J Respir Crit Care Med*, *189*(4), 484. doi:10.1164/rccm.201308-1433IM
- Hodson, M. E., Gallagher, C. G., & Govan, J. R. (2002). A randomised clinical trial of nebulised tobramycin or colistin in cystic fibrosis. *Eur Respir J*, *20*(3), 658-664. Retrieved from <http://www.ncbi.nlm.nih.gov/pubmed/12358344>
- Hodson, M. E., Penketh, A. R., & Batten, J. C. (1981). Aerosol carbenicillin and gentamicin treatment of *Pseudomonas aeruginosa* infection in patients with cystic fibrosis. *Lancet*, *2*(8256), 1137-1139. Retrieved from <http://www.ncbi.nlm.nih.gov/pubmed/6118579>
- Hoegger, M. J., Awadalla, M., Namati, E., Itani, O. A., Fischer, A. J., Tucker, A. J., . . . Welsh, M. J. (2014). Assessing mucociliary transport of single particles in vivo shows variable speed and preference for the ventral trachea in newborn pigs. *Proc Natl Acad Sci U S A*, *111*(6), 2355-2360. doi:10.1073/pnas.1323633111
- Hoegger, M. J., Fischer, A. J., McMenimen, J. D., Ostedgaard, L. S., Tucker, A. J., Awadalla, M. A., . . . Welsh, M. J. (2014). Impaired mucus detachment disrupts mucociliary transport in a piglet model of cystic fibrosis. *Science*, *345*(6198), 818-822. doi:10.1126/science.1255825
- Hoffman, E. A., & Ritman, E. L. (1985). Effect of body orientation on regional lung expansion in dog and sloth. *J Appl Physiol* (1985), *59*(2), 481-491. Retrieved from <http://www.ncbi.nlm.nih.gov/pubmed/4030600>
- Hofmann, W., Sturm, R., Fleming, J. S., Conway, J. H., & Bolt, L. (2005). Simulation of three-dimensional particle deposition patterns in human

lungs and comparison with experimental SPECT data. *Aerosol Science and Technology*, 39(8), 771-781.

doi:10.1080/02786820500237158

Hoiby, N., Flensburg, E. W., Beck, B., Friis, B., Jacobsen, S. V., & Jacobsen, L. (1977). Pseudomonas aeruginosa infection in cystic fibrosis.

Diagnostic and prognostic significance of Pseudomonas aeruginosa precipitins determined by means of crossed immunoelectrophoresis.

Scand J Respir Dis, 58(2), 65-79. Retrieved from

<http://www.ncbi.nlm.nih.gov/pubmed/404701>

Hoo, A. F., Thia, L. P., Nguyen, T. T., Bush, A., Chudleigh, J., Lum, S., . . .

London Cystic Fibrosis, C. (2012). Lung function is abnormal in 3-month-old infants with cystic fibrosis diagnosed by newborn screening.

Thorax, 67(10), 874-881. doi:10.1136/thoraxjnl-2012-201747

Horsley, A. (2009). Lung clearance index in the assessment of airways disease. *Respir Med*, 103(6), 793-799.

doi:10.1016/j.rmed.2009.01.025

Horsley, A. R., Gustafsson, P. M., Macleod, K. A., Saunders, C., Greening,

A. P., Porteous, D. J., . . . Innes, J. A. (2008). Lung clearance index is a sensitive, repeatable and practical measure of airways disease in

adults with cystic fibrosis. *Thorax*, 63(2), 135-140.

doi:10.1136/thx.2007.082628

Hu, S., Hoffman, E. A., & Reinhardt, J. M. (2001). Automatic lung segmentation for accurate quantitation of volumetric X-ray CT images.

IEEE Trans Med Imaging, 20(6), 490-498. doi:10.1109/42.929615

Hussain, K., Hussain, M., Mansoor, S., & Briddon, R. W. (2011). Complete nucleotide sequence of a begomovirus and associated betasatellite

infecting croton (*Croton bonplandianus*) in Pakistan. *Arch Virol*, 156(6), 1101-1105. doi:10.1007/s00705-011-0993-0

Hussain, M., Renate, W. H., & Werner, H. (2011). Effect of intersubject variability of extrathoracic morphometry, lung airways dimensions and respiratory parameters on particle deposition. *J Thorac Dis*, 3(3), 156-170. doi:10.3978/j.issn.2072-1439.2011.04.03

Hwang, T. C., & Kirk, K. L. (2013). The CFTR ion channel: gating, regulation, and anion permeation. *Cold Spring Harb Perspect Med*, 3(1), a009498. doi:10.1101/cshperspect.a009498

Jackson, F. (1982). Epiphenomenal Qualia. *The Philosophical Quarterly*, 32(127), 127-136.

Jain, K., & Smyth, A. R. (2012). Current dilemmas in antimicrobial therapy in cystic fibrosis. *Expert Rev Respir Med*, 6(4), 407-422. doi:10.1586/ers.12.39

Jarrin, N. P., R.; Uribe, J.C.; Benhamadouche, S.; and Laurence, D. . (2009). Reconstruction of Turbulent Fluctuations for Hybrid RANS/LES Simulations using a Synthetic-Eddy Method. *International Journal of Heat and Fluid Flow*,, 30, 435-422.

Javier, R. M., & Jacquot, J. (2011). Bone disease in cystic fibrosis: what's new? *Joint Bone Spine*, 78(5), 445-450. doi:10.1016/j.jbspin.2010.11.015

Jensen, T., Pedersen, S. S., Garne, S., Heilmann, C., Hoiby, N., & Koch, C. (1987). Colistin inhalation therapy in cystic fibrosis patients with chronic *Pseudomonas aeruginosa* lung infection. *J Antimicrob Chemother*, 19(6), 831-838. Retrieved from <http://www.ncbi.nlm.nih.gov/pubmed/3301785>

- Jensen, T. J., Loo, M. A., Pind, S., Williams, D. B., Goldberg, A. L., & Riordan, J. R. (1995). Multiple proteolytic systems, including the proteasome, contribute to CFTR processing. *Cell*, 83(1), 129-135. Retrieved from <http://www.ncbi.nlm.nih.gov/pubmed/7553864>
- Jih, K. Y., & Hwang, T. C. (2013). Vx-770 potentiates CFTR function by promoting decoupling between the gating cycle and ATP hydrolysis cycle. *Proc Natl Acad Sci U S A*, 110(11), 4404-4409. doi:10.1073/pnas.1215982110
- JohnHopkins. (2014). Mechanism in which the mutation of the CFTR gene can lead to defective or inactive CFTR channel. . Retrieved from <http://www.hopkinscf.org/what-is-cf-teen/science-of-cf-teen/cftr-teen/cellular-processing-teen/>
- Kanelis, V., Hudson, R. P., Thibodeau, P. H., Thomas, P. J., & Forman-Kay, J. D. (2010). NMR evidence for differential phosphorylation-dependent interactions in WT and DeltaF508 CFTR. *EMBO J*, 29(1), 263-277. doi:10.1038/emboj.2009.329
- Kelly, A., & Moran, A. (2013). Update on cystic fibrosis-related diabetes. *J Cyst Fibros*, 12(4), 318-331. doi:10.1016/j.jcf.2013.02.008
- Kennedy, M. P., Morice, R. C., Jimenez, C. A., & Eapen, G. A. (2007). Treatment of bronchial airway obstruction using a rotating tip microdebrider: a case report. *J Cardiothorac Surg*, 2, 16. doi:10.1186/1749-8090-2-16
- Kent, G., Iles, R., Bear, C. E., Huan, L. J., Griesenbach, U., McKerlie, C., . . . Tanswell, A. K. (1997). Lung disease in mice with cystic fibrosis. *J Clin Invest*, 100(12), 3060-3069. doi:10.1172/JCI119861

- Kerem, B., Rommens, J. M., Buchanan, J. A., Markiewicz, D., Cox, T. K., Chakravarti, A., . . . Tsui, L. C. (1989). Identification of the cystic fibrosis gene: genetic analysis. *Science*, *245*(4922), 1073-1080. Retrieved from <http://www.ncbi.nlm.nih.gov/pubmed/2570460>
- Kerem, E., Conway, S., Elborn, S., Heijerman, H., & Consensus, C. (2005). Standards of care for patients with cystic fibrosis: a European consensus. *J Cyst Fibros*, *4*(1), 7-26. doi:10.1016/j.jcf.2004.12.002
- Kerem, E., Corey, M., Kerem, B. S., Rommens, J., Markiewicz, D., Levison, H., . . . Durie, P. (1990). The relation between genotype and phenotype in cystic fibrosis--analysis of the most common mutation (delta F508). *N Engl J Med*, *323*(22), 1517-1522. doi:10.1056/NEJM199011293232203
- Kerem, E., Reisman, J., Corey, M., Canny, G. J., & Levison, H. (1992). Prediction of mortality in patients with cystic fibrosis. *N Engl J Med*, *326*(18), 1187-1191. doi:10.1056/NEJM199204303261804
- Khan, T. Z., Wagener, J. S., Bost, T., Martinez, J., Accurso, F. J., & Riches, D. W. (1995). Early pulmonary inflammation in infants with cystic fibrosis. *Am J Respir Crit Care Med*, *151*(4), 1075-1082. doi:10.1164/ajrccm.151.4.7697234
- Kilburn, K. H. (1984). Particles causing lung disease. *Environ Health Perspect*, *55*, 97-109. Retrieved from <http://www.ncbi.nlm.nih.gov/pubmed/6376114>
- Kim, G. S. I., A.J. (1989). Deposition of Inhaled Particles in Bifurcating Airway Models: I. Inspiratory Deposition. *Journal of Aerosol Medicine*, *2*(1), 14. doi:10.1089/jam.1989.2.1.

- Kim, S. J. (2012). Mechanisms of CFTR folding at the endoplasmic reticulum.
Retrieved from
<http://journal.frontiersin.org/article/10.3389/fphar.2012.00201/full>
- Klein, S., Staring, M., & Pluim, J. P. (2007). Evaluation of optimization methods for nonrigid medical image registration using mutual information and B-splines. *IEEE Trans Image Process*, 16(12), 2879-2890. Retrieved from <http://www.ncbi.nlm.nih.gov/pubmed/18092588>
- Knowles, M. R., Clarke, L. L., & Boucher, R. C. (1991). Activation by extracellular nucleotides of chloride secretion in the airway epithelia of patients with cystic fibrosis. *N Engl J Med*, 325(8), 533-538.
doi:10.1056/NEJM199108223250802
- Knowles, M. R., & Drumm, M. (2012). The influence of genetics on cystic fibrosis phenotypes. *Cold Spring Harb Perspect Med*, 2(12), a009548.
doi:10.1101/cshperspect.a009548
- Konstan, M. W., Morgan, W. J., Butler, S. M., Pasta, D. J., Craib, M. L., Silva, S. J., . . . Coordinators of the Epidemiologic Study of Cystic, F. (2007). Risk factors for rate of decline in forced expiratory volume in one second in children and adolescents with cystic fibrosis. *J Pediatr*, 151(2), 134-139, 139 e131. doi:10.1016/j.jpeds.2007.03.006
- Konstan, M. W., Schluchter, M. D., Xue, W., & Davis, P. B. (2007). Clinical use of Ibuprofen is associated with slower FEV1 decline in children with cystic fibrosis. *Am J Respir Crit Care Med*, 176(11), 1084-1089.
doi:10.1164/rccm.200702-181OC
- Kotha, K., & Clancy, J. P. (2013). Ivacaftor treatment of cystic fibrosis patients with the G551D mutation: a review of the evidence. *Ther Adv Respir Dis*, 7(5), 288-296. doi:10.1177/1753465813502115

- Kristufek, P., Brezina, M., Ciutti, P., Strmen, J., & Mayer, M. (1987). Reference values and modelling of lung function development as a transcendent function of age, body height and mass. *Bull Eur Physiopathol Respir*, 23(2), 139-147. Retrieved from <http://www.ncbi.nlm.nih.gov/pubmed/3607328>
- Kuhn, R. J. (2001). Formulation of aerosolized therapeutics. *Chest*, 120(3 Suppl), 94S-98S. Retrieved from <http://www.ncbi.nlm.nih.gov/pubmed/11555562>
- Kulich, M., Rosenfeld, M., Campbell, J., Kronmal, R., Gibson, R. L., Goss, C. H., & Ramsey, B. (2005). Disease-specific reference equations for lung function in patients with cystic fibrosis. *Am J Respir Crit Care Med*, 172(7), 885-891. doi:10.1164/rccm.200410-1335OC
- Kumar, H., Tawhai, M. H., Hoffman, E. A., & Lin, C. L. (2009). The effects of geometry on airflow in the acinar region of the human lung. *J Biomech*, 42(11), 1635-1642. doi:10.1016/j.jbiomech.2009.04.046
- Kwilas, A. R., Yednak, M. A., Zhang, L., Liesman, R., Collins, P. L., Pickles, R. J., & Peeples, M. E. (2010). Respiratory syncytial virus engineered to express the cystic fibrosis transmembrane conductance regulator corrects the bioelectric phenotype of human cystic fibrosis airway epithelium in vitro. *J Virol*, 84(15), 7770-7781. doi:10.1128/JVI.00346-10
- Lambert, A. R., O'Shaughnessy, P., Tawhai, M. H., Hoffman, E. A., & Lin, C. L. (2011). Regional deposition of particles in an image-based airway model: large-eddy simulation and left-right lung ventilation asymmetry. *Aerosol Sci Technol*, 45(1), 11-25. doi:10.1080/02786826.2010.517578

- Lands, L. C., Heigenhauser, G. J., & Jones, N. L. (1992). Analysis of factors limiting maximal exercise performance in cystic fibrosis. *Clin Sci (Lond)*, 83(4), 391-397. Retrieved from <http://www.ncbi.nlm.nih.gov/pubmed/1330400>
- Levitzky, M. G. (1995). *Pulmonary Physiology* (4th editions ed.). United States of America: McGraw Hill Professional.
- Lewindon, P. J., Robb, T. A., Moore, D. J., Davidson, G. P., & Martin, A. J. (1998). Bowel dysfunction in cystic fibrosis: importance of breath testing. *J Paediatr Child Health*, 34(1), 79-82. Retrieved from <http://www.ncbi.nlm.nih.gov/pubmed/9568948>
- Lewis, R. (2002). Targeted Comparative Sequencing Illuminates Vertebrate Evolution. Retrieved from <http://www.the-scientist.com/?articles.view/articleNo/14405/title/Targeted-Comparative-Sequencing-Illuminates-Vertebrate-Evolution/>
- Li, Z., Sanders, D. B., Rock, M. J., Kosorok, M. R., Collins, J., Green, C. G., . . . Farrell, P. M. (2012). Regional differences in the evolution of lung disease in children with cystic fibrosis. *Pediatr Pulmonol*, 47(7), 635-640. doi:10.1002/ppul.21604
- Lin, C. L., Tawhai, M. H., McLennan, G., & Hoffman, E. A. (2007). Characteristics of the turbulent laryngeal jet and its effect on airflow in the human intra-thoracic airways. *Respir Physiol Neurobiol*, 157(2-3), 295-309. doi:10.1016/j.resp.2007.02.006
- Lin, C. L. L., H.; Lee, T.; Weber, L.J. (2005). A level set characteristic galerkin finite element method for free surface flows. *International Journal for Numerical Methods in Fluids*, 49(5), 27.

- Lippmann, M., Yeates, D. B., & Albert, R. E. (1980). Deposition, retention, and clearance of inhaled particles. *Br J Ind Med*, 37(4), 337-362. Retrieved from <http://www.ncbi.nlm.nih.gov/pubmed/7004477>
- Lisowska, A., Wojtowicz, J., & Walkowiak, J. (2009). Small intestine bacterial overgrowth is frequent in cystic fibrosis: combined hydrogen and methane measurements are required for its detection. *Acta Biochim Pol*, 56(4), 631-634. Retrieved from <http://www.ncbi.nlm.nih.gov/pubmed/19997657>
- Littlewood, J. M., Miller, M. G., Ghoneim, A. T., & Ramsden, C. H. (1985). Nebulised colomycin for early pseudomonas colonisation in cystic fibrosis. *Lancet*, 1(8433), 865. Retrieved from <http://www.ncbi.nlm.nih.gov/pubmed/2858720>
- Longest, P. W., & Hindle, M. (2012). Condensational growth of combination drug-excipient submicrometer particles for targeted high efficiency pulmonary delivery: comparison of CFD predictions with experimental results. *Pharm Res*, 29(3), 707-721. doi:10.1007/s11095-011-0596-1
- Loo, M. A., Jensen, T. J., Cui, L., Hou, Y., Chang, X. B., & Riordan, J. R. (1998). Perturbation of Hsp90 interaction with nascent CFTR prevents its maturation and accelerates its degradation by the proteasome. *EMBO J*, 17(23), 6879-6887. doi:10.1093/emboj/17.23.6879
- Lukacs, G. L., & Verkman, A. S. (2012). CFTR: folding, misfolding and correcting the DeltaF508 conformational defect. *Trends Mol Med*, 18(2), 81-91. doi:10.1016/j.molmed.2011.10.003
- Luo, H. Y., Liu, Y., & Yang, X. L. (2007). Particle deposition in obstructed airways. *J Biomech*, 40(14), 3096-3104. doi:10.1016/j.jbiomech.2007.03.027

- LVNG. (2006). I've been diagnosed, now what? *Your lung what you should know*. Retrieved from <https://www.lvng.org/about-lung-cancer/now-what.html>
- Lyon, A., & Bilton, D. (2002). Fertility issues in cystic fibrosis. *Paediatr Respir Rev*, 3(3), 236-240. Retrieved from <http://www.ncbi.nlm.nih.gov/pubmed/12376060>
- Ma, B., & Lutchen, K. R. (2009). CFD simulation of aerosol deposition in an anatomically based human large-medium airway model. *Ann Biomed Eng*, 37(2), 271-285. doi:10.1007/s10439-008-9620-y
- MacConnachie, A. M. (1998). Dornase-alfa (DNase, Pulmozyme) for cystic fibrosis. *Intensive Crit Care Nurs*, 14(2), 101-102. Retrieved from <http://www.ncbi.nlm.nih.gov/pubmed/9814214>
- MacLusky, I., Levison, H., Gold, R., & McLaughlin, F. J. (1986). Inhaled antibiotics in cystic fibrosis: is there a therapeutic effect? *J Pediatr*, 108(5 Pt 2), 861-865. Retrieved from <http://www.ncbi.nlm.nih.gov/pubmed/3517274>
- Maffessanti, M., Candusso, M., Brizzi, F., & Piovesana, F. (1996). Cystic fibrosis in children: HRCT findings and distribution of disease. *J Thorac Imaging*, 11(1), 27-38. Retrieved from <http://www.ncbi.nlm.nih.gov/pubmed/8770824>
- Manske, S. L., Zhu, Y., Sandino, C., & Boyd, S. K. (2015). Human trabecular bone microarchitecture can be assessed independently of density with second generation HR-pQCT. *Bone*, 79, 213-221. doi:10.1016/j.bone.2015.06.006
- Marcotte, J. E., Grisdale, R. K., Levison, H., Coates, A. L., & Canny, G. J. (1986). Multiple factors limit exercise capacity in cystic fibrosis. *Pediatr*

Pulmonol, 2(5), 274-281. Retrieved from

<http://www.ncbi.nlm.nih.gov/pubmed/3774384>

Martonen, T. B. (1993). Mathematical model for the selective deposition of inhaled pharmaceuticals. *J Pharm Sci*, 82(12), 1191-1199. Retrieved from <http://www.ncbi.nlm.nih.gov/pubmed/8308694>

Masters, I. B., Eastburn, M. M., Wootton, R., Ware, R. S., Francis, P. W., Zimmerman, P. V., & Chang, A. B. (2005). A new method for objective identification and measurement of airway lumen in paediatric flexible videobronchoscopy. *Thorax*, 60(8), 652-658.
doi:10.1136/thx.2004.034421

Matsui, H., Grubb, B. R., Tarran, R., Randell, S. H., Gatzky, J. T., Davis, C. W., & Boucher, R. C. (1998). Evidence for periciliary liquid layer depletion, not abnormal ion composition, in the pathogenesis of cystic fibrosis airways disease. *Cell*, 95(7), 1005-1015. Retrieved from <http://www.ncbi.nlm.nih.gov/pubmed/9875854>

Matsuoka, S., Kurihara, Y., Yagihashi, K., Hoshino, M., Watanabe, N., & Nakajima, Y. (2008). Quantitative assessment of air trapping in chronic obstructive pulmonary disease using inspiratory and expiratory volumetric MDCT. *AJR Am J Roentgenol*, 190(3), 762-769.
doi:10.2214/AJR.07.2820

McKone, E. F., Emerson, S. S., Edwards, K. L., & Aitken, M. L. (2003). Effect of genotype on phenotype and mortality in cystic fibrosis: a retrospective cohort study. *Lancet*, 361(9370), 1671-1676.
doi:10.1016/S0140-6736(03)13368-5

McLaughlin, R. A., Williamson, J. P., Phillips, M. J., Armstrong, J. J., Becker, S., Hillman, D. R., . . . Sampson, D. D. (2008). Applying anatomical

optical coherence tomography to quantitative 3D imaging of the lower airway. *Opt Express*, 16(22), 17521-17529. Retrieved from <http://www.ncbi.nlm.nih.gov/pubmed/18958032>

Mearns, M. B. (1972). Treatment and prevention of pulmonary complications of cystic fibrosis in infancy and early childhood. *Arch Dis Child*, 47(251), 5-11. Retrieved from <http://www.ncbi.nlm.nih.gov/pubmed/5018658>

Merlo, C. A., & Boyle, M. P. (2003). Modifier genes in cystic fibrosis lung disease. *J Lab Clin Med*, 141(4), 237-241. doi:10.1067/mlc.2003.29

Meyerholz, D. K., Stoltz, D. A., Namati, E., Ramachandran, S., Pezzulo, A. A., Smith, A. R., . . . Welsh, M. J. (2010). Loss of cystic fibrosis transmembrane conductance regulator function produces abnormalities in tracheal development in neonatal pigs and young children. *Am J Respir Crit Care Med*, 182(10), 1251-1261. doi:10.1164/rccm.201004-0643OC

Mickle, J. E., & Cutting, G. R. (2000). Genotype-phenotype relationships in cystic fibrosis. *Med Clin North Am*, 84(3), 597-607. Retrieved from <http://www.ncbi.nlm.nih.gov/pubmed/10872417>

Miller, A. D. (1992). Human gene therapy comes of age. *Nature*, 357(6378), 455-460. doi:10.1038/357455a0

Miyawaki, S. (2013). *AUTOMATIC CONSTRUCTION AND MESHING OF MULTISCALE IMAGE-BASED HUMAN AIRWAY MODELS FOR SIMULATIONS OF AEROSOL DELIVERY*. (Ph.D.), University of Iowa.

Miyawaki, S., Tawhai, M. H., Hoffman, E. A., & Lin, C. L. (2012). Effect of carrier gas properties on aerosol distribution in a CT-based human

airway numerical model. *Ann Biomed Eng*, 40(7), 1495-1507.

doi:10.1007/s10439-011-0503-2

Molinski, S., Eckford, P. D., Pasyk, S., Ahmadi, S., Chin, S., & Bear, C. E.

(2012). Functional Rescue of F508del-CFTR Using Small Molecule

Correctors. *Front Pharmacol*, 3, 160. doi:10.3389/fphar.2012.00160

Mortola, J. P. (1984). Breathing pattern in newborns. *J Appl Physiol Respir*

Environ Exerc Physiol, 56(6), 1533-1540. Retrieved from

<http://www.ncbi.nlm.nih.gov/pubmed/6735812>

Mott, L. S., Park, J., Gangell, C. L., de Klerk, N. H., Sly, P. D., Murray, C. P., .

. . Australian Respiratory Early Surveillance Team for Cystic Fibrosis

Study, G. (2013). Distribution of early structural lung changes due to

cystic fibrosis detected with chest computed tomography. *J Pediatr*,

163(1), 243-248 e241-243. doi:10.1016/j.jpeds.2012.12.042

Mott, L. S., Park, J., Murray, C. P., Gangell, C. L., de Klerk, N. H., Robinson,

P. J., . . . Arest, C. F. (2012). Progression of early structural lung

disease in young children with cystic fibrosis assessed using CT.

Thorax, 67(6), 509-516. doi:10.1136/thoraxjnl-2011-200912

Murek, M., Kopic, S., & Geibel, J. (2010). Evidence for intestinal chloride

secretion. *Exp Physiol*, 95(4), 471-478.

doi:10.1113/expphysiol.2009.049445

Murphy, K., van Ginneken, B., Reinhardt, J. M., Kabus, S., Ding, K., Deng,

X., . . . Pluim, J. P. (2011). Evaluation of registration methods on

thoracic CT: the EMPIRE10 challenge. *IEEE Trans Med Imaging*,

30(11), 1901-1920. doi:10.1109/TMI.2011.2158349

Nash, K. L., Allison, M. E., McKeon, D., Lomas, D. J., Haworth, C. S., Bilton,

D., & Alexander, G. J. (2008). A single centre experience of liver

disease in adults with cystic fibrosis 1995-2006. *J Cyst Fibros*, 7(3), 252-257. doi:10.1016/j.jcf.2007.10.004

Neuberger, T., Burton, B., Clark, H., & Van Goor, F. (2011). Use of primary cultures of human bronchial epithelial cells isolated from cystic fibrosis patients for the pre-clinical testing of CFTR modulators. *Methods Mol Biol*, 741, 39-54. doi:10.1007/978-1-61779-117-8_4

Newman, K. B., Lynch, D. A., Newman, L. S., Ellegood, D., & Newell, J. D., Jr. (1994). Quantitative computed tomography detects air trapping due to asthma. *Chest*, 106(1), 105-109. Retrieved from <http://www.ncbi.nlm.nih.gov/pubmed/8020254>

Nichols, J. E., Niles, J. A., Vega, S. P., & Cortiella, J. (2013). Novel in vitro respiratory models to study lung development, physiology, pathology and toxicology. *Stem Cell Res Ther*, 4 Suppl 1, S7. doi:10.1186/scrt368

Nixon, G. M., Armstrong, D. S., Carzino, R., Carlin, J. B., Olinsky, A., Robertson, C. F., & Grimwood, K. (2001). Clinical outcome after early *Pseudomonas aeruginosa* infection in cystic fibrosis. *J Pediatr*, 138(5), 699-704. doi:10.1067/mpd.2001.112897

Nolan, G., Moivor, P., Levison, H., Fleming, P. C., Corey, M., & Gold, R. (1982). Antibiotic prophylaxis in cystic fibrosis: inhaled cephaloridine as an adjunct to oral cloxacillin. *J Pediatr*, 101(4), 626-630. Retrieved from <http://www.ncbi.nlm.nih.gov/pubmed/6981695>

O'Neal, W. K., Hasty, P., McCray, P. B., Casey, B., RiveraPérez, J., Welsh, M. J., . . . Bradley, A. (1993). A severe phenotype in mice with a duplication of exon 3 in the cystic fibrosis locus. *Hum Mol Genet*, 2(10), 1561-1569. doi:10.1093/hmg/2.10.1561

- O'Sullivan, B. P., Orenstein, D. M., & Milla, C. E. (2013). Pricing for orphan drugs: will the market bear what society cannot? *JAMA*, *310*(13), 1343-1344. doi:10.1001/jama.2013.278129
- Olivier, A. K., Yi, Y., Sun, X., Sui, H., Liang, B., Hu, S., . . . Engelhardt, J. F. (2012). Abnormal endocrine pancreas function at birth in cystic fibrosis ferrets. *J Clin Invest*, *122*(10), 3755-3768. doi:10.1172/JCI60610
- Ooi, C. Y., & Durie, P. R. (2012). Cystic fibrosis transmembrane conductance regulator (CFTR) gene mutations in pancreatitis. *J Cyst Fibros*, *11*(5), 355-362. doi:10.1016/j.jcf.2012.05.001
- Oppenheimer, E. H., & Esterly, J. R. (1973). Cystic fibrosis of the pancreas. Morphologic findings in infants with and without diagnostic pancreatic lesions. *Arch Pathol*, *96*(3), 149-154. Retrieved from <http://www.ncbi.nlm.nih.gov/pubmed/4722876>
- Oppenheimer, E. H., & Esterly, J. R. (1975). Pathology of cystic fibrosis review of the literature and comparison with 146 autopsied cases. *Perspect Pediatr Pathol*, *2*, 241-278. Retrieved from <http://www.ncbi.nlm.nih.gov/pubmed/1168897>
- Ostedgaard, L. S., Meyerholz, D. K., Chen, J. H., Pezzulo, A. A., Karp, P. H., Rokhlina, T., . . . Stoltz, D. A. (2011). The DeltaF508 mutation causes CFTR misprocessing and cystic fibrosis-like disease in pigs. *Sci Transl Med*, *3*(74), 74ra24. doi:10.1126/scitranslmed.3001868
- Pack, R. J., Al-Ugaily, L. H., & Morris, G. (1981). The cells of the tracheobronchial epithelium of the mouse: a quantitative light and electron microscope study. *J Anat*, *132*(Pt 1), 71-84. Retrieved from <http://www.ncbi.nlm.nih.gov/pubmed/7275793>

- Padst, R. B., R.M. (1994). The immune system of the respiratory tract in pigs. *Vet Immunol Immunopathol.*, 43(1-3), 5.
- Parad, R. B. (1996). Heterogeneity of phenotype in two cystic fibrosis patients homozygous for the CFTR exon 11 mutation G551D. *J Med Genet*, 33(8), 711-713. Retrieved from <http://www.ncbi.nlm.nih.gov/pubmed/8863168>
- Patel, C., Cooper-Charles, L., McMullan, D. J., Walker, J. M., Davison, V., & Morton, J. (2011). Translocation breakpoint at 7q31 associated with tics: further evidence for IMMP2L as a candidate gene for Tourette syndrome. *Eur J Hum Genet*, 19(6), 634-639.
doi:10.1038/ejhg.2010.238
- Pezzulo, A. A., Tang, X. X., Hoegger, M. J., Alaiwa, M. H., Ramachandran, S., Moninger, T. O., . . . Zabner, J. (2012). Reduced airway surface pH impairs bacterial killing in the porcine cystic fibrosis lung. *Nature*, 487(7405), 109-113. doi:10.1038/nature11130
- Pind, S., Riordan, J. R., & Williams, D. B. (1994). Participation of the endoplasmic reticulum chaperone calnexin (p88, IP90) in the biogenesis of the cystic fibrosis transmembrane conductance regulator. *J Biol Chem*, 269(17), 12784-12788. Retrieved from <http://www.ncbi.nlm.nih.gov/pubmed/7513695>
- Pisi, G., & Chetta, A. (2009). Airway clearance therapy in cystic fibrosis patients. *Acta Biomed*, 80(2), 102-106. Retrieved from <http://www.ncbi.nlm.nih.gov/pubmed/19848046>
- Plopper, C. G., Mariassy, A. T., Wilson, D. W., Alley, J. L., Nishio, S. J., & Nettekheim, P. (1983). Comparison of nonciliated tracheal epithelial cells in six mammalian species: ultrastructure and population

densities. *Exp Lung Res*, 5(4), 281-294. Retrieved from

<http://www.ncbi.nlm.nih.gov/pubmed/6662075>

Quanjer, P. H., Tammeling, G. J., Cotes, J. E., Pedersen, O. F., Peslin, R., & Yernault, J. C. (1993). Lung volumes and forced ventilatory flows. *Eur Respir J*, 6 Suppl 16, 5-40. doi:10.1183/09041950.005s1693

Quanjer, P. H., Weiner, D. J., Pretto, J. J., Brazzale, D. J., & Boros, P. W. (2014). Measurement of FEF25-75% and FEF75% does not contribute to clinical decision making. *Eur Respir J*, 43(4), 1051-1058. doi:10.1183/09031936.00128113

Quinton, P. M. (1989). Defective epithelial ion transport in cystic fibrosis. *Clin Chem*, 35(5), 726-730. Retrieved from <http://www.ncbi.nlm.nih.gov/pubmed/2655997>

Quinton, P. M. (1990). Cystic fibrosis: a disease in electrolyte transport. *FASEB J*, 4(10), 2709-2717. Retrieved from <http://www.ncbi.nlm.nih.gov/pubmed/2197151>

Quinton, P. M. (2008). Cystic fibrosis: impaired bicarbonate secretion and mucoviscidosis. *Lancet*, 372(9636), 415-417. doi:10.1016/S0140-6736(08)61162-9

Quinton, P. M. (2010). Role of epithelial HCO₃⁻ transport in mucin secretion: lessons from cystic fibrosis. *Am J Physiol Cell Physiol*, 299(6), C1222-1233. doi:10.1152/ajpcell.00362.2010

Quon, B. S., Schaeffer, M. R., Molgat-Seon, Y., Wilkie, S. S., Wilcox, P. G., & Guenette, J. A. (2015). Physiological mechanisms of dyspnea relief following ivacaftor in cystic fibrosis: a case report. *Respir Physiol Neurobiol*, 205, 105-108. doi:10.1016/j.resp.2014.10.019

- Rabe, K. F., Hurd, S., Anzueto, A., Barnes, P. J., Buist, S. A., Calverley, P., . . . Global Initiative for Chronic Obstructive Lung, D. (2007). Global strategy for the diagnosis, management, and prevention of chronic obstructive pulmonary disease: GOLD executive summary. *Am J Respir Crit Care Med*, *176*(6), 532-555. doi:10.1164/rccm.200703-456SO
- Raia, V., Fuiano, L., & Staiano, A. (2010). The ESPGHAN Cystic Fibrosis Working Group: defining DIOS and constipation in cystic fibrosis with a multicenter study on the incidence, characteristics, and treatment of DIOS. *J Pediatr Gastroenterol Nutr*, *50*(1), 8. doi:10.1097/MPG.0b013e3181a6da59
- Raia, V., Maiuri, L., de Ritis, G., de Vizia, B., Vacca, L., Conte, R., . . . Londei, M. (2000). Evidence of chronic inflammation in morphologically normal small intestine of cystic fibrosis patients. *Pediatr Res*, *47*(3), 344-350. Retrieved from <http://www.ncbi.nlm.nih.gov/pubmed/10709733>
- Ramjeesingh, M., Kidd, J. F., Huan, L. J., Wang, Y., & Bear, C. E. (2003). Dimeric cystic fibrosis transmembrane conductance regulator exists in the plasma membrane. *Biochem J*, *374*(Pt 3), 793-797. doi:10.1042/BJ20030683
- Ramsey, B. W., Davies, J., McElvaney, N. G., Tullis, E., Bell, S. C., Drevinek, P., . . . Group, V. X. S. (2011). A CFTR potentiator in patients with cystic fibrosis and the G551D mutation. *N Engl J Med*, *365*(18), 1663-1672. doi:10.1056/NEJMoa1105185
- Ramsey, B. W., Dorkin, H. L., Eisenberg, J. D., Gibson, R. L., Harwood, I. R., Kravitz, R. M., . . . et al. (1993). Efficacy of aerosolized tobramycin in

patients with cystic fibrosis. *N Engl J Med*, 328(24), 1740-1746.

doi:10.1056/NEJM199306173282403

Ramsey, B. W., Pepe, M. S., Quan, J. M., Otto, K. L., Montgomery, A. B., Williams-Warren, J., . . . Smith, A. L. (1999). Intermittent administration of inhaled tobramycin in patients with cystic fibrosis. Cystic Fibrosis Inhaled Tobramycin Study Group. *N Engl J Med*, 340(1), 23-30. doi:10.1056/NEJM199901073400104

Ranganathan, S. C., Goetz, I., Hoo, A. F., Lum, S., Castle, R., Stocks, J., & London Collaborative Cystic Fibrosis, G. (2003). Assessment of tidal breathing parameters in infants with cystic fibrosis. *Eur Respir J*, 22(5), 761-766. Retrieved from <http://www.ncbi.nlm.nih.gov/pubmed/14621082>

Ratjen, F., Doring, G., & Nikolaizik, W. H. (2001). Effect of inhaled tobramycin on early *Pseudomonas aeruginosa* colonisation in patients with cystic fibrosis. *Lancet*, 358(9286), 983-984. doi:10.1016/S0140-6736(01)06124-4

Reeves, E. P., Molloy, K., Pohl, K., & McElvaney, N. G. (2012). Hypertonic saline in treatment of pulmonary disease in cystic fibrosis. *ScientificWorldJournal*, 2012, 465230. doi:10.1100/2012/465230

Reinhardt, J. M., Ding, K., Cao, K., Christensen, G. E., Hoffman, E. A., & Bodas, S. V. (2008). Registration-based estimates of local lung tissue expansion compared to xenon CT measures of specific ventilation. *Med Image Anal*, 12(6), 752-763. doi:10.1016/j.media.2008.03.007

Ren, C. L., Morgan, W. J., Konstan, M. W., Schechter, M. S., Wagener, J. S., Fisher, K. A., . . . Coordinators of the Epidemiologic Study of Cystic, F. (2007). Presence of methicillin resistant *Staphylococcus aureus* in

respiratory cultures from cystic fibrosis patients is associated with lower lung function. *Pediatr Pulmonol*, 42(6), 513-518.

doi:10.1002/ppul.20604

Respirtech. The inCourage® System. Retrieved from

<http://www.respirtech.com/incourage-airway-clearance-therapy>

Rich, D. P., Anderson, M. P., Gregory, R. J., Cheng, S. H., Paul, S., Jefferson, D. M., . . . Welsh, M. J. (1990). Expression of cystic fibrosis transmembrane conductance regulator corrects defective chloride channel regulation in cystic fibrosis airway epithelial cells. *Nature*, 347(6291), 358-363. doi:10.1038/347358a0

Riordan, J. R. (2008). CFTR function and prospects for therapy. *Annu Rev Biochem*, 77, 701-726.

doi:10.1146/annurev.biochem.75.103004.142532

Riordan, J. R., Rommens, J. M., Kerem, B., Alon, N., Rozmahel, R., Grzelczak, Z., . . . et al. (1989). Identification of the cystic fibrosis gene: cloning and characterization of complementary DNA. *Science*, 245(4922), 1066-1073. Retrieved from

<http://www.ncbi.nlm.nih.gov/pubmed/2475911>

Rodarte, J. R., Hubmayr, R. D., Stamenovic, D., & Walters, B. J. (1985).

Regional lung strain in dogs during deflation from total lung capacity. *J Appl Physiol* (1985), 58(1), 164-172. Retrieved from

<http://www.ncbi.nlm.nih.gov/pubmed/3968007>

Rogan, M. P., Stoltz, D. A., & Hornick, D. B. (2011). Cystic fibrosis transmembrane conductance regulator intracellular processing, trafficking, and opportunities for mutation-specific treatment. *Chest*, 139(6), 1480-1490. doi:10.1378/chest.10-2077

- Rogers, C. S., Hao, Y., Rokhlina, T., Samuel, M., Stoltz, D. A., Li, Y., . . . Prather, R. S. (2008). Production of CFTR-null and CFTR-DeltaF508 heterozygous pigs by adeno-associated virus-mediated gene targeting and somatic cell nuclear transfer. *J Clin Invest*, *118*(4), 1571-1577. doi:10.1172/JCI34773
- Rogers, C. S., Stoltz, D. A., Meyerholz, D. K., Ostedgaard, L. S., Rokhlina, T., Taft, P. J., . . . Welsh, M. J. (2008). Disruption of the CFTR gene produces a model of cystic fibrosis in newborn pigs. *Science*, *321*(5897), 1837-1841. doi:10.1126/science.1163600
- Rommens, J. M., Iannuzzi, M. C., Kerem, B., Drumm, M. L., Melmer, G., Dean, M., . . . et al. (1989). Identification of the cystic fibrosis gene: chromosome walking and jumping. *Science*, *245*(4922), 1059-1065. Retrieved from <http://www.ncbi.nlm.nih.gov/pubmed/2772657>
- Roscetto, E., Vitiello, L., Muoio, R., Soriano, A. A., Iula, V. D., Vollaro, A., . . . Catania, M. R. (2015). In vitro interaction of *Stenotrophomonas maltophilia* with human monocyte-derived dendritic cells. *Front Microbiol*, *6*, 723. doi:10.3389/fmicb.2015.00723
- Rossi, U. G., & Owens, C. M. (2005). The radiology of chronic lung disease in children. *Arch Dis Child*, *90*(6), 601-607. doi:10.1136/adc.2004.051383
- Rowe, S. M., Heltshe, S. L., Gonska, T., Donaldson, S. H., Borowitz, D., Gelfond, D., . . . Network, G. I. o. t. C. F. F. T. D. (2014). Clinical mechanism of the cystic fibrosis transmembrane conductance regulator potentiator ivacaftor in G551D-mediated cystic fibrosis. *Am J Respir Crit Care Med*, *190*(2), 175-184. doi:10.1164/rccm.201404-0703OC

- Rowe, S. M., Miller, S., & Sorscher, E. J. (2005). Cystic fibrosis. *N Engl J Med*, 352(19), 1992-2001. doi:10.1056/NEJMra043184
- Rowntree, R. K., & Harris, A. (2003). The phenotypic consequences of CFTR mutations. *Ann Hum Genet*, 67(Pt 5), 471-485. Retrieved from <http://www.ncbi.nlm.nih.gov/pubmed/12940920>
- Santis, G., Hodson, M. E., & Strickland, B. (1991). High resolution computed tomography in adult cystic fibrosis patients with mild lung disease. *Clin Radiol*, 44(1), 20-22. Retrieved from <http://www.ncbi.nlm.nih.gov/pubmed/1873946>
- Sato, S., Ward, C. L., & Kopito, R. R. (1998). Cotranslational ubiquitination of cystic fibrosis transmembrane conductance regulator in vitro. *J Biol Chem*, 273(13), 7189-7192. Retrieved from <http://www.ncbi.nlm.nih.gov/pubmed/9516408>
- Saynor, Z. L., Barker, A. R., Oades, P. J., & Williams, C. A. (2014). The effect of ivacaftor in adolescents with cystic fibrosis (G551D mutation): an exercise physiology perspective. *Pediatr Phys Ther*, 26(4), 454-461. doi:10.1097/PEP.0000000000000086
- Sbarbati, A., Bertini, M., Catassi, C., Gagliardini, R., & Osculati, F. (1998). Ultrastructural lesions in the small bowel of patients with cystic fibrosis. *Pediatr Res*, 43(2), 234-239. doi:10.1203/00006450-199804001-01393
- Schmidt, A., Zidowitz, S., Kriete, A., Denhard, T., Krass, S., & Peitgen, H. O. (2004). A digital reference model of the human bronchial tree. *Comput Med Imaging Graph*, 28(4), 203-211. doi:10.1016/j.compmedimag.2004.01.001

- Scholte, B. J., Davidson, D. J., Wilke, M., & De Jonge, H. R. (2004). Animal models of cystic fibrosis. *J Cyst Fibros*, 3 Suppl 2, 183-190.
doi:10.1016/j.jcf.2004.05.039
- Senn, J. (1998). Cystic Fibrosis and Gene Therapy. Retrieved from <https://www.ndsu.edu/pubweb/~mcclean/plsc431/students98/senn.htm>
- Sermet-Gaudelus, I. (2013). Ivacaftor treatment in patients with cystic fibrosis and the G551D-CFTR mutation. *Eur Respir Rev*, 22(127), 66-71.
doi:10.1183/09059180.00008512
- Serohijos, A. W., Hegedus, T., Aleksandrov, A. A., He, L., Cui, L., Dokholyan, N. V., & Riordan, J. R. (2008). Phenylalanine-508 mediates a cytoplasmic-membrane domain contact in the CFTR 3D structure crucial to assembly and channel function. *Proc Natl Acad Sci U S A*, 105(9), 3256-3261. doi:10.1073/pnas.0800254105
- Serpa Neto, A., Cardoso, S. O., Manetta, J. A., Pereira, V. G., Esposito, D. C., Pasqualucci Mde, O., . . . Schultz, M. J. (2012). Association between use of lung-protective ventilation with lower tidal volumes and clinical outcomes among patients without acute respiratory distress syndrome: a meta-analysis. *JAMA*, 308(16), 1651-1659.
doi:10.1001/jama.2012.13730
- Shamsi, M. B., Kumar, K., & Dada, R. (2011). Genetic and epigenetic factors: Role in male infertility. *Indian J Urol*, 27(1), 110-120.
doi:10.4103/0970-1591.78436
- Shaw, T. J., Wakely, S. L., Peebles, C. R., Mehta, R. L., Turner, J. M., Wilson, S. J., & Howarth, P. H. (2004). Endobronchial ultrasound to assess airway wall thickening: validation in vitro and in vivo. *Eur*

Respir J, 23(6), 813-817. Retrieved from

<http://www.ncbi.nlm.nih.gov/pubmed/15218991>

Sheikh, S. I., Long, F. R., McCoy, K. S., Johnson, T., Ryan-Wenger, N. A., & Hayes, D., Jr. (2015a). Computed tomography correlates with improvement with ivacaftor in cystic fibrosis patients with G551D mutation. *J Cyst Fibros*, 14(1), 84-89. doi:10.1016/j.jcf.2014.06.011

Sheikh, S. I., Long, F. R., McCoy, K. S., Johnson, T., Ryan-Wenger, N. A., & Hayes, D., Jr. (2015b). Ivacaftor improves appearance of sinus disease on computerised tomography in cystic fibrosis patients with G551D mutation. *Clin Otolaryngol*, 40(1), 16-21.

doi:10.1111/coa.12310

Sinaasappel, M., Stern, M., Littlewood, J., Wolfe, S., Steinkamp, G., Heijerman, H. G., . . . Doring, G. (2002). Nutrition in patients with cystic fibrosis: a European Consensus. *J Cyst Fibros*, 1(2), 51-75.

Retrieved from <http://www.ncbi.nlm.nih.gov/pubmed/15463811>

Sinha, C., Zhang, W., Moon, C. S., Actis, M., Yarlagadda, S., Arora, K., . . . Naren, A. P. (2015). Capturing the Direct Binding of CFTR Correctors to CFTR by Using Click Chemistry. *Chembiochem*, 16(14), 2017-2022. doi:10.1002/cbic.201500123

Sly, P. D., Brennan, S., Gangell, C., de Klerk, N., Murray, C., Mott, L., . . . Australian Respiratory Early Surveillance Team for Cystic, F. (2009). Lung disease at diagnosis in infants with cystic fibrosis detected by newborn screening. *Am J Respir Crit Care Med*, 180(2), 146-152.

doi:10.1164/rccm.200901-0069OC

Smith, M. L., Kohart, N. A., Newmyer, B. A., & Cline, M. A. (2009).

Gamma(2)-melanocyte stimulating hormone decreases food intake in

chicks. *Neurosci Lett*, 465(3), 210-213.

doi:10.1016/j.neulet.2009.08.021

Smyth, R. L., Croft, N. M., O'Hea, U., Marshall, T. G., & Ferguson, A. (2000).

Intestinal inflammation in cystic fibrosis. *Arch Dis Child*, 82(5), 394-

399. Retrieved from <http://www.ncbi.nlm.nih.gov/pubmed/10799435>

Snyder, P. M., McDonald, F. J., Stokes, J. B., & Welsh, M. J. (1994).

Membrane topology of the amiloride-sensitive epithelial sodium

channel. *J Biol Chem*, 269(39), 24379-24383. Retrieved from

<http://www.ncbi.nlm.nih.gov/pubmed/7929098>

Song, G. K., S.; and Lorenz, C. (2010). *Fast elastic image registration," Med.*

Image Anal. Clinic: A Grand Challenge.

Spencer, R. M., Schroeter, J. D., & Martonen, T. B. (2001). Computer

simulations of lung airway structures using data-driven surface

modeling techniques. *Comput Biol Med*, 31(6), 499-511. Retrieved

from <http://www.ncbi.nlm.nih.gov/pubmed/11604154>

Spicuzza, L., Sciuto, C., Di Dio, L., Mattina, T., Leonardi, S., del Giudice, M.

M., & La Rosa, M. (2012). Mild cystic fibrosis in patients with the rare

P5L CFTR mutation. *J Cyst Fibros*, 11(1), 30-33.

doi:10.1016/j.jcf.2011.08.009

Steagall, W. K., Elmer, H. L., Brady, K. G., & Kelley, T. J. (2000). Cystic

fibrosis transmembrane conductance regulator-dependent regulation

of epithelial inducible nitric oxide synthase expression. *Am J Respir*

Cell Mol Biol, 22(1), 45-50. doi:10.1165/ajrcmb.22.1.3789

Stettler, N., Kawchak, D. A., Boyle, L. L., Propert, K. J., Scanlin, T. F.,

Stallings, V. A., & Zemel, B. S. (2000). Prospective evaluation of

growth, nutritional status, and body composition in children with cystic

fibrosis. *Am J Clin Nutr*, 72(2), 407-413. Retrieved from

<http://www.ncbi.nlm.nih.gov/pubmed/10919935>

- Stick, S. M., Brennan, S., Murray, C., Douglas, T., von Ungern-Sternberg, B. S., Garratt, L. W., . . . Australian Respiratory Early Surveillance Team for Cystic, F. (2009). Bronchiectasis in infants and preschool children diagnosed with cystic fibrosis after newborn screening. *J Pediatr*, 155(5), 623-628 e621. doi:10.1016/j.jpeds.2009.05.005
- Stoltz, D. A., Meyerholz, D. K., Pezzulo, A. A., Ramachandran, S., Rogan, M. P., Davis, G. J., . . . Welsh, M. J. (2010). Cystic fibrosis pigs develop lung disease and exhibit defective bacterial eradication at birth. *Sci Transl Med*, 2(29), 29ra31. doi:10.1126/scitranslmed.3000928
- Strom, C. M., Crossley, B., Redman, J. B., Buller, A., Quan, F., Peng, M., . . . Sun, W. (2004). Cystic fibrosis screening: lessons learned from the first 320,000 patients. *Genet Med*, 6(3), 136-140. doi:10.109701.GIM.0000127275.52925.05
- Sturm, R. (2011). Stochastic Modeling of Particle Deposition in Lungs of Cystic Fibrosis Patients. *ISRN Pulmonology*, 2011(Article ID 510860), 11. doi:10.5402/2011/510860
- Sturm, R., & Hofmann, W. (2006). A computer program for the simulation of fiber deposition in the human respiratory tract. *Comput Biol Med*, 36(11), 1252-1267. doi:10.1016/j.compbiomed.2005.07.004
- Stutts, M. J. B., R.C. (1999). *Cystic Fibrosis in Adults* (Y. J. R. K. M.R. Ed.). Philadelphia: Lippincott-Raven Publishers.
- Subramaniam, R. P., Asgharian, B., Freijer, J. I., Miller, F. J., & Anjilvel, S. (2003). Analysis of lobar differences in particle deposition in the human lung. *Inhal Toxicol*, 15(1), 1-21. doi:10.1080/089583703044451

- Sun, X., Sui, H., Fisher, J. T., Yan, Z., Liu, X., Cho, H. J., . . . Engelhardt, J. F. (2010). Disease phenotype of a ferret CFTR-knockout model of cystic fibrosis. *J Clin Invest*, *120*(9), 3149-3160. doi:10.1172/JCI43052
- Sun, Y., O'Sullivan, B. P., Roche, J. P., Walvick, R., Reno, A., Baker, D., . . . Albert, M. S. (2011). Using hyperpolarized ³He MRI to evaluate treatment efficacy in cystic fibrosis patients. *J Magn Reson Imaging*, *34*(5), 1206-1211. doi:10.1002/jmri.22724
- Suri, R. (2005). The use of human deoxyribonuclease (rhDNase) in the management of cystic fibrosis. *BioDrugs*, *19*(3), 135-144. Retrieved from <http://www.ncbi.nlm.nih.gov/pubmed/15984899>
- Tarran, R., Grubb, B. R., Parsons, D., Picher, M., Hirsh, A. J., Davis, C. W., & Boucher, R. C. (2001). The CF salt controversy: in vivo observations and therapeutic approaches. *Mol Cell*, *8*(1), 149-158. Retrieved from <http://www.ncbi.nlm.nih.gov/pubmed/11511368>
- Tebbutt, S. J., Wardle, C. J., Hill, D. F., & Harris, A. (1995). Molecular analysis of the ovine cystic fibrosis transmembrane conductance regulator gene. *Proc Natl Acad Sci U S A*, *92*(6), 2293-2297. Retrieved from <http://www.ncbi.nlm.nih.gov/pubmed/7534416>
- Thiberville, L., Moreno-Swirc, S., Vercauteren, T., Peltier, E., Cave, C., & Bourg Heckly, G. (2007). In vivo imaging of the bronchial wall microstructure using fibered confocal fluorescence microscopy. *Am J Respir Crit Care Med*, *175*(1), 22-31. doi:10.1164/rccm.200605-684OC
- Thomas, K. R., Folger, K. R., & Capecchi, M. R. (1986). High frequency targeting of genes to specific sites in the mammalian genome. *Cell*,

44(3), 419-428. Retrieved from

<http://www.ncbi.nlm.nih.gov/pubmed/3002636>

Thompson, V. (2014). what does cystic fibrosis feel like?, Cystic fibrosis lifestyle foundation. Retrieved from <http://www.cflf.org/blog/what-does-cystic-fibrosis-feel>

Tian, G. L., P.W.; Su, G.; Hindle, M. (2011). Characterization of respiratory drug delivery with enhanced condensational growth using an individual path model of the entire tracheobronchial airways. *Ann Biomed Eng.*, 39(3), 17. doi:10.1007/s10439-010-0223-z

Timonen, K. L., Randell, J. T., Salonen, R. O., & Pekkanen, J. (1997). Short-term variations in oscillatory and spirometric lung function indices among school children. *Eur Respir J*, 10(1), 82-87. Retrieved from <http://www.ncbi.nlm.nih.gov/pubmed/9032497>

Trotman-Dickenson, B. (2014). Cystic lung disease: achieving a radiologic diagnosis. *Eur J Radiol*, 83(1), 39-46. doi:10.1016/j.ejrad.2013.11.027

Trout, L., King, M., Feng, W., Inglis, S. K., & Ballard, S. T. (1998). Inhibition of airway liquid secretion and its effect on the physical properties of airway mucus. *Am J Physiol*, 274(2 Pt 1), L258-263. Retrieved from <http://www.ncbi.nlm.nih.gov/pubmed/9486211>

Tschirren, J., Hoffman, E. A., McLennan, G., & Sonka, M. (2005). Intrathoracic airway trees: segmentation and airway morphology analysis from low-dose CT scans. *IEEE Trans Med Imaging*, 24(12), 1529-1539. doi:10.1109/TMI.2005.857654

Turnbull, E. L., Rosser, M. F., & Cyr, D. M. (2007). The role of the UPS in cystic fibrosis. *BMC Biochem*, 8 Suppl 1, S11. doi:10.1186/1471-2091-8-S1-S11

- Tzeng, Y. S., Hoffman, E., Cook-Granroth, J., Maurer, R., Shah, N., Mansour, J., . . . Albert, M. (2007). Comparison of airway diameter measurements from an anthropomorphic airway tree phantom using hyperpolarized ³He MRI and high-resolution computed tomography. *Magn Reson Med*, 58(3), 636-642. doi:10.1002/mrm.21285
- UK, T. D. M. (2010). Teenager battles cystic fibrosis on 30 pills a day to take part in cheerleading competition. Retrieved from <http://www.dailymail.co.uk/health/article-1246777/Teenager-battles-cystic-fibrosis-thirty-pills-day-compete-cheerleading-competitions.html>
- Ukil, S., & Reinhardt, J. M. (2009). Anatomy-guided lung lobe segmentation in X-ray CT images. *IEEE Trans Med Imaging*, 28(2), 202-214. doi:10.1109/TMI.2008.929101
- University, W. (2014). Restrictive/ obstructive airway disease. Retrieved from <http://www2.nau.edu/~daa/lecture/pft.htm>
- Valerius, N. H., Koch, C., & Hoiby, N. (1991). Prevention of chronic *Pseudomonas aeruginosa* colonisation in cystic fibrosis by early treatment. *Lancet*, 338(8769), 725-726. Retrieved from <http://www.ncbi.nlm.nih.gov/pubmed/1679870>
- van Gool, K., Norman, R., Delatycki, M. B., Hall, J., & Massie, J. (2013). Understanding the costs of care for cystic fibrosis: an analysis by age and health state. *Value Health*, 16(2), 345-355. doi:10.1016/j.jval.2012.12.003
- Van Goor, F., Hadida, S., Grootenhuys, P. D., Burton, B., Cao, D., Neuberger, T., . . . Negulescu, P. (2009). Rescue of CF airway epithelial cell function in vitro by a CFTR potentiator, VX-770. *Proc Natl Acad Sci U S A*, 106(44), 18825-18830. doi:10.1073/pnas.0904709106

- Van Goor, F., Straley, K. S., Cao, D., Gonzalez, J., Hadida, S., Hazlewood, A., . . . Negulescu, P. (2006). Rescue of DeltaF508-CFTR trafficking and gating in human cystic fibrosis airway primary cultures by small molecules. *Am J Physiol Lung Cell Mol Physiol*, 290(6), L1117-1130. doi:10.1152/ajplung.00169.2005
- Van Scott, M. R., Yankaskas, J. R., & Boucher, R. C. (1986). Culture of airway epithelial cells: research techniques. *Exp Lung Res*, 11(2), 75-94. Retrieved from <http://www.ncbi.nlm.nih.gov/pubmed/3530735>
- Varadhan, R., Karangelis, G., Krishnan, K., & Hui, S. (2013). A framework for deformable image registration validation in radiotherapy clinical applications. *J Appl Clin Med Phys*, 14(1), 4066. doi:10.1120/jacmp.v14i1.4066
- Vasquez, K. M., Marburger, K., Intody, Z., & Wilson, J. H. (2001). Manipulating the mammalian genome by homologous recombination. *Proc Natl Acad Sci U S A*, 98(15), 8403-8410. doi:10.1073/pnas.111009698
- Vender, R. L. (2008). Cystic fibrosis lung disease in adult patients. *Postgrad Med*, 120(1), 64-74. doi:10.3810/pgm.2008.04.1762
- Vercauteren, T., Perchant, A., Malandain, G., Pennec, X., & Ayache, N. (2006). Robust mosaicing with correction of motion distortions and tissue deformations for in vivo fibered microscopy. *Med Image Anal*, 10(5), 673-692. doi:10.1016/j.media.2006.06.006
- Verkman, A. S., & Galletta, L. J. (2009). Chloride channels as drug targets. *Nat Rev Drug Discov*, 8(2), 153-171. doi:10.1038/nrd2780

- Vernon, H., Clark, K., & Bressler, J. P. (2011). In vitro models to study the blood brain barrier. *Methods Mol Biol*, 758, 153-168. doi:10.1007/978-1-61779-170-3_10
- Vertex. (2013). Treatment with VX-661 and Ivacaftor in a Phase 2 Study Resulted in Statistically Significant Improvements in Lung Function in People with Cystic Fibrosis Who Have Two Copies of the F508del Mutation. Retrieved from <http://investors.vrtx.com/releasedetail.cfm?ReleaseID=743425>
- Vickress, J., Battista, J., Barnett, R., Morgan, J., & Yartsev, S. (2016). Automatic landmark generation for deformable image registration evaluation for 4D CT images of lung. *Phys Med Biol*, 61(20), 7236-7245. doi:10.1088/0031-9155/61/20/7236
- Vinchurkar, S., Backer, L. D., Vos, W., Holsbeke, C. V., Backer, J. D., & Backer, W. D. (2012). A case series on lung deposition analysis of inhaled medication using functional imaging based computational fluid dynamics in asthmatic patients: effect of upper airway morphology and comparison with in vivo data. *Inhal Toxicol*, 24(2), 81-88. doi:10.3109/08958378.2011.644351
- Voelkel, N. F., MacNee, W. (2008). *Chronic obstructive lung disease*. Hamilton, Ontario: BC Decker Inc.
- Vos, W., De Backer, J., Poli, G., De Volder, A., Ghys, L., Van Holsbeke, C., . . . De Backer, W. (2013). Novel Functional Imaging of Changes in Small Airways of Patients Treated with Extrafine Beclomethasone/Formoterol. *Respiration*, 86(5), 393-401. Retrieved from <http://www.karger.com/DOI/10.1159/000347120>

- Vreman, A. W. (2004). An eddy-viscosity subgrid-scale model for turbulent shear flow: Algebraic theory and applications. *Physics of fluids*, 16(10), 11. Retrieved from <http://www.vremanresearch.nl/Vreman-PF2004-subgridmodel.pdf>
- Wainwright, C. E. (2014). Ivacaftor for patients with cystic fibrosis. *Expert Rev Respir Med*, 8(5), 533-538. doi:10.1586/17476348.2014.951333
- Ward, C. L., Omura, S., & Kopito, R. R. (1995). Degradation of CFTR by the ubiquitin-proteasome pathway. *Cell*, 83(1), 121-127. Retrieved from <http://www.ncbi.nlm.nih.gov/pubmed/7553863>
- Weibel, E. R. (1963). Principles and methods for the morphometric study of the lung and other organs. *Lab Invest*, 12, 131-155. Retrieved from <http://www.ncbi.nlm.nih.gov/pubmed/13999512>
- Weibel, E. R. (1973). Morphological basis of alveolar-capillary gas exchange. *Physiol Rev*, 53(2), 419-495. Retrieved from <http://www.ncbi.nlm.nih.gov/pubmed/4581654>
- Weisman, R. (2015). FDA clears vertex's new treatment for cystic fibrosis. Retrieved from <https://www.bostonglobe.com/business/2015/07/02/fda-approves-vertex-cystic-fibrosis-medicine/jzn9eCDenCq4rEI671mDOM/story.html>
- Welsh M.J., T. L.-C., Boat T.F., Beaudet A.L. (1996). *Cystic fibrosis* (t. edn Ed.). New York: McGraw-Hill.
- Welsh, M. J., & Ramsey, B. W. (1998). Research on cystic fibrosis: a journey from the Heart House. *Am J Respir Crit Care Med*, 157(4 Pt 2), S148-154. doi:10.1164/ajrccm.157.4.nhlbi-13

- West, J. B. (2012). *Pulmonary Pathophysiology: the essentials* (9th edition ed.). Baltimore, MD, USA: Lippincott Williams & Wilkins, a Wolters Kluwer Business.
- Whitcutt, M. J., Adler, K. B., & Wu, R. (1988). A biphasic chamber system for maintaining polarity of differentiation of cultured respiratory tract epithelial cells. *In Vitro Cell Dev Biol*, 24(5), 420-428. Retrieved from <http://www.ncbi.nlm.nih.gov/pubmed/3372447>
- Widdicombe, J. H. (1986). Cystic fibrosis and beta-adrenergic response of airway epithelial cell cultures. *Am J Physiol*, 251(4 Pt 2), R818-822. Retrieved from <http://www.ncbi.nlm.nih.gov/pubmed/3021002>
- Widmaier, E. P. R., H.; Strang, K.T. (2011). *Vander's human physiology: the mechanism of body function, 2nd edition* (2nd edition ed.): McGraw-Hill.
- Wielputz, M. O., Weinheimer, O., Eichinger, M., Wiebel, M., Biederer, J., Kauczor, H. U., . . . Puderbach, M. (2013). Pulmonary emphysema in cystic fibrosis detected by densitometry on chest multidetector computed tomography. *PLoS One*, 8(8), e73142. doi:10.1371/journal.pone.0073142
- Wiesel, J. M., Gamiel, H., Vlodaysky, I., Gay, I., & Ben-Bassat, H. (1983). Cell attachment, growth characteristics and surface morphology of human upper-respiratory tract epithelium cultured on extracellular matrix. *Eur J Clin Invest*, 13(1), 57-63. Retrieved from <http://www.ncbi.nlm.nih.gov/pubmed/6409625>
- Williams, S. H., Sahota, V., Palmai-Pallag, T., Tebbutt, S. J., Walker, J., & Harris, A. (2003). Evaluation of gene targeting by homologous

recombination in ovine somatic cells. *Mol Reprod Dev*, 66(2), 115-125.
doi:10.1002/mrd.10340

Williamson, J. P., James, A. L., Phillips, M. J., Sampson, D. D., Hillman, D. R., & Eastwood, P. R. (2009). Quantifying tracheobronchial tree dimensions: methods, limitations and emerging techniques. *Eur Respir J*, 34(1), 42-55. doi:10.1183/09031936.00020408

Wilmot, I., Schnieke, A. E., McWhir, J., Kind, A. J., & Campbell, K. H. (1997). Viable offspring derived from fetal and adult mammalian cells. *Nature*, 385(6619), 810-813. doi:10.1038/385810a0

Wilschanski, M., Miller, L. L., Shoseyov, D., Blau, H., Rivlin, J., Aviram, M., . . . Kerem, E. (2011). Chronic ataluren (PTC124) treatment of nonsense mutation cystic fibrosis. *Eur Respir J*, 38(1), 59-69.
doi:10.1183/09031936.00120910

Wilschanski, M., Rivlin, J., Cohen, S., Augarten, A., Blau, H., Aviram, M., . . . Kerem, E. (1999). Clinical and genetic risk factors for cystic fibrosis-related liver disease. *Pediatrics*, 103(1), 52-57. Retrieved from <http://www.ncbi.nlm.nih.gov/pubmed/9917439>

Wine, J. J. (1999). The genesis of cystic fibrosis lung disease. *J Clin Invest*, 103(3), 309- 312.

Wine, J. J. (2010). The development of lung disease in cystic fibrosis pigs. *Sci. Transl. Med.*, 2, 29ps20.

Wine, J. J., & Joo, N. S. (2004). Submucosal glands and airway defense. *Proc Am Thorac Soc*, 1(1), 47-53. doi:10.1513/pats.2306015

Wolcott, M. W., & Murphy, J. D. (1957). The changing picture of lung abscess therapy. *Dis Chest*, 32(1), 62-69. Retrieved from <http://www.ncbi.nlm.nih.gov/pubmed/13437912>

- Wu, K., Gamazon, E. R., Im, H. K., Gleeher, P., White, S. R., Solway, J., . . .
Huang, R. S. (2014). Genome-wide interrogation of longitudinal FEV1
in children with asthma. *Am J Respir Crit Care Med*, *190*(6), 619-627.
doi:10.1164/rccm.201403-0460OC
- Xia, G., Tawhai, M. H., Hoffman, E. A., & Lin, C. L. (2010). Airway wall
stiffening increases peak wall shear stress: a fluid-structure interaction
study in rigid and compliant airways. *Ann Biomed Eng*, *38*(5), 1836-
1853. doi:10.1007/s10439-010-9956-y
- Xu, Z., Pissarra, L. S., Farinha, C. M., Liu, J., Cai, Z., Thibodeau, P. H., . . .
Sheppard, D. N. (2014). Revertant mutants modify, but do not rescue,
the gating defect of the cystic fibrosis mutant G551D-CFTR. *J Physiol*,
592(Pt 9), 1931-1947. doi:10.1113/jphysiol.2014.271817
- Yamamoto, T., Kabus, S., Klinder, T., von Berg, J., Lorenz, C., Loo, B. W.,
Jr., & Keall, P. J. (2011). Four-dimensional computed tomography
pulmonary ventilation images vary with deformable image registration
algorithms and metrics. *Med Phys*, *38*(3), 1348-1358.
doi:10.1118/1.3547719
- Yin, Y., Choi, J., Hoffman, E. A., Tawhai, M. H., & Lin, C. L. (2010).
Simulation of pulmonary air flow with a subject-specific boundary
condition. *J Biomech*, *43*(11), 2159-2163.
doi:10.1016/j.jbiomech.2010.03.048
- Yin, Y., Choi, J., Hoffman, E. A., Tawhai, M. H., & Lin, C. L. (2013). A
multiscale MDCT image-based breathing lung model with time-varying
regional ventilation. *J Comput Phys*, *244*, 168-192.
doi:10.1016/j.jcp.2012.12.007

Yin, Y., Hoffman, E. A., & Lin, C.-L. (2009). *Local tissue-weight-based nonrigid registration of lung images with application to regional ventilation.*

Yin, Y., Hoffman, E. A., & Lin, C. L. (2009). Mass preserving nonrigid registration of CT lung images using cubic B-spline. *Med Phys*, 36(9), 4213-4222. Retrieved from <http://www.ncbi.nlm.nih.gov/pubmed/19810495>

Zahm, J. M. G., D.; Dupuit, F.; Hinrasky, J.; Porteous, D.; Dorin, J.R.; Puchelle, E. (1997). Early alterations in airway mucociliary clearance and inflammation of the lamina propria in CF mice. *Am J Physiol*, 272(3 Pt 1), C853-859. Retrieved from <http://ajpcell.physiology.org/content/ajpcell/272/3/C853.full.pdf>

Zhu, X., Dor, F. J., & Cooper, D. K. (2007). Pig-to-non-human primate heart transplantation: immunologic progress over 20 years. *J Heart Lung Transplant*, 26(3), 210-218. doi:10.1016/j.healun.2006.12.005

Zielenski, J. (2000). Genotype and phenotype in cystic fibrosis. *Respiration*, 67(2), 117-133. doi:29497